UNIVERSITY OF OKLAHOMA

GRADUATE COLLEGE

BOTTOM HOLE ANALYSES OF GAS KICK (INFLOW) AND GAS RESERVOIR CHARACTERIZATION WHILE DRILLING UNDERBALANCED

A Dissertation

SUBMITTED TO THE GRADUATE FACULTY

in partial fulfillment of the requirements for the

degree of

Doctor of Philosophy

By

OLUKAYODE JACOB AREMU
Norman, Oklahoma
2005

Downloaded from SHAREOK. Persistent Handle URL: https://hdl.handle.net/11244/856

UMI Number: 3163312



UMI Microform 3163312

Copyright 2005 by ProQuest Information and Learning Company.
All rights reserved. This microform edition is protected against unauthorized copying under Title 17, United States Code.

ProQuest Information and Learning Company
300 North Zeeb Road
P.O. Box 1346
Ann Arbor, MI 48106-1346

BOTTOM HOLE ANALYSES OF GAS INFLOW AND GAS RESERVOIR CHARACTERIZATION WHILE DRILLING UNDERBALANCED

A Dissertation APPROVED FOR THE

MEWBOURNE SCHOOL OF PETROLEUM AND GEOLOGICAL ENGINEERING

BY

_____
Dr. Samuel O. Osisanya
(Committee Chair)

_____
Dr. Chandra Rai

_____
Dr. Subhash N. Shah

_____
Dr. Richard Hughes

_____
Dr. Thomas A. Dewers

© Copyright by Olukayode Jacob Aremu 2005
All Rights Reserved.

ACKNOWLEDGEMENT

The author is indebted to Dr. Samuel O. Osisanya for his counseling, encouragement, financial support and thorough review that have resulted in the completion of this study. My special thanks go to Dr. Chandra Rai, Dr. Subhash Shah, Dr. Richard Hughes, and Dr. Thomas A. Dewers for their willingness to serve on my dissertation committee, and for their priceless comments and suggestions that have contributed to the successful completion of this study. I would also like to sincerely and gratefully thank Dr. Djebbar Tiab for exposing me to presenting at professional conferences, and providing me with useful comments for improving the quality of this work.

A special note of gratitude goes to the faculty members, and staff of the Mewbourne School of Petroleum and Geological Engineering for their various moral, educational, and financial provisions.

I am grateful to my two sons, IfeOluwa and OlaOluwa, my wife, my entire family and friends locally and internationally for their supports and prayers.

Finally, I would like to thank God Almighty for seeing me through this program; for His care, provisions and absolute love towards my family.

O. J. Aremu

Norman, Oklahoma

May 2005

TABLE OF CONTENTS

ACKNOWLEDGEMENT..……iv

LIST OF TABLES……...x

LIST OF FIGURES…….xi

ABSTRACT……..xv

CHAPTER ONE

FORMULATION OF THE PROBLEM……1

1.1 INTRODUCTION……..1

1.2 LITERATURE REVIEW……...4

1.3 OBJECTIVES AND METHODOLOGY……...12

1.3.1 Objectives……...13

1.3.2 Methodology……...14

1.4 ORGANIZATION OF THE DISSERTATION…….15

CHAPTER TWO

THEORETICAL BACKGROUND OF GAS INFLOW ANALYSIS…….....19

2.1 INTRODUCTION…….19

2.2 ABNORMAL FORMATION PRESSURE CONCEPTS…….20

2.3 TECHNIQUES FOR PREDICTING ABNORMAL PRESSURE…22

2.4 THEORETICAL ANALYSIS OF GAS INFLOW……...26

2.5 CONCEPTS OF GAS BUBBLE FORMATION……..33

2.5.1 Background and Principles of Gas Bubble Development…..33

2.6 MECHANICS OF WELLBORE PRESSURE BUILDUP……41

2.6.1 Wellbore Storage Analyzes……....47

CHAPTER THREE

MODELING OF GAS BUBBLY INFLOW AT THEWELLBORE-SAND FACE CONTACT FOR OPENED WELLBORE SCENARIOS……49

3.1 INTRODUCTION…….49

3.2 MODEL HYPOTHESES AND DESCRIPTION……..51

3.2.1 Model Hypotheses……..51

3.2.2 Model Description……..52

3.3 DEVELOPMENT OF THE GENERALIZED MODEL……54

3.3.1 Development of a Bubble……...54

3.3.2 Analysis of Forces on a Developing Bubble……..59

3.3.3 Coupling of Model Forces……..61

3.3.3.1 Expatiation on the Terms in the Coupled Model……61

3.4 THE GENERALIZED MODEL…….65

3.5 APPLICATION OF THE GENERAL MODEL TO THE PHYSICAL PROCESSES……...67

3.5.1 Stage 1 – Inception of Gas Inflow while Drilling and Circulating Drilling Fluid……67

3.5.2 Stage 2 – Suspension of Drilling and Mud Circulation……...69

3.6 MODEL SIMULATION, RESULTS AND DISCUSSIONS…….71

3.6.1 Error Analysis of the Modeling……...71

3.6.2 Apparent Bubble Size Profile at Instant of Gas Inflow…….77

3.6.3 Effect of Porosity……...77

3.6.4 Effects of Formation Radial Permeability…….86

3.6.5 Effects of Permeability Heterogeneity ……..89

3.6.6 Effect of Drag Forces on Apparent Bubble Sizes …….93

3.6.7 Effect of Mud Plastic Viscosity…….95

3.6.8 Effect of Rate of Penetration…….99

3.7 SUMMARY……...99

CHAPTER FOUR

MODELING OF WELLBORE STORAGE EFFECTS ON ANNULAR PRESSURE ANALYSIS OF A GAS-KICK WELL…….105

4.1 INTRODUCTION…….105

4.2 MODEL HYPOTHESES AND DESCRIPTION……..106

4.2.1 Model Hypotheses…….106

4.2.2 Model Description…….108

4.3 MODEL DEVELOPMENT……...110

4.3.1 Casing Pressure Module……119

4.4 MODELING TECHNIQUE……..120

4.4.1 Background to Pressure Build-up Computations……..121

4.4.2 Computing Pressure Rises During Shut-in……125

4.5 SIMULATION RESULTS AND DISCUSSIONS……...126

4.5.1 Effect of Reservoir Permeability on Pressure Rises……..127

4.5.2 Effects of Nominal Gas Kick Size or Volume……...131

4.5.3 Effect of Pressure Build-Up on the Annular Gas Density….137

4.5.4 Apparent Bubble Size Profile at the Instant of Inflow During Shut-in……140

4.5.5 Integration of All the Modeling Stages……..142

4.5.6 Effect of Hydrostatic Pressure During Shut-in Period……...145

4.6 SUMMARY……...146

CHAPTER FIVE

VALIDATION OF MODELS AND PRACTICAL APPLICATIONS……...151

5.1 INTRODUCTION…….151

5.2 VALIDATION OF MODELS……...152

5.2.1 Prediction of Surface Mud Pit Gain……...155

5.2.2 Modeling of Bottom-Hole Pressure Rise During Well Shut-in……157

5.3 QUANTITATIVE PREDICTION OF GAS INFLOW DURING UNDER-BALANCED DRILLING……...164

5.4 ESTIMATION OF THE GAS RESERVOIR PERMEABILITY AND PORE-PRESSURE……..165

5.4.1 Improving on the Existing Approaches…….166

5.4.2 Proposed Approach for Estimating the Reservoir Pressure and Permeability……167

5.5 SUMMARY……...171

CHAPTER SIX

CONCLUSIONS AND RECOMMENDATIONS…….173

6.1 CONCLUSIONS……...173

6.2 RECOMMENDATION..……...175

NOMENCLATURE…….176

REFERENCES…….181

APPENDIX A …….. .. 193

A1. RADIAL-CYLINDRICAL DIFFERENTIAL EQUATION …….... 194

A2. RADIAL-SPHERICAL DIFFUSIVITY FLOW EQUATION ….... 209

A3. DERIVATION OF VISCOUS DRAG FORCES …..... 216

APPENDIX B.……..218

B1. COMPUTER PROGRAM INTERFACE FORMS FOR COMPUTATIONS……219

B2. COMPUTER PROGRAMMING CODES……221

APPENDIX C……...……213

C1. EXAMPLE OF SIMULATION RESULTS FOR THE COMPUTED APPARENT GAS BUBBLE SIZES…….239

C2. EXAMPLE OF CASING AND BOTTOM-HOLE PRESSURE BUILD-UP SIMULATION RESULTS……241

APPENDIX D……...243

D. PLOT OF ANNULAR GAS DENSITY AGAINST THE SHUT-IN-TIME……...243

LIST OF TABLES

TABLE	TITLE	PAGE
2.1	Suggested types of formation pressure seals……...21	
3.1	Compiled base case data for modeling……72	
3.2	Comparison of experimental and literature data for the surface tension…….74	
3.3	Viscous stabilizing effect on the apparent bubble sizes……...98	
4.1	Modeling data……117	
4.2	Conventional drilling fluid pressure design data……...142	
5.1	Validation Data……..	

LIST OF FIGURES

FIGURE	TITLE	PAGE
1.1	Schematic representation of the top view of a "bent" shaped single bubble in the annulus containing viscous fluid	6
1.2	Forces responsible for the bubble development	16
2.1	Graphical representation of the existence of abnormal pressure depth	23
2.2	Example Illustration of Bowers unloading concept of abnormal pressure generation	24
2.3	Improvements on pressure predictions by spline function over regression analysis approach	27
2.4	U-tube modeling of wellbore configuration	28
2.5	Theoretical illustration of gas bubble upward flow in the annulus	30
2.6	Photographic display of bubble formation in a viscous fluid at high gas flow rate	36
2.7	Theoretical and experimental result comparison (smooth curves represent the theoretical results)	38
2.8	Viscosity effect on bubble volume by Satyanarayan et al	42
2.9	Effect of gas supply openings on bubble volume by Satyanarayan et al	43
2.10	Bottom-hole shut-in (curve a), and surface shut-in (curve b) of South Texas well no. 1 showing gas humping at the later shut-in time	46
3.1	Schematic representation of the modeled physical processes	55
3.2	Schematic of forces acting on a forming bubble	57
3.3	Example of error analysis plot for bubble volume prediction at formation interval, h =3 inches	75
3.4	Example of error analysis plot for bubble volume prediction at formation interval, h = 6 inches	76

3.5 Apparent bubble size distributions for the base case data during drilling and flow-check periods……78

3.6 Annular cumulative gas volume during drilling and flow-check periods….79

3.7 Rate of mud gain at the surface mud pit during drilling and flow-check periods……...80

3.8 Effect of porosity on the apparent bubble size profile for stages 1 and 2….82

3.9 Effect of porosity on the cumulative inflow gas volume during stages 1 and 2……83

3.10 Magnified porosity effect on the cumulative inflow gas volume at greater drilled interval for stage 1……..84

3.11 Experimental determination of the effects of pore volume compressibility on the initial porosity of consolidated sandstones……86

3.12 Class averages of the rock properties for the various rock types…….87

3.13 Effect of permeability on bubble size profile for stages 1 and 2……..89

3.14 Effect of permeability on cumulative inflow gas volume during stages 1 and 2……90

3.15 Effect of permeability on the rate of increase in the surface mud pit volume during stages 1 and 2……..…….91

3.16 Effect of permeability anisotropy on apparent bubble sizes…….94

3.17 Effect of viscous drag forces on apparent bubble sizes……96

3.18 Effect of mud plastic viscosity on bubble size profile……..97

3.19 Effect of ROP on the apparent gas bubble sizes……...100

3.20 Rate of change in the apparent gas bubble sizes at different rates of penetration……101

3.21 Rate of change in mud pit volume for different ROPs…….102

4.1 Schematic illustrations of modeled physical processes: (A) during flow-check or before shut-in; (B) well shut-in……111

4.1 Schematic illustrations of continuous shut-in period……..112

4.2 Bottom-hole pressure build-up profiles for various permeability values…128

4.3 Rate of further flow of gas into the wellbore during shut-in……...129

4.4 Surface casing pressure rise during shut-in…….130

4.5 Bottom-hole pressure (BHP) profile for an assumed 10-bbl nominal gas kick size at well shut-in…….……...134

4.6 Casing pressure profile for an assumed 10-bbl nominal gas kick size at well shut-in……..135

4.7 Shut-in inflow rates for an assumed 10- bbl nominal gas kick size at well shut-in……..136

4.8 Bottom-hole pressure derivative curves……..138

4.9A Variation of annular gas density with continuous wellbore pressure build-up for different permeable reservoirs……139

4.9B Expanded plot of the variation of annular gas density with changing wellbore pressure……....139

4.10 Bubble size profile or pattern for the additional gas inflow during well shut-in for various gas kick volumes……..141

4.11 Integration of apparent bubble size profile for all the modeling stages.....143

4.12 Cumulative annular gas volume and corresponding required stabilization time…….144

4.13 Apparent gas bubble size profile for the conventional drilling fluid pressure design…….……..148

4.14 Effect of drilling fluid hydrostatic pressure on the apparent bubble size profile for the three stages of gas inflow analysis……..149

5.1 Comparison of simulation results for the surface pit volume for the developed model and Nickens model…….156

5.2 Comparison of the predictions for bottom-hole pressure rise by Nickens model and the developed model…….……159

5.3 Reproduced plots of the gas kick experimental results at the LSU-Goldking well no. 1……...161

5.4 Surface casing pressure rise without wellbore storage effect considerations…….163

5.5 Reservoir pressure sensitivity study at constant reservoir permeability….169

5.6 Reservoir permeability sensitivity study at constant reservoir pressure….170

ABSTRACT

This study presents two new models developed to analyze gas flow between the reservoir and the wellbore while drilling underbalanced. Three drilling operational stages were considered in the analyses. These stages are the continuous drilling and mud circulation; suspension of drilling and mud circulation with the wellbore still opened; and, the shut-in of the wellbore. The first model, called gas bubbly model distinguishes the inflow pattern of gas into a liquid from that of liquid inflow into a liquid, while the second model, a wellbore pressure build-up model, is based on the concepts of increasing annular fluid density during well shut-in. The limitations of these models are the assumption of isothermal wellbore conditions, application of radial unsteady flow equation, and that none of the gas inflow has been produced.

The models couple the viscous, surface tension, inertia, buoyancy, force of fluid ejection from the bit nozzles, and the reservoir forces at the wellbore-sand face contact to analyzing the three drilling operational stages. By incorporating these forces and conducting the analyses at the wellbore-sand face contact, practical characteristics of gas bubbly inflow into a denser fluid system is achieved, thus improving gas formation productivity evaluation while drilling. The improvements are achieved through the reduction of the wellbore effects such as the gas bubble coalescence and breakage, and bubble expansion and compression that are not possible to practically quantify during annular upward flow of gas bubbles.

Among many outcomes from the study are:

1. The radial flow equation of gas inflow into the wellbore during underbalanced should be applied deeper than a partially penetrated depth of ≤ 1 ft

2. Porosity effect on cumulative gas production is not apparent for smaller drilled gas formation intervals, but for longer intervals, gas formations with lower porosity produce more gas volume than ones with higher porosity due to greater pore space compression. This is in agreement with published data.

THE CHIEF TECHNICAL CONTRIBUTIONS OF THIS STUDY ARE:

1. Models that take into account the practical characteristics of gas inflow into denser fluid systems are developed. This allows the gas inflow to be treated differently from the liquid inflow.
2. Quantitative analyses of gas inflow at the bottom of the hole are made possible by this study. This approach thus reduces the influences of the wellbore effects on the gas formation productivity evaluation, which is presently approached as the differences in the surface fluid injection rate and the annular outflow rate.

CHAPTER ONE

FORMULATION OF THE PROBLEM

1.1 Introduction

Since the inception of rotary drilling operations, the occurrence of abnormal formation pressure that can lead to a kick and subsequent blowout has plagued the oil/gas well drilling industry. One of the major functions of drilling fluids is to exert adequate circulating and hydrostatic pressures on any formation at any depth as long as the sediment remains bare opened.[1&2] Consequently, drilling engineers put the highest priority on the design of wells suspected of being abnormally pressured. Inadequate control of the influx, such as formation gas, has been identified to lead to blowout due to the readily expansion nature of the gas. Severe consequences of the blowout, such as potential loss of life, loss of the well, and environmental damage have caused most well kick studies to be geared towards achieving successful control of gas influxes or gas kicks.[3-47, 50-52]

There are presently two methods[50,53-54] used to control gas influx during drilling operations. One of the methods is known as the “Driller’s Method”. This method involves continuous circulation of mud with the intent of being able to circulate the initial gas influx out of the well. Afterwards, the circulating mud is gradually weighed-up while circulating to exert sufficient backpressure on the formation to prevent further gas influx. The second control method is known as

"Wait-and-Weight" or "Engineer's Method". This method involves terminating mud circulation, and evaluating the gas kick while the well is shut-in. The Engineer's method demands weighing up of the mud to the required mud weight before circulation to kill the well. These two methods have proven successful at different occasions. However, the driller's method has been mostly adopted for controlling gas kick taken at offshore locations because of the adverse effect of low temperature on the static mud density.

To successfully adopt a control method, accurate dynamic description of the distribution of the gas in the annulus is required. Unfortunately, such information are not easy to come-by. Consequently, sophisticated gas kick experiments, empirical and semi-empirical correlations developed for air-water flow, and analytical means have been used to analyze the flow of gas kicks with the assumption of a gas distribution pattern. For simplicity, most of these approaches assume that the gas flows into the annulus as a single bubble and migrates upward as a single slug. This assumption has been found to be conservative, in that it over-estimates the behavior or distribution of gas in the annulus and also the density of the fluid. On the other hand, some studies[55,72&83] assumed that gas kick exists as uniform bubble size distributed in the annulus.

One of these studies[55] was able to show that predictions and analyses for parameters such as the casing pressure and pit gain are considerably lower when a uniformly distributed bubble size is assumed than for the assumption of single slug flow. Also, non-linearity of the surface casing pressure prediction with increasing shut-in time was attributed to gas bubble fragmentation during upward migration of

the gas bubbles.[72] The gas fragmentation theory was realized after unsuccessful correlation of the predictions from single gas bubble assumption and field observations. With these findings, over-estimated predictions through the single slug flow assumption as well as the assumption itself has been considered unsatisfactory. To buttress the findings, it is apparent that the presence of turbulent flow at the bottom hole, during gas inflow into the wellbore, should cause gas dispersion into gas bubbles of varying sizes depending on the gas influx rate.

There seem to be more devotion to analyzing gas kick after it had occurred. That is, more focus has been directed onto the gas kick control than the causes of gas kick. Therefore, all the present gas kick models have no choice other than to make assumptions about a gas distribution pattern, and the volume of mud pit gain as the bases for their simulations. Some authors[55,72] concluded that there is the need for more realistic description of gas distribution in the annulus in order to accurately predict gas kick.

Although gas distribution in the annulus has been convincingly identified to exist in bubbles rather than as a single slug, consideration of the existence of varying sizes of gas bubbles is still lacking. One obvious reason is the complexity involved in analysis if the currently adopted approach, through gas bubble velocity, for analyzing gas kick is to be employed. It is apparent that drilling into pressurized gas-containing formation occurred before noticing, at the surface, that under balanced pressure condition has been created down-hole. Such continuous drilling into the formation causes more interval of the sediment to be exposed. As longer interval is exposed, increasing rate of gas influx is undoubtedly expected, which should induce different

sizes of gas bubbles at the same turbulent flow conditions. This realistic physical process therefore results in the introduction of varying gas bubbles sizes into the annulus. For such complex gas distribution, it would be inappropriate to analyze the gas kick situation through the use of a simple small-scale-developed gas velocity correlation that is independent on bubble sizes. Unfortunately, this has been the basis of the currently adopted gas kick analysis. These correlations are discussed in Chapter 2.

1.2 Literature Review

Most of the drilling operation problems are closely related to improper mud conditioning. Zamora et al[77] provided a comprehensive analysis of mud-related drilling problems, and stated the importance of maintaining excellent mud properties such as mud weight and viscosity in preventing both hole instability and gas influx. They also emphasized that gas hydrate formation could only result when gas influx is allowed into the wellbore during drilling under chilled conditions.

Extensive studies[55,72,78-81] have been carried out to analyze gas flow in the annulus when gas kick is taken during onshore drilling operations. These analyses have been extended to offshore drilling operations by considering the imposed hydrostatic head of the water depth. LeBlanc et al[78] introduced a mathematical model for gas kick behavior during displacement or control using both “Driller’s and Wait-and-Weight methods”. The model assumes that the gas kick starts as a large single bubble, and continuously migrates upward as a single bubble from the bottom of the well bore to the surface. Analysis of each of the two control methods utilizes the

assumption that continuous reduction in hydrostatic pressure as the bubble rises to the surface leads to bubble expansion. Comparison of their results from the model with field cases resulted in poor agreement. This is because of the inadequate assumption of the gas bubble distribution in the annulus.

Rader et al[72] conducted experiments on the behavior of a single large gas bubble in the annulus. Their work claimed to have revealed some valuable factors that affect a single bubble rise. These factors include the shape profile of the single bubble in annulus; and, the non-linear trend of the observed rates of casing pressure rise during well shut-in as opposed to constant rate of casing pressure rise being predicted and used by the existing gas kick models. They found that the assumption of bullet shape of a single bubble migrating upward in an annulus is incorrect. Instead, a shape that resembles a "bent hot dog bun" was observed to exist in the annulus for a large single bubble. **Figure 1.1** shows a schematic diagram of this annulus bubble shape. The degree of curvature of such a single large bubble has been observed to be dependent on the viscosity of the liquid or mud.

Consequently, a shape correction factor was incorporated into the various correlations developed for air-water flow in cylindrical tubes to describe the flow of air in drilling fluid. In order to justify their observations of non-linearity of the rate of shut-in casing pressure rise, they assumed that the gas kick initially exists as single bubble at the bottom of the hole. Afterwards, the single bubble starts to break into numerous slugs of gas as the upward migration continues during well shut-in. This speculation was used as a line of defense for the poor agreement between their results and field cases. Mathews[79] utilized a similar approach as Rader et al, but his study

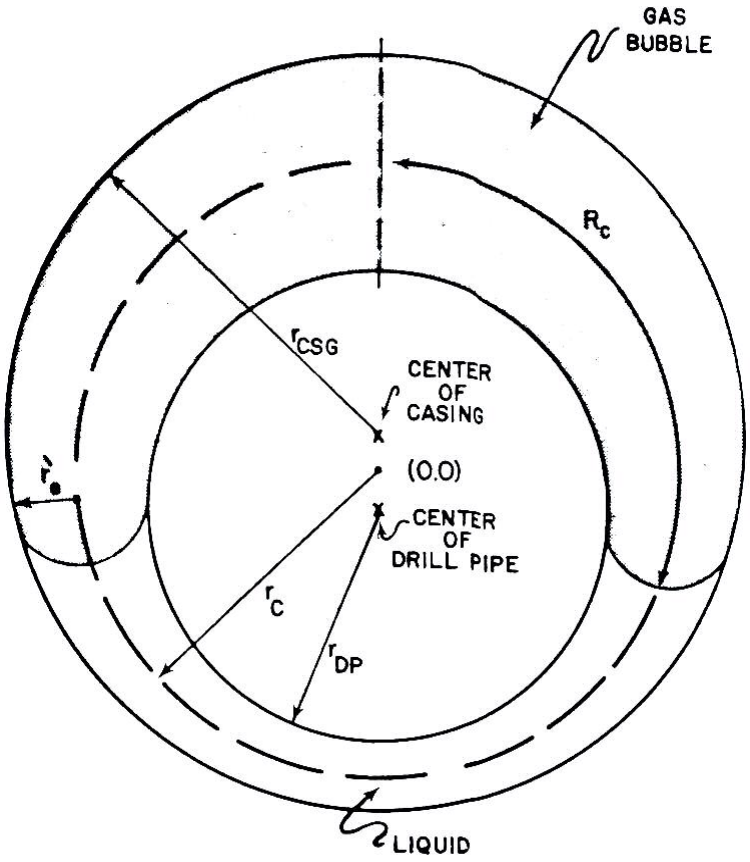

Fig. 1.1 – Schematic representation of the top view of a "bent" shaped single bubble in the annulus containing viscous fluid[79]

also resulted in poor agreement between the results from the model and field cases.

Following the proposition of inappropriate single bubble flow assumption to analyzing gas kick by Rader et al.[72], Nickens[55&80] performed an analytical study on the transient behavior of liquid/gas flow system. The study incorporates some sets of transient mass- and momentum-balance equations that relate gas and mud densities; gas void (volume) fraction; gas and mud velocities; and, pressure and temperature. These equations are based on vertical-hole geometry, and one-dimensional flow analysis. The semi-empirical correlation developed for the gas slip velocity of the air-water systems, and single- and two-phase frictional relationships were included in the analysis. He emphasized the importance of considering the possible influx of considerable amount of gas after the BOP and choke have been closed. He also stated that accurate knowledge of gas distribution pattern in the annulus helps to adequately analyze gas behavior during well shut-in and kick control. In light of this, he assumed three cases of different combination of ROP and formation permeability. Each of these cases was assumed to result in a uniform bubble size distribution of gas in the annulus rather than a single bubble. However, no justification was provided that these cases would actually produce discretely distributed gas flow. Despite all the inadequacies, the results showed a better agreement because of the assumed discretely distributed bubbly gas flow pattern.

Zuber and Findlay[81] derived a theoretical relationship that linearly relates the mean gas velocity to the velocity of the two-phase (homogeneous) region and the gas slip velocity. The magnitude of the slope or gradient of such expression was reported to be dependent on the distribution pattern of bubbles in the annulus. Their work was

based on the flow of air in water, and therefore, the effect of fluid viscosity was not considered. The homogeneous velocity was calculated by combining the volumetric flow rates for the gas and liquid, and the cross-sectional area of the system.

Johnson and White[82] conducted a large-scale experiment to observe the gas flow pattern in a clear polymer fluid that closely resembles drilling fluid used in the field. The basis of their analysis was on the linear relationship developed by Zuber and Findlay.[81] Johnson and White[82] showed that gas kick rises as larger gas bubbles, and faster in a viscous fluid than in water. The formation of larger bubbles was attributed to the stabilizing effect of the viscous fluid. Equating the drag force expression of the Stokes' formula to the buoyancy force on a bubble of specific diameter, it could be realized that the terminal velocity of the bubble must increase in fluids of decreasing viscosities. However, with all things equal, larger bubbles are readily formed in higher fluid viscosities. A force balance exercise for the above mentioned forces (Stoke's formula) would indicate that the terminal velocity of any bubble size is proportional to the square of the bubble size, any slight increase in the fluid viscosity that promotes larger bubble size should cause increase in the terminal velocity. Therefore, the experimental observations by Johnson and White[82] could be considered as being consistent with the existing theory.

Although Johnson and White[82] stated a range of the liquid superficial velocity, its effects on the variations of bubble sizes were not presented. However, the plots of bubble slip velocity and the slope from Zuber and Findlay[81] expression versus the various gas void fractions show that there are glaring variations in the slip velocity of gas bubbles in the two-phase region. That is, as the gas volume or gas void fraction

increases, the bubble slip velocity increases. However, when they plotted the mean gas velocity against the homogeneous velocity for gas void fractions of higher value than 7.5%, a constant gas slip velocity value resulted. This clearly shows inconsistency in the analysis of the experimental observations.

Otake et al[109] conducted a comprehensive experimental study using high speed cinematography to monitor the 3-D movements of a single bubble, and an isolated bubble from a swarm of bubbles. From the observations of the bubbles in various stagnant viscous liquids of varying properties, bubble terminal velocity was seen to increase with increase in the bubble equivalent diameter. Such velocity increase is pronounced in more viscous liquids. Also, larger gas bubble sizes were observed to readily form in more viscous liquids than in water. This observation supports the experimental results of Johnson and White[82]. The Otake et al[109] results indicated that larger gas bubbles are formed through the coalescence of smaller gas bubbles at a position close to the gas supply source. Moreover, with increase in the gas flow rate from the gas supply source, the position at which these larger gas bubbles starts to form gets closer to the source of gas supply. A logical explanation for the formation of larger bubbles as the gas flow rate increases is due to the increased cluttering of smaller gas bubbles at a position very close to the source of gas supply. Hence, for a certain high viscosity fluid, increased gas flow rate causes larger bubbles to form at decreasing distance from the gas supply source.

Maus et al[54] developed a gas kick computer program that utilizes the mass and momentum balance equations, which relates the different phases in the annulus. They, like some other authors, treated the annulus flow as a single bubble flow. The study

involved the evaluation of various field parameters - mud pit gain, return flow rate, and standpipe pressure - that are usually interpreted to indicate the occurrence and significance of gas kicks. Their analyses were oversimplified because it was strongly based on the assumptions of linear relationships that were empirically adopted from the simulation results. Although they attempted to simulate the effects of reservoir and drilling operation parameters on the rate of kick notification, their approach was limiting and inconsistent because the assumed linear relationships may not hold for all gas kick case scenarios. However, the flow rate of the returning drilling mud was chosen as being the most sensitive means of early kick detection because of the slower rates at which other parameters change.

Hoberock and Stanbery[83] introduced the concept of transmission line to analyze gas kick taken during onshore drilling operations. This involves treating a borehole system as a continuum. Although the approach was initially designed for the flow of Newtonian fluid in a cylindrical geometry, adequate modifications were done for its use for non-Newtonian fluid flow in annular geometry. This study assumes that the initial gas distribution pattern is in discrete bubbles, which later grows into slug flow. However, no evidence for such gas distribution existence was provided. Moreover, the popular correlation by Zuber and Findlay[81] and the gas slip velocity developed for the air-water flow system were used. The results from their model showed over-prediction of mud-pit gain as compared to the experimental outcomes from the test well at Louisiana State University.[81] An apparent realization from this study is the fact that the study forced its modeling procedures to some specific test well results, thereby, not representing a general procedure.

Thomas et al[84] and White and Walton[85] compared the effects of gas solubility in oil- and water-base muds on the gas kick detection rates. The results showed that there is delay in mud-pit gain when oil-base mud is used as compared to when water-base mud is used. Such results show that gas could readily dissolve in oil base mud than in water base mud, and at the surface conditions, gas evolves from the oil base mud, hence causing slower rate of mud pit gain for the oil base mud. Therefore, significant amount of gas influx might be allowed into the oil-base mud compared to when water-base mud is used. Such comparisons are not part of the goals for the present study.

Choe and Juvkam-Wold[86] realized the inconsistencies in the use of the mass- and momentum governing equations by the past authors. They noticed that the assumptions used by individuals to simplify these equations had made the resulting expressions from finite difference solution susceptible to errors. Therefore, they introduced two-phase unsteady flow in the annulus that incorporated variations in annular geometry. Pseudo-pressure function for the gas, instead of ordinary pressure parameter, was used for their modeling and analysis. Likewise, as their predecessors, the authors assumed that the entire gas flows into the annulus and stops flowing. This therefore creates four regions in the annulus namely: a single-phase region of old mud before gas influx, the two-phase mixture region, a single-phase region of old mud, and a single-phase region of kill mud underneath. The inclusion of a single-phase region of old mud underneath the two-phase mixture is practically not feasible. This is because gas continues to flow into the annulus until the kill mud gets to the formation face and suppresses further gas inflow. Therefore, overall three flow

regions should have been considered. Consequently, comparison between the results from their model and field data consistently showed over-estimation and under-estimation before and after the gas reaches the surface respectively.

1.3 Objectives and Methodology

A major goal of any gas kick simulation is to adequately evaluate the pressure of the gas reservoir encountered. Such evaluation helps to control the gas kick satisfactorily. Due to the change of an initial single-phase annular flow to a two-phase flow system when a gas kick is taken, analysis of gas kick has become very challenging and complex. From the literature reviews, it is apparent that accurate gas distribution pattern in the annulus is essential for predicting and controlling a gas kick. However, no work has been recorded in the literature that provides such opportunity.

In addition to the above motivation for the present study, it is impractical to assume that gas kick analysis should be based solely on the upward migration of gas bubble whether during well dynamic or static conditions. As will be fully discussed in Chapter 4, the contribution of such gas bubble migration to pressure rise during well shut-in has been observed in practice during well testing operations to be minimal and occurs during the late period of pressure stabilization. Moreover, if the rise in annular pressure due solely to bubble upward migration ever occurs, the time of occurrence is short, and such occurrence dies off at pressure stabilization. Moreover, the effect of bubble migration on pressure rise is dampened by higher annular fluid

compressibility when the well is closed at the surface, which is usually the operational procedure used after a kick is taken.

All of the above, thus, point to the fact that the present approaches to gas kick analysis need to be thoroughly investigated, and possible alternatives to analyzing gas kick developed.

1.3.1 Objectives

There are four major objectives for this study.

1. To develop a new mathematical model for wellbore and surface casing pressure predictions based on varying annular fluid compressibility rather than by gas bubble migration.
2. To mathematically simulate the inflow of gas during gradual bit penetration into pressurized gas formation under three operating conditions: during continuous drilling and circulation of drilling fluid; when the drilling operation and the circulation of drilling fluid are suspended for any reason; and during well shut-in. This will involve a different approach from the known present approaches. It is a new concept that provides mathematical relation of the forces resulting from the gas inflow, drilling operation, and dynamic and static conditions of drilling fluid.
3. To show that when gas inflows during underbalanced drilling operations, the gas exists as bubbles of different sizes, and not as a single bubble or uniformly distributed bubbles of the same size.

4. To perform a parametric study of the effects of various factors such as gas influx rate, drilling fluid properties, ROP, and gas reservoir permeability and porosity on gas bubble sizes at the wellbore-sand face contact to alleviate the wellbore effects on gas formation productivity evaluation.

1.3.2 Methodology

The present study intends to mathematically describe realistic gas kick behavior and its instantaneous distribution from the time the bit penetrates the pressurized gas formation until attempts for control is made. This new concept will serve as solution to the lingering quest for reasonable gas kick distribution in the annulus. The study is conducted on the whole gas kick periods - from the inception of gas influx to the kick control period, which are divided into three stages based on the different well conditions existing within each period. Each of these operating periods are analyzed separately and later combined to obtain a general insight of the whole two-phase system. For the purpose of this study, the three drilling periods have been referred to as stages and they are as follows:

I. Stage 1 – Instantaneous gas influx while drilling and circulating
II. Stage 2 – Suspension of drilling and mud circulation
III. Stage 3 – Well shut-in on gas kick

For each of the above stages, the forces that are responsible for the establishment or formation of bubbles are considered. These forces are:

I. The viscous force from the drilling fluid viscosity

II. The surface tension force that exist on the surface of the forming bubble, which is related to the hydraulic radius of the gas sand or reservoir being drilled
III. The inertia force due to the movement of the fraction of drilling fluid surrounding the forming bubble as the forming bubble expands, and
IV. The buoyancy force due to the submerged bubble volume

Among all of these forces, the buoyancy force is the only force that supports the continuous expansion of the bubble, while the other forces oppose the expansion of the bubble. These forces are schematically presented in **Fig. 1.2.** Force balance between the associated forces resulted in a complex model that could only be solved by iterative procedure.

Consequently, a computer simulation program is designed to carry out such iterative steps until a minimal error is reached. In the design of the simulation program, considerable reduction of the overall execution time for the iterative steps is given a higher priority in order to quicken the time for the analysis. Among the results generated by this computer program are the numbers of iteration required for the attainment of minimum error, the error analysis plots for each iterative procedure carried out, various bubble sizes as drilling operation continues before kick detection and during well shut-in, and bottom-hole and casing pressure rise.

1.4 Organization of the Dissertation

Chapter 2 of the dissertation presents a complete review of the theoretical background of the gas kick. It provides a description of the causes of abnormal formation pressure that initiates gas kick. The consequences of such occurrences, the

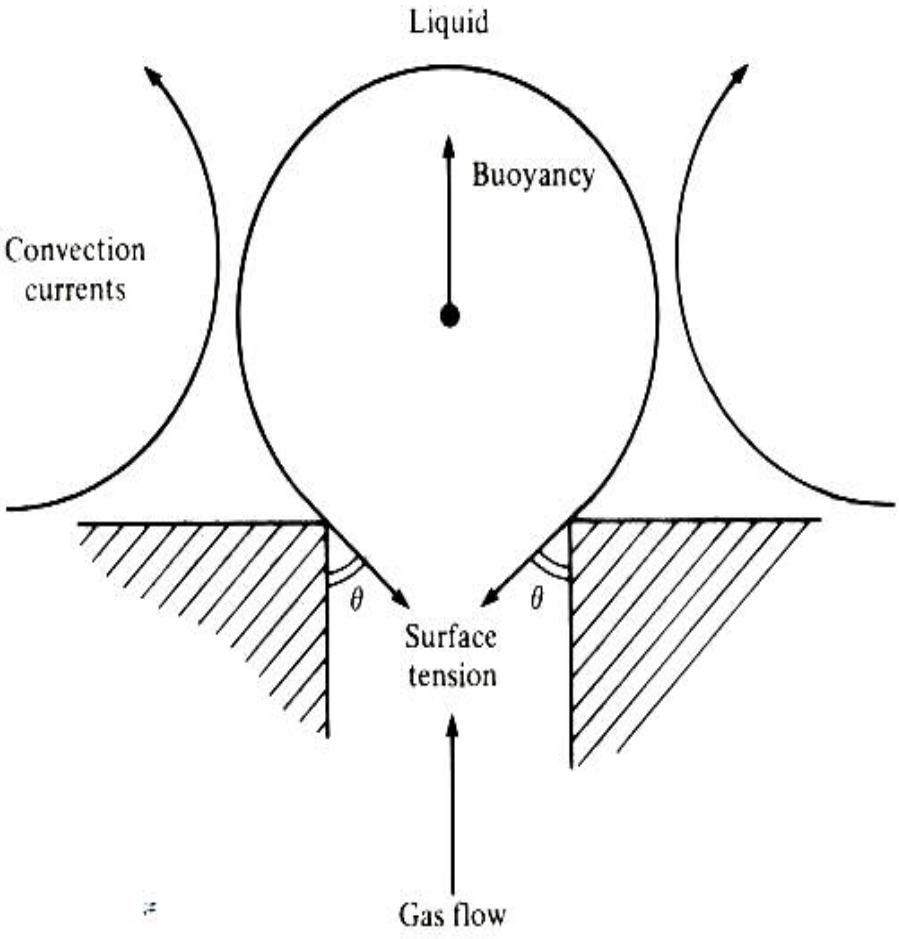

Fig. 1.2 – Forces responsible for the bubble development

identifications of the when higher formation pressure is being penetrated, and the procedures for the kick control methods are also presented. Under this chapter, detailed descriptions are provided for bubble formation in a flowing and static vertical column containing different viscous fluids. Lastly, different gas flow patterns that have been identified in the literature are thoroughly discussed.

In Chapter 3, the general mathematical model for gas distribution in the annulus is presented. The overall model assumptions, model development, model evaluations, and discussions on the sensitivity analysis of various factors on gas bubble size distribution are presented. The general model is applied to the first two stages: during drilling and flow-check.

Chapter 4 comprises of the last physical process: well shut-in. In order to evaluate the gas reservoir pressure for adequate drilling fluid weight-up, the wellbore needs to be shut-in until surface casing pressure stabilization is attained. This Chapter presents a new mathematical model for predicting casing and bottom-hole pressure buildup by employing the wellbore storage concept. Detailed discussions on the modeling techniques, and the simulation results are presented. Modifications to the assumptions in Chapter 3 are provided to suit the stage 3 of this study. Under the analysis of the simulation results the following were conducted: the effects of reservoir permeability, as well as nominal gas kick size or volume on both casing and bottom-hole pressure build-up rate, effect of the bottom-hole build-up on the annular gas density variations, profile of instantaneous bubble sizes inflow into the annulus during shut-in, and the integration of all the modeling stages.

Chapter 5 discusses the application of the introduced concepts to under-balanced, near-balanced or flow-drilling operations. Model evaluation and validation with some presently existing gas kick models and their published data are also provided.

Chapter 6 presents the summary, conclusions and recommendations.

CHAPTER TWO

THEORETICAL BACKGROUND OF GAS INFLOW ANALYSIS

2.1 Introduction

Normally, during drilling operations, over-balanced condition of bottom-hole circulating pressure over the formation pressure is desired to prevent inflow of formation fluid into the wellbore. If, however, a higher than expected formation pressure is encountered downhole, under-balanced pressure condition results, which allows formation fluid to flow into the wellbore. More consideration is usually devoted to controlling inflow of gas into the wellbore because of the tendency for gas bubbles to carry the high formation pressure to the surface, which could be disastrous.

To prevent the occurrence of gas inflow or kick, thorough formation pressure analysis of the drilling environments is usually conducted both at the well planning stage and during drilling operation. In light of this, many methods[1-49] of detecting the existence of overpressured formation, and predicting the overpressure or abnormal pressure magnitude are readily available in the industry. Each of these methods is subject to limitations based on the assumptions underlying its methodology.

Whenever gas kick occurs, the gas flows in mixture with the flowing drilling fluid or migrate upwardly when drilling fluid circulation is suspended. Experimental analyses[62,111,112] of airflow in water have identified various patterns to which air or gas could adopt while flowing with or migrating in a liquid. Each of these gas flow

patterns has been characterized based on the superficial velocities of the liquid and that of the gas. Superficial velocity of any fluid is defined as the velocity at which such fluid would flow in the same medium as a single phase.

In this chapter, various theories relating to causes of gas inflow into the wellbore, and currently employed techniques for abnormal pressure prediction are briefly presented. In a physical sense, inflow of gas into either static or a flowing liquid should result in formation of series of gas bubbles and not a single gas bubble at any inflow rate of the gas. This is because, at any gas inflow rate, force balance on each of the formed gas bubble causes the bubble to detach from its source and thus, allows another bubble to form.[62-70] Hence, theories of bubble formation at the wellbore-gas reservoir contact would be the major area of focus in this study. In light of that, physical theories that have been experimentally proven would be summarized in this chapter. The second section of this chapter would discuss the theories on wellbore pressure build-up that are used in Chapter 4 for analyzing surface and bottom hole pressure rise during well shut-in on gas-drilling fluid mixture.

2.2 Abnormal Formation Pressure Concepts

Existence of overpressure requires some means of formation isolation by seals from its surroundings.[2-6] The origin of a pressure seal could be physical, chemical, or a combination of both. **Table 2.1** shows some suggested formation pressure seals.[2] A consequence of these sealing processes is the development of a partially or completely closed system. One of the requirements of a closed system is the inhibition of further migration of hydrocarbons from and into the closed system

while the internal chemical/diagenetical processes continue. A system that is not in communication with its surrounding is considered abnormal, and thus, subjects its internal components to more than normal pressure or overpressure.

Table 2.1 - Suggested types of formation pressure seals [2]

Type of Seal	Nature of Trap	Examples
Vertical	Massive shales and siltstones Massive salts Anhydrite Gypsum Limestone, marl, chalk dolomite	Gulf Coast, U.S.A., Zech stein in North Germany North Sea, Middle east U.S.A., U.S.S.R.
Transverse	Faults Salt and shale diapirs	Worldwide
Combination of vertical and transverse seals		worldwide

The most prominent occurrence area or region of overpressures has been identified to be in deltaic environments, where sand/shale sequences dominate. Such occurrence is geologically based, which then makes the abnormal pressure analyses in geologic provinces to differ from each other. In the early times, the general concepts of overpressure development have been attributed to non-equilibrium compaction of shale sediments during sediment deposition.[3] The non-equilibrium compaction has been attributed to a sediment deposition rate that is greater than the rate at which the inherent shale fluid or water is expelled from the sediment during deposition. However, recent studies[4,6,19&29] have identified other factors, such as fluid expansion

due to elevated temperature, impact of tectonic forces, and transformation of shale mineralogy, as responsible for formation over pressuring.

2.3 Techniques for Predicting Abnormal Pressure

While normal pressure gradient prediction is easily conducted through some widely accepted generalized expressions,[5,6] abnormal pressure predictions are based on regional experience,[7-10] regression analysis on real-time drilling data,[11-20] and calibration of off-set field data.[21-45] As could be noticed with the larger numbers of literature available for pre-drill methods, more attention has been devoted to such prediction methods because of the need for estimating pressures during well planning. After the planning stage, any subsequent pressure analyses are then improved upon by incorporating the newly acquired pressure data from drilling operations. Figure 2.1 shows typical plots that aid in identifying the existence of abnormal pressure at certain depth.

Unfortunately, all pre-drill methods are based on calibrating data from offset wells and offset field seismic survey data. One of the currently used pre-drill formation pressure prediction method is that by Bowers.[32] This approach relates two seismic attributes (sonic velocity and effective stress) empirically to generate expressions for predicting abnormal pressure. Figure 2.2 shows a typical relationship of these seismic attributes. The figure displays virgin and unloading curves that represent the relationships between the seismic attributes during the normal compaction of the sediment, and the effects of fluid expansion due to increased temperature on the pore pressure respectively. The empirical correlations developed

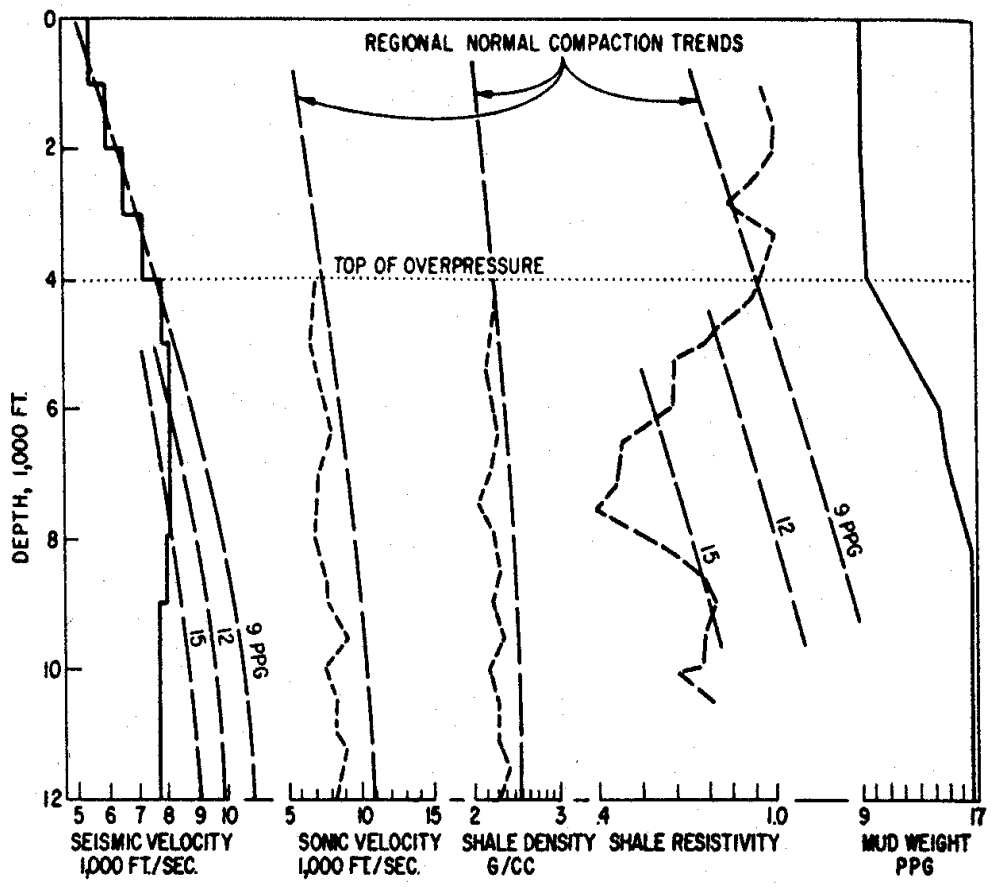

Fig. 2.1 – Graphical representation of the existence of abnormal pressure depth[23]

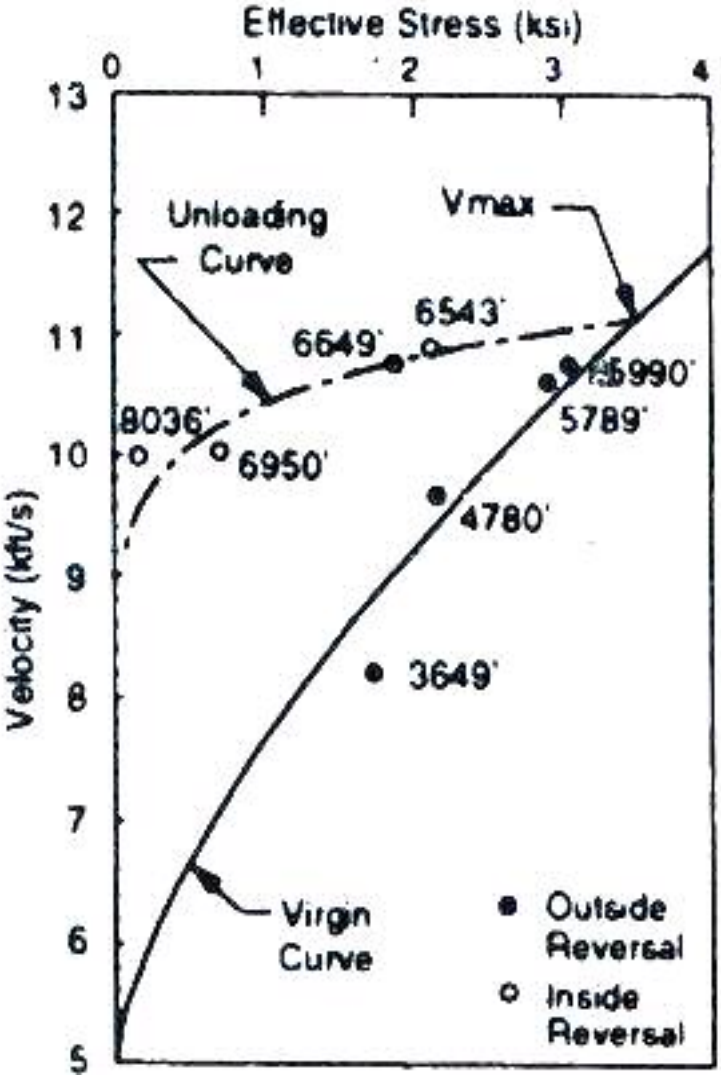

Fig. 2.2 – Example illustration of unloading concept of abnormal pressure generation (Bowers[32])

between sonic velocity and effective stress for the normal compaction (virgin curve) and that for the overpressure caused by the combination of under-compaction and fluid expansion phenomena (unloading curve) are given in Eqs. 2.1 – 2.5 as follows:

For virgin curve:

$$v_s = 5000 + A\sigma_v{}^B \quad \ldots 2.1$$

For unloading curve:

$$v_s = 5000 + A\left[\sigma_{v,max}\left(\sigma_v \big/ \sigma_{v,max}\right)^{(1/U)}\right]^B \quad \ldots 2.2$$

$$\sigma_{v,\max} = \left(\frac{v_{s,max} - 5000}{A}\right)^{1/B} \quad \ldots 2.3$$

A and B are parameters calibrated with offset well sonic velocity and effective stress data. $\sigma_{v,\max}$ and $v_{s,\max}$ are the estimates at the onset of unloading from the normal or virgin curve, as shown in **Fig. 2.2**. U is another parameter that measures the degree of plasticity of the sediments. U = 1 means that there is no permanent deformation. In practice, values of U range from 3 to 8. U can be solved-for by using the following relations:

$$\left(\sigma_v / \sigma_{v,\max}\right) = \left(\sigma_{vc} / \sigma_{v,\max}\right)^U \quad \ldots 2.4$$

where,

$$\sigma_{vc} = \left(\frac{v_s - 5000}{A}\right)^{1/B} \quad \ldots 2.5$$

One disadvantage of this approach is that there are many parameters to be estimated, and summed-up errors from the estimates of these parameters could negatively affect

the precision of the predicted pore pressure. Moreover, Bowers[32] related data points by regression analysis, as other studies on abnormal pressure prediction used for their various approaches. Unfortunately, with considerable scattering of data points, prediction from regression analysis incorporates summed-up error of all errors developed in fitting the scattered data points. This source of prediction inaccuracy was later detected, and a proposed solution was presented by the use of Spline Functions for data calibration.[45] **Figure 2.3** shows improved accuracy in the formation pressure predictions using the Spline Function (PLF) over the regression analysis.

2.4 Theoretical Analysis of Gas Inflow

The theoretical evaluation of gas inflow, and of providing pressure-controlled procedures of circulating the gas out of the wellbore is based on a "U" tube classical model. **Figure 2.4** shows a schematic representation of a U-tube, which is usually adopted to simulate the connectivity of the inside of drill-pipe and the annulus. Over the years, two approaches have been adopted, whose differences are based on different operational control procedures. All of the approaches associated with this classical model are based on the assumption that the gas inflows into the wellbore as a single bubble, which flows or migrates upwardly as entity.

One of these approaches is the "Drillers' or Circulate method, which involves displacing the gas kick with the original mud weight, being previously used to drill, using a much higher circulating pump pressure. This higher circulating pump pressure should be greater than the stabilized shut-in drill pipe pressure that must have been

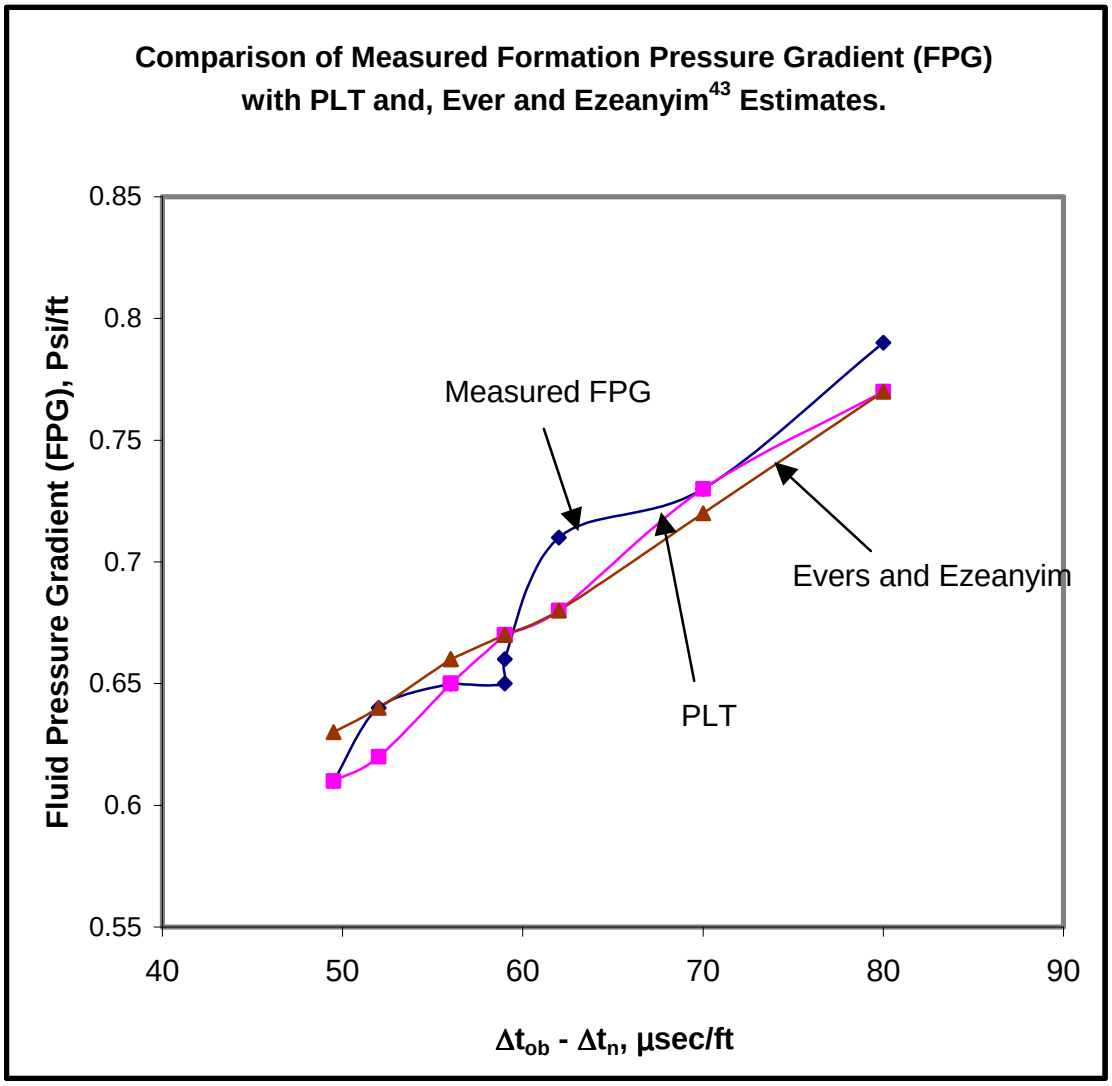

Fig. 2.3 – Improvements on pressure predictions by spline function over regression analysis approach

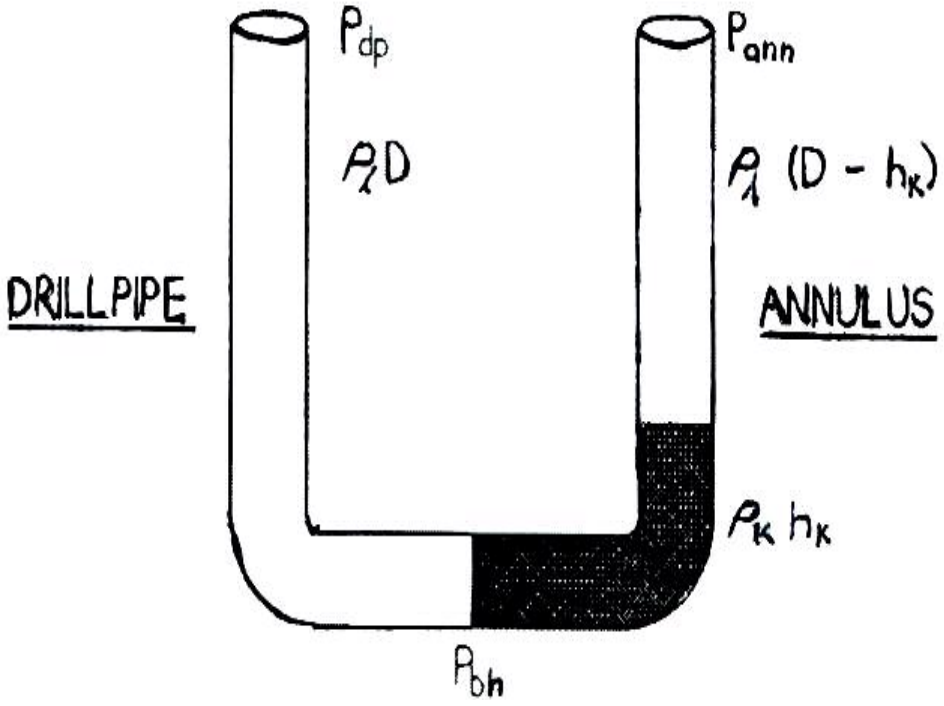

Fig. 2.4 – U-tube modeling of wellbore configuration[53]

previously obtained by shutting-in the well after gas inflow detection. Afterwards, the pump circulating pressure is reduced after the kill mud of higher density has been successfully circulated into the entire wellbore. Hence, this method requires two complete wellbore circulations.

The second method is the Engineers' or Wait and Weight Method. This method involves the evaluation of the reservoir gas inflow into the wellbore during well shut-in. Instead of circulating the inflow out of the annulus with the original drilling mud, as for the case of Driller's method, a kill mud is prepared and circulated through out the entire wellbore after attaining stabilized casing and drill pipe pressures. Contrary to Driller's method, Engineer's method involves only one complete wellbore circulation.

Figure 2.5 schematically displays a single gas bubble migrating upward in the annulus during well shut-in after gas inflow detection. With the assumption that the gas inflow is in form of a single gas bubble that occupies the entire annular diameter, a pressure balance in the annulus during shut-in of the well is given as:[113]

$$P_{csg} + 0.052\rho_l h_a + 0.052\rho_{gas} h_{gas} + 0.052\rho_l h_b = P_{pore} \quad \ldots 2.6$$

Where P_{csg} and P_{pore} are the surface casing pressure and the reservoir fluid pore pressure respectively. With the assumption of a negligible gas density, **Eq. 2.6** becomes:

$$P_{csg} + 0.052\rho_l h_a + 0.052\rho_l h_b = P_{pore} \quad \ldots 2.7$$

Equation 2.7 is re-written as:

$$P_{csg} - 0.052\rho_l h_{gas} = P_{pore} - 0.052\rho_l h_w \quad \ldots 2.8$$

Inside the drill-string, the right-hand side expression of **Eq. 2.8** can be

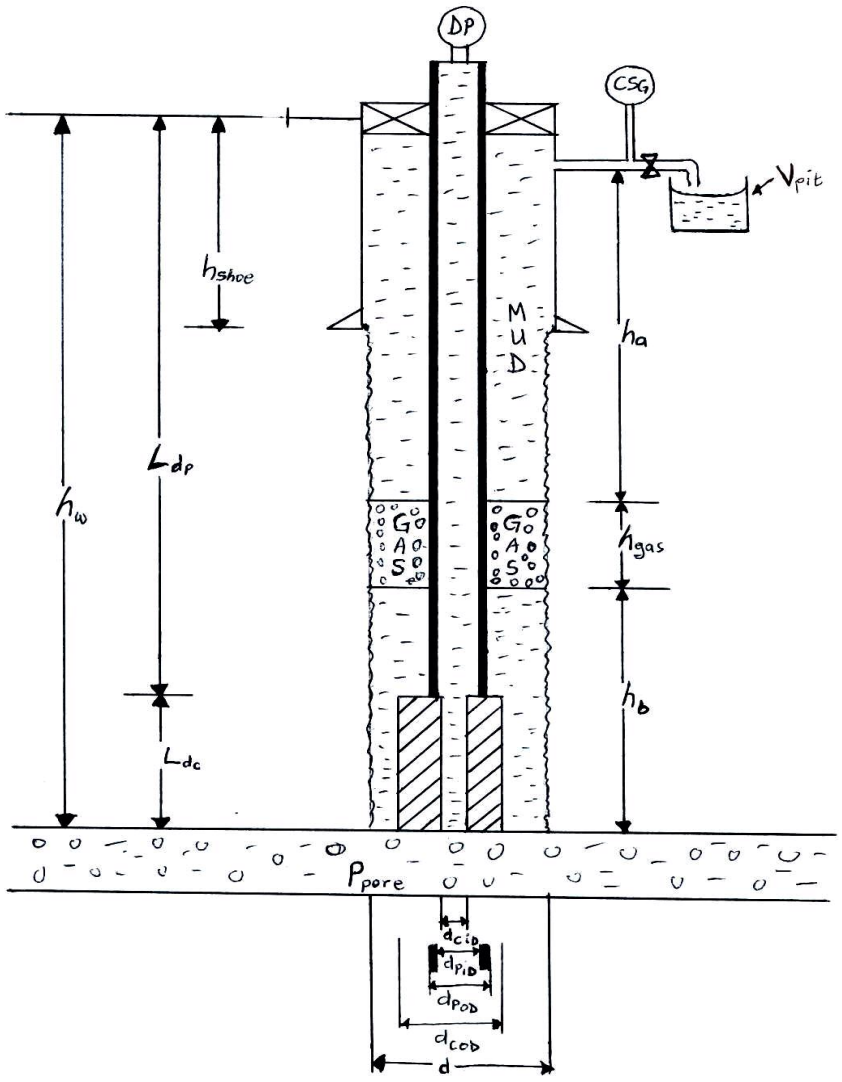

Fig. 2.5 – Theoretical illustration of gas bubble upward flow in the annulus[113]

translated as:

$$P_{pore} - 0.052\rho_l h_w = SIDPP \quad \ldots 2.9$$

Equation 2.8 is rewritten as:

$$P_{csg} - 0.052\rho_l h_{gas} = SIDPP \quad \ldots 2.10$$

There are changes in the gas bubble volume due to expansion as the gas bubble migrates upward. At a particular depth in the annulus, the annular height occupied by the gas would depend on its new volume attained at such depth. That is,

$$h_{gas} = \frac{V_{gas}}{V_{ann}} \quad \ldots 2.11$$

Where V_{ann} is the annular capacity around the drill-string. The attained volume of the gas at any depth, V_{gas}, is usually obtained from the ideal gas law as follows:

$$\frac{P_{pore}V_{pit}}{T_f} = \frac{P_{gas}V_{gas}}{T_{gas}} \quad \ldots 2.12$$

Where P_{gas} is the pressure in the gas bubble at a particular depth above the bottom-hole, and it is given as:

$$P_{gas} = P_{csg} + 0.052\rho_l h_a \quad \ldots 2.13$$

Combining **Eqs. 2.10 to 2.13** results in a quadratic expression for the surface casing pressure in terms of the varying depth, h_a, from the surface to the top of the bubble. This expression is given as follows:

$$aP_{csg}^2 + bP_{csg} + c = 0 \quad \ldots 2.14$$

Where,

$$a = 1$$

$$b = -\left(SIDPP - 0.052\rho_l h_a\right)$$

$$c = -0.052\rho_l\left(h_a SIDPP + \frac{P_{pore}V_{pit}T_{gas}}{V_a T_f}\right)$$

In **Eq. 2.11**, a gas bubble of certain volume is assumed to have entered the annulus at once with its internal pressure being equal to the reservoir pressure. This gas bubble volume is then immediately reflected at the surface mud pit as a gain or rise in the mud pit volume, V_{pit}. This is practically inadequate because it has been discovered that the response of the surface mud pit to gas inflow is low until the gas occupies a significant annular volume.[54] Hence, before gas kick detection, gas would increasingly enter the annulus as drilling operation continues into the gas formation. Realistically, the gas continues to enter the annulus in bubbles of different sizes/volumes due to the turbulent forces from the circulating drilling fluid. However, for sake of convenience, all these differently sized bubbles that entered the annulus at certain drilling period and at certain interval of the gas formation are lumped together to form a single spherical gas bubble for such interval and drilling period. This accounts for the phrase “apparent bubble size” used in this study.

Gas bubbles are susceptible to expansion as they flow or migrate upward the annulus before gas kick detection. Therefore, the gain in the mud pit volume at the time of detection would be the combination of the volumes of all the bubbles at the instant of their entrance into the annulus or at the wellbore-sand face contact and the respective extent of expansion that each bubble had undergone. Such inevitable gas bubble expansion causes reduction in its internal pressure. Hence, at the time of

detection, the annular gas volume indicated by the gain in the volume of the surface mud pit would practically not be at the reservoir pressure.

In practice, the above assumption is usually undertaken because the total volume of all the bubbles at the instant of their inflow cannot be accounted for. A theoretical analysis that treats such complexity or unknown is presented in Chapter 3 of this study. That is, in Chapter 3 a means of estimating the volumes of the series of gas bubbles as drilling and mud circulation progress, and during the suspension of mud circulation would be provided. By implementing this new approach, improvement in the above-discussed gas inflow or kick evaluation would be realized.

2.5 Concepts of Gas Bubble Formation

Experimental and theoretical studies[62,109,111,112] have demonstrated that gas inflow into a stationary liquid exists inform of gas bubbles proximal to the source of the gas supply. With high inflow rate, the number of these bubbles clustering together increases. The continued degree of clustering promotes the development of larger sized bubbles as the inflow rate increases. Thus, depending on the gas inflow rate, larger bubbles could start off from the lower part of the system, or be formed as a result of coalescence of bubbles at the upper portion of the system.[82,109,112]

As earlier mentioned, various existing theories relating to the formation of bubble would be reviewed because it is the concept upon which the study in Chapter 3 is based.

2.5.1 Background and Principles of Gas Bubble Development

The theories behind bubble development have been solely based on the assumption of non-dissolution of the gas phase in the liquid phase. Also, equivalent spherical size is assumed for all developed bubbles. As technology advances, a number of forces have been identified to be responsible for the development of gas bubbles. Different combinations of these forces that have resulted in evaluating volume of a bubble that develops would be considered in this section. Up to date, the following forces have been recognized to dictate bubble sizes:[57,63-67]

a. Liquid surface tension
b. Liquid viscous force
c. Inertia force of the liquid, and
d. Buoyancy force on the bubble

Taking into consideration only the equality between the buoyancy force and the surface tension on bubble formation, the radius of the bubble formed has been given as:[57]

$$\left(\frac{4}{3}\right)\pi r_B^3 g\left(\rho_l - \rho_g\right) = 2\pi r_o \sigma \qquad \text{… 2.15}$$

The LHS expression of Eq. 2.15 is the buoyancy equation that relates the density difference between the fluids and the volume of the bubble formed. The RHS, however, represents the surface tension of the liquid, which acts around the formed bubble while still attached to the gas supply opening of radius r_o. Re-arranging Eq. 2.15 gives the radius of the bubble as follows:

$$r_B \approx 1.145\left[\frac{\sigma r_o}{g\left(\rho_l - \rho_g\right)}\right]^{1/3} \quad \ldots 2.16$$

The radius of the bubble calculated from Eq. 2.16 is the expanding bubble radius just before the bubble uplifts from the gas supply opening, but still attached to the gas supply opening through a stretched neck. During this period, more gas still flows into the bubble, which results in further expansion of the bubble before it is finally detached from the gas supply source. For a system of low constant gas flow rate, the time required for the bubble to move from the gas supply opening before detachment is required to be able to compute the final bubble volume attainable at detachment. Application of the equation of motion to the terminal rising velocity of the bubble results in the following expression for the final bubble volume in inviscid or non-viscous liquid.[57]

$$V_{DB} = 1.138\frac{q_g^{6/5}}{g^{3/5}} \quad \ldots 2.17$$

Davidson and Schuler[63] developed an approximate bubble volume that forms at gas flow rates between 0 and 50-ml/s in a static viscous liquid under the assumption that the formed bubble is spherical. Flow rates ranging from 0 –2-ml/s were considered as low rate, while gas flow rates higher than 2-ml/s were considered to be higher rates of flow for their study. Another approach of the forming bubble moving from the gas supply opening, other than the establishment of a neck linking the bubble and the supply point was considered by the authors. The bubble was assumed to have its center at the gas supply source when it starts to form. However, the center of the bubble moves gradually upward as it expands with the lower end of

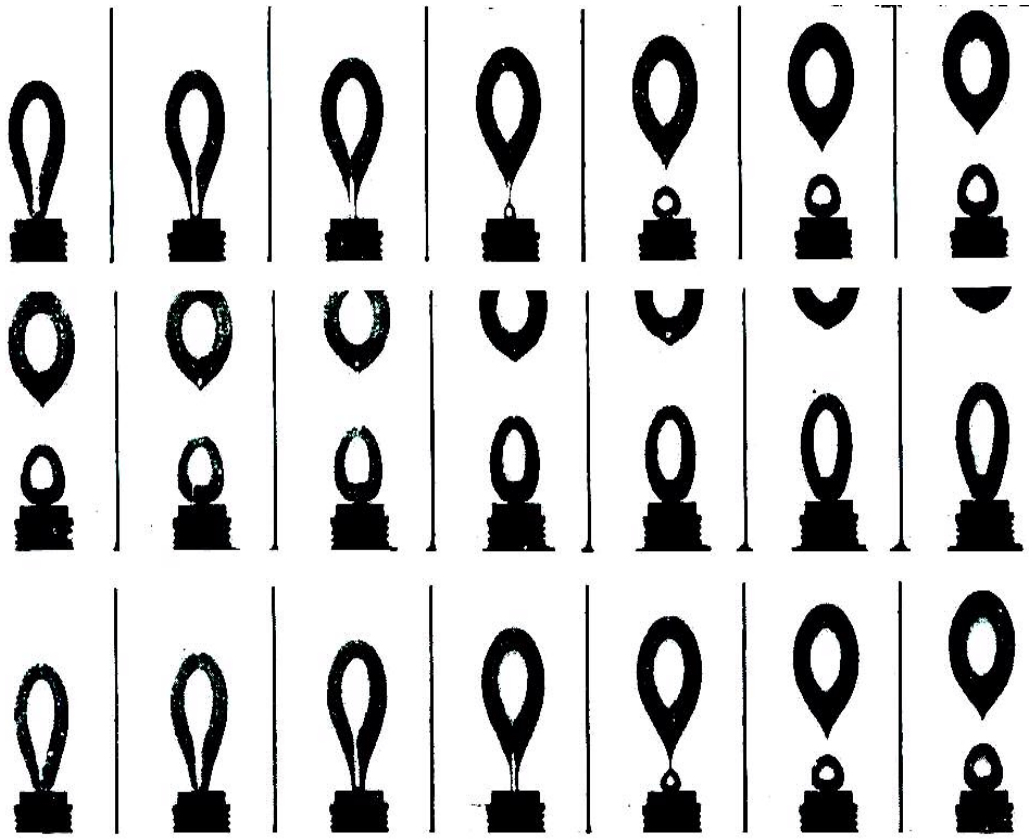

Gas flow rate	= 24 m/s
Viscosity	= 711 cp
Density	= 1.25 g/ml
Radius of orifice	= 0.096 cm
Bubble volume	= 2.5 ml

Fig. 2.6 – Photographic display of bubble formation in a viscous fluid at high gas flow rate[63]

the spherical bubble still buried inside the gas supply opening. An example photograph of bubble formation in a static viscous fluid of 711-cp, density of 1.25-g/ml, at the orifice radius of 0.096-cm for a gas flow rate of 24-ml/s is shown in Fig. 2.6. Considering Stokes expression for the bubble velocity after time, t, as:

$$v_B = \frac{2r^2 g(\rho_l - \rho_g)}{9\mu_l} \qquad \ldots 2.18$$

and knowing the gas flow rate, the variations in the upward distance moved by the center of the bubble with time was derived. From this derivation, the following expression for the final bubble volume was obtained.

$$V_{Db} = 4.87\pi^{1/4}\left(\frac{\mu_l q_g}{g(\rho_l - \rho_g)}\right)^{3/4} \qquad \ldots 2.19$$

Figure 2.7 shows a comparison between the experimental results and the theoretical calculations using Eq. 2.19. For the cases considered in their study, it could be seen that as the viscosity increases, the two results are in close agreement at low gas flow rates, while slight differences exist as the gas rate increases. Also, for low viscous fluids, there are inconsistencies in the comparison at both low and high gas flow rates.

Sullivan et al.[66] followed the bubble development pattern by Davidson and Schuler[63], but considered additional forces such as the bubble momentum force, inertia force, acceleration force, and viscous force. However, their study was based on the horizontal flow of the bubble along a flat surface after the spherical shape of the bubble is defined.

Obvious existence of a neck formed by the bubble when uplifting from the gas supply opening as shown in Fig. 2.6 at high gas flow rates made Kumar and Kuloor[67]

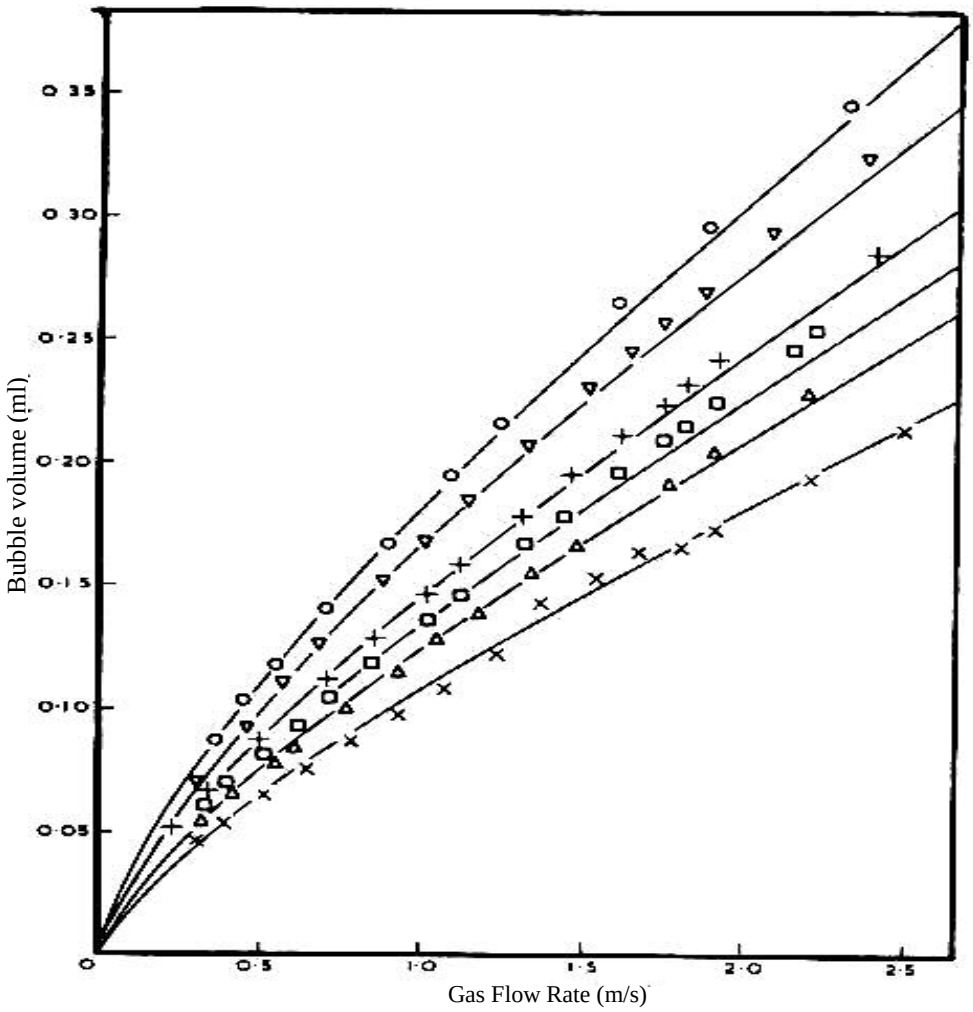

Orifice radius = 0.0334 cm + = 764 cp
Ring radius = 1.10 cm = 695 cp
Liquid seal = 5.0 cm Δ = 626 cp
O = 1040 cp x = 515 cp
∇ = 915 cp

Fig. 2.7 – Theoretical and experimental result comparison[63] (smooth curves represent the theoretical results)

equate only the buoyancy force to the inertia force of the fluid moving downward around the forming bubble. They pioneered the division of the bubble formation into two stages: expansion stage, which is characterized by the continuous gas flow into the forming bubble to cause bubble expansion before uplifting of the bubble commences; and, the detachment stage that starts at the instant that bubble uplifting commences until the neck of the bubble breaks away from the gas supply source. Their approach is based on the assumption that the bubble is spherically shaped right from its appearance at the gas supply opening until detachment. They provided explicit mathematical influence of another concept, known as virtual gas mass[69], on the bubble size. The expression derived for the expansion stage is given as:

$$V_B = \left[\frac{q_g^2 \left(\rho_g + \frac{11}{16} \rho_l \right)}{12\,\pi \left(\frac{3}{4\,\pi} \right)^{2/3} \left(\rho_l - \rho_g \right)} \right]^{3/5} \qquad \ldots 2.20$$

Application of Newton's law of motion to the instantaneous bubble velocity from the gas supply opening, and the consideration of continuous gas flow into the expanded bubble during upward movement before detachment resulted in the following expression for the final bubble radius.

$$r_B = \frac{P}{4q_g}\left(V_{Db}^2 - V_B^2\right) - \frac{9N}{q_g}\left(V_{Db}^{1/3} - V_B^{1/3}\right) + \frac{1}{q_g}\left(3NV_{Db}^{1/3} - \frac{P}{2}V_B^2\right)\left(\ln V_{Db} - \ln V_B\right) \qquad \ldots 2.21$$

where,

$$P = \frac{(\rho_l - \rho_g)g}{q\left(\rho_g + \frac{11}{16}\rho_l\right)} \qquad \ldots 2.22$$

and

$$N = \frac{q}{12\pi\left(\frac{3}{4\pi}\right)^{\frac{2}{3}}} \qquad \ldots 2.23$$

To solve for the final bubble volume, V_{Db}, Eq. 2.21 has to be iterated after calculating the bubble volume and radius at the end of the expansion stage from Eq. 2.20. From the comparison of results for the theoretical analysis and some experiments, noticeable differences in the estimated bubble volumes were observed as the volumetric flow rate increases.

Ramakrishnan et al[64] and Satyanarayan et al[65] provided some generalized expressions for bubble volume or size under the constant gas flow and constant gas pressure conditions, respectively, for bubbles formed at gas supply source submerged in viscous fluids. These studies are general in the sense that all the recognized forces - buoyancy force, surface tension, inertial force, and viscous or drag force – that control bubble development were considered. These two studies followed the modeling approach by Kumar and Kuloor[67]. Consequently, the forms of their results are similar to that of Kumar and Kuloor[67]. The expressions derived by Satyanarayan et al[65] for estimating a bubble volume at constant gas pressure is given as follows:

$$V_{Db}\rho_l g = \frac{11G^2 V_{Db}^{-2/3}\rho_l}{64\pi\left(\frac{3}{4\pi}\right)^{2/3}}A - \frac{11G^2 V_{Db}^{-1}\rho_l}{512\pi^2\left(\frac{3}{4\pi}\right)^{2}}B + \frac{3G\mu_l V_{Db}^{-1/3}}{2\left(\frac{3}{4\pi}\right)^{1/3}}C + \pi D\sigma \qquad \ldots 2.24$$

where A, B, C are arbitrary parameters defined as follows:

$$A = \left[P + \left(\frac{3}{4\pi} \right)^{1/3} V_{Db}^{1/3} \rho_l g - \frac{2\sigma V_{Db}^{-1/3}}{\left(\frac{3}{4\pi} \right)^{1/3}} \right] \quad \ldots 2.25$$

$$B = \left[4\left(\frac{3}{4\pi} \right)^{1/3} V_{Db}^{1/3} P + 3\left(\frac{3}{4\pi} \right)^{2/3} V_{Db}^{2/3} \rho_l g - 10\sigma \right] \quad \ldots 2.26$$

$$C = \left[P + \left(\frac{3}{4\pi} \right)^{1/3} V_{Db}^{1/3} \rho_l g - \frac{2\sigma V_{Db}^{-1/3}}{\left(\frac{3}{4\pi} \right)^{1/3}} \right]^{1/2} \quad \ldots 2.27$$

and,

$$P = P_g - \rho_l g h \quad \ldots 2.28$$

The study by Satyanarayan et al[65] is applicable to systems with varying gas inflow rates, but under constant gas supply pressure that is synonymous to the assumption of constant reservoir gas pressure at the time of drilling through such reservoir. This approach was, therefore, used as the platform for the present study with necessary modifications to suit Petroleum Engineering applications. Figures 2.8 and 2.9 show some examples of the agreement between the theoretical and experimental results provided by Satyanarayan et al[65].

2.6 Mechanics of Wellbore Pressure Buildup

Under this section, basic theoretical and practical concepts of the causes of wellbore storage are reviewed. Various analogies derivable from these concepts are utilized in developing a new model for the bottom-hole and surface

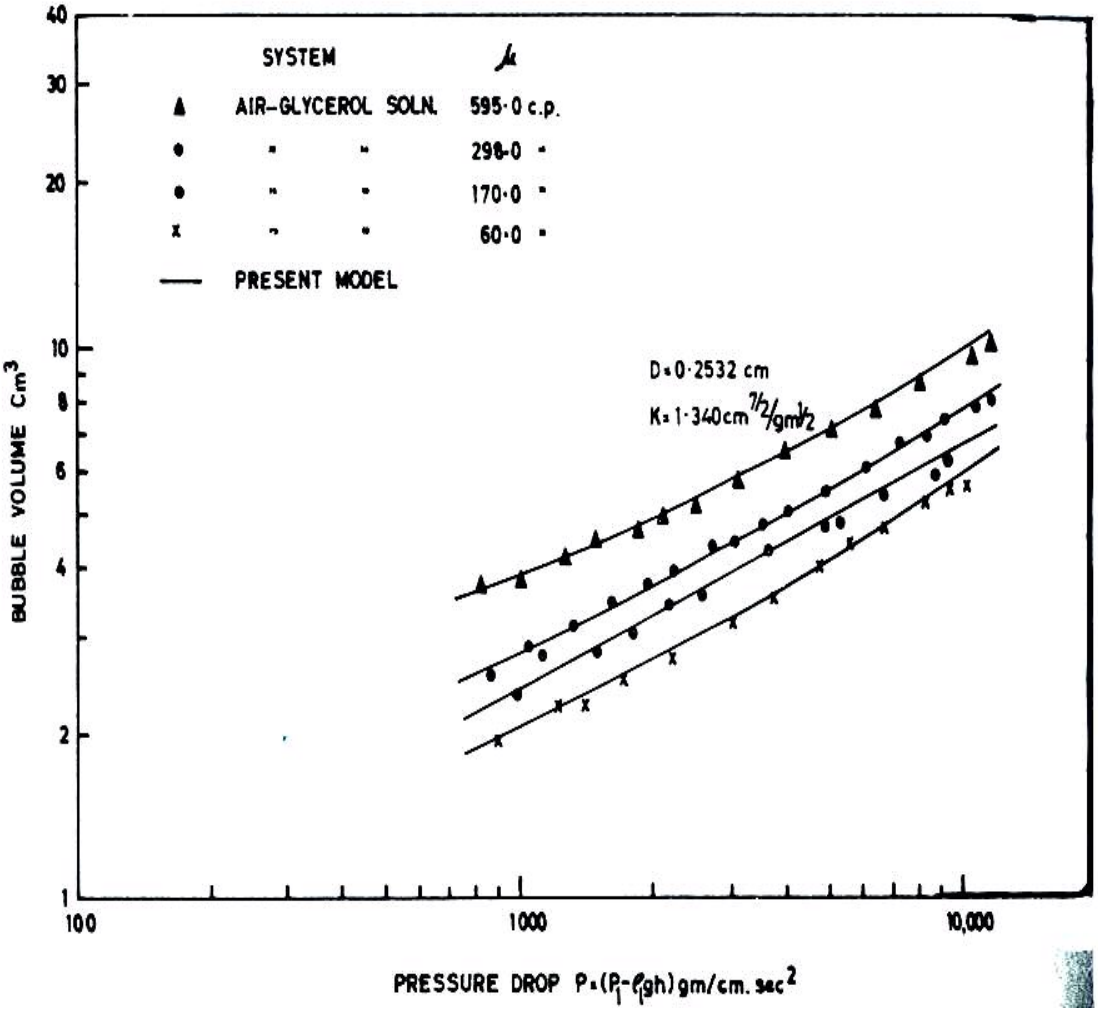

Fig. 2.8 – Viscosity effect on bubble volume by Satyanarayan et al[65]

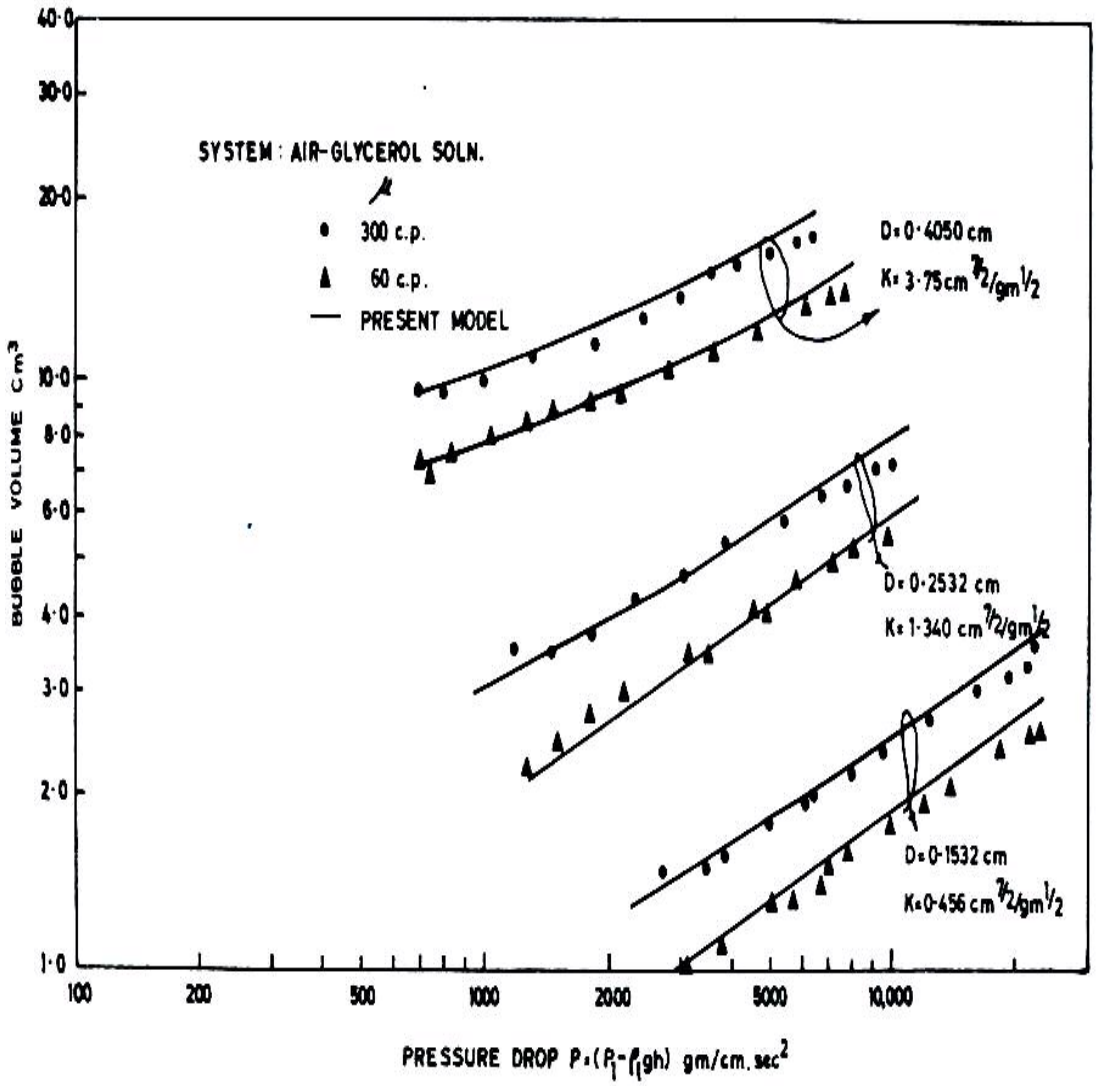

Fig. 2.9 – Effect of gas supply openings on bubble volume by Satyanarayan et al[65]

casing pressure rise during well shutting-in on drilling fluid that is contaminated by gas inflow from a gas formation. This model is developed and presented in Chapter 4.

Since the needs to evaluate well completion and reservoir properties began, it has become a custom to allow the reservoir to regain, to a reasonable extent, its original status prior to drilling into it. In doing so, the wellbore is usually shut-in to promote pressure build-up both in the wellbore and in the reservoir. Subsequently, the measured pressure buildup data are analyzed to obtain reasonable information about the reservoir properties, and the productivity of the wellbore.

Three factors have been recognized to control pressure build-up in wellbores. These are the wellbore storage effect, near wellbore damage or skin [93-96,99,102-107], and gas upward migration in a liquid known as the phase segregation. Such gas phase segregation has been identified to cause “gas humping” or build-up pressure abnormality [93-95,100-107]. Among these factors, only the near wellbore damage or skin is not considered in this study. This is because the physical processes being modeled involve reservoir gas inflow into the wellbore, which are opposite in fluid flow direction to drilling fluid invasion into the reservoir that could cause near wellbore damage or skin.

There are two wellbore conditions that could promote wellbore storage. One of the conditions is when shutting-in a wellbore on a partially filled annulus containing either only liquid or combination of liquid and gas, with the gas as the dispersed phase. Such condition causes the entire fluid to rise upwardly until a restriction such as a packer or wellhead is encountered. The rise in fluid level results only due to the continuous fluid inflow from more pressured reservoir than the

wellbore pressure. This, then, causes pressure to build-up inside the wellbore, and the imposition of backpressure on the reservoir. Under this scenario the wellbore storage is represented as the change in the volume of the wellbore fluids per unit change in the bottom hole pressure.

$$C = \frac{\Delta V_{wb}}{\Delta P_{bh}} \qquad \ldots 2.29$$

When a unit conversion is conducted on **Eq. 2.29**, an expression for estimating the annular volume rise during wellbore storage is presented as follows:

$$V_{ann} = C\left(\frac{\rho_l g}{144 g_c}\right) \qquad \ldots 2.30$$

Where ρ_l is in lb_m/ft^3, C is the wellbore storage coefficient of bbl/psi unit, g_c is the force-mass conversion factor, and V_{ann} is the volumetric fluid rise in the annulus per unit foot. The second wellbore condition is when the wellbore is completely filled with a mixture of liquid and gas. Due to buoyancy effect on the gaseous phase, the gas bubbles migrate upward. This phenomenon has been proposed to cause pressure build-up abnormality that is seldom observed in practice. Dated back to 1958, Stegemeier and Mathews[100] pioneered the quantitative demonstration of pressure build-up abnormality due to phase segregation resulting from the relative upward migration of the gaseous phase. Such abnormality is generally referred to as “gas humping”. Humping of build-up pressure data is a situation whereby the bottom hole pressure suddenly rises above the reservoir pressure at certain later shut-in time.

Shortly afterwards, the abnormal pressure rise falls back to the reservoir pressure. A practical illustration of pressure build-up data affected by gas humping is shown in **Fig. 2.10** as the dotted curve. On the contrary, the solid curve in **Fig. 2.10**

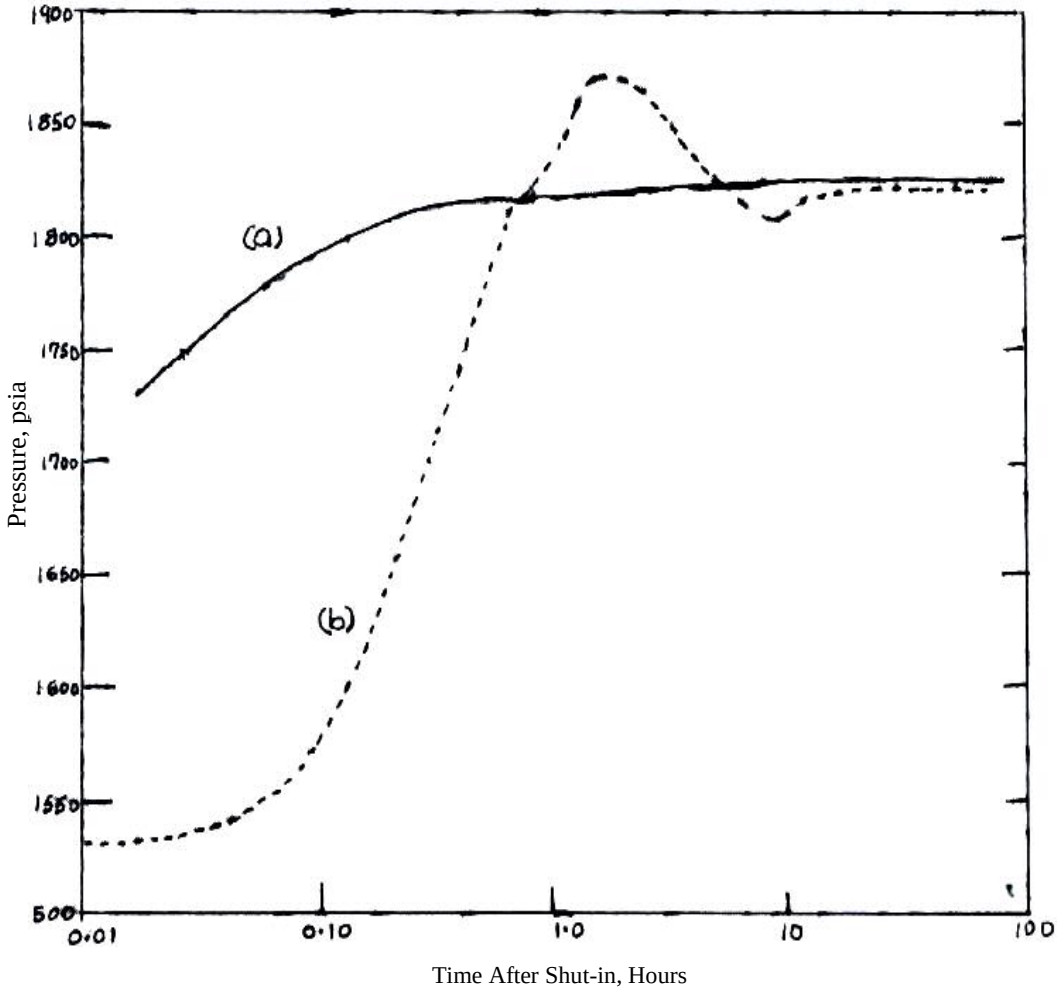

Fig. 2.10 – Bottom-hole shut-in (curve a), and surface shut-in (curve b) of South Texas well No. 1 showing gas humping at the later shut-in time[101]

represents the pressure build-up profile with minimal wellbore storage for downhole shut-in practices. This figure shows that when a well is shut-in at the surface on a fluid system that contains a mixture of liquid and gaseous phases, wellbore storage is definitely expected to relatively affect the early time pressure data before pressure stabilization.

Although from a theoretical point of view, Pitzer et al[101] admitted that pressure humps could be caused by gas-phase segregation, however, they concluded that its influence is significantly reduced in wells completed without a packer. Such wellbore condition is synonymous to the drilling operational periods. During these periods no packer is installed inside the wellbore. This could imply that the influence of gaseous phase upward migration on the pressure build-up is negligible. From a well in the Gulf of Mexico, Pitzer et al[101] observed that the pressure humping continuously reduces in magnitude as the gas-oil ratio increases. It was also stated that such pressure buildup anomalous have been noticed in wells that had mechanical problems such as leaking packers or tubing, which introduces uncertainties in distinguishing the cause of pressure humping.

Considering the above discussions, this study assumes that the upward migration of the gaseous phase could not be the sole phenomenon responsible for pressure build-up when a well is shut-in on gas inflow or kick. Hence, the principles of wellbore storage phenomenon, which is physically proven to exist when mixture of liquid and gaseous phases is pressurized,[93-96,99] is implemented in Chapter 4 to predict and analyze bottom-hole and surface casing pressure rise.

2.6.1 Wellbore Storage Analyzes

For this study, it is assumed that the wellbore being drilled is completely filled-up with drilling mud before gas inflow commences. Also, after gas inflow, the wellbore is still filled up with both drilling mud and gas during shut-in, and none of the gas is produced yet. By these assumptions, and considering the fluid compressibility expression for slightly compressible fluid as follows:

$$c_{fl} = \frac{1}{V_{wb}} \cdot \frac{\Delta V_{wb}}{\Delta P_{bh}} \quad \ldots 2.31$$

Equation 2.29 can be re-arranged to contain **Eq. 2.31** as follows:

$$\frac{C}{V_{wb}} = \frac{1}{V_{wb}} \cdot \frac{\Delta V_{wb}}{\Delta P_{bh}} = c_{fl} \quad \ldots 2.32$$

Equation 2.32 is the expression usually considered for wellbore storage coefficient for a completely filled wellbore, and it could be re-written as:[95]

$$C = V_{wb} c_{fl} \quad \ldots 2.33$$

and in dimensionless form as:

$$C_D = \frac{5.6146C}{2\pi\phi c_t h r_w^2} \quad \ldots 2.34$$

Equation 2.33 indicates that if two systems of the same constant volume, but different initial quantities of gas in the same liquid type are compressed by an external source at the same rate, the system with larger initial gas compress more. Consequently, the system with the larger initial gas volume would tolerate intake of more fluid to fill up the system's constant volume after such compression. With this case scenario, the system with larger initial gas volume system is said to have higher wellbore storage.

CHAPTER THREE

MODELING OF GAS BUBBLY INFLOW AT THE WELLBORE-SAND FACE CONTACT FOR OPENED WELLBORE SCENARIOS

3.1 Introduction

The major goals of any kick simulation are to predict the surface out-flow rate of drilling fluid from the annulus; gain in the surface mud pit volume; and wellbore pressure distribution. Due to the change from an initial single-phase flow of mud to a two-phase flow system when a gas inflow occurs, analysis of gas inflow has become very challenging and complex. In an attempt to solve this problem, several assumptions have been made to simplify the physical processes governing the occurrence of gas inflow.

The most common assumption is that all of the gas enters the annulus during drilling as a single bubble or slug flow.[77] Gas inflow analysis by this assumption is the simplest approach because the pressure-volume-temperature relationships for the gaseous phase could be applied.[55,79,61&83] Another assumption is that the gas exists as uniformly distributed bubbles in the annulus. This assumption is usually incorporated into the fluid mass and momentum equations, which require velocity expressions and volumetric fractional contents for each of the various fluid phases.[78&80] To satisfy these requirements, empirical and semi-empirical velocity correlations derived for air-water flow and other viscous Newtonian liquids[58,59,81,86,97] are used. Since this

approach cannot predict the gas volume at the wellbore-sand face contact for every formation interval drilled, an assumed volumetric fraction of the gaseous phase is usually made. Generally, volumetric fractions of 20% to 25% are considered depending on the assumed fluid flow pattern for the analysis. Unfortunately, it is virtually impossible to know the fluid flow pattern existing inside the annulus during drilling. Also, several bubble flow phenomena such as bubble coalescence, varied bubble sizes at different parts of the annulus, and varied bubble velocity occur that cannot be adequately accounted for. Therefore, assuming a particular flow pattern, and volumetric fraction of the gas could result in erroneous analysis.

From Chapter 2, it was clear that there is need to know the gas volume at the instant of inflow into the annulus. Such total gas volume would have the reservoir pressure as the internal pressure of all the gas bubbles before undergoing expansion due to the lower wellbore pressure when upward starts. Unfortunately, there is presently no gas inflow analysis that could predict the gas volume at the instant of inflow into the annulus. It is therefore the purpose of this chapter to present a mathematical model that is capable of predicting gas bubble size profile at the instant of gas inflow into the annulus. This model is applicable to any stage of the gas inflow or kick occurrence as long as the necessary conditions of such stage are understood and incorporated. Such applications are provided in Chapters 3, 4 and 5

As stated in Chapter 1, the study has been divided into three stages to simulate the various periods of gas inflow starting from the inception of gas influx to the kick control. The first two stages are considered in this chapter. These are:

A. Stage 1 – Gas influx inception while drilling and circulating

B. Stage 2 – Flow-check (suspension of drilling and mud circulation)

3.2. Model Hypotheses and Description

3.2.1. Model Hypotheses

The major hypotheses considered for the development of the mathematical models in this study are as follows:

1. Flow phase

- Flow pattern in the system is turbulent inside the drill pipe, and drill collars. No emphasis is made on the hydraulics since sophisticated hydraulic software are already available for the industry.
- Single, incompressible, mud exists inside the drill string at all times, while two-phase with compressible gas phase exists in the annular space during gas kick.

2. Continuous phase

- The density and rheological properties of the continuous fluid (drilling fluid or mud) are constant both inside the drill string and in the annulus. Changes in the annular phase properties are due to the presence of the formation gas.
- Bingham fluid rheological model was used for this study. However, the simulation procedures can be adjusted for other rheological models as long as the corresponding frictional pressure expressions for such fluid model are utilized.

3. Hole Geometry

- Vertical hole is considered.

4. Cuttings

- No effect of cuttings is considered, although, such effect could play some noticeable influence on bubble coalescence in the annulus.

5. Bubble Shape

- All gas bubbles whether larger or smaller than the one-half (1/2) of the annular diameter are represented by their equivalent spherical volume and size (diameter).

6. Bit

- All resulting sizes of gas bubbles from the cutting action of the bit are assumed to form a total gas bubble size as every inch of the formation is drilled.

7. Other hypotheses

- Isothermal condition is assumed

3.2.2. Model Description

The physical processes, modeled, during stages 1 and 2 are described as follows and illustrated in **Fig. 3.1**.

I. During the drilling operations, achievement of turbulent fluid flow condition is usually preferred at the bit-formation contact to aid the uplifting and upward flowing of the cuttings being generated by the bit-cutting action. When the resulting equivalent circulating density or mud circulating pressure at the bottom hole is lower than the formation pressure, formation gas and/or liquid enters the annular section of the wellbore. When a small height or

interval of such gas formation is initially penetrated, the inflow rate of the formation gas is low. The low gas influx rate results in the formation of smaller bubbles (**Fig. 3.1A**). As these bubbles are released from the bottom hole, they flow upward to the surface at the combined mudflow rate and their corresponding slip velocities.

II. As further bit penetration ensues, increased formation height or interval is exposed. This causes increase in the gas inflow rate into the well bore, thereby, producing much larger bubble sizes (**Fig. 3.1B**). The bubble sizes increase as more formation interval is drilled.

III. At the notification of significant gas inflow or kick by the surface equipment, further drilling and mud circulation are suspended. A visual check for fluid outflow rate from the annulus is conducted to ascertain the severity of the gas inflow. During this period, referred to in this study as the “Flow-Check” period, the wellbore would still be opened to the surface. If a significant gas inflow into the annulus occurs, high rate of mud outflow from the annulus would be noticed. At this time, the only pressure being exerted on the gas formation or reservoir is the hydrostatic pressure of the mud column. A lower hydrostatic pressure than the mud circulating or flowing pressure would increase the rate of gas inflow into the annulus. Thus, resulting in the development of larger gas bubbles during the flow check period (**Fig. 3.1C**). However, during the flow-check stage, equal size of gas bubble is introduced into the wellbore because further drilling of the formation that could cause increasing gas inflow rate is suspended (**Fig. 3.1D**).

IV. After the confirmation of significant gas influx into the well bore, the well is usually shut-in to estimate the formation pressure. The density or weight of the mud is increased to the estimated formation pressure to subdue further inflow of the gas into the wellbore.

3.3. Development of the Generalized Model

As earlier mentioned, the major modeling procedures are applicable to all of the three stages. However, the practical wellbore conditions during each of the three stages are different. Such different wellbore conditions result in different bottom hole pressures for each stage.

3.3.1 Development of a Bubble

The development of a gas bubble during the static or dynamic conditions of a wellbore involves the flow of gas from the gas reservoir or gas containing sediment into a liquid-filled annulus. As presented by Davidson and Schuler[63], one of the factors that determines the size or volume of a bubble formed at a specific period is the pressure differential between the gas source and the liquid-filled container. In petroleum engineering, the gas source is the gas formation, while the liquid-filled container is the annulus containing the drilling mud. The wellbore pressure could be dynamic, as the case of flowing or circulating mud pressure at the bottom-hole, or could be static.

These different pressures are translated to their corresponding forces. Therefore, depending on the drilled interval and its corresponding gas inflow rate into

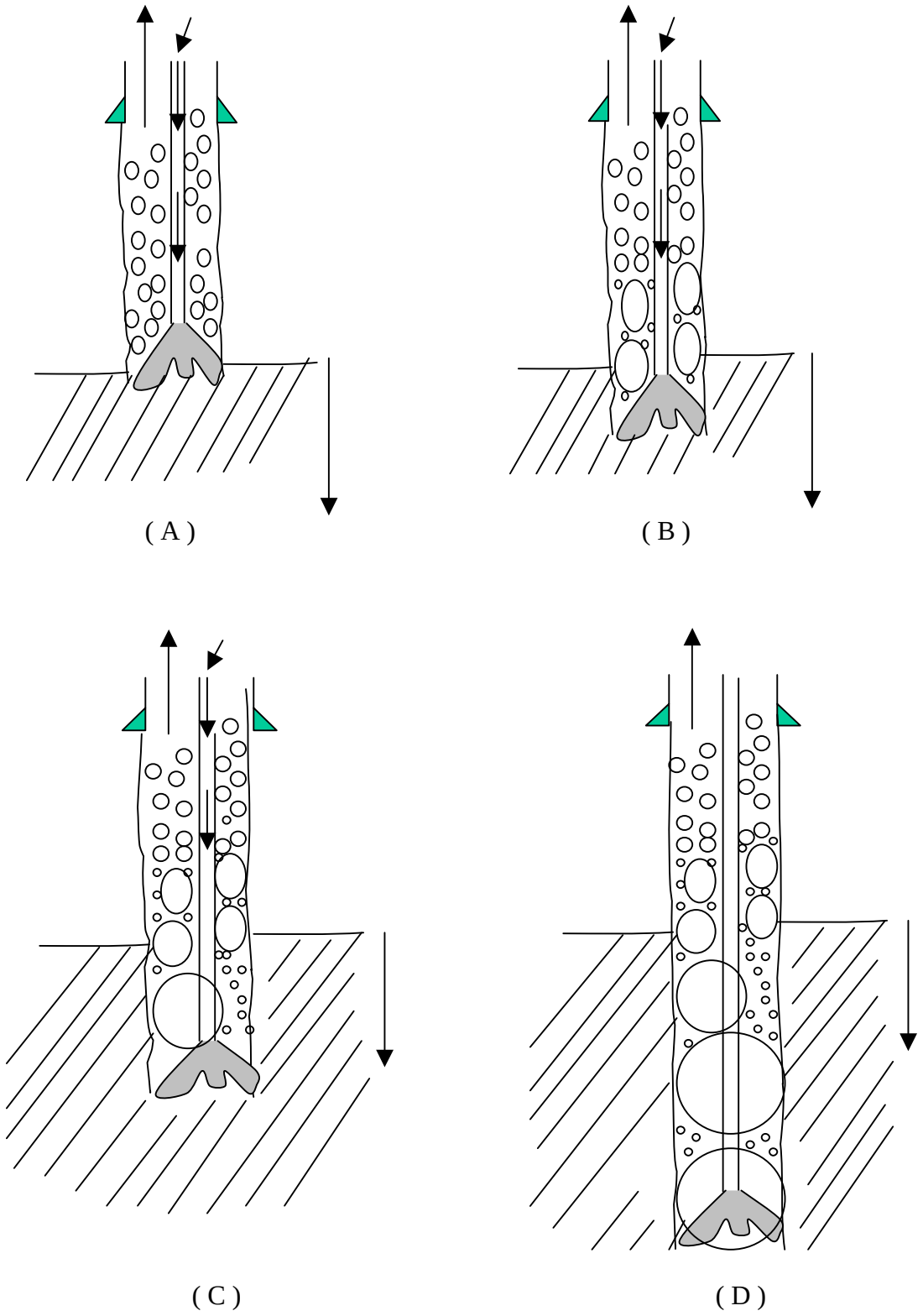

Fig. 3.1 – Schematic representation of the modeled physical processes

the annulus, a force balance is conducted to estimate the volume or size of gas bubble that enters the annulus during a specific time period. For any force balance to occur, there must be some forces that support the development of the gas bubble. That is, allowing the gas bubble to expand. Such forces are considered to act outwardly from the reservoir face. Also, some forces that discourage or oppose the development of a gas bubble must be present. These second set of forces are derivable from either the dynamic or static impact of mud column on the gas bubble development, and the mud viscous force. Thus, they are considered to act on the developing gas bubble. **Figure 3.2** shows a schematic of bubble formation and the various forces responsible for its development and expansion.

For this study, the major opposing force to the bubble development is the corresponding bottom hole pressure force, P_{bh}, that results from drilling or non-drilling operational conditions. This pressure comprises of: the pressure exerted on the gas bubble by the jetting action of the flowing drilling fluid from the bit nozzles, P_{wb}, and, the pressure differential due to the surface tension. Both of these bottom hole pressure components act on and around the developing gas bubble respectively. While the gas bubble is developing, the pressure differential due to the surface tension surrounding a developing bubble of radius r_b could be represented as follows:

$$P_{res} - P_{wb} > \frac{2\sigma}{144 r_b} \qquad \ldots 3.1$$

Taking the total bottom hole pressure, P_{bh}, to be:

$$P_{bh} = P_{wb} + \frac{2\sigma}{144 r_b} \qquad \ldots 3.2$$

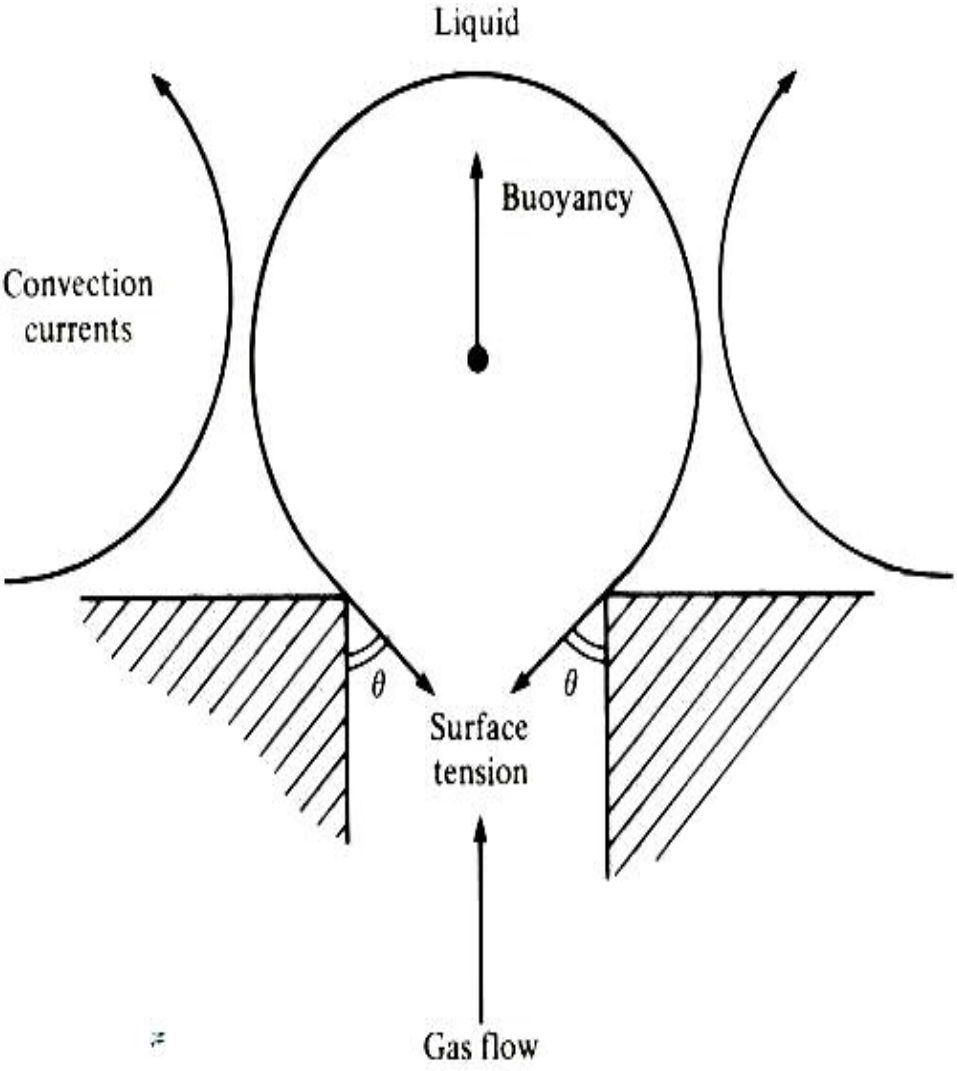

Fig. 3.2 – Schematic of forces acting on a forming bubble

Substituting **Eq. 3.1** into **Eq. 3.2**, we have:

$$P_{res} - P_{wb} > 0 \qquad \ldots 3.3$$

Therefore, the excess pressure expressed by **Eq. 3.3**, which is greater than zero, causes the continuous gas inflow into the developing bubble from the reservoir at a particular gas inflow rate. When the gas inflow rate changes, which occurs when another inch of the formation is drilled, another gas bubble is assumed to form after the previous gas bubble is uplifted. That is, a particular gas inflow rate would correspond to a gas bubble volume. Larger gas bubbles are formed as the gas inflow rate increases.

Such pressure difference expressed in **Eq. 3.3** is incorporated into the solved diffusivity equation[95] for the gas flow rate. This equation and other related expressions that are independent of the reservoir drainage radius and are derived in appendix A for radial-cylindrical gas inflow into a partially penetrated wellbore.

$$q_g = \frac{kh\left(P_{res}^2 - P_{bh}^2\right)B_g}{34176P_D * \left(T * \mu_g * Z_g\right)_{res}} \qquad \ldots 3.4$$

Where q_g is the gas inflow rate, expressed in Mcuft/hr.

$$P_D = \frac{1}{2}\left[\ln\left(t_D\right) + 0.81\right] \qquad \ldots 3.5$$

and,

$$t_D = \frac{2.634 \times 10^{-4} Kt}{\phi \mu_g c_g r_w^2} \qquad \ldots 3.6$$

Equations 3.4 and 3.5 are the approximate solutions to the diffusivity equation for gas flow in radial direction inside gas reservoirs during transient period. These equations

are approximations because the resulting diffusivity equation involving pseudopressure terms transformation for the reservoir gas flow is non-linear, and thus can only be solved numerically. In order to perform analytical processes for reservoir gas flow, Al-Hussainy et al[134] introduced this pseudopressure transformation, as presented in appendix A. These authors[134] performed numerical techniques on the resulting gas flow diffusivity equation, and found that the dimensionless pseudopressure term, ψ_D, can be approximated by the dimensionless pressure term, P_D, for the slightly compressible fluid at the following conditions:

$$\psi_D(t_D) = p_D(t_D) = \frac{1}{2}\left[\ln t_D + 0.80907\right], \text{ for } 100 \le t_D \le \frac{1}{4}\left(\frac{r_e}{r_w}\right)^2 \qquad \ldots \text{D52}$$

The transient flow period is included in the analysis because of the possible variations in rate of penetration (ROP) that might be desired to drill through formations. This rate of penetration would control the exposure time for a particular interval, and thus, partly determines the volumetric inflow of the gas into the wellbore.

Another consideration in this study is the fact that partially penetrated wellbores into massive reservoirs have been realized to better be modeled by hemi-spherical inflow of the reservoir fluid into the wellbore.[135,137-140] However, the various analyses available for hemispherical flow analysis require that the entire formation interval be known before analysis. On the contrary, during drilling the exact formation thickness or length is not known until the formation is completely drilled through. Hence, the first approximation is to assume that radial flow exist all through the drilled height for analysis, and perform simulation for reservoir heterogeneity.

3.3.2 Analysis of Forces on a Developing Bubble

Figure 3.2 shows that there is presence of surface tension around a developing or fully developed gas bubble within a liquid system. Therefore, with the assumption of spherically developed bubbles, an opposing force due to liquid surface tension is expressed as follows:

$$F_{ST} = \pi d_H \sigma \qquad \ldots 3.7$$

Equation 3.7 incorporates the assumption of zero contact angle between the contacting fluid phases, therefore cosine of the contact angle is equal to 1. By assuming that the reservoir is composed of hydraulic tubes of different sizes that are distributed non-uniformly, the hydraulic radius, r_H, of such porous reservoir sand or formation can be approximated as follows[87]:

$$r_H = \frac{\phi \overline{D}_p}{6(1-\phi)} \qquad \ldots 3.8$$

$\overline{D}_p$ is the sand particle diameter. The hydraulic diameter, d_H, is assumed to be:

$$d_H = 2r_H \qquad \ldots 3.9$$

Tiab and Donaldson[88] published the average particle sizes or diameters for various known earth sediments. From the grain size table presented by these authors[88], the average sand particle of 0.25mm, for medium grained sand sediment, was chosen as the average sand size for this study.

That is,

$$\overline{D}_p = 0.25 \text{ mm} = 8.2 \times 10^{-4} \text{ ft} \qquad \ldots 3.10$$

Combining **Eqs. 3.7** through **3.10**, and expressing the parameters in field units, we have:

$$F_{ST} = \frac{8.2 \times 10^{-4} \pi \phi \sigma}{3(1-\phi)} \qquad \ldots 3.11$$

Another opposing force on the developing bubble is that due to the inertia of the drilling fluid fraction surrounding the developing bubble. Owing to the continuous expansion of this bubble, the surrounding fraction of the liquid or mud is subjected to a downward movement. The resulting liquid movement is expressed in differential form[65] as follows:

$$F_I = \frac{d(M v_b)}{d_b t} \qquad \ldots 3.12$$

Where, M is the virtual mass of the gas bubble and the bubble volume

$$M = V\left(\rho_g + \frac{1}{1}\rho_l\right)\frac{1}{6} \qquad \ldots 3.13$$

v_b is the velocity of

$$v_b = \frac{d_b r}{d_b t} \qquad \ldots 3.14$$

The third dual end to last state, and the expression respectively given

$$F_v = 6\pi r_b \mu_p v_b \qquad \ldots 3.15$$

and,

$$V_b = \frac{4}{3}\pi r_b^3 \qquad \ldots 3.16$$

The only supporting or upward force on the developing bubble is the buoyancy force. The buoyancy force is dependent on the bubble volume and the density difference between the drilling fluid and the gaseous phases that exist in the annulus. The buoyancy expression is given as follows:[89]

$$F_{BF} = V_b(\rho_l - \rho_g)g \qquad \ldots 3.17$$

3.3.3 Coupling of Model Forces

During the bubble development, the differential pressure between the bottom hole pressure and that of the formation encourages the continuous growth of the bubble, as expressed by **Eq. 3.3**. Such pressure differential, also, promotes inequality between the total upward and total downward acting forces. It is assumed that at the instant of equality between the total upward and the total downward forces, the bubble stops to develop or grow. Once the bubble stops growing, it is uplifted from the bottom-hole towards the surface.

Then, equating **Eq. 3.17** to the summation of **Eqs. 3.11**, **3.12** and **3.15** results in the coupled model to be evaluated for the bubble size or volume at a specific gas inflow rate. Thus, we have:

$$V_b(\rho_l - \rho_g)g = \frac{d(Mv_b)}{d_b} + \frac{8.2\times10^{-4}\pi\phi\sigma}{t\ 3(1-\phi)} + 6\pi\ r_b\mu v_b \qquad \ldots 3.18$$

3.3.3.1 Expatiation on the Terms in the Coupled Model

The terms in **Eq. 3.18** that need further expatiation are the first and third terms at the RHS. In **Eq. 3.4** the gas inflow rate is assumed constant, at a particular exposed

formation interval, while the gas is flowing into the forming or developing bubble. Such constancy of flow rate could be considered reasonable because the entire flow time of gas during drilling is comparably shorter than when the reservoir is actually placed on production. Hence, any reservoir pressure drop and changes in the flow rate over the period for gas inflow during drilling are considered insignificant in this study. As the bubble grows or develops, the change in bubble volume is dependent on the change in bubble radius, as expressed by **Eq. 3.16**. Also, the change in volume of a particular bubble with respect to the change in time that is required for the gas to flow into the bubble is equivalent to the gas inflow rate. Therefore, substituting **Eq. 3.2** into **Eq. 3.4**, and expressing the parameters in field units, we have:

$$q_g = \frac{dV_b}{dt_b} = \frac{khB_g\left[P_{res}^2 - \left(P_{wb} + \frac{2\sigma}{144r_b}\right)^2\right]}{34176P_D * \left(T * \mu_g * Z_g\right)_{res}} \quad \ldots 3.19$$

where,

q_g = gas inflow rate, cu ft/hr

The gas formation volume factor, in SCF/cu ft, is given as follows[33]:

$$B_g = 0.02829\frac{Z_g T_{res}}{P_{res}} \quad \ldots 3.20$$

Equation 3.20 assumes that the atmospheric pressure is 14.7 psia, surface temperature of 60°F (520°R), and a compressibility factor of 1 at these standard conditions.

Defining a parameter as follows:

$$\eta_1 = \frac{k_g}{3 * \left(T * \mu_g * Z_g\right)_r} B \quad 1 \quad e \quad 7 \quad s \quad 6 \quad \ldots \quad 3$$

Then,

$$q_g = \frac{dV_b}{dt_b} = \eta_1 \frac{h}{P_D}\left[P_{res}^2 - \left(P_{wb} + \frac{2\sigma}{144 r_b}\right)\right] \quad \ldots 3.22$$

Differentiation of the first term at the RHS of **Eq. 3.18** is expressed as:

$$\frac{d(M v_b)}{dt_b} = M\frac{dv_b}{dt_b} + v_b\frac{dM}{dt_b} \quad \ldots 3.23$$

In **Eq. 3.23**, the differential terms need to be solved for. Therefore, differentiating **Eq. 3.13** with respect to time, and substituting **Eq. 3.22** into the differentiated expression, we have:

$$\begin{aligned}\frac{dM}{dt_b} &= \left(\rho_g + \frac{7.48\times 11}{16}\rho_l\right)\frac{dV_b}{dt_b} \\ &= \left(\rho_g + \frac{11}{16}\times 7.48\rho_l\right)\eta_1\frac{h}{P_D}\left[P_{res}^2 - \left(P_{wb} + \frac{2\sigma}{144 r_b}\right)^2\right]\end{aligned} \quad \ldots 3.24$$

Application of Chain-rule of differentiation to the RHS term of **Eq. 3.14** yields:

$$v_b = \frac{dV_b}{dt_b}\cdot\frac{dr_b}{dV_b} \quad \ldots 3.25$$

When **Eq. 3.16** is differentiated with respect to r_b, and taking the reciprocal of the result, we have:

$$\frac{dr_b}{dV_b} = \frac{1}{4\pi\ r_b^2} \quad \ldots 3.26$$

Substituting **Eqs. 3.22** and **3.26** into **Eq. 3.25** yields the rate at which the bubble develops, which corresponds to the rate at which the radius of the bubble increases. This results to:

$$v_b = \eta_1 \frac{h}{P_D}\left[P_{res}^2 - \left(P_{wb} + \frac{2\sigma}{144 r_b}\right)\right] \cdot \frac{1}{4\pi r_b^2} \quad \ldots 3.27$$

That is,

$$v_b = function(r_b, t_b) \quad \ldots 3.28$$

Therefore, when v_b is differentiated with respect to t_b, the Chain-rule of differentiation is applied, and **Eq. 3.14** is substituted into the resulting expression from the Chain rule application. , we have:

$$\frac{dv_b}{dt_b} = \frac{dv_b}{dr_b} \cdot \frac{dr_b}{dt_b} = v_b \frac{dv_b}{dr_b} \quad \ldots 3.29$$

Then, the growth rate of the bubble with respect to the change in the bubble radius is evaluated by differentiating **Eq. 3.27** with respect to r_b. This yields:

$$\frac{dv_b}{dr_b} = \frac{\left\{\frac{16}{144}\eta_1\sigma\frac{h}{P_D}\pi\left(P_{wb} + \frac{2\sigma}{144 r_b}\right)\right\} - \left\{\eta_1 \frac{h}{P_D}\left[P_{res}^2 - \left(P_{wb} + \frac{2\sigma}{144 r_b}\right)^2\right] \cdot 8\pi r_b\right\}}{16\pi^2 r_b^4} \quad \ldots 3.30$$

Which becomes,

$$\frac{dv_b}{dr_b} = \frac{\eta_1 h\left\{\frac{2\sigma}{144}\left(P_{wb} + \frac{2\sigma}{144 r_b}\right) - r_b\left[P_{res}^2 - \left(P_{wb} + \frac{2\sigma}{144 r_b}\right)^2\right]\right\}}{2\pi P_D r_b^4} \quad \ldots 3.31$$

When **Eqs. 3.27** and **3.31** are substituted into **Eq. 3.29**, **Eq. 3.29** could be re-written as:

$$\frac{dv_b}{dt_b} = \frac{\eta_1^2 h^2}{8\pi^2 P_D^2 r_b^6}\left\{\frac{2\sigma}{144}\left(P_{wb} + \frac{2\sigma}{144r_b}\right)\left[P_{res}^2 - \left(P_{wb} + \frac{2\sigma}{144r_b}\right)^2\right] - r_b\left[P_{res}^2 - \left(P_{wb} + \frac{2\sigma}{144r_b}\right)^2\right]^2\right\} \quad \ldots 3.32$$

Thus, substituting **Eqs. 3.22**, **3.24** and **3.32** into **Eq. 3.23** solves for the differential equation of the first term in the general solution, **Eq. 3.18**, while the growth rate of the bubble radius that is required in the last term of the general solution is given in **Eq. 3.27**.

3.4 The General Model

Having solved all the required terms of **Eq. 3.18**, the expressions in **Eqs. 3.13, 3.24, 3.27, 3.32**, and **3.23** were coupled together and substituted into **Eq. 3.18** to obtain a general model for the physical processes being modeled. The summarized expression for the general model is given as follows.

$$\frac{V_B\left(7.48\rho_l - \rho_g\right)g}{32.174} = \Omega B + \Psi A^2 + \frac{8.2\times10^{-4}\pi\phi\sigma}{3\left(1-\phi\right)} + \Gamma A \quad \ldots 3.33$$

All along, the subscript, b, has been used to represent the developing stage of the bubble. To distinguish the developing stage from the final volume of a bubble, the general model in **Eq. 3.33** has this subscript replaced by an uppercase letter B**.** Hence, **Eq. 3.33** contains the final bubble volume, V_B, when the buoyancy force balances the total of all the downward forces.

Since the final bubble volume, V_B, is embedded in various terms at both sides of **Eq. 3.33**, a computer iterative program was developed for estimating the bubble volume as every inch of the formation or gas containing sediment is penetrated by the bit. This computer program is coded in Visual Basic 6.0 Language. The details of the coding are presented in **Appendix B2**. The various parameters in the preceding general model, **Eq. 3.33** are defined as follows:

$$\Omega = \frac{2\eta_1^2 h^2 \left(\rho_g + \frac{11*7.48}{16} \rho_l \right)}{9 P_D^2 V_B} \quad \ldots 3.34$$

$$\Psi = \frac{\eta_1^2 h^2 \left(\rho_g + \frac{11*7.48}{16} \rho_l \right)}{(36\pi)^{1/3} V_B^{2/3} P_D^2} \quad \ldots 3.35$$

$$\Gamma = \frac{3\eta_1 \mu_p h \pi^{1/3}}{4\ 7\ 9.8 P_D (6)^{1/3} V_B^{1/3}} \quad \ldots 3.36$$

$$\eta_1 = \frac{k\ B_g}{3\ 4\ 1*7 T_b 6 \mu_g Z_g} \quad \ldots 3.37$$

$$B_g = 0.0\ 2\ 8 \frac{Z_g T_b\ h}{2\ 9 P_{r\ e\ s}}, \quad {}^3 f\ S\ C\ F \quad \ldots 3.38$$

$$A = \left(P_{r\ e\ s}^2 - Y^2 \right) \quad \ldots 3.39$$

$$Y = P_{w\ b} + \left(\frac{4\pi}{3} \right)^{1/3} * \frac{\sigma}{7\ 2 V_B^{1/3}} \quad \ldots 3.40$$

$$B = \frac{\sigma}{7\ 2} A\ Y - \left(\frac{3}{4\pi} \right)^{1/3} V_B^{1/3} A^2 \quad \ldots 3.41$$

All of the variables used in this modeling procedure have been converted to field units.

3.5 Application of the General Model to the Physical Processes

As earlier mentioned, the application of the general model to the first two stages of the entire physical processes under consideration will be presented in this section of the study. Also, it had been stated that the major difference between these stages is the different bottom hole pressures due to the different operational conditions existing during each stage. Consequently, the bottom hole pressure, P_{bh}, needs to be evaluated for each of the first two stages.

3.5.1 Stage 1 – Inception of Gas Inflow While Drilling and Circulating Drilling Fluid.

The operational condition under this stage involves the bit penetration into the gas formation and circulation of the drilling fluid until the gas inflow into the annulus is significant, and detected at the surface. Existence of such a drilling condition is a must; otherwise, there would not be any need to analyze any gas inflow.

Following the concept of energy balance of fluid flow from the surface to the bottom-hole through the drillstring, as presented by Bourgoyne et al[31], and taking the frictional pressure drops in the drill string into consideration, the following expression was derived as the imposing pressure by the circulating drilling fluid through the jets of the bit.

$$P_{wb1} = 0.052\rho_l D_{bh} + \Delta P_{pump} - \left(\Delta P_t\right)_f - 8.074\times10^{-4}\bar{\nu}_{dc}^{2}\rho_l - \frac{8.311\times10^{-5}\rho_l q_l^2}{C_d^2 A_t^2}$$

… 3.42

where,

$\left(\Delta P_t\right)_f = \left(\Delta P_{dc} + \Delta P_{dp}\right)_f$ - Total frictional pressure drop inside the drill string, psi

For the flow of a Bingham plastic fluid inside a cylindrical geometry of specific length, L, the following expression is used for the turbulent frictional pressure drop:[50]

$$\Delta P_f = \frac{\rho_l^{0.75}\left(\bar{\nu}\right)^{1.75}\mu_p^{0.25}L}{1800d^{1.25}} \quad \text{… 3.43}$$

The average velocity of flow through a cylindrical geometry is also given as:

$$\bar{\nu} = \frac{q_l}{2.448d^2} \quad \text{… 3.44}$$

and, the cross-sectional area across the three nozzles of a tri-cone roller bit is given as:

$$A_t = \frac{\pi}{4(32)^2}\left(d_{nz1}^2 + d_{nz2}^2 + d_{nz3}^2\right) \quad \text{… 3.45}$$

where,

ΔP_{dc} = total frictional pressure drop in the drill Collars, psi

ΔP_{dp} = total frictional pressure drop in the drill pipes, psi

$D_{bh} = L_{dc} + L_{dp}$ - True Vertical Depth (TVD), ft

Thus, the bottom hole pressure for stage 1 is given as:

$$P_{bh} = P_{wb1} + \frac{2\sigma}{144r_e} \quad \text{… 3.46}$$

Substituting **Eq. 3.46** into the general model, **Eq. 3.33**, results in the following expressions for stage 1:

$$A_1 = \left(P_{res}^2 - Y_1^2\right) \quad \ldots 3.47$$

$$Y_1 = P_{wb1} + \left(\frac{4\pi}{3}\right)^{1/3} * \frac{\sigma}{72 V_{B1}^{1/3}} \quad \ldots 3.48$$

$$B_1 = \frac{\sigma}{72} A_1 Y_1 - \left(\frac{3}{4\pi}\right)^{1/3} V_{B1}^{1/3} A_1^2 \quad \ldots 3.49$$

Equations 3.47 through **3.49** are substituted into the RHS terms of the general model, and the developed computer program is used to perform iterations for the determination of each of the various gas bubble sizes and volumes during drilling and circulation of the drilling fluid.

3.5.2 Stage 2 – Suspension of Drilling and Mud Circulation

When the gas inflow or gas kick is detected through a surface kick detection equipment, a visual check for the out-flow rate of the drilling fluid from the annulus is usually conducted. The effectiveness of such check for the annular out-flow rate is achieved by the suspension of both drilling and circulation of drilling fluid. With no circulation of the drilling fluid, any notable annular out-flow signifies a significant inflow of the reservoir fluid into the wellbore. Such high annular outflow rate is an indication that a formation with higher formation pressure than the designed drilling fluid bottom hole circulating and hydrostatic pressure is encountered.

At this stage 2, the drilling fluid is static and the well is still opened to the surface, therefore, the hydrostatic pressure of the drilling fluid at the bottom hole is the only fluid pressure available to act against the gas formation pressure. The hydrostatic pressure of a liquid column at a depth, D_{bh}, is generally expressed as:[31]

$$P_{wb2} = 0.052\rho_l D_{bh} \quad \ldots 3.50$$

In **Eq. 3.50**, P_{wb2} is in psi, ρ_l is in lbm/gal and D_{bh} is in ft.

Thus, when **Eq. 3.50** is substituted into the developed general model, **Eqs. 3.39** through **3.41**, similar expressions as obtained for the stage 1, but with differently defined parameters are obtained as follows:

$$A_2 = \left(P_{res}^2 - Y_2^2\right) \quad \ldots 3.51$$

$$Y_2 = P_{wb2} + \left(\frac{4\pi}{3}\right)^{1/3} * \frac{\sigma}{72V_{B2}^{1/3}} \quad \ldots 3.52$$

$$B_2 = \frac{\sigma}{72} A_2 Y_2 - \left(\frac{3}{4\pi}\right)^{1/3} V_{B2}^{1/3} A_2^2 \quad \ldots 3.53$$

Likewise, as stated under the solutions for the operational stage 1, the determined bubble sizes or volume at this stage are different from those at other stages. Since no drilling activity takes place during the flow check period, the same interval of the gas formation is exposed for the duration of the flow check. Hence, the gas inflow rate is constant, and could be higher than that at the end of stage 1 if the bottom-hole circulating pressure of the drilling fluid is lower than its hydrostatic pressure.

For consistency, the duration for the development of each gas bubble during stage 2 is taken as the time it requires to drill an inch interval of the gas formation.

Thus, with higher gas inflow rate for this stage, larger constant gas bubble is formed during each time interval.

3.6 Model Simulation, Results and Discussions

A base case data for the modeling was compiled from the literature[54,55,84,98], and published textbooks[50&88]. Furthermore, the surface pump ratings were extracted from a text book[50]. However, the frictional pressure loss in the surface equipment was neglected. **Table 3.1** displays the data used for this simulation.

Since the developed model requires estimation of the drilling fluid surface tension, which is usually not available in the literature, a simple capillary experiment using a capillary-like straw was conducted. Drilling fluid samples of various viscosities and components were prepared in the laboratory for the experiment. The intention was to obtain as many surface tension data as possible. There were difficulties in estimating the contact angles for low viscous water-based bentonite and polymer-based drilling fluids. However, experimental results for some other viscous drilling fluids were considered reasonable after comparing with the literature data[65]. **Table 3.2** shows the comparison and the selected surface tension (in bold) for the analyses.

3.6.1 Error Analysis of the Modeling

Due to the potential significant error that could result from any simulation procedure, an error analysis procedure was designed and incorporated in the modeling. The goal of the error analysis was to achieve the lowest possible absolute

Table 3.1 – Compiled base case data for modeling

Bottom Hole Assembly:					
Riser size	=	19	in. ID		
Casing Size	=	11	in. ID		
Drill pipe Size	=	5	in. OD		
Drill pipe Size	=	4.41	in. ID		
Drill Collars	=	8	in. OD		
Drill Collars	=	2.81	in. ID		
Bit diameter	=	9.875	ins.		
Bit nozzle sizes	=	12	/32 in x 3		
Total area of the three nozzles	=	0.33147	in^2		
Bit nozzles' discharge Coefficient, Cd	=	0.95	constant		
Choke Line	**=**	**3**	in. ID		
Maximum Surface Pump Horse power	=	1000	hp		
Drilling Fluid and Formation Properties:					
Mud Flow Rate	=	400	gpm		
Surface Pump discharge pressure	=	1620	psi		
Drilling Fluid density	=	8.4	ppg	= 61.4	lb/ft^3
Mud Plastic viscosity	=	24	cp		
Mud Yield Point	=	18	$lbf/100ft^2$		
Average velocity in drill pipe (DP)	=	8.4	ft/sec		
Average velocity in drill collars (DC)	=	20.7	ft/sec		
Average velocity through Nozzles	=	387.1	ft/sec		
Mud apparent viscosity for DP	=	87	cp		
Mud apparent viscosity for DC	=	40	cp		
Mud apparent viscosity for Bit Nozzles	=	24	cp		
Mud Surface tension, σ	=	1.30E-02	lb_f/ft		
Mud flowing Reynolds Number	=	3323	Inside DP		
Mud flowing Reynolds Number	=	11254	Inside DC		
Mud flowing Reynolds Number	=	139439	Nozzles' exit		
Friction Pressure loss in Drill pipe	=	376	psi		
Friction Pressure loss in Drill collars	=	151	psi		
Flowing BHP (FBHP)	=	4332	psi		
Formation Pressure	=	4600	psi		
Formation Permeability	=	300	md		
Formation Porosity	=	0.3	fraction		
Mud Hydrostatic Pressure	=	4368	psi		

Table 3.1 – Compiled Base Case Data for Modeling (contd.)

Temperature:			
Surface	*70 ^{o}F*	=	*530 ^{o}R*
Bottom hole	*180 ^{o}F*	=	*640 ^{o}R*
Hole Geometry - VERTICAL HOLE:			
Riser Length	1000 ft from surface		
Last Casing Shoe Depth	4000 ft from the mud line		
Open-Hole section	5000 ft from last Casing Shoe		
Drill Collars' Length	450 ft		
Time Required to drill h-ft of formation	0.033 hr		
Open-hole radius, r_w	4.938 ins.	=	0.411 ft
Penetration Rate	30 ft/hr		
Formation Fluid - GAS - properties:			
Viscosity of gas at 1 ATM	0.01244 cp		
Viscosity ratio	1.85		
Gas Viscosity, μ_g at 4600 psia & 180°F	0.023014 cp		
Gas gravity, $S.G_g$	0.6		
Gas Constant, R	10.7		
Gas pseudo-critical pressure	671 psia		
Gas pseudo-critical temp.	358 ^{o}R		
Gas pseudo-reduced pressure	6.85544		
Gas pseudo-reduced temperature	1.787709		
Gas Compressibility factor, z at 4600 psia	0.975		
Gas Density, ρ_g	11.98778 lb/ft^3		
dZ/dP slope at 4600 psia	7.27E-05 psi^{-1}		
Gas compressibility, C_g	0.000143 psi^{-1}		
Gas Formation Volume Factor, Bg	0.003838 ft^3/SCF		
Gas Formation Volume Factor, Bg	0.000684 bbl/SCF		

error for each of the iterative step. Achieving such lowest absolute iteration error determines the apparent gas bubble volume or size that satisfies the expressions at both sides of **Eq. 3.33** for each iterative step. This error analysis was designed for cumulative inches of each drilled formation interval.

Table 3.2 – Comparison of experimental and literature data for the surface tension

	Literature Data[65]		Capillary Test	
Density, lb_m/gal	8.33	10.4	8.4	**8.4**
Viscosity, cp	60	600	70	**24**
Surface Tension, lb_f/ft	2.40E-03	4.93E-03	3.51E-03	**0.0013**

Figures 3.3 and **3.4** show two example plots of error analysis obtained for the bubble volumes after drilling the first ¼ - and one-half foot (½ -ft) of the formation. These are semi-logarithmic plots of the absolute error from successive steps of iteration for each accumulated inches of the drilled intervals. The iterative steps by the computer program are designed in such a way that as long as the absolute error in the next step is lower than that of the preceding step, the iterative procedures continue. The apparent bubble size is recorded for a particular formation interval when the absolute error becomes minimal.

The iteration end-points or lowest absolute errors obtained for all the instances simulated were to the order of 10^{-2} in order to optimize the run-time for the computer program. Absolute error as low as to the order of 10^{-5} could be obtained after very long computer run-time. However, the improvements in the iterated bubble volumes

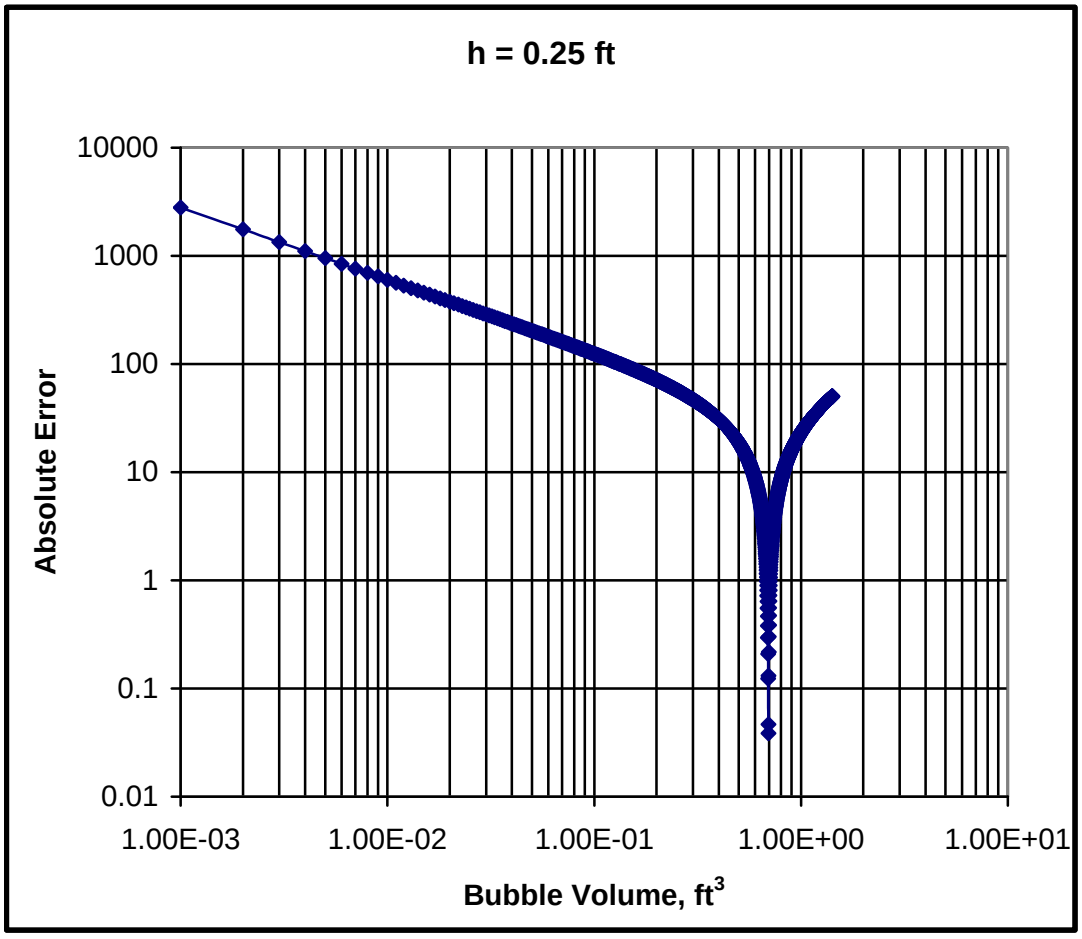

Fig. 3.3 – Example of error analysis plot for bubble volume prediction at formation interval, h =3 inches

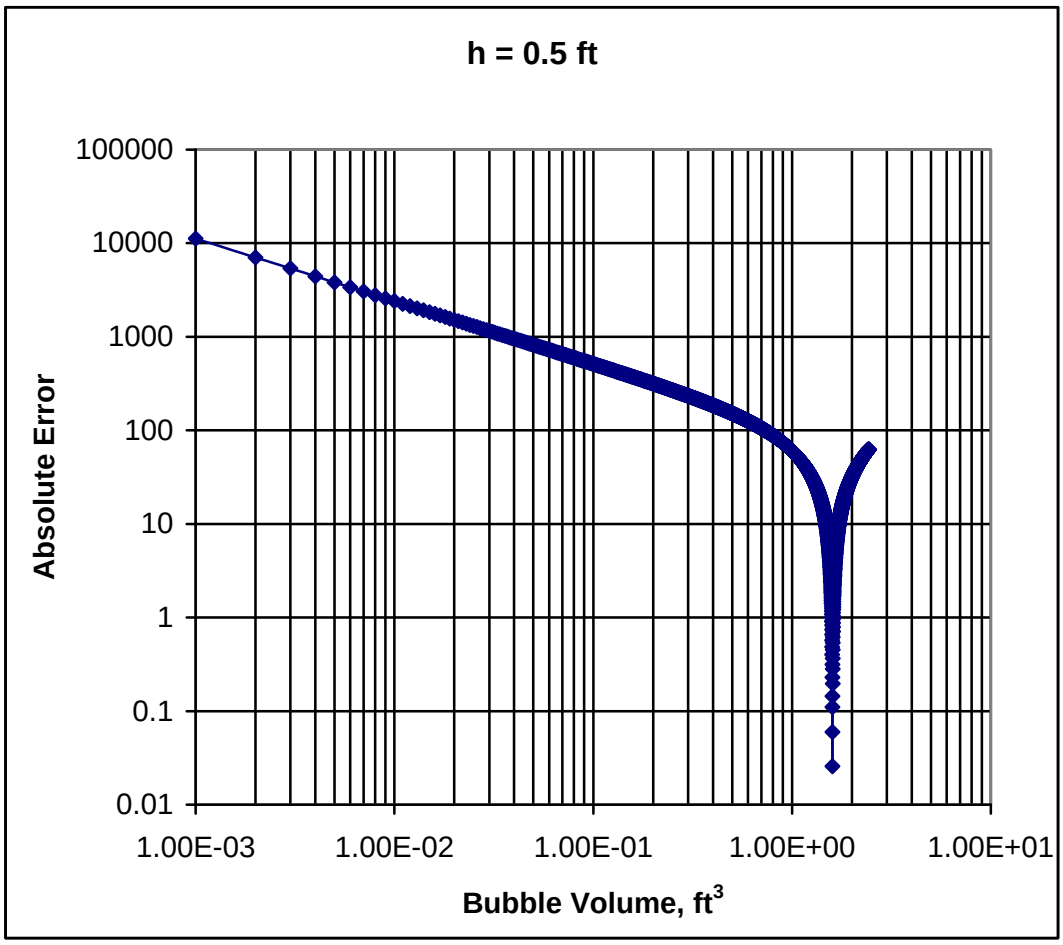

Fig. 3.4 – Example of error analysis plot for bubble volume prediction at formation interval, h = 6 inches

are extremely low, which do not justify the enormous run-time used by the computer program.

3.6.2 Apparent Bubble Size Profile at Instant of Gas Inflow

As explained in Chapter 2, the estimates of bubble sizes provided in this study are referred to as apparent bubble sizes because of the complexity in determining the sizes of series of gas bubbles that enter the annulus after drilling a formation interval. These series of gas bubbles are generated as a result of the turbulent action of the circulating drilling fluid. Instead, for a particular drilled gas formation interval, all these various sizes of bubbles are lumped together to form a single spherical bubble of an apparent size equaling the summation of all the sizes of these series of bubbles. All of the bubble size analyses are conducted at the wellbore-sand face contact.

Figures 3.5 and **3.6** show that with continuous drilling, the apparent gas bubble sizes, being released into the annulus, increases polynomially. The drop in the apparent bubble size at the end of the polynomial trend in **Fig. 3.5** is due to the change from the drilling operational stage to the flow-check stage, which is characterized by the higher mud hydrostatic pressure during the flow check period than the bottom-hole mud circulating pressure during the actual drilling periods. For comparison sake, the simulation results for higher bottom-hole circulating pressure than the mud hydrostatic pressure are presented in Chapter 4. **Figure 3.7** shows the cumulative mud pit volume gain, which is equivalent to the total volume of all the gas bubbles that entered the annulus during the drilling and flow check periods (stages 1 and 2).

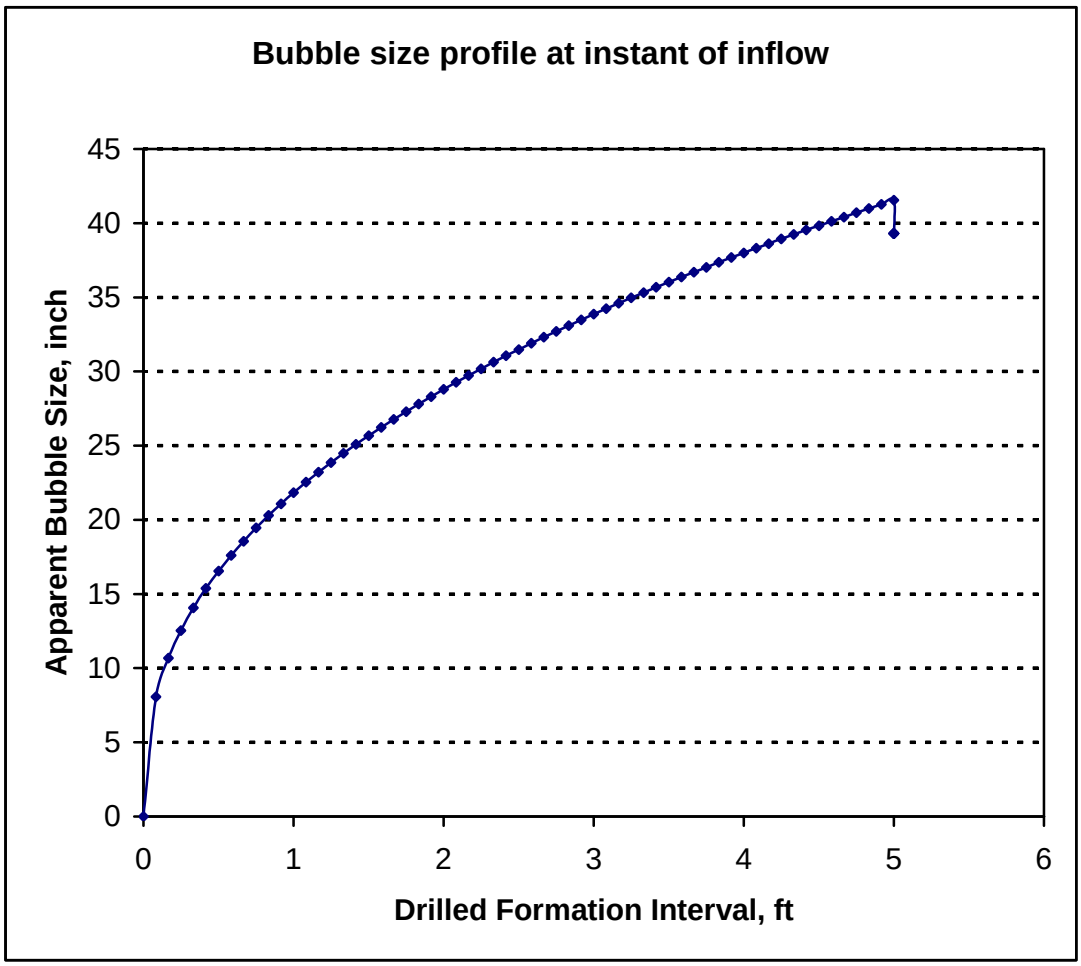

Fig. 3.5 – Apparent bubble size distributions for the base case data during drilling and flow-check periods

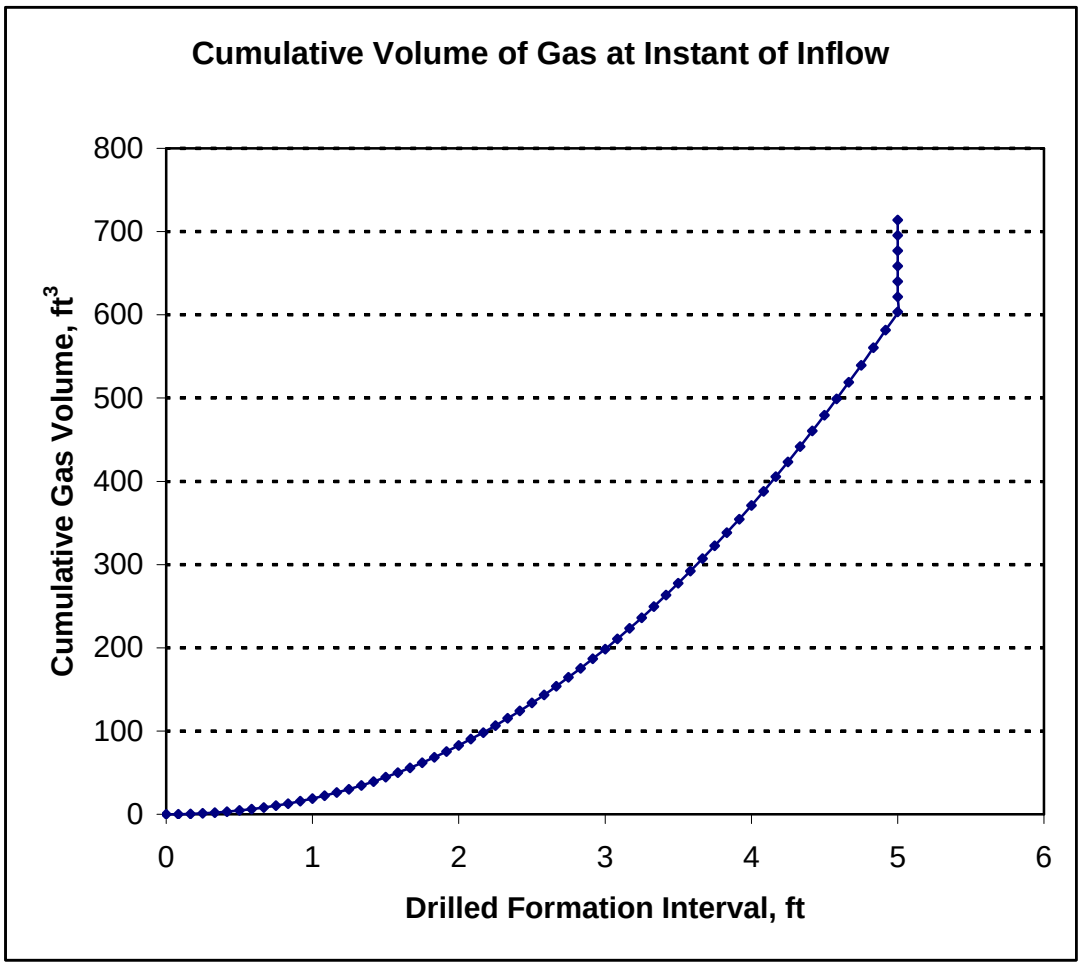

Fig. 3.6 – Annular cumulative gas volume during drilling and flow-check periods

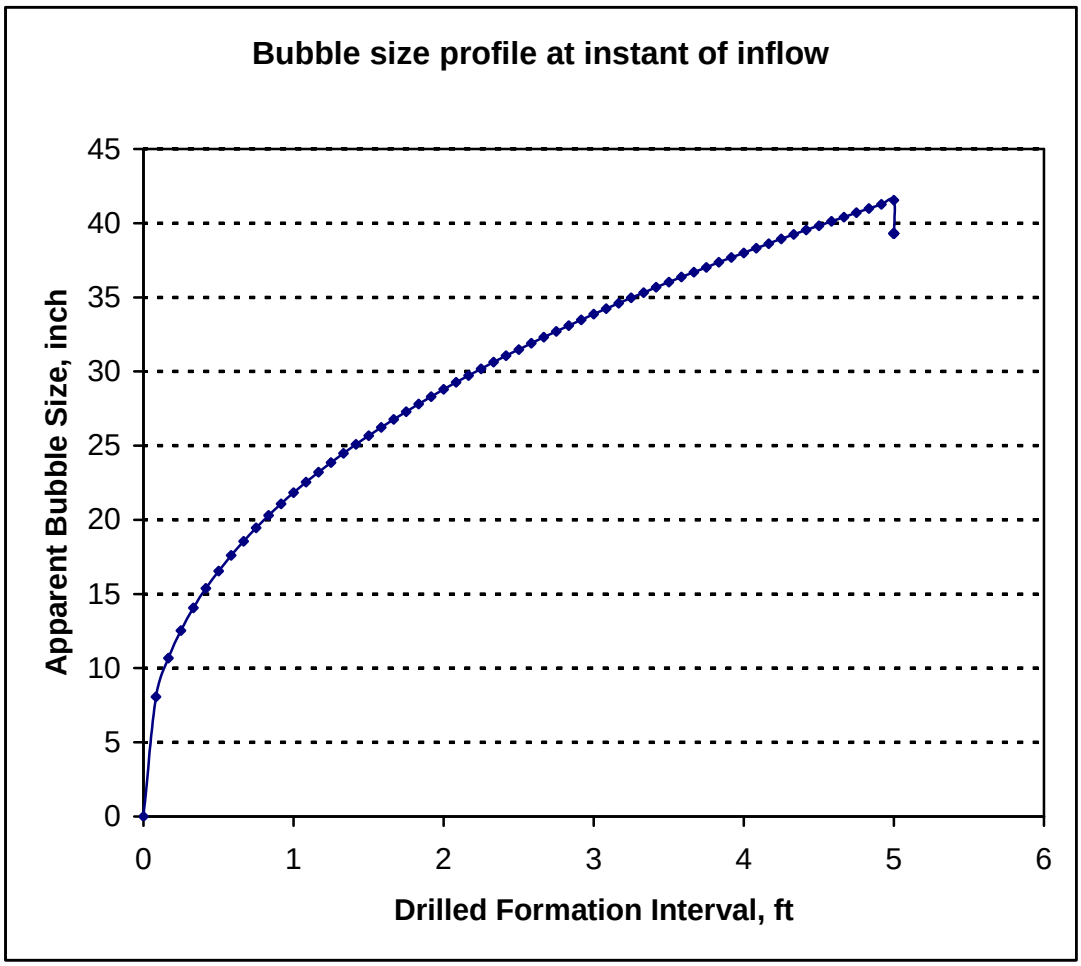

Fig. 3.7 – Rate of mud gain at the surface mud pit during drilling and flow-check periods

3.6.3 Effect of Porosity

The effects of porosity were investigated by considering two porosity values of 0.05 and 0.5. **Figure 3.8** presents the apparent bubble size profile for these two porosity values. Similar trend of polynomial increase in the bubble size is observed for both porosity values as the gas formation interval increases. At each gas formation interval, the cumulative plot for all the apparent bubble volumes that had entered the annulus is presented in **Fig. 3.9** for each porosity value. Due to the large-scale interval on the cumulative bubble volume axis, little effect of the porosity could be seen. However, when the plot scale interval is reduced for the later sections of these plots, as shown in **Fig. 3.10**, obvious differences in the plots could be seen for the two gas formation permeability cases. With all other reservoir and wellbore properties held constant, **Fig. 3.10** shows that the quantitative production, at the sand face, from a less porous reservoir is greater than that from a more porous reservoir. Also, the magnitudes of the differences in the volumetric production increase with increase in the permeability. These results are based on the same period of production, and the same pressure differential between the wellbore and the reservoir pressures.

A possible explanation for these analytical results could be due to the difference in the matrix volume or quantity in the two porous gas formations with different porosity values. For gas formations of equal gross thickness, higher porosity gas formations, undoubtedly, have more matrix fractional volume than lower porosity gas formations. Hence, for a gas formation without any external pressure replenishment, such a strong water aquifer, any pressure relief would cause the larger matrix of the less porous formation to undergo more displacement or re-arrangement.

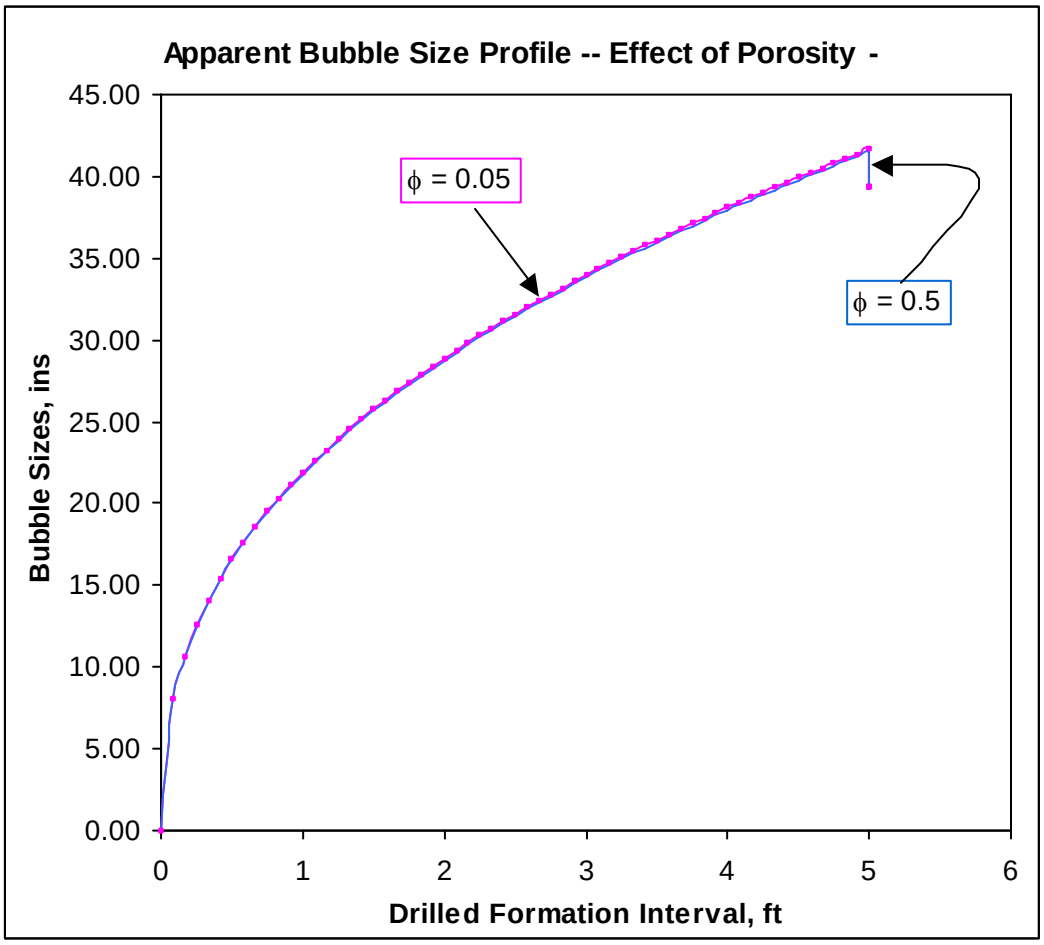

Fig. 3.8 – Effect of porosity on the apparent bubble size profile for stages 1 and 2

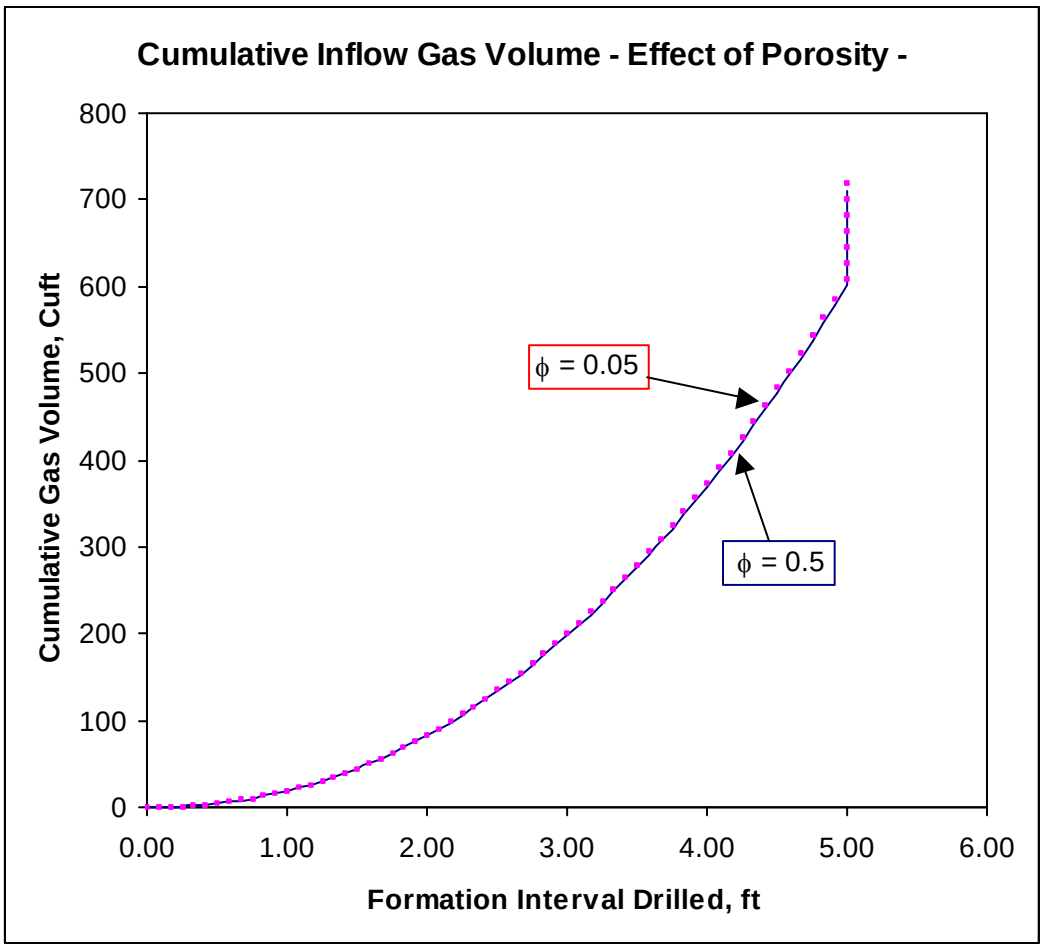

Fig. 3.9 – Effect of porosity on the cumulative inflow gas volume during stages 1 and 2

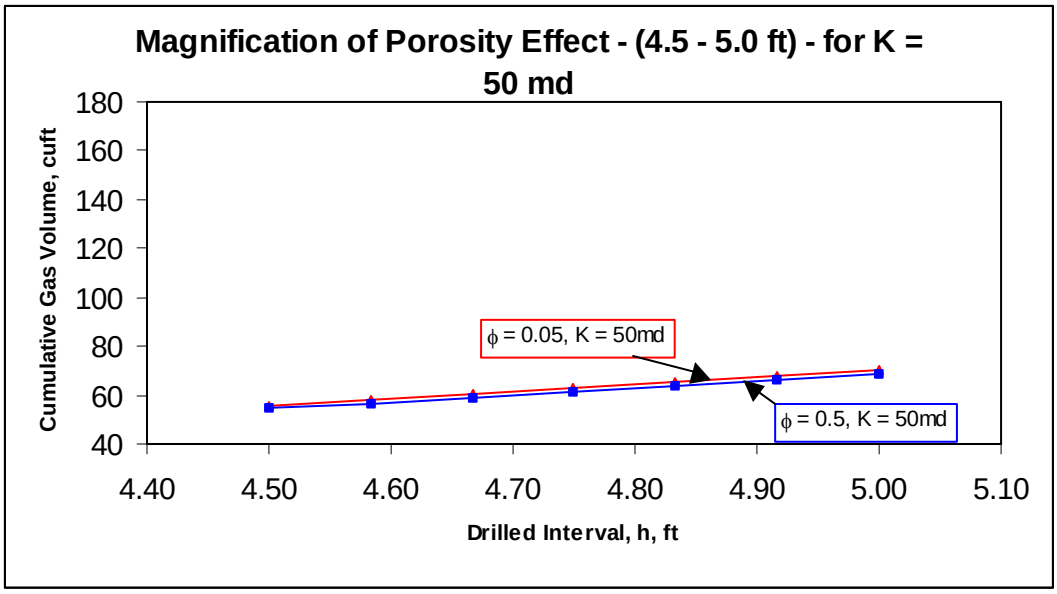

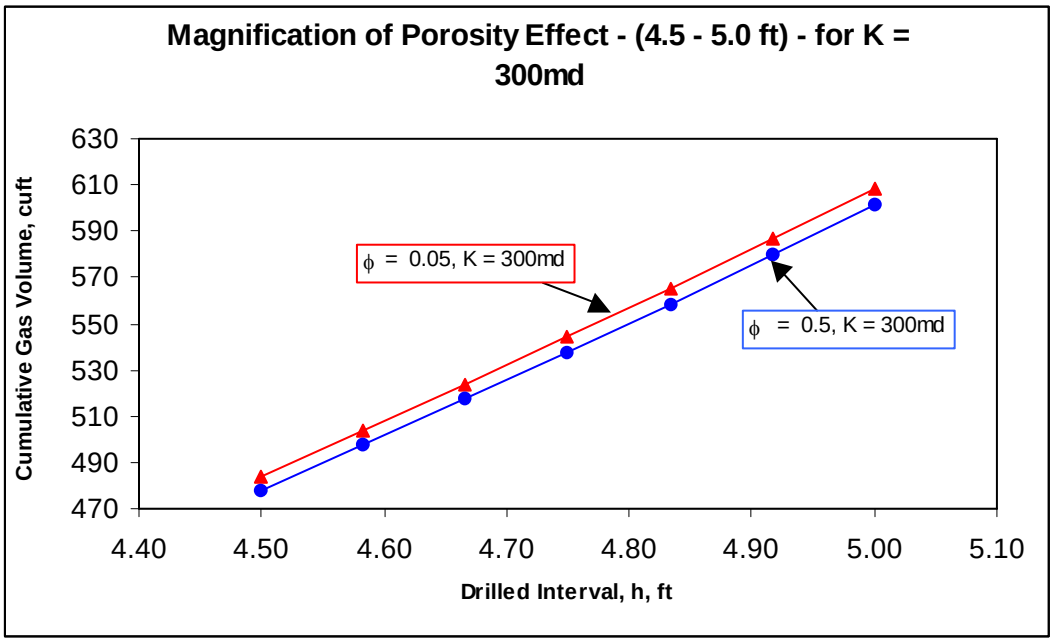

Fig. 3.10 – Magnified porosity effect on the cumulative inflow gas volume at greater drilled interval for stage 1

This is necessary to compensate for the decline in the magnitude of the reservoir fluid pressure. Such re-arrangement would cause pore space compression by the matrix, and thus, reduction in pore volume would result. Therefore, the greater the pore space compression, the greater the reservoir fluids expulsion from the reservoir. By these simulation results, a gas formation with significant variation in the in-situ porosity values may experience severe in-situ pore space reduction at its local sections with lower porosity values. This effect could also trigger increasing permeability impairment, and hence, limit the ultimate recovery from such gas formation.

To support these simulation results, Newman[129] conducted series of experiments on consolidated, friable, limestone and unconsolidated reservoir rocks to study the impact of initial porosity on the pore-volume compressibility. A total of 256 samples of sandstone and limestone from 40 reservoirs were used for the experiment. **Figure 3.11** shows the experimental results for the consolidated reservoir rocks. The class averages of these rock properties for the rock types are reproduced in **Fig. 3.12**. These experimental results show that the fractional reduction in pore volume increases with decreasing initial porosity as fluids are produced. This, thus, experimentally agrees with the presented analytical results by the present theoretical study.

3.6.4 Effect of Formation Radial Permeability

The physical meaning of formation permeability is the ease at which fluids flow through a porous medium. Therefore, for a higher permeability medium, a higher rate of fluid flow through the porous medium is expected. So, it is not

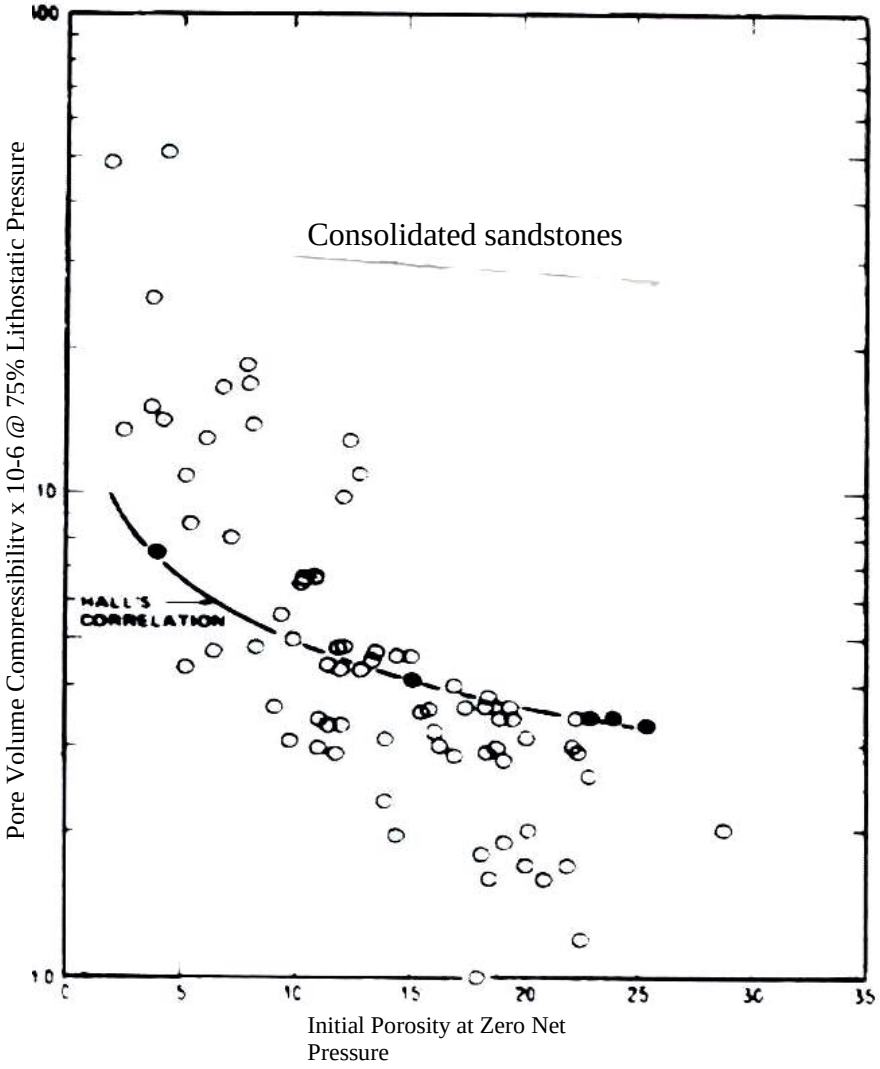

Fig. 3.11 – Experimental determination of the effects of pore volume compressibility on the initial porosity of consolidated sandstones[129]

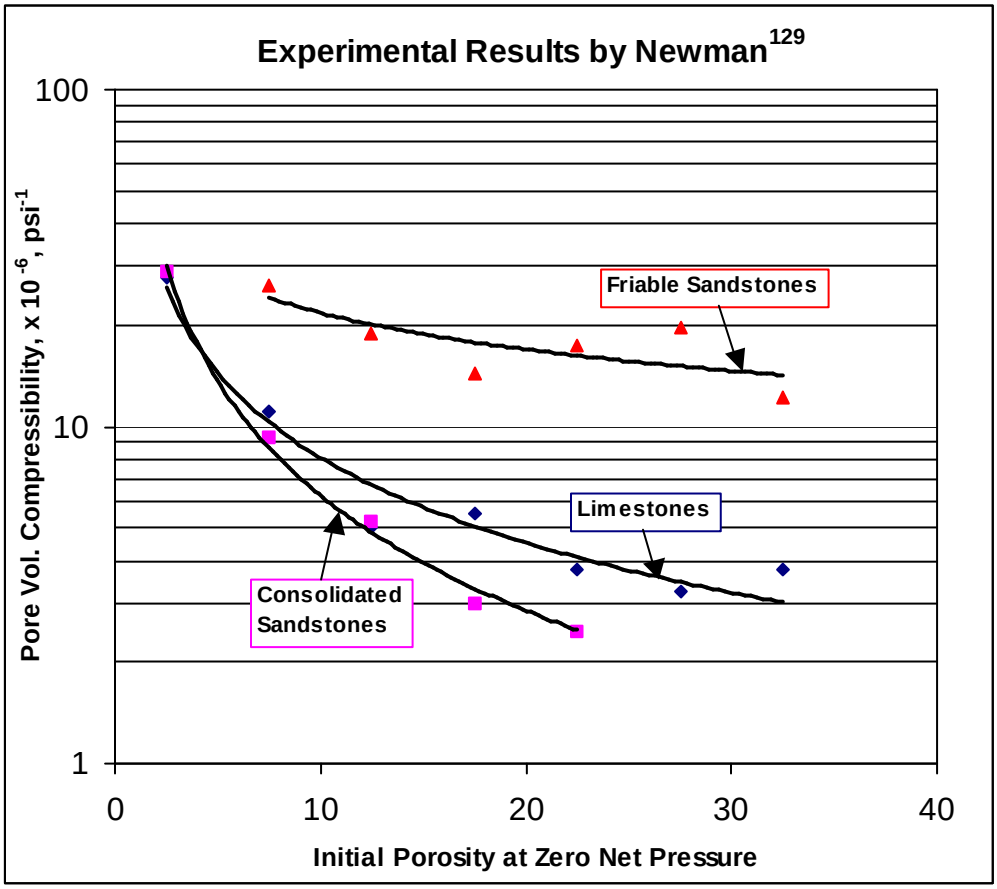

Fig. 3.12 – Class averages of the rock properties for the various rock types

surprising that increase in apparent bubble sizes at the wellbore-sand face contact, and increase in the surface mud pit volume are predicted as the reservoir permeability increases in **Figs. 3.13** through **3.15**.

A closer look at **Fig. 3.13** indicates that there is a comparison between the apparent bubble sizes during the flow-check stage (stage 2) for all the permeability values considered. For all of these permeability values, smaller bubble size occurs during the flow- check stage due to a higher bottom hole pressure – mud hydrostatic pressure – than the bottom-hole circulating pressure when drilling and circulating the mud (stage 1). Interestingly, the magnitude of the decrease in gas bubble size is directly proportional to the magnitude of the permeability. That is, higher permeability resulted in higher drop in apparent bubble size during the flow-check stage.

A possible explanation for such analytical observation could be due to the fact that for higher permeability formation, the greater pressure impulse of the hydrostatic pressure travels faster into the gas formation to alleviate the rate of gas inflow. For the considered permeability cases of 50-md, 300-md and 400-md permeability the resulting drop in the apparent bubble sizes are 1.09-inches, 2.24-inches and 2.52-inches respectively. An agreement to these results is provided in Chapter 4 during wellbore pressure rises or buildup while shutting-in on the gas inflow.

3.6.5 Effect of Permeability Heterogeneity

The effect of directional variation of permeability in the vertical and radial directions on the apparent gas bubble sizes is introduced into the modeling by

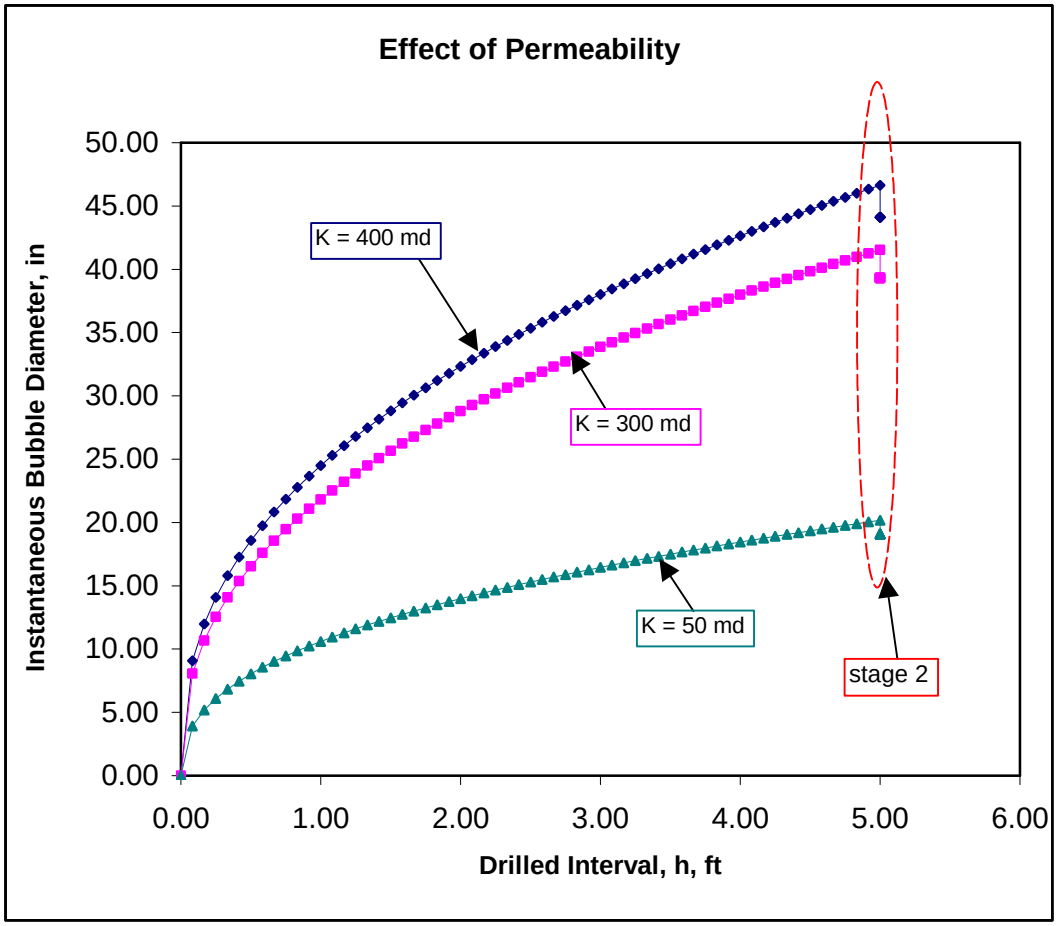

Fig. 3.13 – Effect of permeability on bubble size profile for stages 1 and 2

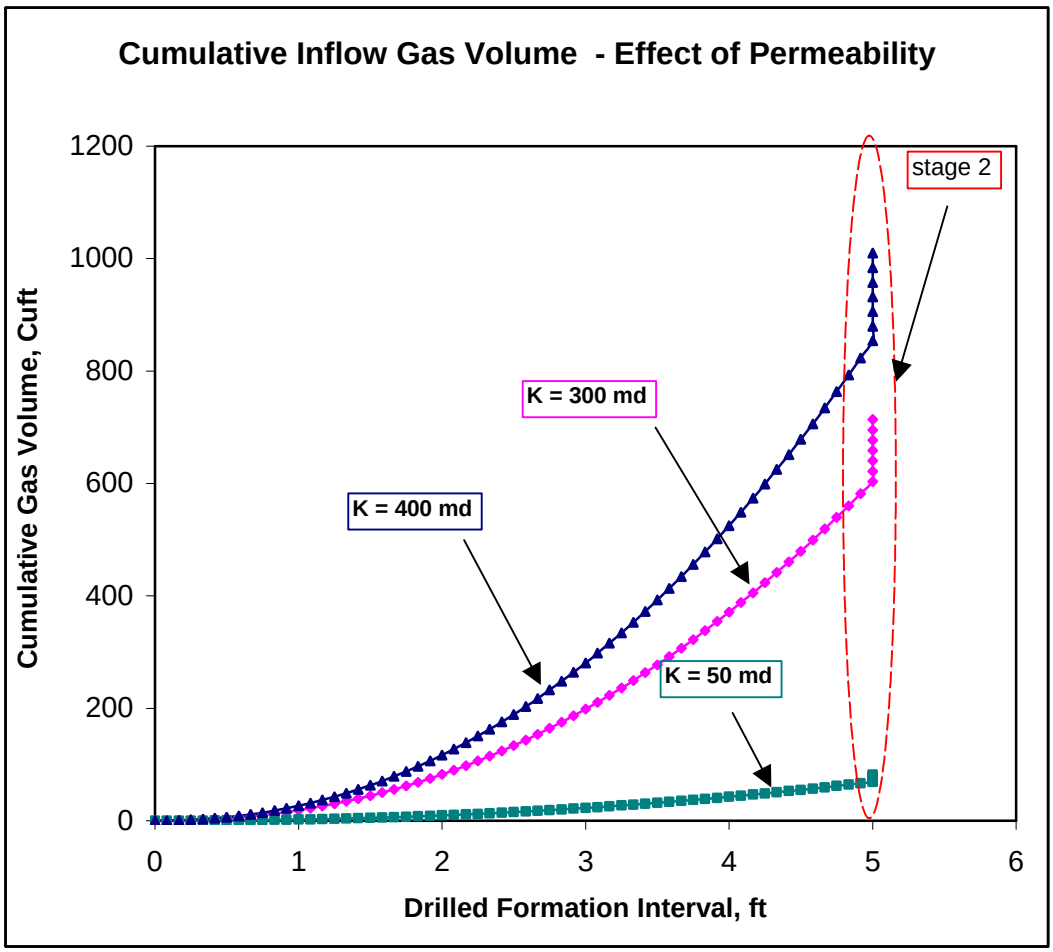

Fig. 3.14 – Effect of permeability on cumulative inflow gas volume during stages 1 and 2

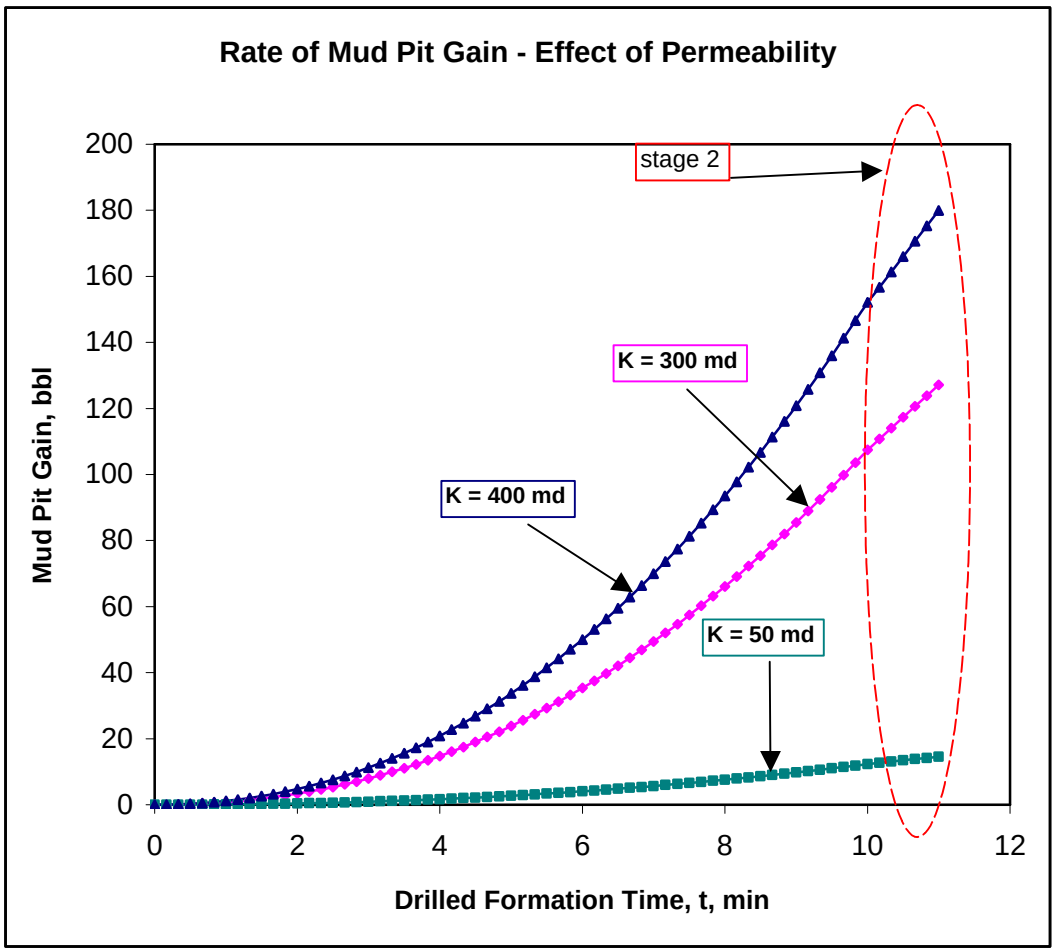

Fig. 3.15 – Effect of permeability on the rate of increase in the surface mud pit volume during stages 1 and 2

considering five permeability anisotropic ratios of 1.0, 1.5, 2.0, 4.0, 8.0. The anisotropic ratio is represented in this study as the effective permeability for a heterogeneous porous medium, and is given as:[131, 139]

$$K_{eff} = \sqrt{\frac{k_r}{k_v}} \qquad \ldots 3.54$$

Where, K_{eff} represents the effective permeability of the gas formation, k_r and k_v are the radial and vertical permeabilities respectively. This effective permeability is used to replace the average permeability term k in the gas bubbly model in equation 3.33.

Figure 3.16 shows the simulation results for the five anisotropic ratios. The figure indicates that there is increase in the apparent bubble sizes as the formation interval increases for all the anisotropy ratios. However, for $K_{eff} \leq 2.0$, which signify higher vertical flow, there is instability in the apparent gas bubble sizes that inflow into the wellbore at lower gas formation intervals. This probably indicates that the gas flow in the vertical direction affects the radial gas flow into the wellbore at drilled formation interval less than 1-ft. However, as the effective permeability increases for any drilled formation interval, which indicates lesser influences of vertical flow, the instability in the apparent gas bubble subsides. These results buttress the suggestion of using a hemispherical flow model to analyze the apparent bubble sizes for small drilled intervals of high vertical permeability gas sands.

3.6.6 Effect of Drag Forces on Apparent Bubble Sizes

During the bubble development, it is assumed that the instantaneous growth

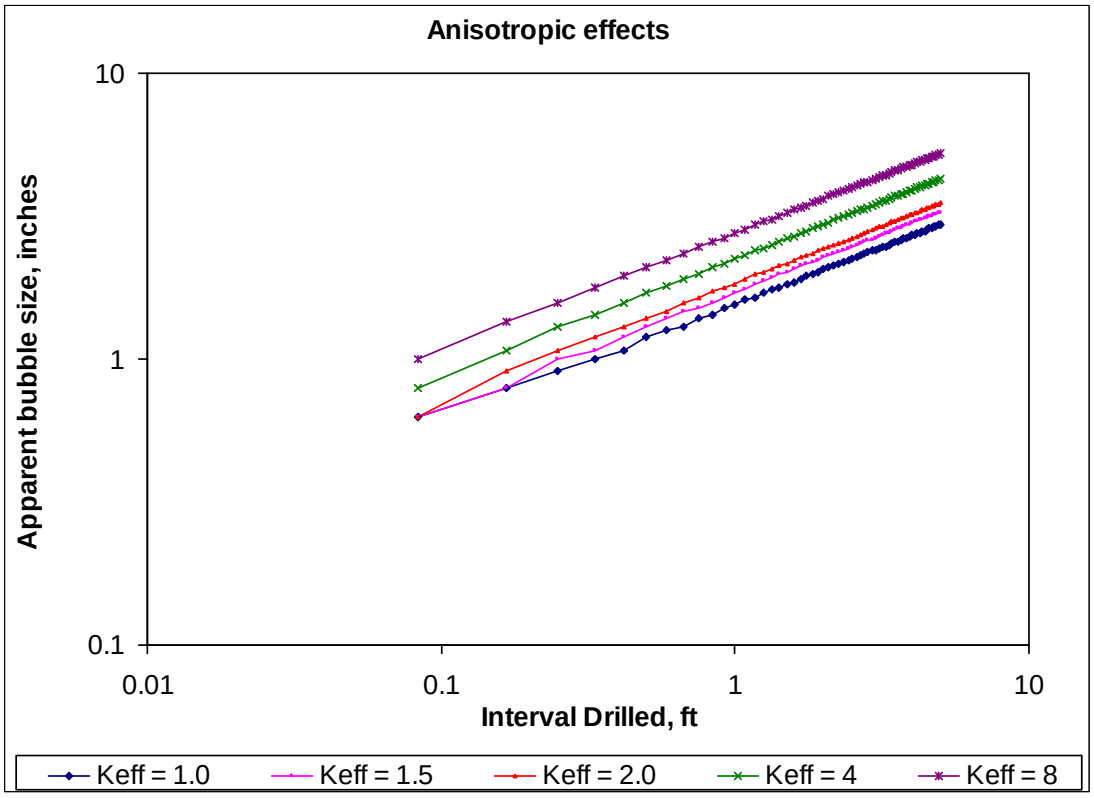

Fig. 3.16 – Effect of permeability anisotropy on apparent bubble size

of the bubble is as a result of laminar flow of gas into an enclosure that eventually form a bubble. The bubble growth is opposed by the viscosity of the drilling fluid surrounding the growing bubble, hence, a viscous drag or force due to the drilling fluid viscosity must be overcome for gas bubble to continue growing.

There are two basic types of viscous forces. These are the pressure or form drag and the friction drag. The derivations of these forces are given in **appendix A**. The form and the friction viscous forces are respectively given as:[141]

$$F_D = 3\pi\mu\upsilon D = 6\pi\mu\upsilon r \quad \ldots 3.55$$

$$F_D = 12\pi\mu\upsilon D = 24\pi\mu\upsilon \text{ r} \quad \ldots 3.56$$

Equation 3.55 which is generally referred to as the Stoke's law had been considered for modeling in this study rather than the friction viscous force since there is an opposing pressure to the bubble growth which acts on the maximum cross sectional area of the growing bubble perpendicularly. Instead of the used form viscous force, the friction viscous force was used in the model to ascertain its effect on the apparent bubble size. **Figure 3.17** shows no difference in the use of either of these viscous forces. This is not surprising because the forces introduced in this study only control the rate of growth of the gas bubbles, they do not control the size of the gas bubble.

3.6.7 Mud Plastic Viscosity

In order to investigate the influence of mud viscosity on the apparent gas bubble size profile, three mud plastic viscosity values were chosen. These values (15, 24-, and 33-cp plastic viscosities) are within the range of practical mud plastic viscosity. **Figure 3.18** shows the apparent gas bubble size profile for these mud

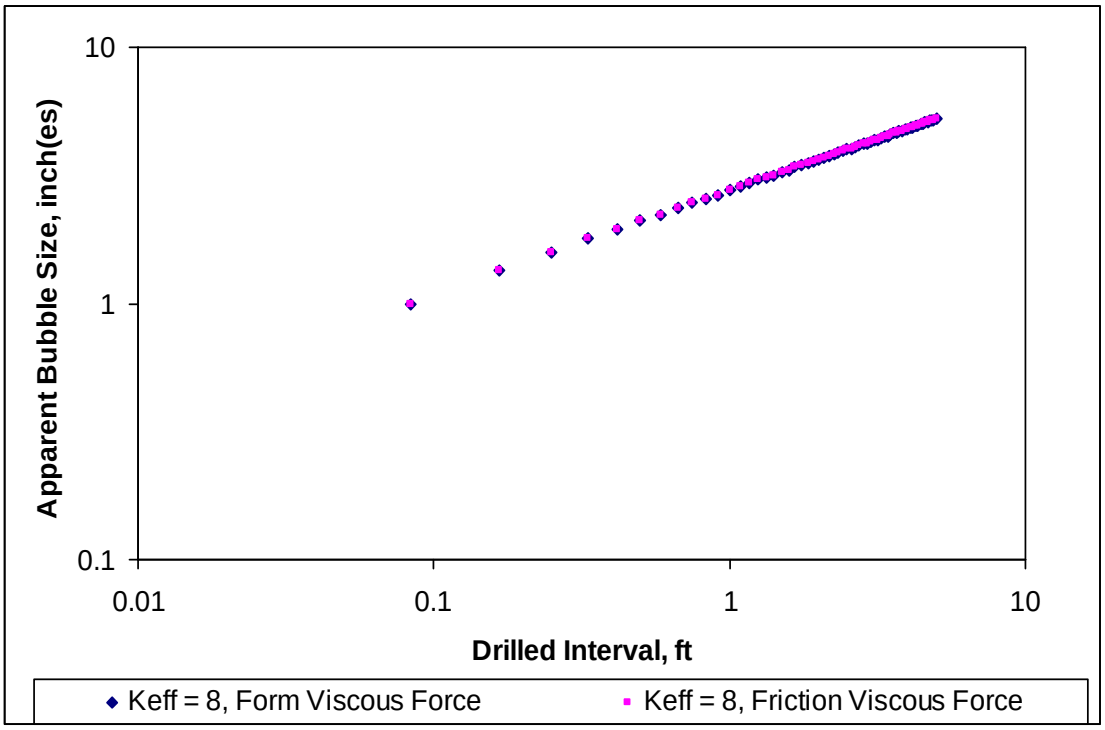

Fig. 3.17 – Effect of viscous forces on apparent bubble sizes

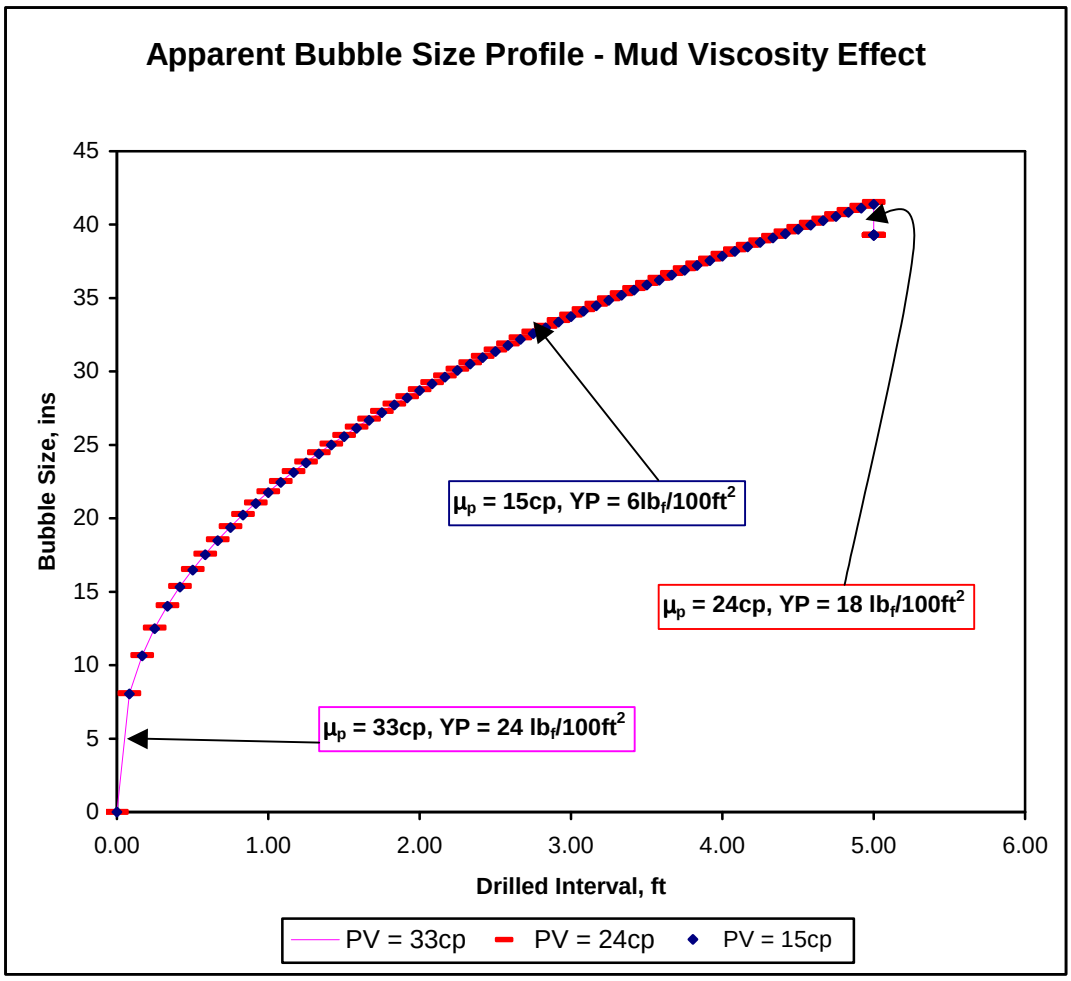

Fig. 3.18 – Effect of mud plastic viscosity on bubble size profile

plastic viscosity values. Little to no increases in the apparent sizes of the gas bubbles are observed with increasing mud plastic viscosities for increasing formation intervals. This is because the stabilizing effect of a viscous fluid on the size of gas bubble that could be allowed to form is not pronounced within the chosen viscosity range. However, for highly viscous fluids, with the viscosity values in hundreds, notable increases in the bubble sizes with increasing fluid viscosities have been experimentally presented by Johnson and White[88], Otake et al[109], and Satyanarayan et al[65]. **Table 3.3** presents slight increases in the apparent gas bubble sizes as the viscosity increases, which theoretically agree with such literature experimental results.

Table 3.3 – Viscous stabilizing effect on the apparent bubble sizes

Drilled Form. Interval, h, ft	Bubble Vol., cuft	Bubble Size (dia.), ins	Drill Time t, minutes	Cum. Gas Volume, cuft	Cum Gas Volume, SCF	Cum Pit gain, bbl
Mud Plastic Viscosity = 15cp						
0	0.00	0.00	0	0	0	0
1	3.12	21.74	2	18.6	4838.9	3.3
2	7.16	28.69	4	81.7	21280.5	14.5
3	11.64	33.74	6	196.3	51155.1	35.0
4	16.44	37.85	8	366.9	95605.6	65.4
5	21.48	41.39	10	596.7	155494.3	106.3
Mud Plastic Viscosity = 33cp						
0	0.00	0.00	0	0	0	0
1	3.14	21.79	2	18.7	4870.2	3.3
2	7.20	28.75	4	82.2	21418.0	14.6
3	11.71	33.81	6	197.6	51486.1	35.2
4	16.54	37.94	8	369.3	96223.7	65.8
5	21.62	41.48	10	600.6	156499.1	107.0

3.6.8 Effect of Rate of Penetration

The effect of the changes in rate of penetration, ROP, from 30 ft/hr to 50 ft/hr on the apparent gas bubble sizes is not apparent as shown in **Fig. 3.19**. This is because irrespective of the rate of drilling a certain formation interval, the same rate of gas inflow is obtained due to the equally drilled formation interval. However, the required drill time for the same formation interval decreases with increase in the ROP. **Figure 3.20** indicates that a 50-ft/hr ROP drills a formation interval of 5-ft faster than 30-ft/hr ROP. This causes the inflow of larger gas bubble sizes for the 50-ft/hr ROP than those for the 30-ft/hr ROP as the drill time increases. Hence, the same maximum mud pit gain is achieved faster with 50-ft/hr ROP than with 30-ft/hr ROP, as shown in **Fig. 3.21**.

3.7 Summary

In summary, theoretically and experimentally proven forces that control the formation of bubbles have been employed to adequately establish the various gas bubble size profiles that possibly inflow into the annulus when underbalanced condition exists at the bottom-hole of a wellbore. Two stages of gas inflow have been analyzed. These stages are the stage 1 – when simultaneous drilling and mud circulating are embarked upon, and stage 2 – when drilling and mud circulation are suspended to check for mud outflow from the annulus. From the previously presented analyses of the simulation results, the following are new findings:

During the opened wellbore stages (stages 1 and 2), increase in permeability of gas formations causes increase in the apparent bubble sizes/volumes under the

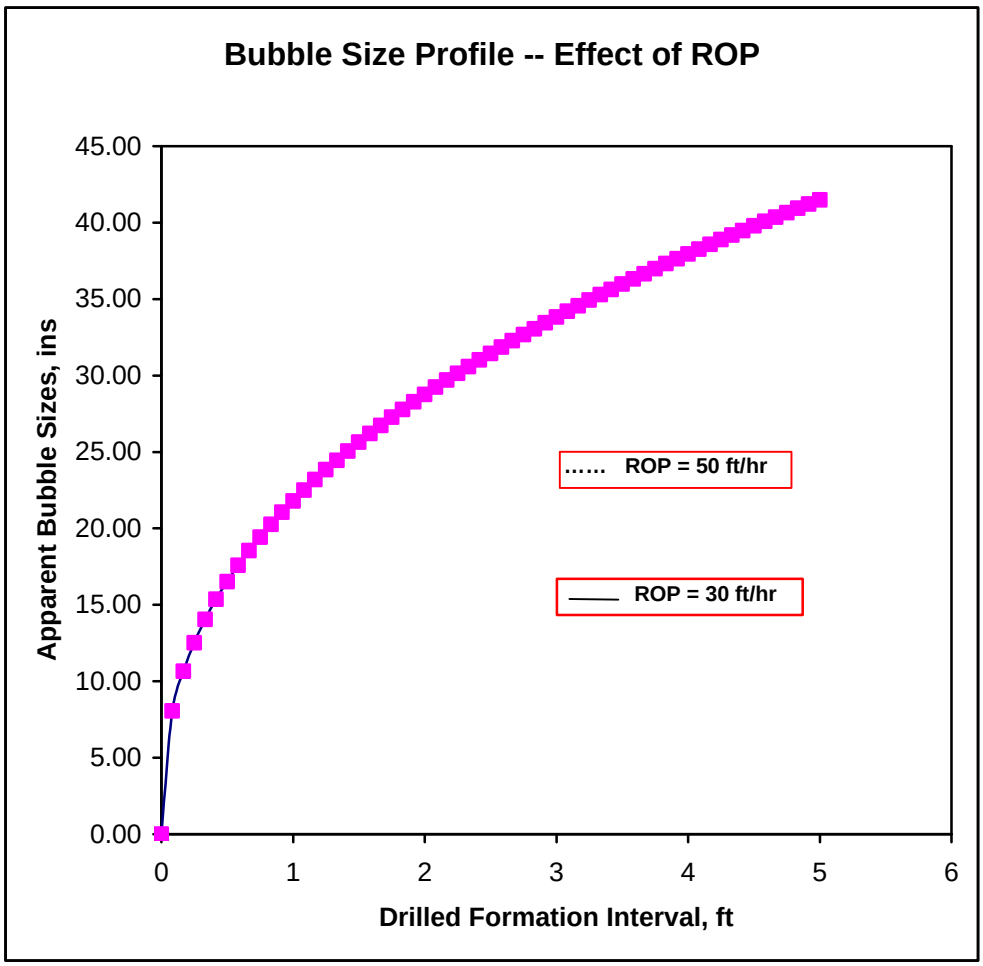

Fig. 3.19 – Effect of ROP on the apparent gas bubble sizes

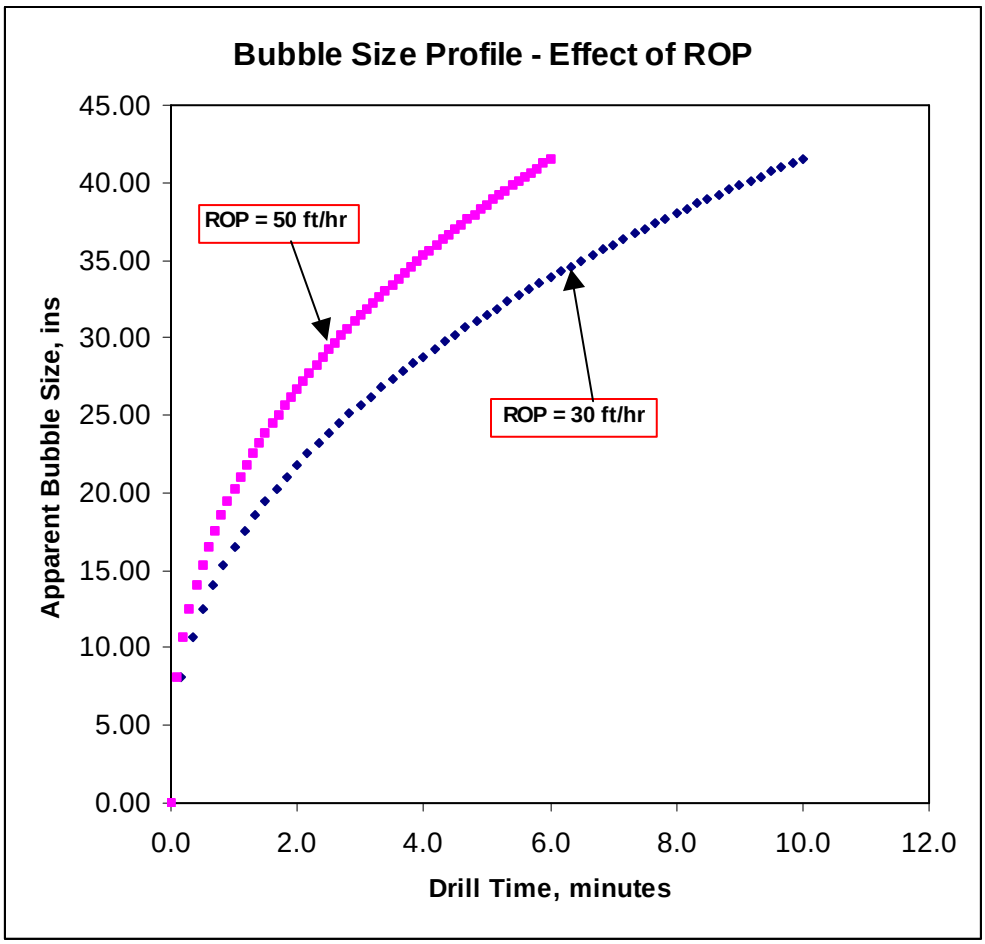

Fig. 3.20 – Rate of change in the apparent gas bubble sizes at different rates of penetration

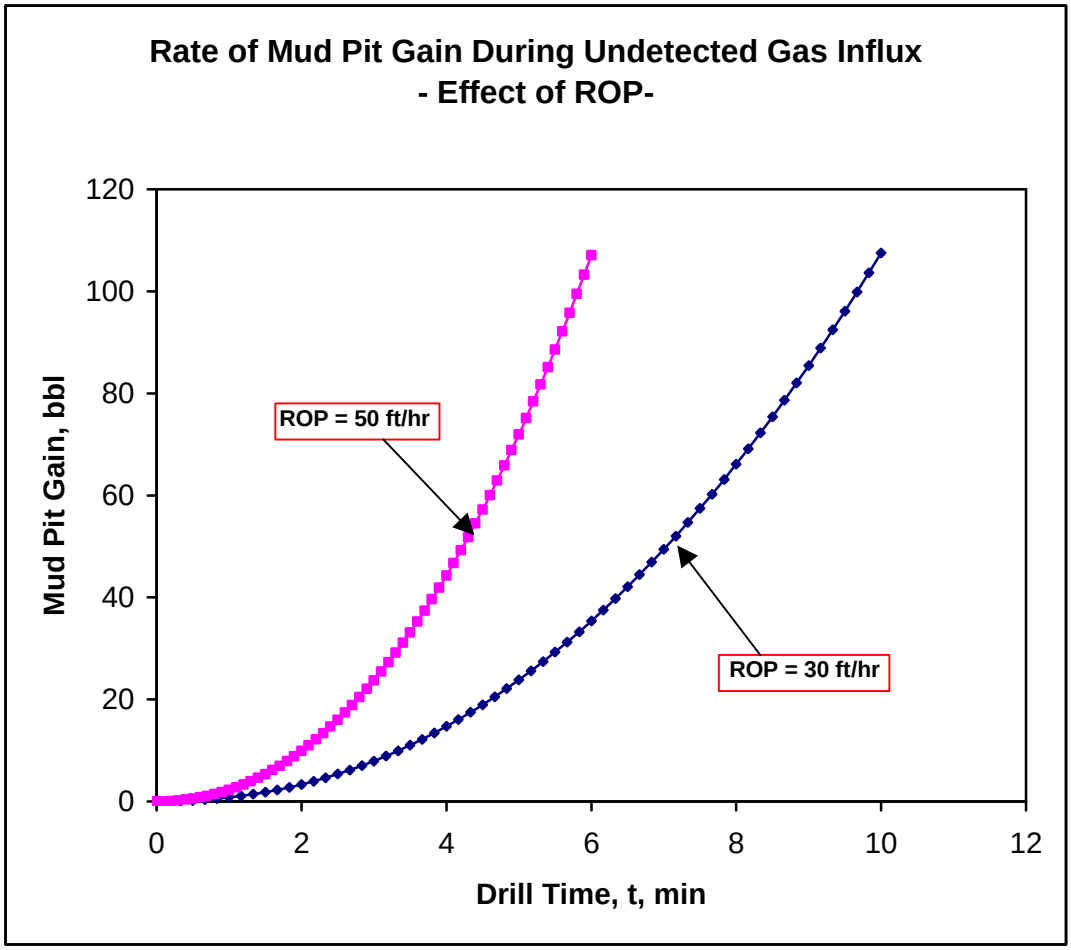

Fig. 3.21 –Rate of change in mud pit volume for different ROPs

same conditions of drilling, and of the same other reservoir properties. Consequently, there is increase in the rate at which the surface mud pit rises during these stages.

Also, increase in permeability has been shown to promote traces of higher rate of backpressure transmission from the wellbore into the gas formation when the wellbore or bottom hole pressure becomes greater than its previous magnitude. Therefore, under this condition, increase in permeability would indicate increasing reduction in the gas inflow rate. More discussions on this finding will be provided in Chapter 4.

Introduction of permeability anisotropy into the modeling procedures has shown that gas inflow into a wellbore of ≤ 1-ft partial penetration under the conditions stipulated for analysis in this study is hemispherical rather than the usual radial flow assumption by some authors of gas kick analysis.

Porosity effect on gas production is not apparent at smaller drilled formation interval range. However, at greater formation interval, cumulative gas production showed that gas formation with lower porosity would produce more cumulative gas volume than formation with higher porosity due to the greater pore space compression by the greater matrix volume in lower porosity gas formation. Also, with increasing gas formation permeability, there is increasing cumulative gas production from a low porosity gas formation than for a higher porosity gas formation. Agreement with these simulation results, and series of published experimental results on the influence of pore volume compressibility on the initial porosity of various rock types was provided. Therefore, for a gas formation with significant variation in its in-situ local porosities, variations in the porosity damages could result. This effect could

also trigger increasing permeability impairment, and hence, limit the ultimate recovery from such gas formation.

Furthermore, it was theoretically confirmed that the viscosity stabilizing effect would cause larger apparent gas bubble size in highly viscous fluid than in less viscous fluid. However, due to the lower range of practical viscosity values used in drilling operations, insignificant differences in the bubble sizes were obtained for such small viscosity range.

CHAPTER FOUR

MODELING OF WELLBORE STORAGE EFFECTS ON ANNULAR PRESSURE ANALYSIS OF A GAS-KICK WELL

4.1 Introduction

As mentioned in the preceding chapters, the concluding stage of evaluating gas inflow, before any control procedure is embarked upon, is the shut-in of the wellbore. Shutting-in a wellbore on a gas kick provides an opportunity to evaluate the pressure of the formation penetrated. However, in practice, the most valuable shut-in information that determines the success of any gas kick control are the surface instantaneous shut-in drill pipe and shut-in casing or annular pressures.

To adequately prevent further gas inflow, on-site analysis of these surface pressure rises is crucial in estimating the additional mud weight needed for control. All of the currently existing models for such analysis are based on gas bubble velocity approach. Gas velocity is primary in estimating the upward distance traveled by the gas bubbles. However, to satisfactorily approach the wellbore pressure build-up through gas velocity concept, an excellent knowledge of the contributions from all the existing gas bubbles or distribution patterns must be ascertained. It is also necessary to know the status (such as their depths, and volumes attained) of every gas bubbles at the closure of the wellbore for pressure build-up. All of these, coupled with the negligible influence that bubble migration has on the pressure build-up, point to the

fact that it is practically inappropriate to consider gas bubble velocity as the sole parameter responsible for any pressure build-up.

Regrettably, all of the currently existing studies[58-62,72,82&92] on the pressure build-up during shut-in of a gas kick have undoubtedly analyzed wellbore pressure buildup as a consequence of gas bubble velocity or upward migration. Definitely, it is agreed that upward gas migration does exist during shut-in due to buoyancy effect. However, it could not single-handedly be responsible for the pressure build-up in a gas containing system, where gas compressibility could play a significant, if not dominant, role. Moreover, the gas velocity expressions used in the current gas kick analyses are usually based on one or more of the many correlations for air bubble velocity in water. From Stokes' theories,[114] it is crystal clear that the performances of differently sized gas bubbles in air/water systems are different from those existing in viscous fluids such as drilling fluid.

Due to the established influence of wellbore storage effect on the pressure rise as explained in Chapter 2, the primary objective of the present chapter is to implement the wellbore storage concept to analyzing pressure rise in the wellbore and at the surface when the well is shut-in.

4.2 Model Hypotheses and Description

4.2.1 Model Hypotheses

For the wellbore pressure buildup modeling, the following hypotheses have been adopted. Some of the following hypotheses are repetitions of those presented in Chapter 3.

1. Hole Geometry

- Vertical hole is considered, with the drill bit on bottom of hole.

2. Status of Fluid Phases

- The continuous phase, drilling mud, is static, while the dispersed phase, gas is allowed to migrate upward with no further expansion after well complete closure.
- Before shutting-in the well, the bubbles at the upper sections would have expanded, and, thus, would be more susceptible to compression. Such compression would cause reduction in the volume of these bubbles immediately at shut-in, and during the shut-in period. Conversely, bubbles at the vicinity of the bottom-hole would expand due to lower wellbore pressure than the reservoir pressure. However, at any shut-in time, all deformable bubbles would have same volume since they are all under the same imposed pressure from the reservoir.
- As a consequence of the above hypothesis, at and during shut-in, the densities of all the deformable gas bubbles are equal and subjected to equal instantaneous wellbore or bottom-hole pressure.
- The gas phase is considered highly compressible, and controls the rate at which the entire annular fluid system is compressed.
- The drilling mud is assumed incompressible.

3. Cuttings

- The effect of the weight of cuttings on the bottom-hole pressure is neglected.

- At and during shut-in, the bit nozzles are assumed unplugged by the drill cuttings.

4. Bubble Shape

- There are non-deformable discrete bubbles separating the larger bubbles. The separating discrete bubbles disallow the coalescence of the larger bubbles.
- A larger bubble takes the shape of a bent hot dog around the drill pipe

5. Other Hypotheses

- Isothermal condition is considered inside the annulus
- Shutting-in of the well is considered to take some finite time, and the time taken is assumed to be known
- Engineers' method of kick control is used

4.2.2. Model Description

Figures 4.1A to 4.1D schematically illustrate the description of the model during pressure build-up in the annulus after a well kick. For better understanding of the modeling procedure, three instantaneous periods of pressure build-up analysis are considered. The initial period is when the annular drilling fluid is contaminated by the gas inflow from the gas reservoir. The second period is viewed as instantaneous isolation of the pressurized annulus from the influences of reservoir forces. This period allows the deeper (recently released) gas bubbles into the wellbore to expand, and the already expanded shallower bubbles to contract their volumes. The final and third period involves the removal of the instantaneous isolation so that the annular fluid system can be pressurized by the reservoir again. Since the gas bubbles in the

annular fluid system are capable of further compression, this final period allows additional inflow of gas bubbles into the annulus. However, there is continuous decrease in subsequent gas bubbles released into the annulus at later periods. These periods continue in cyclic form until the gas bubbles in the annulus cannot be compressed anymore. The following are the detailed descriptions of these processes.

1. Before shut-in, the bubble sizes are as shown in **Fig. 4.1A**. That is, the shallower bubbles would have migrated upward and undergone expansion than the deeper bubbles. At shut-in, the time required to completely close the well must be noted. With the assumption of an instantaneous isolation of the wellbore from the gas formation immediately after shut-in, the highest pressure at the bottom hole would be the hydrostatic pressure of the drilling mud inside the drill pipe since the annulus contains the gas phase. Therefore, immediately at shut-in, the surface casing pressure and the annular fluid would respond to the annular pressurization by the hydrostatic pressure of drilling mud in the drill pipe as shown in **Fig. 4.1B**.
2. When the instantaneous isolation is relaxed, the gas formation would pressurize the fluids in the drill pipe and in the annulus. But because it is assumed that there is no gas inflow into the drill pipe, there would be no gaseous phase compression inside the drill pipe. Therefore, the surface drill pipe pressure would rise rapidly because of faster pressure transmission through much denser drilling fluid to balance the gas formation pressure at that side of the system. On the other hand, the surface casing pressure would rise slowly because the annular pressurization by the gas formation is slowed

down by presence of compressible gaseous phase. Such gas phase compression reduces the initial total annular volume occupied by the gas. Therefore, the pressurization by the formation would introduce an equivalent volume of gas bubble into the annulus to retain the initial annular volume of the gaseous phase at all times. By this action, the annular gas phase volume is kept constant with increased mass of the gaseous phase. This causes the gas density to correspondingly increase with time. Completion of these periods processes is shown in **Fig. 4.1B**.

3. Further reservoir pressurization on the annular fluid system causes continuous cyclic repetition of the three periods. These processes continue until the surface casing and the bottom hole or wellbore pressures stabilized, which is an indication that the bottom-hole pressure now equalizes the gas reservoir pressure. At this time, all of the gas bubbles would have been compressed to the same density as at the instant inflow of each gas bubble into the wellbore. Afterwards, no further pressurization or annular gas compression by the gas formation is allowed by the wellbore. Two cyclic repetitions of these processes, before pressure stabilization, are schematically presented in **Figs. 4.1C** and **4.1D**. It should be noted that the stabilized surface pressures are sometimes referred to as instantaneous drill pipe and casing pressures.

4.3. Model Development

This section discusses the development of the modeling steps of pressure variation in the wellbore of a gas kick well using the wellbore storage concept. Since

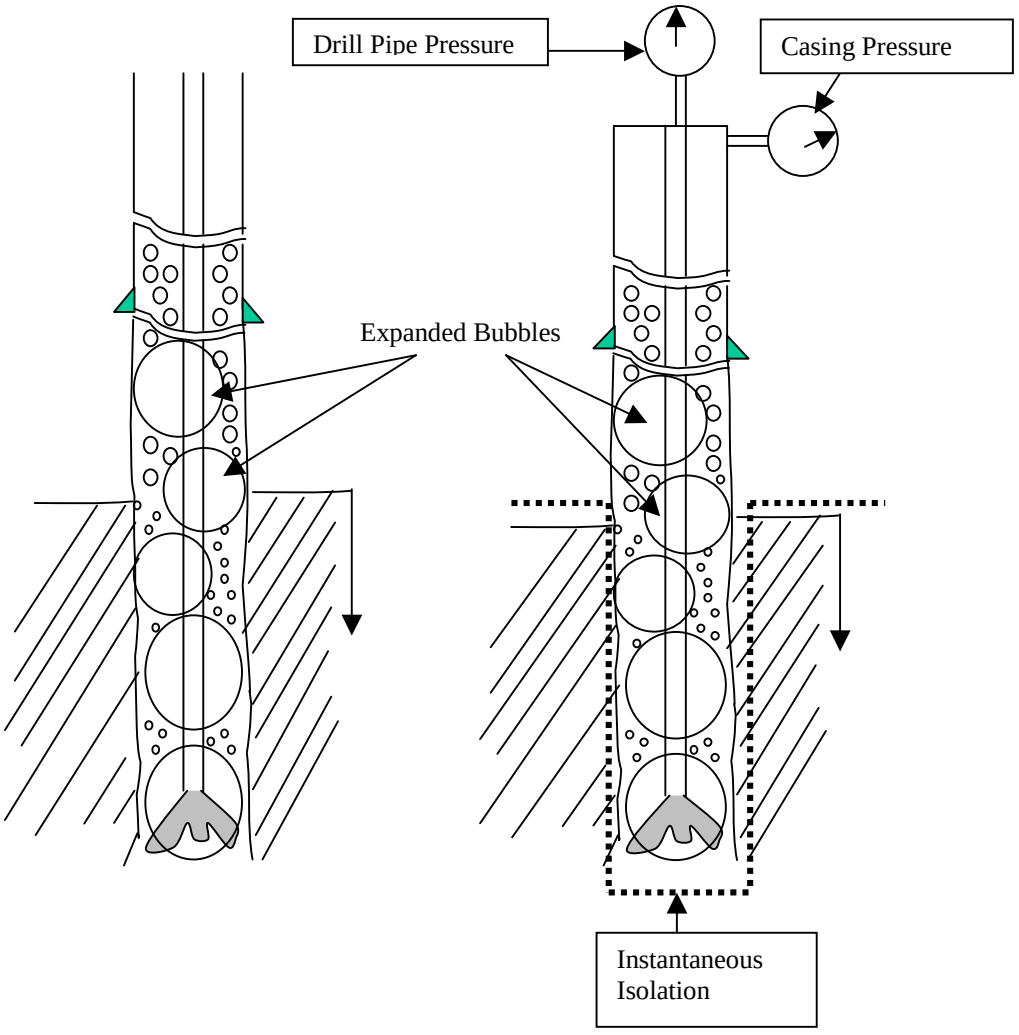

Fig. 4.1 – Schematic illustrations of modeled physical processes: (A) during flow-check or before shut-in; (B) well shut-in

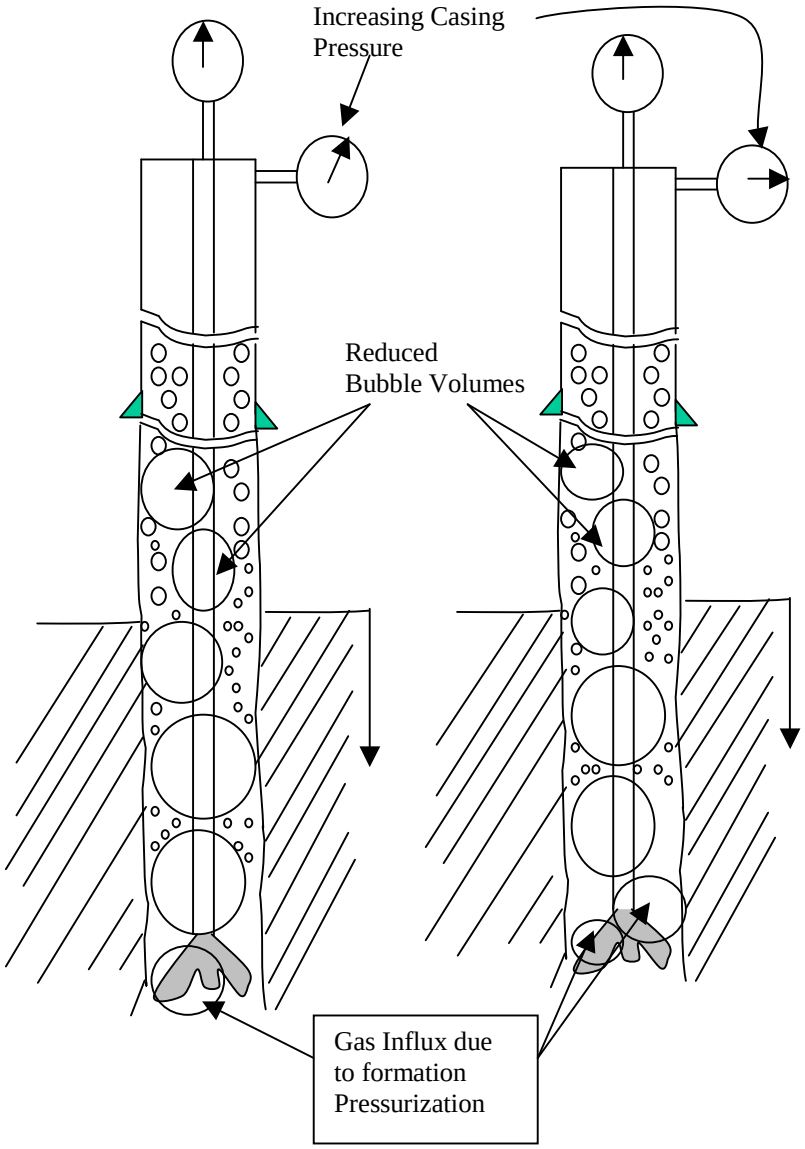

Fig. 4.1 – Schematic illustrations of continuous shut-in period

the annulus comprises mostly of incompressible drilling mud and some gaseous phase (highly compressible), the annular fluid system is considered to be slightly compressible. That is, not as compressible as when the entire annulus is filled with gas. For slightly compressible fluid system, the standard compressibility expression under isothermal condition is given as[91]:

$$c_{g,wb} = \left(\frac{1}{\rho_g} \cdot \frac{d\rho_g}{dP_{bh}} \right)_{wb} \quad \ldots 4.1$$

By applying Chain Rule to **Eq. 4.1**, we have:

$$c_{g,wb} = \left(\frac{1}{\rho_g} \cdot \frac{d\rho_g}{dt} \cdot \frac{dt}{dP_{bh}} \right)_{wb} \quad \ldots 4.2$$

Re-arranging **Eq. 4.2**, we have

$$\left(\frac{dP_{bh}}{dt} \right)_{wb} = \left(\frac{1}{\rho_g c_g} \cdot \frac{d\rho_g}{dt} \right)_{wb} \quad \ldots 4.3$$

The density of a substance, in this case for the gas, is expressed as follows:

$$\rho_{g,wb} = \left(\frac{m_g}{V_g} \right)_{wb} \quad \ldots 4.4$$

where,

m_g = mass of gas bubble, lbm

V_g = portion of the annular volume occupied by the gas, cuft

Differentiating **Eq. 4.4** with respect to time, t, yields:

$$\left(\frac{d\rho_g}{dt} \right)_{wb} = \left(\frac{V_g \frac{dm_g}{dt} - m_g \frac{dV_g}{dt}}{V_g^2} \right)_{wb} \quad \ldots 4.5$$

At any instantaneous time, t, any pressure imposed on the annular gas compresses a constant gas mass that causes additional gas inflow from the reservoir. Such compression results in increased gas mass of the entire annular gaseous phase at instantaneous time t+Δt for the constant annular gas volume. However, the mass of each already existing gas bubble, before the additional inflow, is assumed to remain the same. Therefore, the increase in the entire annular gaseous mass is as a result of the additional gas inflow by the wellbore storage effect. It should be noted that the consequential change in density for each of the gas bubble is due to the change in its volume only. Thus, at any instant, the reservoir pressurizes a constant annular gaseous mass for additional inflow. At that instant of reservoir pressurization,

$$\left(\frac{dm_g}{dt}\right)_{wb} \approx 0 \qquad \ldots 4.6$$

Also, since the successive additional gas bubbles are as a result of reduction in the entire annular gaseous volume, we have

$$\left(\frac{Change\ in\ Gaseous\ Volume}{Change\ in\ Time}\right)_{wb} \equiv -\left(\frac{dV_g}{dt}\right)_{wb} \qquad \ldots 4.7$$

Substituting **Eqs. 4.6** and **4.7** into **Eq. 4.5** yields an expression in terms of the gas density and volume:

$$\left(\frac{d\rho_g}{dt}\right)_{wb} = \left(\frac{\rho_g}{V_g}\cdot\frac{dV_g}{dt}\right)_{wb} \qquad \ldots 4.8$$

When **Eq. 4.8** is substituted into **Eq. 4.3**, we have,

$$\left(\frac{dP_{bh}}{dt}\right)_{wb} = \left(\frac{1}{c_g V_g}\cdot\frac{dV_g}{dt}\right)_{wb} \qquad \ldots 4.9$$

Equation 4.9 is another expression generally used to express the isothermal gas compressibility. Thus, all of the above assumptions, and analyses, which are the implementation of all the hypotheses for this chapter, are consistent with the conventional engineering analysis. Substituting **Eq. 3.4** into **Eq. 4.9**, and re-arranging yields:

$$\frac{dP_{bh}}{\left(P_{res}^2 - P_{bh}^2\right)} = \left(\frac{1}{c_g V_g}\right)_{wb} \cdot \frac{khB_g}{34176 T_{bh} \mu_g Z_g} \cdot \frac{dt}{P_D} \qquad \ldots 4.10$$

Two constant parameters could be defined from **Eqs. 3.5** and **3.6** as follows:

$$I_c = \frac{2.63 \times 10^{-4} k}{\phi \mu_g c_g r_w^2} \qquad \ldots 4.11$$

and,

$$J_c = \left[\ln I_c + 0.81\right] \qquad \ldots 4.12$$

Therefore, **Eq. 3.5** simplifies to:

$$P_D = 0.5\left[J_c + \ln t\right] \qquad \ldots 4.13$$

Substituting **Eq. 4.13** into **Eq. 4.10** and integrating results in:

$$\int \frac{dP_{bh}}{\left(P_{res}^2 - P_{bh}^2\right)} = \left(\frac{1}{c_g V_g}\right)_{wb} \cdot \frac{khB_g}{34176 T_{bh} \mu_g Z_g} \cdot 2 \int \frac{dt}{\left(J_c + \ln t\right)}$$

$$\ldots 4.14$$

Where the LHS of **Eq. 4.14** is integrated as

$$\int \frac{dP_{bh}}{\left(P_{res}^2 - P_{bh}^2\right)} = \frac{1}{P_{res}} \tanh^{-1} \frac{P_{bh}}{P_{res}} \qquad \ldots 4.15$$

However, the integration of the RHS of **Eq. 4.14** is as presented below up to **Eq. 4.22**

Let,

$$u = J_c + \ln t \qquad \ldots 4.16$$

Differentiating **Eq. 4.16** with respect to time, t, we have

$$du = \frac{1}{t} dt$$

Then,

$$dt = t \ du \qquad \ldots 4.17$$

But, from **Eq. 4.16**,

$$\ln t = \left(u - J_c\right)$$

Which then leads to:

$$t = e^{\left(u - J_c\right)} \qquad \ldots 4.18$$

Therefore, substituting **Eqs. 4.17** and **4.18** into the RHS integrand of **Eq. 4.14**, we have:

$$\int \frac{dt}{J_c + \ln t} = \int \frac{e^{\left(u - J_c\right)}}{u} \ du \qquad \ldots 4.19$$

The RHS integrand of **Eq. 4.19** is much easier to solve compared to its LHS integrand. Since J_c is a constant parameter, re-arranging RHS expression of **Eq. 4.19** results in the following expression:

$$\int \frac{dt}{J_c + \ln t} = \frac{1}{e^{J_c}} \int \frac{e^u}{u} \ du \qquad \ldots 4.20$$

The RHS integrand is evaluated as:[108]

$$\int \frac{e^u}{u} \ du = \ln u + \frac{u}{1 \cdot 1!} + \frac{u^2}{2 \cdot 2!} + \frac{u^3}{3 \cdot 3!} + \frac{u^4}{4 \cdot 4!} + \frac{u^5}{5 \cdot 5!} + \cdots\cdots \qquad \ldots 4.21$$

The successive evaluation of each of the terms in the above series, for the same value

of u , increases up to a particular term. Beyond this term, the evaluation of the subsequent terms continuously decreases rapidly. Also, as the parameter u increases in value, there is increase in the number of terms before rapid decrease in the evaluation of subsequent terms commences. Therefore, it is inadequate to just truncate the series in **Eq. 4.21** without proper evaluation of the series. This fact is taken care of during the computer simulation processes, so that the evaluation of the highest term, after decreased evaluation in term commences, is at least 10^{-5} as u increases. This lowest value of 0.00001 was arbitrarily chosen to satisfy maximum decimal places of 4 usually desired in engineering computations. So, substitution of **Eq. 4.21** into **Eq. 4.20** yields:

$$\int \frac{dt}{J_c + \ln t} = \frac{1}{e^{J_c}} \left[\begin{array}{l} \ln(J_c + \ln t) + \dfrac{(J_c + \ln t)}{1 \cdot 1!} + \dfrac{(J_c + \ln t)^2}{2 \cdot 2!} + \dfrac{(J_c + \ln t)^3}{3 \cdot 3!} + \\ \dfrac{(J_c + \ln t)^4}{4 \cdot 4!} + \dfrac{(J_c + \ln t)^5}{5 \cdot 5!} + \cdots\cdots\cdots\cdots \end{array} \right] \qquad \ldots 4.22$$

If a parameter is defined as:

$$\delta_s = \left[\begin{array}{l} \ln(J_c + \ln t) + \dfrac{(J_c + \ln t)}{1 \cdot 1!} + \dfrac{(J_c + \ln t)^2}{2 \cdot 2!} + \dfrac{(J_c + \ln t)^3}{3 \cdot 3!} + \\ \dfrac{(J_c + \ln t)^4}{4 \cdot 4!} + \dfrac{(J_c + \ln t)^5}{5 \cdot 5!} + \cdots\cdots\cdots\cdots \end{array} \right] \qquad \ldots 4.23$$

Then, substituting **Eqs. 4.15** and **4.22** into the solution of the model, **Eq. 4.14,** completely solves for the model. Therefore, we have the complete solution expressed as follows:

$$\frac{1}{P_{res}} \tanh^{-1} \frac{P_{bh}}{P_{res}} = \frac{2}{e^{J_c}} \cdot \frac{khB_g \delta_s}{34176 c_g V_g T_{bh} \mu_g Z_g} + Y_{\text{int}} \qquad \ldots 4.24$$

Where,

Y_{int} = the constant of integration

For simplicity sake, another arbitrary parameter can be defined as:

$$\Pi_c = \frac{2}{34176e^{J_c}} \cdot \frac{khB_g}{c_g V_g T_{bh} \mu_g Z_g} \quad \ldots 4.25$$

Therefore, **Eq. 4.24** is re-written as

$$P_{bh} = P_{res} \tanh\left[P_{res}\left(\Pi_c \delta_s + Y_{\text{int}}\right)\right] \quad \ldots 4.26$$

Equation 4.26 is then the general solution with a constant of integration for predicting the wellbore pressure build-up for a well shut-in on gas kick of known specific volume or size before shut-in.

In order to evaluate the constant of integration, Y_{int} , the initial condition at the time of complete well shut-in is used. The actual time, expressed in hours, which is required to shut-in the well must be known. This initial condition corresponds to the previously illustrated initial period of all the three periods considered for the modeling. Thus, at this initial condition, the hydrostatic pressure of the drilling fluid would be the bottom-hole pressure. If $t = t_{cl}$ and $P = P_{hyd}$ at the completion of wellbore closure, where t_{cl} is the time required to completely close the wellbore before the actual well shut-in period starts, and P_{hyd} is the hydrostatic pressure, then substituting the wellbore shut-in time into **Eq. 4.23** gives the following equation:

$$\delta_{s,int} = \left[\begin{array}{l} \ln\left(J_c + \ln t_{cl}\right) + \dfrac{\left(J_c + \ln t_{cl}\right)}{1 \cdot 1!} + \dfrac{\left(J_c + \ln t_{cl}\right)^2}{2 \cdot 2!} + \dfrac{\left(J_c + \ln t_{cl}\right)^3}{3 \cdot 3!} + \\ \dfrac{\left(J_c + \ln t_{cl}\right)^4}{4 \cdot 4!} + \dfrac{\left(J_c + \ln t_{cl}\right)^5}{5 \cdot 5!} + \cdots\cdots\cdots\cdots \end{array}\right] \quad \ldots 4.27$$

When $P = P_{hyd}$ is substituted into **Eq. 4.26**, the constant of integration is solved for as:

$$Y_{\text{int}} = \frac{1}{P_{res}} \tanh^{-1}\left(\frac{P_{hyd}}{P_{res}}\right) - \left(\Pi_c * \delta_{s,\text{int}}\right) \quad \ldots 4.28$$

With known constant of integration, the solution to the model, **Eq. 4.26,** can then be evaluated for the wellbore or bottom hole pressure build-up as shut-in time increases.

4.3.1 Casing Pressure Module

Build-up of surface casing pressure is modeled as a changing annular gas density phenomenon. For the physical processes under consideration in this study, the pressures in the annulus are acting in various directions. The gas pressure from the reservoir at the reservoir-wellbore contact is acting upward while the annular pressure due to fluid column acts downward. As presented earlier, wellbore storage causes increase in gas mass and, thus, increase in gas density for constant gas volume. Such changes in gas density during shut-in make the computation of the hydrostatic pressure of the annular fluid system more complex.

From the model hypotheses, drilling mud in the annulus is considered incompressible while the annular gas is highly compressible. Therefore, integration of **Eq. 4.1**, and the evaluation of the resulting constant of integration at the reservoir conditions for the gaseous phase yields:

$$\overline{\rho}_g = e^{\left(P_{bh} - Y_\rho\right) C_{g,wb}} \quad \ldots 4.29$$

Where Y_ρ is another constant of integration, and it is expressed in terms of the reservoir conditions as:

$$Y_\rho = P_{res} - \left(\frac{1}{C_{g,res}} \right) \ln \rho_{g,res} \quad \ldots 4.30$$

Since the drilling mud density is expressed in lbm/gal, the gas density in **Eq. 4.29** should also be expressed in lbm/gal (ppg). With known total annular volume, from volumetric calculations, and the mud pit gain at the surface before the well is completely closed, the annular gas volumetric fraction is represented as:

$$\lambda_g = \frac{V_{spg}}{V_{ann}} \equiv \frac{V_{g,ann}}{V_{ann}} \quad \ldots 4.31$$

Implementing a volumetric averaging technique, the average density of the annular fluid system is estimated as follows:

$$\bar{\rho}_f = \frac{\overline{\rho_g} V_{g,ann} + \rho_l V_{l,ann}}{V_{ann}} = \bar{\rho}_g \lambda_g + \rho_l \left(1 - \lambda_g\right) \quad \ldots 4.32$$

Therefore, the hydrostatic pressure of the annular fluid system can be estimated from:

$$P_{hyd,ann} = 0.052 \bar{\rho}_f D \quad \ldots 4.33$$

The annular fluid hydrostatic pressure in **Eq. 4.33** is computed for every wellbore buildup pressure value to obtain the corresponding surface casing pressure rise.

4.4 Modeling Technique

The procedure adopted in the simulation is presented in this section. A computer program written in Visual Basics 6.0 was developed to perform the

simulation. The modeling data used are the same as those used in Chapter 3. These data are, again, presented in **Table 4.1**. The data in bold are literature[55] data.

The major purpose of the modeling, in Chapter 4, is to predict the casing pressure rise, which relatively determines the bottom-hole pressure rise. For application of this study, varying the reservoir permeability and/or reservoir pressure helps to match the predicted casing pressure rise to the measured casing pressure rise up to the initial stabilization period. At the initial pressure stabilization, the reservoir pressure used for the history matching of the casing pressure rise could be assumed to be the reservoir pressure. Hence, such predicted reservoir pressure could be the basis for controlling the well. Another purpose of this modeling is the ability to predict what time, from when complete well shut-in commences, would a particular gas kick scenario be expected to attain its initial pressure stabilization. Predicting shorter time than actual could result in assuming lower pressure for the reservoir. Hence, this could cause the occurrence of multiple kicks at the same borehole depth. Prediction of such early time of initial pressure stabilization is possible if the predicted rates of pressure rise for the casing and the bottom-hole are too rapid, as usually presented by the currently existing approaches.

4.4.1 Background to Pressure Build-up Computations

Before any pressure rise computation using the model developed in this Chapter 4, the models developed and applied in Chapter 3 must have provided the total volume of gas inflow into the annulus before shutting-in the well. The two

Table 4.1 – Modeling Data

Bottom Hole Assembly:					
Riser size	**=**	**19**	in. ID		
Casing Size	**=**	**11**	in. ID		
Drill pipe Size	**=**	**5**	in. OD		
Drill pipe Size	**=**	**4.41**	in. ID		
Drill Collars	**=**	**8**	in. OD		
Drill Collars	**=**	**2.81**	in. ID		
Bit diameter	=	9.875	ins.		
Bit nozzle sizes	=	12	/32 in x 3		
Total area of the three nozzles	=	0.33147	in^2		
Bit nozzles' discharge Coefficient, Cd	=	0.95	constant		
Choke Line	**=**	**3**	in. ID		
Maximum Surface Pump Horse power	=	1000	hp		
Drilling Fluid and Formation Properties:					
Mud Flow Rate	=	400	gpm		
Surface Pump discharge pressure	=	1620	psi		
Drilling Fluid density	=	8.4	ppg	= 61.4	lb/ft^3
Mud Plastic viscosity	=	24	cp		
Mud Yield Point	=	18	$lbf/100ft^2$		
Average velocity in drill pipe (DP)	=	8.4	ft/sec		
Average velocity in drill colars (DC)	=	20.7	ft/sec		
Average velocity through Nozzles	=	387.1	ft/sec		
Mud apparent viscosity for DP	=	87	cp		
Mud apparent viscosity for DC	=	40	cp		
Mud apparent viscosity for Bit Nozzles	=	24	cp		
Mud Surface tension, σ	=	1.30E-03	lb_f/ft		
Mud flowing Reynolds Number	=	3323	Inside DP		
Mud flowing Reynolds Number	=	11254	Inside DC		
Mud flowing Reynolds Number	=	139439	Nozzles' exit		
Friction Pressure loss in Drill pipe	=	376	psi		
Friction Pressure loss in Drill collars	=	151	psi		
Flowing BHP (FBHP)	=	4332	psi		
Formation Pressure	=	4600	psi		
Formation Permeability	**=**	300	md		
Formation Porosity	**=**	0.3	fraction		
Mud Hydrostatic Pressure	=	4368	psi		

Table 4.1 – Modeling Data (Contd.)

Temperature:			
Surface	***70 ^{o}F***	**=**	***530 ^{o}R***
Bottom hole	***180 ^{o}F***	**=**	***640 ^{o}R***
Hole Geometry - VERTICAL HOLE:			
Riser Length	**1000 ft from surface**		
Last Casing Shoe Depth	**4000 ft from the mud line**		
Open-Hole section	**5000 ft from last Casing Shoe**		
Drill Collars' Length	**450 ft**		
Time Required to drill h-ft of formation	0.033 hr		
Open-hole radius, r_w	**4.938 ins.**	**=**	**0.411 ft**
Penetration Rate	**30 ft/hr**		
Formation Fluid - GAS - properties:			
Viscosity of gas at 1 ATM	0.01244 cp		
Viscosity ratio	1.85		
Gas Viscosity, μ_g	0.023014 cp		
Gas gravity, $S.G_g$	0.6		
Gas Constant, R	10.7		
Gas pseudo-critical pressure	671 psia		
Gas pseudo-critical temp.	358 ^{o}R		
Gas pseudo-reduced pressure	6.85544		
Gas pseudo-reduced temperature	1.787709		
Gas Compressibility factor, z	0.975		
Gas Density, ρ_g	11.98778 lb/ft^3		
dZ/dP slope at 4600 psia	7.27E-05 psi^{-1}		
Gas compressibility, C_g	0.000143 psi^{-1}		
Gas Formation Volume Factor, Bg	0.003838 ft^3/SCF		
Gas Formation Volume Factor, Bg	0.000684 bbl/SCF		

periods responsible for this total volume of gas inflow before shut-in are designated as stages 1 and 2 in Chapter 3. This computed total gas volume by simulation in Chapter 3 is the total gas volume as at the time of inflow into the wellbore (wellbore-reservoir contact). That is, the volume does not include the effects of expansion and/or coalescence of the bubbles on their volumes while flowing/migrating upward. These effects were not addressed because of the obvious uncertainties in evaluating the bubble behaviors while in the annulus. Hence, at this stage, the internal pressure in each of these gas bubbles is the reservoir pressure.

However, to simulate the possible expansion that these bubbles would have undergone at well shut-in, all of the gas bubbles are subjected to the hydrostatic pressure of the drilling fluid, which is externally applied to each of the gas bubbles. Due to lower annular fluid hydrostatic pressure than the reservoir pressure, which is inside each of the gas bubbles, each of the gas bubbles would expand after inflow into the wellbore. This procedure is simulated by imposing the concept of instantaneous isolation of the reservoir that was earlier presented as one of the hypotheses in this chapter. Therefore, this procedure results in increased gas volume immediately at well shut-in than when the bubbles were released into the wellbore. It is upon this expanded gas volume that the pressure rise would take place. This procedure is realistic because if no gas expansion were simulated, it would not be possible for the reservoir pressure to be greater than the internal pressure of each of the bubbles. Thus, no gas bubble compression that gives rise to wellbore storage during the shut-in period would be entertained. It is assumed that the gas expansion would have displaced certain volume of drilling fluid equivalent to the extent of expansion of all

the gas bubbles while shutting-in the well.

4.4.2 Computing Pressure Rises During Shut-in

The variables considered for this modeling are:

a. Reservoir pressure
b. Reservoir permeability
c. Formation or reservoir interval drilled to achieve the total quantity of unexpanded gas volume
d. Unexpanded annular gas volume
e. Expanded annular gas volume immediately at shut-in
f. The reservoir gas viscosity and compressibility factor, which vary anytime the reservoir pressure is changed

For any particular simulation scenario, variable (d) is obtained from the model results of the simulation developed in Chapter 3 at particular values of variables a, b, c, and f. All of these values constitute a set of simulation result. Another set could be obtained by varying either the reservoir pressure or the reservoir permeability to achieve a desired total quantity of unexpanded volume of gas inflow. For example, having different values of reservoir permeability at constant reservoir pressure to achieve equal total quantity of unexpanded gas inflow for these different cases requires different values of interval to be drilled into the reservoir or formation. In order to obtain the same total quantity of unexpanded gas inflow for different reservoir permeabilities, different gas inflow rates must be involved. Such different gas inflow rates undoubtedly correspond to different drilled formation intervals.

For the simulation results presented in the following section, the reservoir pressure is held constant at 4600-psi while the reservoir permeability was varied. The variation in reservoir permeability consequentially corresponds to the required drilled formation intervals as explained above. On the other hand, with varying reservoir permeability but constant drilled formation interval, different unexpanded volumes of the gas inflow would result.

The general model stated in **Eq. 4.26** and the associated **Eqs. 4.11** through **4.13**, **4.25**, and **4.28** are coded in VB programming language to compute the bottom-hole pressure rise. The casing pressure rise is computed using **Eqs. 4.29** through **4.33**. The VB coding for these expressions is presented in the shut-in pressure rise module in **Appendix B2**. Once each set of the simulation results obtained from the models in Chapter 3 are inputted into their respective text boxes on the VB forms in **Appendix B1**, the programming module for the shut-in pressure rise computations in **Appendix B2** would execute the program and displays the results for casing and bottom-hole pressure build-up with shut-in time. If desired, plots of these casing, and bottom-hole pressure rises could be displayed as well. Typical pressure build-up results for a particular case scenario are presented in **Appendix C2**.

4.5 Simulation Results and Discussions

The simulation results of the newly developed model in this chapter are divided into two parts. The first part is completely independent of the analyses in the preceding Chapter 3. This part was conducted to establish the pressure build-up trends influenced by wellbore storage effect for a wellbore shut-in during a gas kick.

Excellent similarities in the resulting pressure-rise trends with those practically observed during pressure transient testing (curve (b) in **Fig. 2.10)** are established. In practice, for a typical shut-in procedure, the surface casing and drill pipe buildup pressures are taken and recorded every 15-minutes.[53] It shows that pressure rise in a well shut-in on gas-containing systems requires sufficient time to build. This is unlike the extremely rapid pressure build-up rates that have been predicted by all the currently existing approaches to gas kick analysis. This statement would be explained further in Chapter 5 during model validation and comparison with the existing approaches for gas kick analysis.

The second part of the simulation results involves the integration of the results in Chapter 3 and 4 to achieve a complete over-view of the status of a gas kick in the wellbore from its inception up to when its control is initiated. In Chapter 3 it was shown that reservoir permeability and formation or reservoir pressure prediction play significant roles in determining the sizes of gas bubbles and its volume at the instant of gas-kick into the wellbore. Therefore, for a constant reservoir pressure, comparisons of simulation results from the developed model in Chapter 4 would be based on the arbitrarily selected three different reservoir permeabilities.

4.5.1 Effect of Reservoir Permeability on Pressure Rises

At the same rate of penetration and for the same 5-ft interval drilled into the gas containing sediments of different permeability values of 50-md, 300-md and 400-md, **Figures 4.2** through **4.4** show that the rate of bottom-hole and surface casing pressure rise increases as the permeability decreases. This is because at the time of

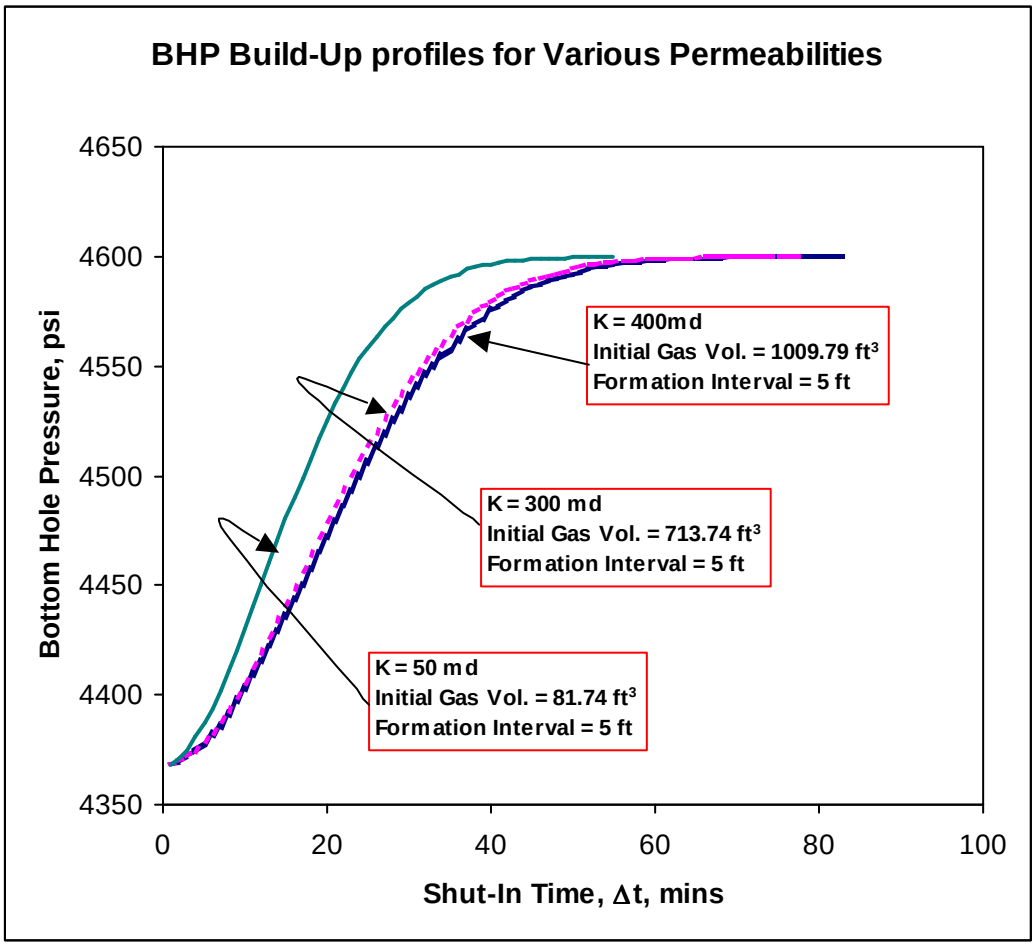

Fig. 4.2 – Bottom-hole pressure build-up profiles for various permeability values

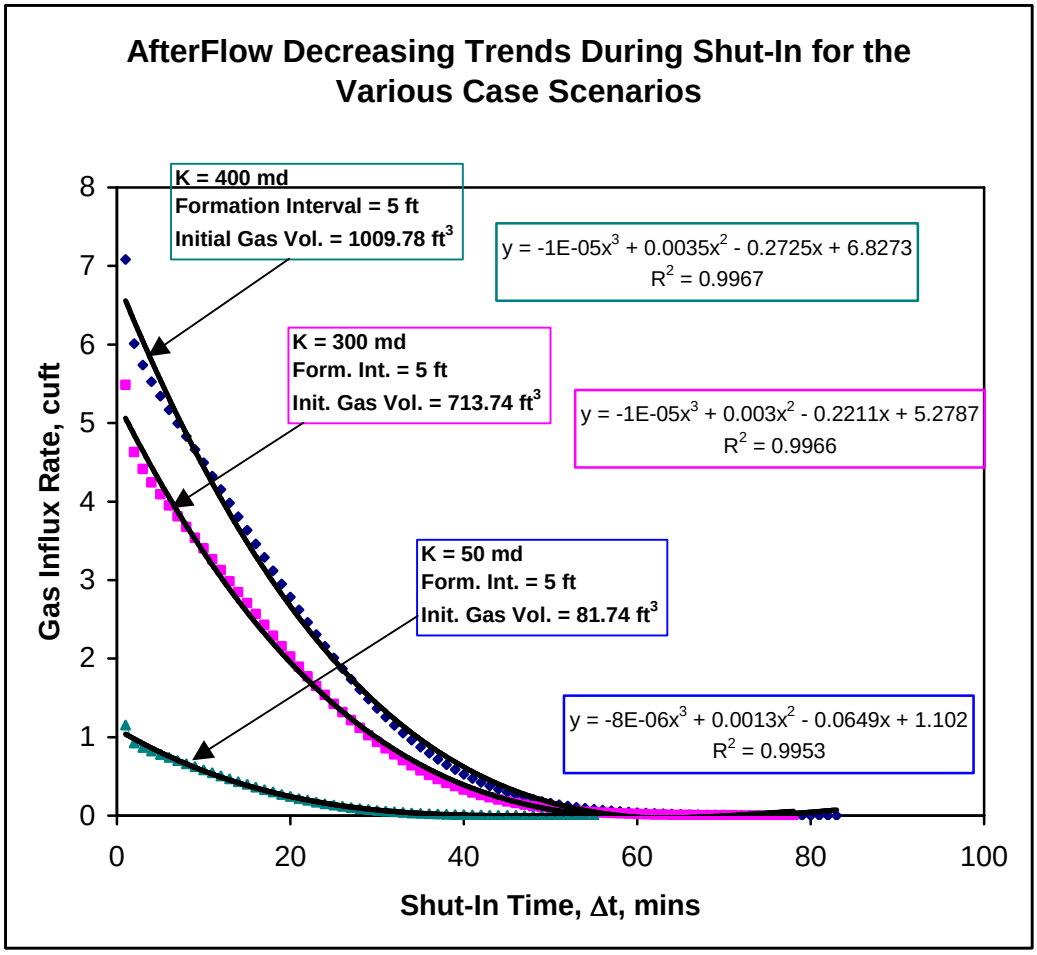

Fig. 4.3 – Rate of further flow of gas into the wellbore during shut-in

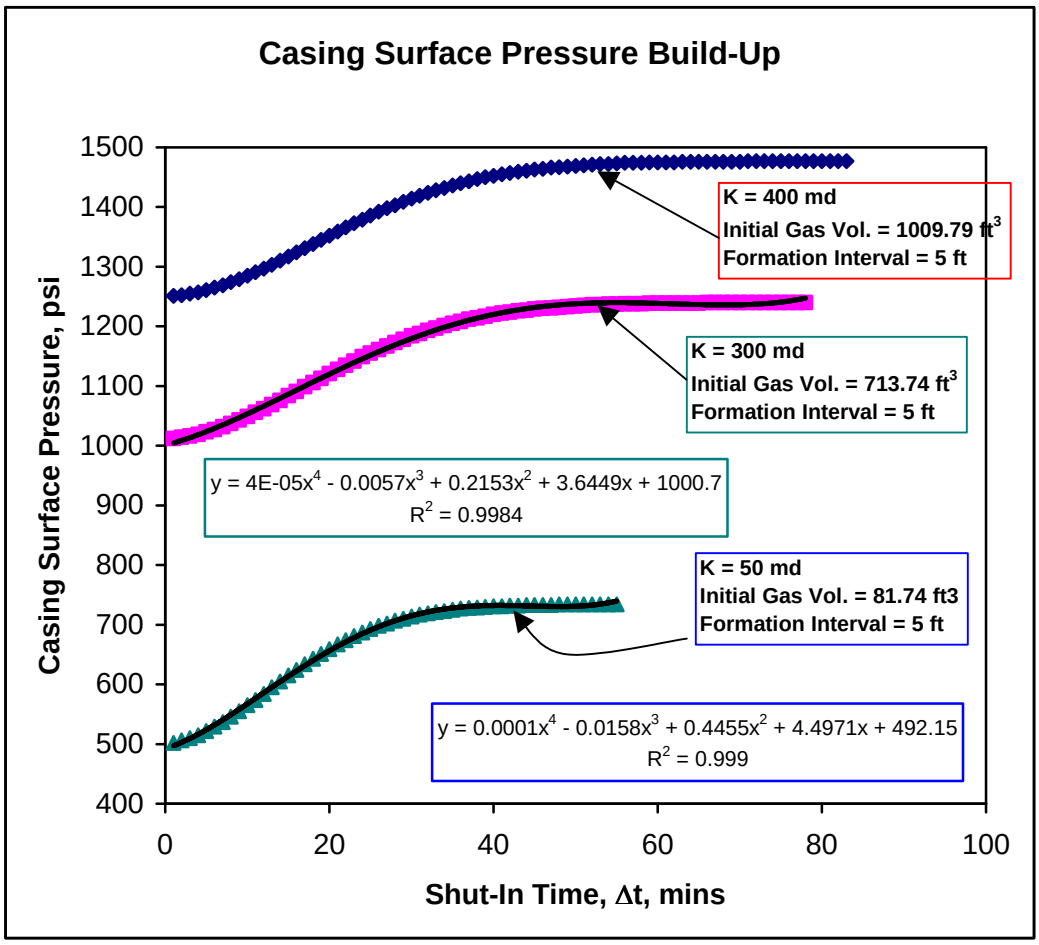

Fig. 4.4 – Surface casing pressure rise during shut-in

noticing a gas-kick on surface equipment, drilling a 5-ft interval into a low permeable reservoir would have caused a smaller volume of gas inflow into the annulus than drilling the same interval into a higher permeable reservoir. Therefore, for the same reservoir pressure imposed on different annular gas volumes, it takes a shorter time to compress a smaller gas volume to its maximum density than compressing a larger gas volume to the same maximum density.

These figures show a trend of gradual wellbore or bottom-hole pressure buildup, which is the characteristic of pressure buildup in well testing. For these particular scenarios, the figures indicate that gas formations with the same pore pressure, but different permeability have different rates to achieve the initial pressure stabilization. That is, with smaller annular gas volume and the same reservoir pressure, low permeable formations would build-up its wellbore pressure faster than highly permeable formations. Therefore, surface casing pressure observed in the field should be expected to stabilize quickly for low permeable formations.

Under the same reservoir pressure for all the permeability cases, **Fig. 4.3** shows that lower gas flow rate from the low permeability formation would result in lower total wellbore storage during shut-in.

4.5.2 Effects of Nominal Gas Kick Size or Volume

All of the currently existing gas kick analyses are based on assuming a nominal gas inflow size or volume.[54,55,72,80,84&86] This is because when a gas kick occurs, the kick detection equipment on the surface are designed to alert the drilling crew whenever certain pre-set conditions are satisfied. The most common kick

detector on surface is the pit, which is usually set at a 10 or 20-barrel gain in the pit volume. Other indicators of kick occurrence could be sudden changes in the rate of drilling, known as drilling break. However, drilling break could also occur when drilling from harder formation into softer formation. Therefore, drilling break might not necessarily be caused by well kick. When drilling break occurs, any gain in the surface mud pit is usually checked to gain insight on what might probably be happening downhole.

These pit gain sizes or volumes are assumed to correspond directly to the gas volume inside the annulus at the time of kick alertness. However, at the time of kick alertness, the size of gas bubbles would have increased due to expansion than the original size at the instant of inflow into annulus. This means that the total pit gain is the volume of the gas bubble at the instant of inflow into the annulus, plus the volume of drilling mud displaced due to expansion. Moreover, at the time of kick detection, these expanded gas bubbles would have been relieved of their reservoir pressure with which they entered into the wellbore. Unfortunately, for simplicity and as discussed in Chapter 2, such expanded gas volume is still assumed to exist at the reservoir pressure by the currently existing approaches.

In this section, 56.13-cuft of gas is assumed to flow into the annulus, and this is equivalent to 10-bbls of mud displaced out of the annulus. This 56.13-cuft of gas is the unexpanded volume of the gas bubbles at the instant of inflow into the annulus. Possible increase in the total gas volume due to expansion, at the time of complete well shut-in, is achieved as previously explained. This procedure causes larger annular gas volume than 56.13-cuft, and consequently lower density. The 10-barrel

gas volume was chosen because at the end of a 5-ft drilling break for all the permeability cases, 50-md reservoir could not introduce a cumulative gas volume of 20-bbls. With the assumed equal pit gain, all of the three permeability cases therefore have equal annular gas volume available at different inflow rates at the same reservoir pressure during well shut-in.

Figures 4.5 through **4.7** show similar trends, as previously presented, for the wellbore pressure, casing pressure, and rate of afterflow for the formations with different permeabilities. However, the figures now show that the rates of rise of the bottom-hole and surface casing pressures for the 50-md reservoir are slower than for the 300 or 400-md permeability formations. These results are opposite to the results presented in **Figs. 4.2** and **4.4**. This is because for the same reservoir pressurization and equal initial annular gas volume at the time of complete well shut-in, the higher rate of gas inflow from the 300 or 400-md formations would continuously introduce larger quantity of gas mass into the annulus than the 50-md formation. Since the annular gas volume is the same for all the permeability cases, the introduction of larger gas mass by the 300 or 400-md formation would result in rapid increase in the annular gas density up to the maximum gas density. Such rapidity of gas density increase also causes rapid decline in the subsequent inflow rate from the 300 or 400-md formations. A shut-in time is reached when the rates of inflow from the formations are equal, as shown by the dashed circle in **Fig. 4.7**, which, however, is not present in **Fig. 4.3**. When the maximum annular gas density is attained, initial pressure stabilization occurs at the surface and downhole.

From the analysis of the results in Chapter 3, a trace of wellbore backpressure

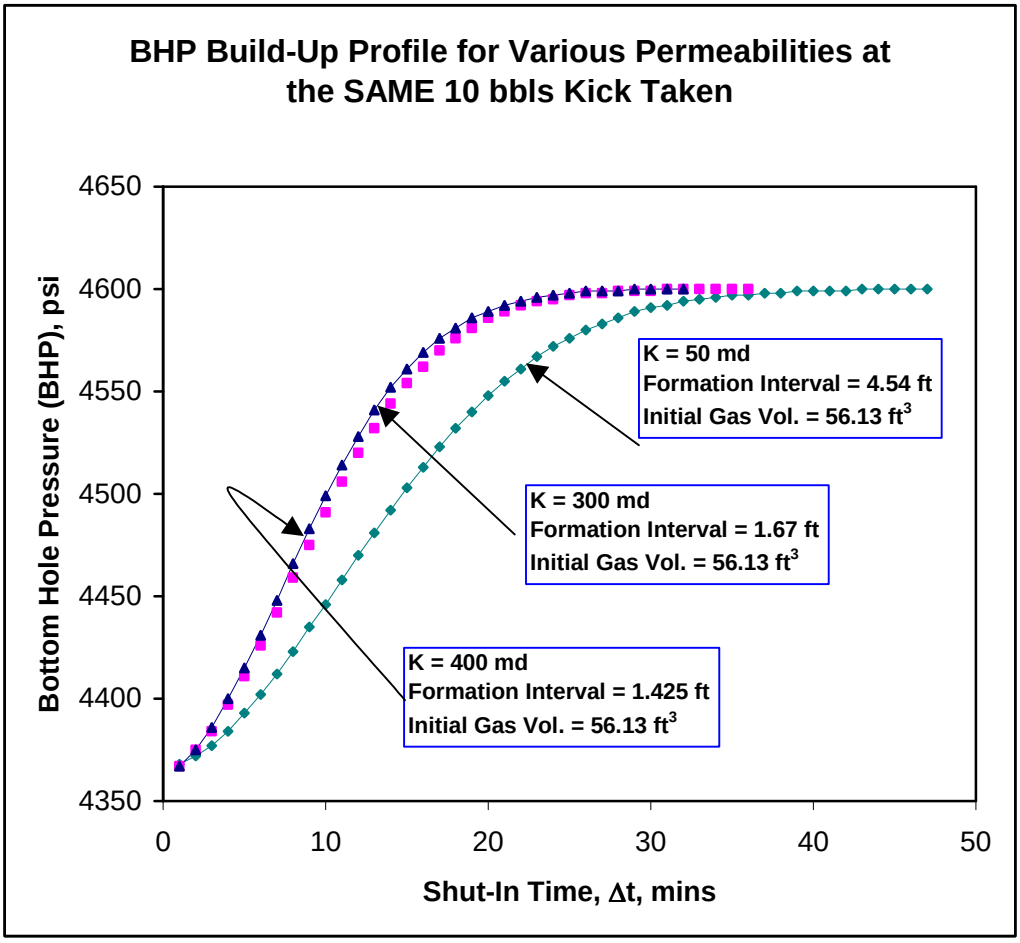

Fig. 4.5 – Bottom-hole pressure (BHP) profile for an assumed 10-bbl nominal gas kick size at well shut-in

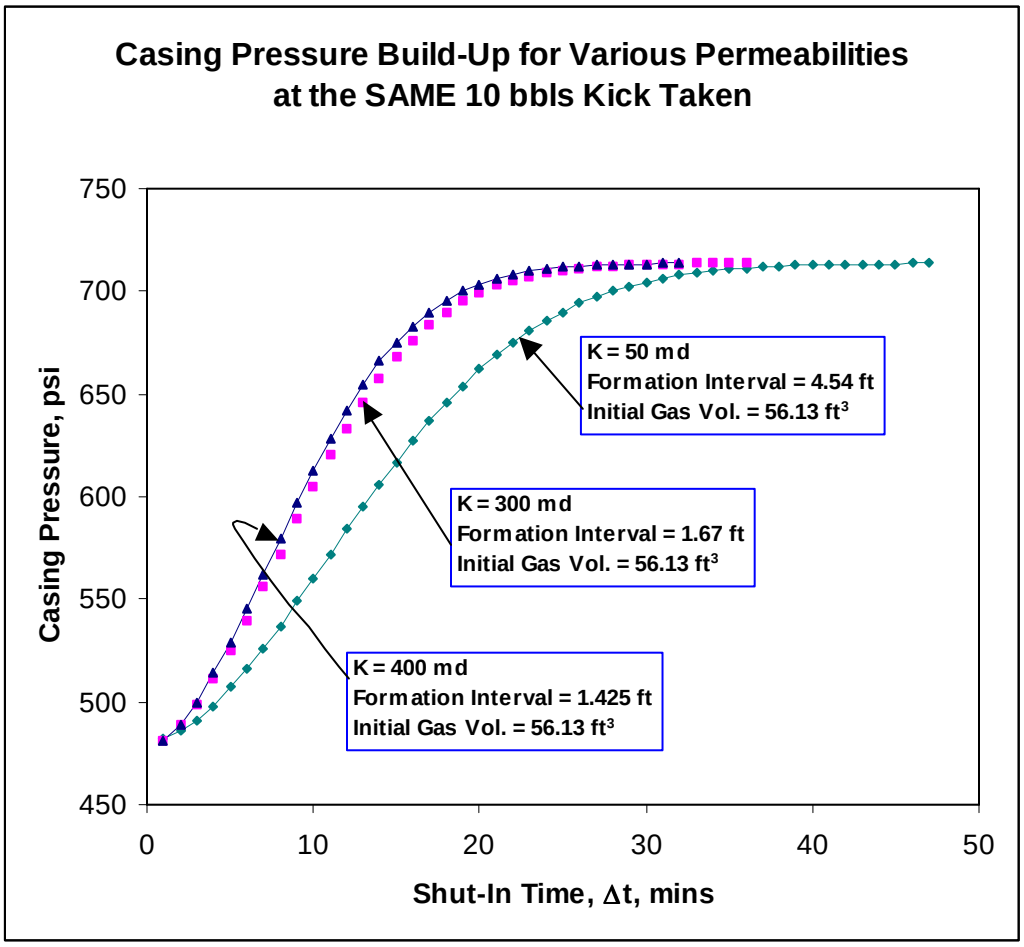

Fig. 4.6 – Casing pressure profile for an assumed 10-bbl nominal gas kick size at well shut-in.

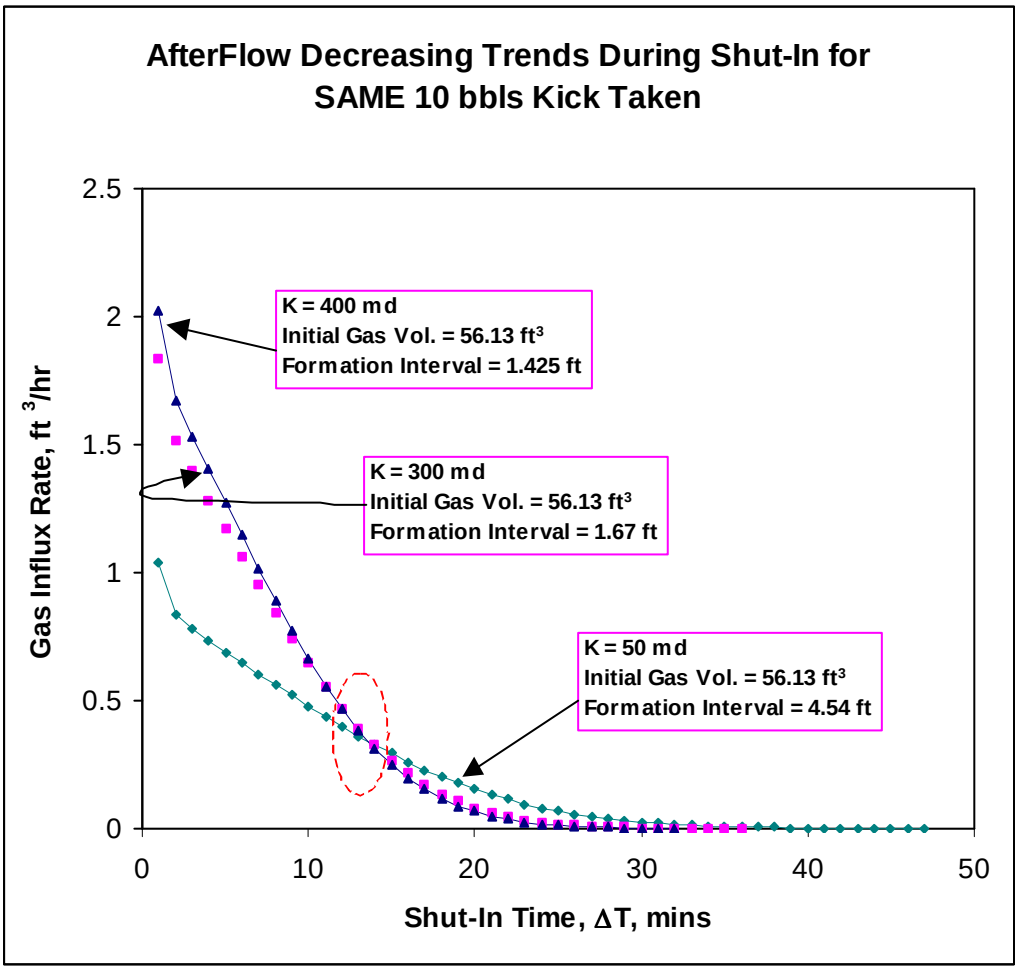

Fig. 4.7 – Shut-in inflow rates for an assumed 10- bbl nominal gas kick size at well shut-in

on highly permeable formations was noticed to cause rapid subsiding rate of additional gas inflow from such formations. Such observation is enhanced and reinforced by the resulting lower inflow rate from the 300 or 400-md formations than that from the 50-md formation after the occurrence of the above-mentioned inflow rate equalization. That is, after the inflow rate equalization, the influence of the formation on the annulus decreases considerably for higher permeability reservoirs. **Figure 4.8** shows the bottom-hole pressure derivative curves, and indicates that much lower bottom-hole pressure changes are observed for higher permeability reservoirs.

4.5.3 Effect of Pressure Build-Up on the Annular Gas Density

A major characteristic of a gas is its ability to respond to a greater external pressure by reduction of its volume. If such volumetric reduction continues due to increasing externally imposed pressure on a constant gas mass system, the gas molecules correspondingly exert increased opposite pressure to balance the externally applied pressure. This causes increase in the gas density because gas mass is constant. Therefore, gas density continues to increase as long as the imposed pressure is greater than the internal pressure of a gas bubble.

Figures 4.9A and 4.9B show the relationship between the rising wellbore pressure and the annular gas density for the various permeability cases. These figures show that irrespective of the sediment or formation permeability, at the same build-up bottom-hole pressure, the same average gas density exists in the annulus. This could only be assured for the same wellbore configuration if and only if the same reservoir pressure acts on the annulus fluid, and the same drilling break was conducted before

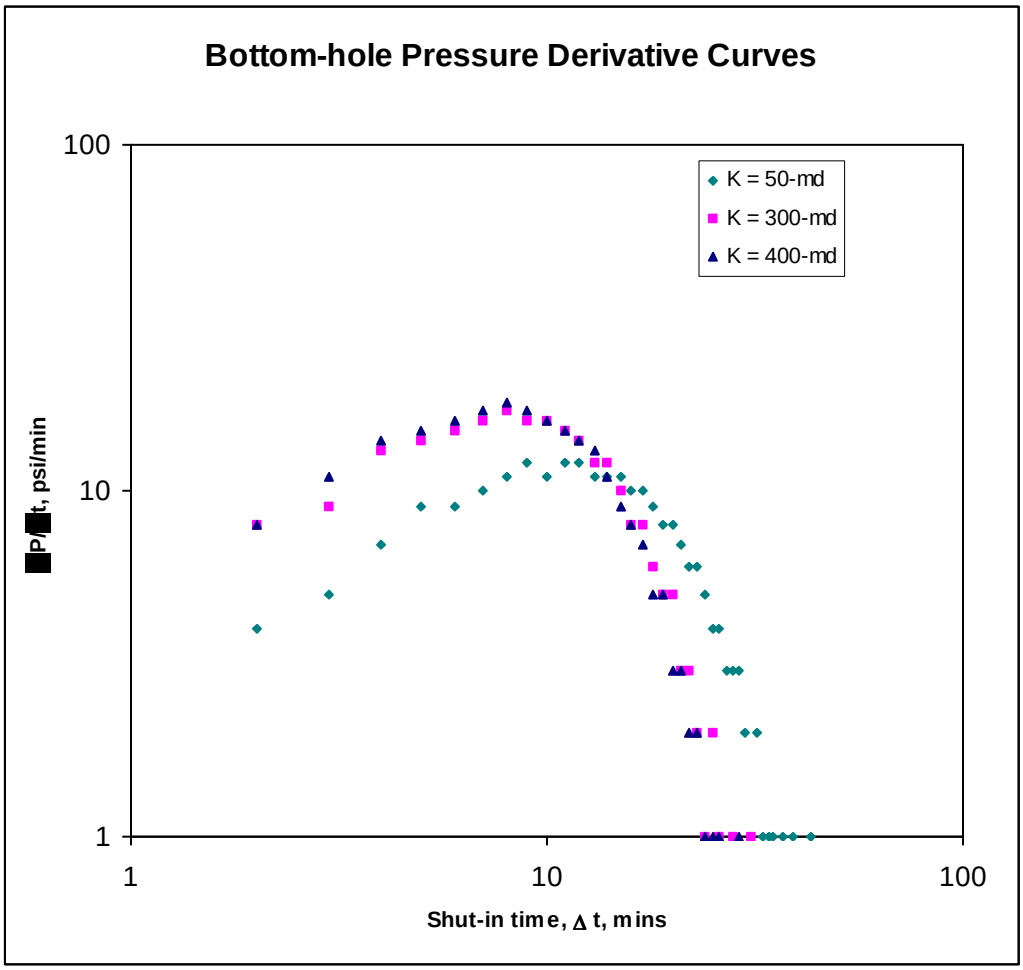

Fig. 4.8 – Bottom-hole pressure derivative curves

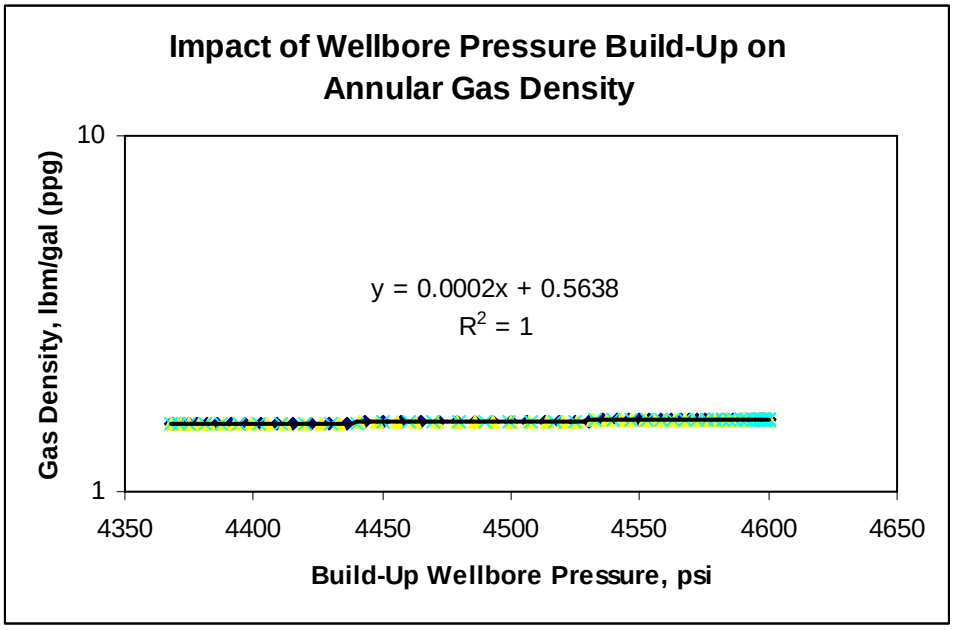

Fig. 4.9A – Variation of annular gas density with continuous wellbore pressure build-up for different permeable reservoirs

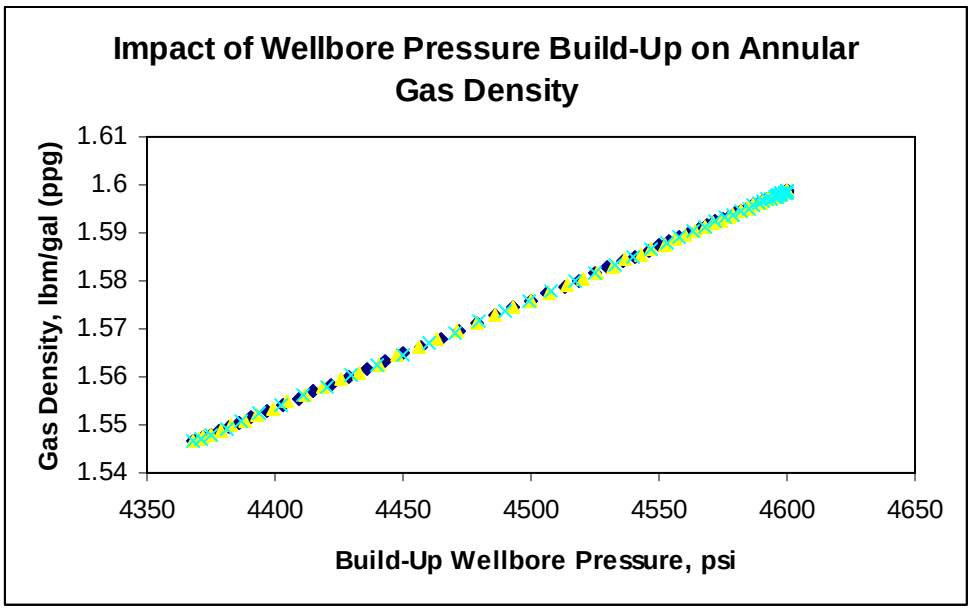

Fig. 4.9B – Expanded plot of the variation of annular gas density with changing wellbore pressure

shutting-in. If, however, the annular gas density variation is plotted against the shut-in time, similar patterns as in **Fig. 4.2** are obtained because of different rates of inflow during shut-in. This is presented in **Appendix D**.

In practice, it is usually assumed that when a well is shut-in on a gas-kick, the small variations in the gas density do not aid any wellbore pressure build-up. From the presented simulation results, a small gas density variation was achieved, as always practically assumed. However, such low gas density variation has been shown to generate considerable pressure build-up single-handedly.

Due to the need for instantaneous system equilibrium at every wellbore pressure build-up, the instantaneous average gas pressure in all the gas bubbles should equate the wellbore pressure. Therefore, at the time of pressure stabilization, the average gas pressure in the annulus would approximately be equal to the formation pressure.

4.5.4 Bubble Size Profile at the Instant of Inflow During Shut-in

To conclude on the bubble size distribution that was discussed in Chapter 3 for the gas kick analysis, this section presents an explanation of possible instantaneous bubble size distribution at the instant of gas inflow during the shut-in period. Normally, as shut-in time increases, the rates of inflow decline, which should correspondingly results in successive decrease in the bubble sizes. **Figure 4.10** shows that the bubble sizes during the shut-in period decrease polynomially until the inflow ceases, which signifies pressure stabilization. This figure also shows that at any shut-in time interval, the volume of the gas bubble resulting from the inflow is larger for

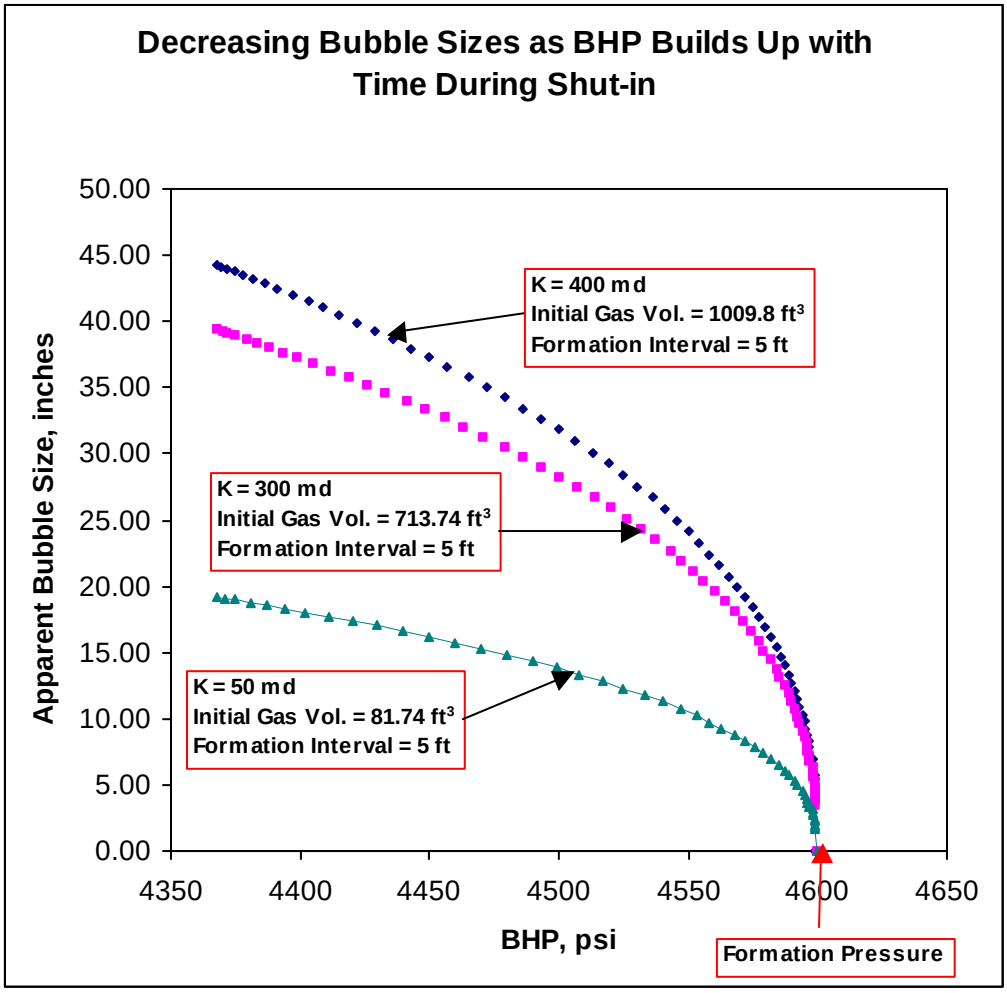

Fig. 4.10 – Bubble size profile or pattern for the additional gas inflow during well shut-in for various gas kick volumes

formations with high permeability due to the higher inflow rate.

4.5.5 Integration of All the Modeling Stages

Coupling of all of the modeling stages requires relating common varying parameters for all the stages. Since no drilling activities occur during well shut-in, relating drilled formation interval to the bubble sizes as presented in Chapter 3 would be inappropriate. Therefore, drilling time from Chapter 3 (stages 1 and 2), and shut-in time from Chapter 4 (stage 3) were chosen in order to relate to the bubble size distribution for all the modeling stages. **Figure 4.11** shows the coupled results of all the stages for the same permeability variations, used in this study. This plot shows that at any stage of the gas kick analysis before any kick control procedure is initiated, formations with high permeability would introduce large size gas bubbles into the annulus than formations with low permeability. This, consequently, means that higher permeability formations would introduce larger total additional gas volume into the annulus during the shut-in period.

Figure 4.12 shows the differences in cumulative gas kick volumes, and the required total time for wellbore pressure stabilization. It should be recalled that for the base case data, the drilling fluid flowing bottom hole pressure during drilling operation was deliberately designed to be lower than the hydrostatic pressure of the drilling fluid. This was achieved as follows. At a particular well depth and a constant mud weight, the hydrostatic pressure is constant when mud circulation ceases. However, during drilling and mud circulation, computed flowing bottom-hole pressure through the drill-string could vary depending on the magnitude of fluid

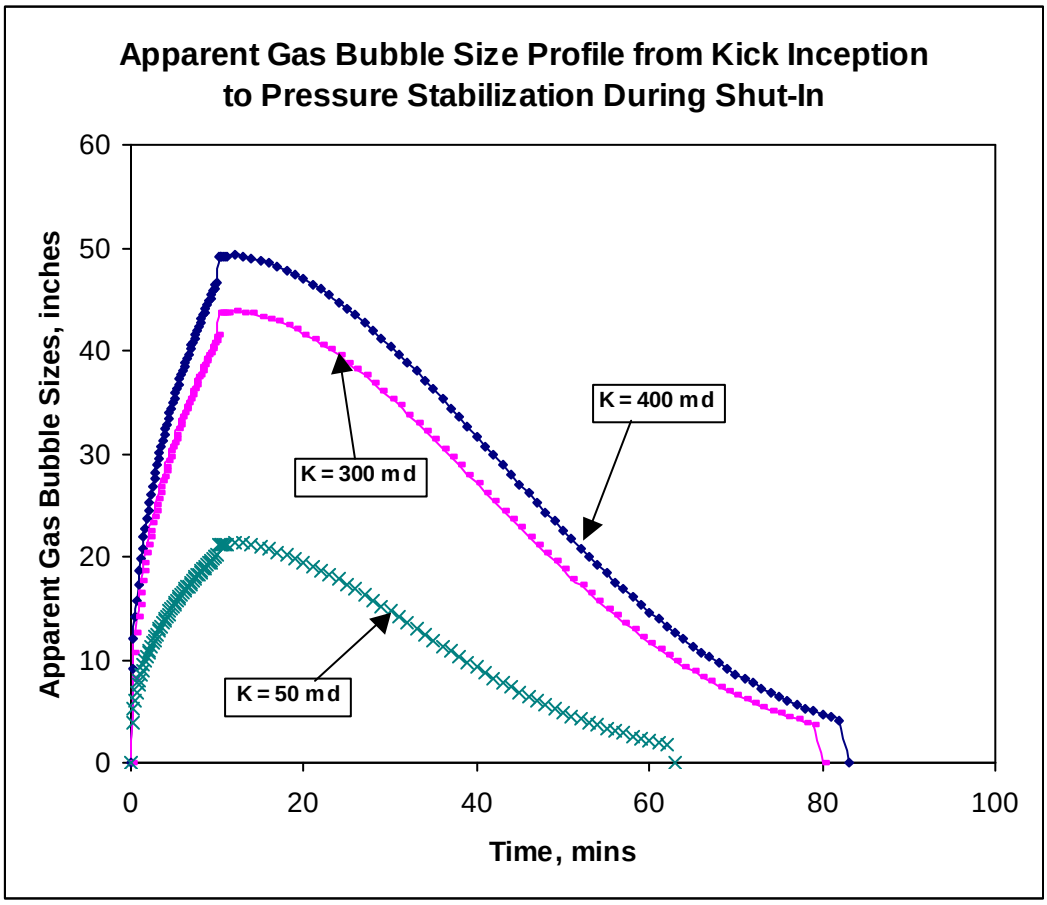

Fig. 4.11 – Integration of apparent bubble size profile for all the modeling stages

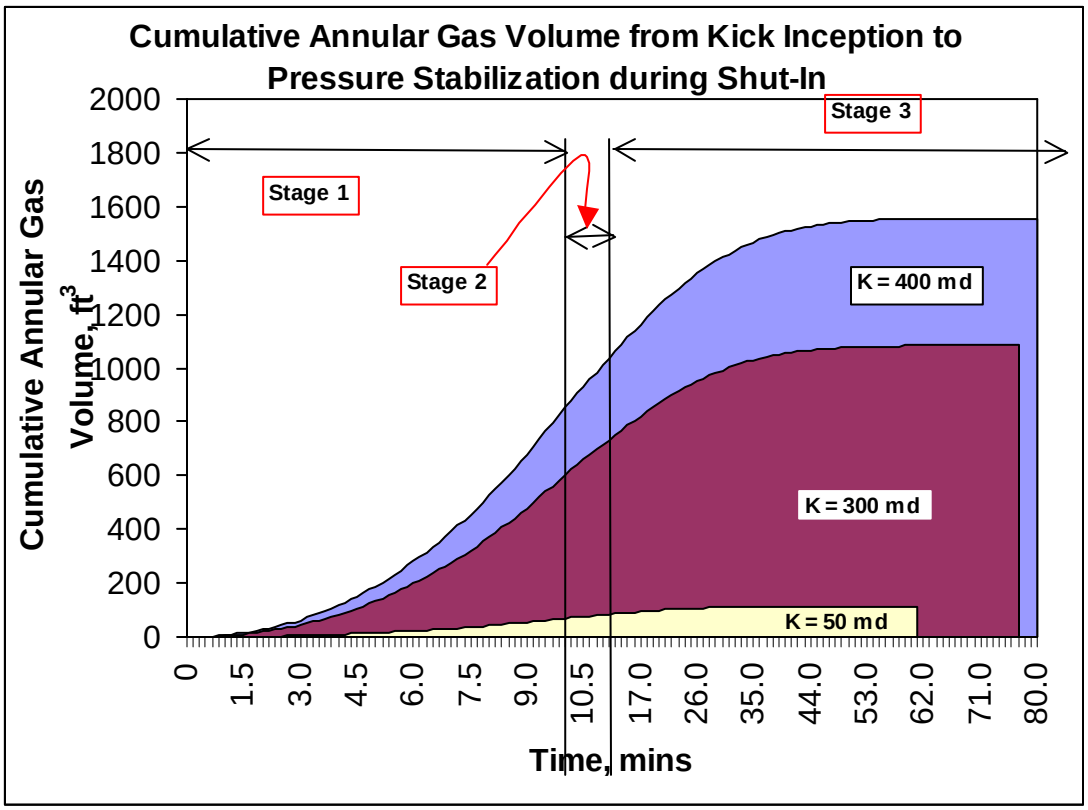

Fig. 4.12 – Cumulative annular gas volume and corresponding required stabilization time

pressure loss inside the string. This fluid pressure loss also depends on the extent of the pipe roughness, viscosity, and the flow rate of the fluid inside the pipe. With all other parameters held constant, a certain fluid flow rate inside the drill-string could result in excessive frictional pressure loss. If care is not taken, the pressure loss could be significant to cause lower mud flowing bottom-hole pressure than the hydrostatic pressure.

4.5.6 Effect of Hydrostatic Pressure During Shut-in Period

This section presents the effect of mud density on the entire results of the gas inflow. Whenever drilling and mud circulation are suspended, the only force that could subdue the pore pressure or formation pressure is the hydrostatic pressure of the drilling fluid. If, however, a large pressure differential exists between the designed hydrostatic pressure and the formation pressure, there would be differences in the total volumes of formation fluids that would inflow from the time the mud circulation ceases.

Re-designing the drilling fluid flow parameters such as the surface pump pressure, the drilling fluid density, and the desired flow rate in **Table 4.1** results in another table of data presented in **Table 4.2**. For the sake of consistency, the same circulating bottom-hole pressure was retained as closely as possible, but the hydrostatic pressure was reduced. The desired flow rate and the drilling fluid density were reduced to 381-gal/min and 8.2-lb/gal respectively. These lowered the required surface pump discharge pressure and hydrostatic pressure to 1543-psi and 4264-psi respectively with constant flowing bottom-hole pressure of 4332-psi.

Implementation of the procedures for all the three stages modeled in this study using the data displayed in **Table 4.2** results in the bubble size distribution shown in **Fig. 4.13**. This figure shows that for any permeability case, there is increase in the gas bubble sizes at the instant of suspending mud circulation because of lower hydrostatic pressure. However, the subsequent size of gas bubbles decreases as pressure stabilization is being approached. Superposition of **Figures 4.11** and **4.13** is presented in **Fig. 4.14.** Figure 4.14 shows that for the lower hydrostatic pressure, the initial total annular gaseous volume at shut-in is higher than that of the higher hydrostatic pressure case scenario. Similar results are obtained for the cumulative gas mass/volume that entered the annulus during the shut-in period.

4.6 Summary

A different approach to the wellbore and casing pressure build-up during a gas-kick control was presented. This approach showed consistency with field observations of pressure build-up during well testing As a consequence, a new model that is based on wellbore storage concept was presented to achieve this goal.

Completion of the instantaneous gas bubble size distributions in the annulus that was started in Chapter 3 was achieved. Effects of various factors on the pressure rise were analyzed. It was noticed that permeability and the initial annular gaseous volume before shut-in play significant roles in determining the duration for pressure stabilization as well as quantitatively determining the rate of gas inflow during shut-in. For formations with different permeability but with equal initial annular gaseous volume, the rate of gas inflow, during shut-in, decreases more rapidly for the highly

Table 4.2 – Conventional drilling fluid pressure design data

Bottom Hole Assembly:			
Riser size	=	19	in. ID
Casing Size	=	11	in. ID
Drill pipe Size	=	5	in. OD
Drill pipe Size	=	4.41	in. ID
Drill Collars	=	8	in. OD
Drill Collars	=	2.81	in. ID
Bit diameter	=	9.875	ins.
Bit nozzle sizes	=	12	/32 in x 3
Total area of the three nozzles	=	0.33147	in^2
Bit nozzles' discharge Coefficient, Cd	=	0.95	constant
Choke Line	=	3	in. ID
Maximum Surface Pump Horse power	=	1000	hp
Drilling Fluid and Formation Properties:			
Mud Flow Rate	=	381	gpm
Surface Pump discharge pressure	=	1543	psi
Drilling Fluid density	=	8.2	ppg = 61.4 lb/ft^3
Mud Plastic viscosity	=	24	cp
Mud Yield Point	=	18	$lbf/100ft^2$
Average velocity in drill pipe (DP)	=	8.0	ft/sec
Average velocity in drill colars (DC)	=	19.7	ft/sec
Average velocity through Nozzles	=	368.8	ft/sec
Mud apparent viscosity for DP	=	90	cp
Mud apparent viscosity for DC	=	41	cp
Mud apparent viscosity for Bit Nozzles	=	24	cp
Mud Surface tension, σ	=	1.30E-02	lbf/ft
Mud flowing Reynolds Number	=	2982	Inside DP
Mud flowing Reynolds Number	=	10257	Inside DC
Mud flowing Reynolds Number	=	129561	Nozzles' exit
Friction Pressure loss in Drill pipe	=	339	psi
Friction Pressure loss in Drill collars	=	136	psi
Mud Flowing BHP (FBHP)	=	**4332**	psi
Formation Pressure	=	4600	psi
Formation Permeability	=	300	md
Formation Porosity	=	0.3	fraction
Mud Hydrostatic Pressure	**=**	**4264**	psi

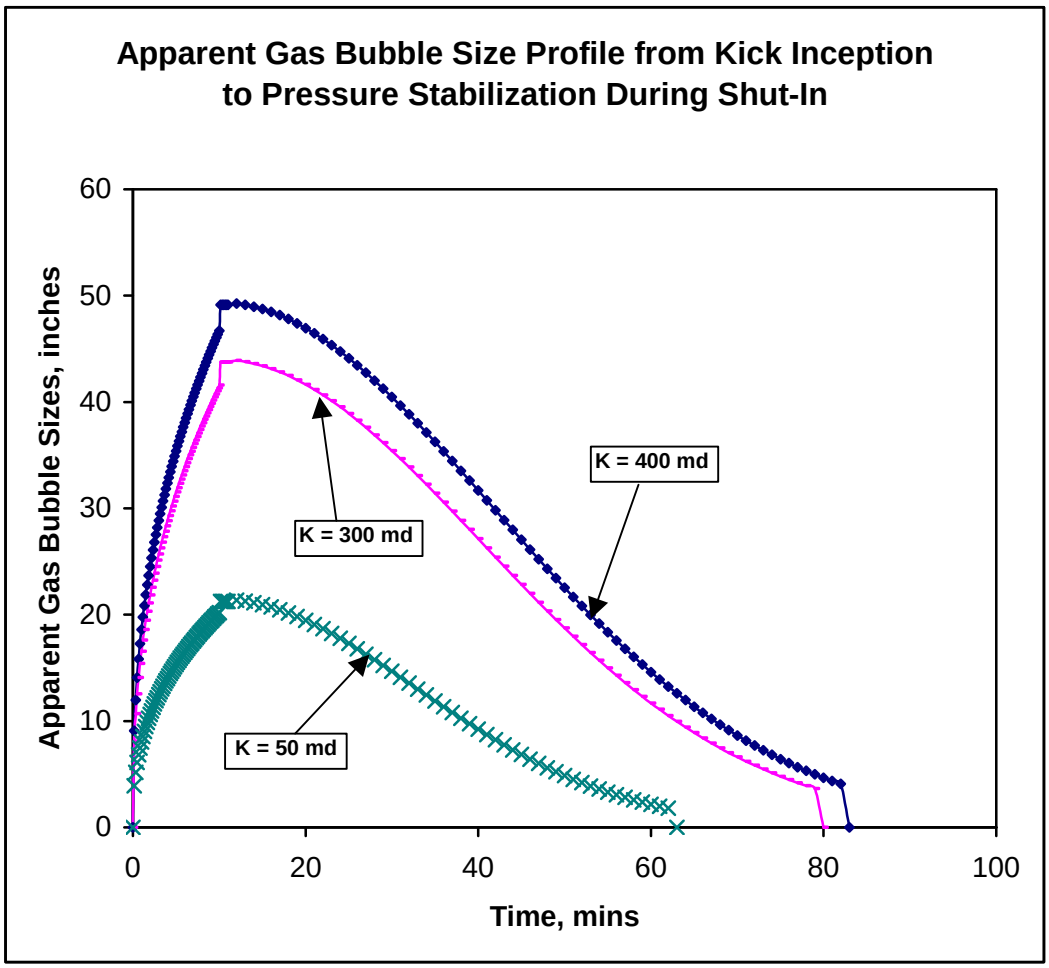

Fig. 4.13 – Apparent gas bubble size profile for the conventional drilling fluid pressure design

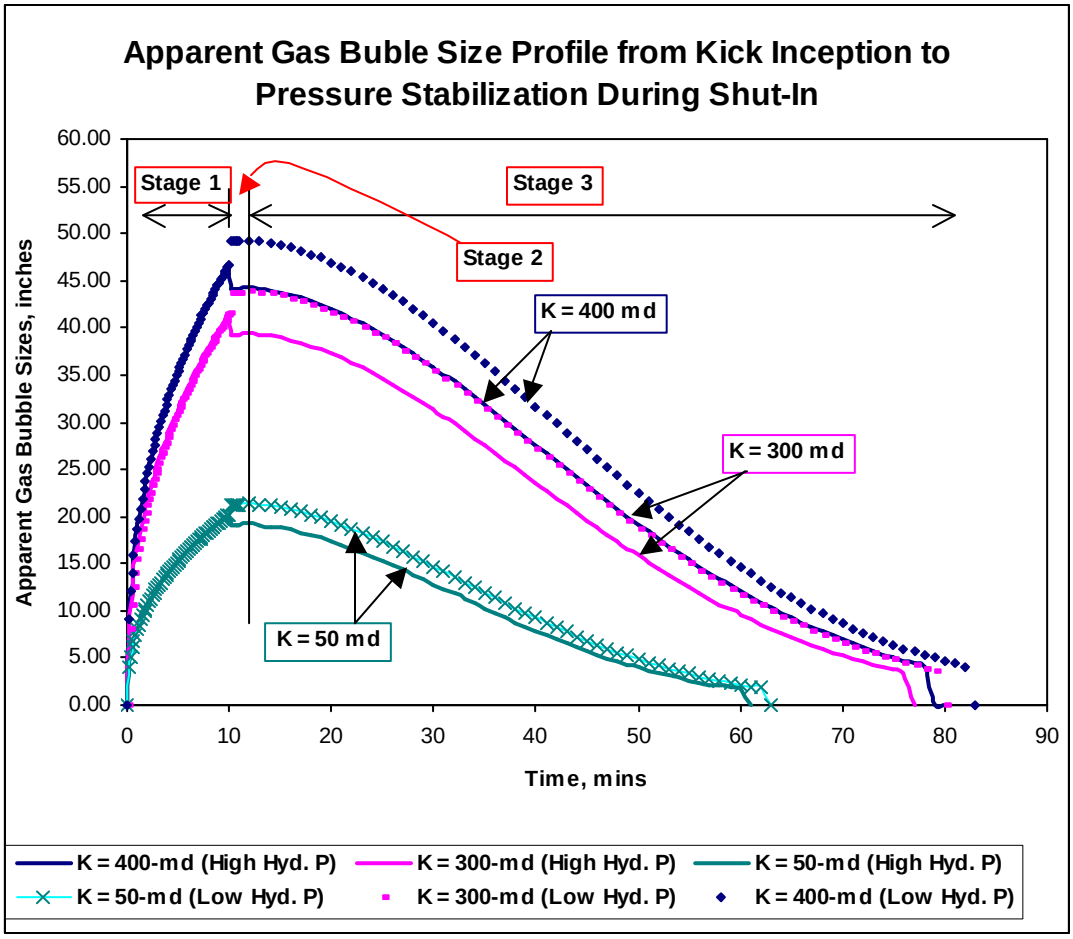

Fig. 4.14 – Effect of drilling fluid hydrostatic pressure on the apparent bubble size profile for the three stages of gas inflow analysis

permeable formations. Finally, it has been shown that the practically assumed small variation in gas density during well shut-in is also theoretically achievable. However, such small variation in gas density could single-handedly generate wellbore pressure build-up.

CHAPTER FIVE

VALIDATION OF MODELS AND PRACTICAL APPLICATIONS

5.1 Introduction

So far two models have been developed and presented. One of the models was utilized in Chapters 3 and 4 to predict the gas bubble sizes/volumes at the instant of inflow into the wellbore. Predictions from this model help in improving the theoretical gas inflow analysis presented in Chapter 2 regarding the total gas volume existing at the reservoir pressure. The second model predicts the surface and bottom-hole pressure variations for a gas-kick during well shut-in.

In order to validate these models, an existing published model on gas kick analysis (validating model), and a field simulated experimental work at the Louisiana State University are chosen. The validating model analyzed only stages 1 and 3 of the three stages presented in this current study. This validating model considered the periods during drilling and shutting-in.

An obvious area of application of the present study is in under-balanced or inflow drilling operations. Some sections in this chapter would be devoted to the quantification of gas inflow during under-balanced drilling, and the estimation of reservoir permeability during well shut-in for a short period while drilling under-balanced.

5.2 Validation of Models

The existing modeling approach by Nickens[55] has been considered to validate the models developed in this study. For proper validation of the modeling approach by the present study, comparison of simulated results from this study and those presented by Nickens[55] was conducted. The developed model from this study and Nickens model were evaluated using the simulation data presented by Nickens. These data are the bolded part of the data presented in **Table 5.1**. Other data are those needed to successfully conduct gas inflow evaluation using the new model. These data are reasonably chosen and calculated using standard engineering expressions from the literatures[50].

As mentioned earlier, Nickens approach is based on the assumption that the gas bubbles exist as uniformly sized and distributed bubbles. This assumption implies that the effect of increasing gas inflow rate on the bubble size as more interval of the formation is exposed is considered negligible. Such assumption is invalid because it has been observed experimentally that gas bubble sizes increase as the inflow rate increases even in more viscous liquids, such as drilling fluids.[109] Moreover, it has been discovered that a bubble trailing another leading bubble moves faster than the leading bubble due to a vorticity force created by the leading bubble. The increase in the velocity of the trailing bubble causes coalescence of the two bubbles to form bigger bubbles[114,116] that could be randomly distributed in the annulus.

There are other gas bubble activities, as the bubbles flow or migrated upwardly that possibly affect the wellbore pressure rises that cannot be technically and adequately accounted for. Such activities are pronounced after the initial

Table 5.1 – Validation Data

Bottom Hole Assembly:		
Riser size	**19**	**in. ID**
Casing Size	**11**	**in. ID**
Drillpipe Size	**5**	**in. OD**
Drillpipe Size	**4.41**	**in. ID**
Drill Collars	**8**	**in. OD**
Drill Collars	**2.81**	**in. ID**
Bit diameter	**9.875**	**ins.**
Bit nozzle sizes	**12/32 in x 3**	
Total area of the three nozzles	0.331	in2
Bit nozzles' discharge Coefficient, Cd	0.95	constant
Choke Line	3	in. ID
Maximum Surface Pump Horse power	1000	hp
Maximum Pump Discharge Pressure	2880	psi
Maximum Flow Rate	595	gal/min
Drilling Fluid and Formation Properties:		
Mud Flow Rate	**400**	**gpm**
Surface Pump discharge pressure	1936	psi
Drilling Fluid density	**10**	**ppg = 75 lb/ft^3**
Mud Plastic viscosity	**15**	**cp**
Mud Yield Point	**8**	**$lb_f/100ft^2$**
Average velocity in drill pipe	8.40	ft/sec
Average velocity in drill collar	20.69	ft/sec
Average velocity through Nozzles	387.15	ft/sec
Mud apparent viscosity for DP	43	cp
Mud apparent viscosity for DC	22	cp
Mud apparent viscosity for Nozzles	15	cp
Mud Surface tension, σ	0	lbf/ft
Mud flowing Reynolds Number	8003	Inside the Drill Pipe
Mud flowing Reynolds Number	24269	Inside the Drill Collars
Mud flowing Reynolds Number	266701	At nozzles' exits
Friction Pressure loss in Drill pipe	381	psi
Friction Pressure loss in Drill collars	153	psi
Flowing BHP (FBHP)	5258	psia
Formation Pressure	**5558**	**psia**
Formation Permeability	**300**	**md**
Formation Porosity	**0.3**	**fraction**
Mud Hydrostatic Presssure	**5200**	**psia**

Table 5.1 – Validation Data (contd.)

Temperature:			
Surface	***70 ^{o}F***	**=**	***530 ^{o}R***
Bottom hole	***180 ^{o}F***	**=**	***640 ^{o}R***
Hole Geometry - VERTICAL HOLE:			
Riser Length	**1000 ft from surface**		
Last Casing Shoe Depth	**4000 ft from the mud line**		
Open-Hole section	**5000 ft from last Casing Shoe**		
Drill Collars' Length	**450 ft**		
Drilled Formation Height, h	1 ft		
Time Required to drill h ft	0.033 hr		
Open-hole radius, r_w	**4.938 ins.**	**=**	**0.411 ft**
Penetration Rate	**30 ft/hr**		
Formation Fluid - GAS - properties:			
Viscosity of gas at 1 ATM	0.0124 cp		
Viscosity ratio	2.02		
Gas Viscosity, μ_g	0.025 cp		
Gas gravity, $S.G_g$	0.6		
Gas Constant, R	10.7		
Gas pseudo-critical pressure	671 psia		
Gas pseudo-critical temp.	358 ^{o}R		
Gas pseudo-reduced pressure	8.283		
Gas pseudo-reduced temperature	1.788		
Gas Compressibility factor, z	1.044		
Gas Density, ρ_g	14 lb/ft^3		
dZ/dP slope at 5558 psia	0.053 psi^{-1}		
Gas compressibility, C_g	0.000104 psi^{-1}		
Gas Formation Volume Factor, Bg	0.003401 ft^3/SCF		
Gas Formation Volume Factor, Bg	0.000606 bbl/SCF		

stabilization period (wellbore storage effect).[101] Due to the complexity of gas bubble flow, it is quite impractical to assume that a particular gas bubble distribution exist in the annulus. Likewise, it is inappropriate to consider any average gas bubble velocity correlation of the assumed bubble distribution as being the controlling factor for gas inflow or wellbore pressure evaluation.

5.2.1 Prediction of Surface Mud Pit Gain

With the assumption of non-dissolution of gas in a liquid system, such as water-based mud, a means of detecting gas inflow into the annulus during drilling is the gain in the surface mud pit. Although this method of detection has been evaluated as being slower in reacting to gas inflow than other means such as change in the standpipe or surface pump pressure[54], it remains one of the most important means of evaluating and detecting gas inflow[115].

Using the data presented in **Table 5.1**, the surface mud pit gains were computed from **Eqs. 3.33** through **3.45** presented in Chapter 3. **Figure 5.1** shows the comparison of these results for the developed model and those obtained by Nickens (validating model). This figure shows that the surface mud pit gain, before surface alertness of gas inflow, increases polynomially with the drilling time. An excellent agreement in the trends of the results from the two models is displayed. However, the slight difference in the magnitude of the results may be due to different gas properties used for computation by the two models. Moreover, the developed model computes for only the gas bubbles sizes/volumes at the instant of inflow into the wellbore from the reservoir. Hence, results from the developed model do not incorporate any bubble

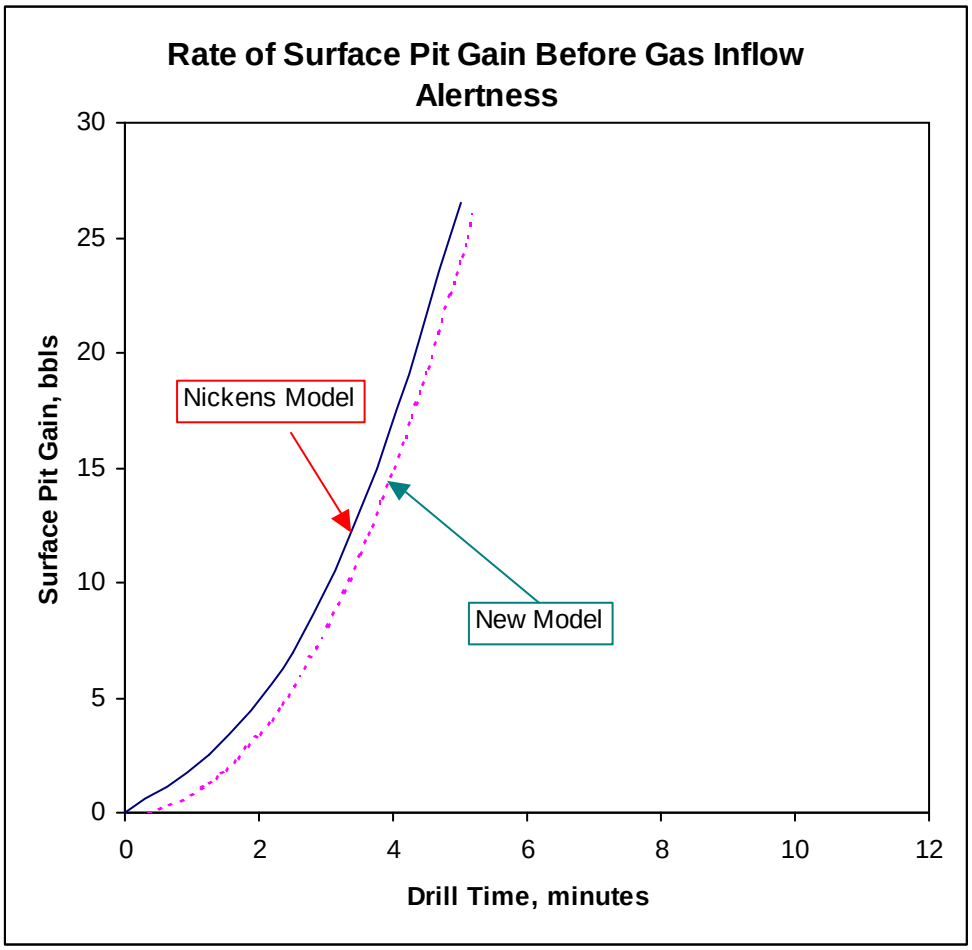

Fig. 5.1 – Comparison of simulation results for the surface pit volume for the developed model and Nickens model

expansion that might have occurred while each of the bubbles flows upward with the circulating drilling fluid. Such expansion could definitely be responsible for the lower predictions by the developed model, if and only if the Nickens model is taken to incorporate the bubble expansion effects, though not vividly stated in the paper.

Another reason for the different results could be attributed to the fact that the new model did not simulate the stage 2 (flow check period) of the present study. Simulating stage 2 requires the knowledge of the time used to watch if the well could flow on its own. Unfortunately, such information is not available among the simulation data presented by Nickens[55]. During stage 2, as presented in Chapter 3, gas inflow continues, and this would definitely cause increase in the annular gas volume with more increase in the pit gain.

5.2.2 Modeling of Bottom-Hole Pressure Rise During Well Shut-in

In practice, whenever a gas inflow into the wellbore occurs, further drilling and circulation of drilling fluid is suspended to visually observe if the well would flow on its own at the surface. If there is significant annular flow, the well is shut-in to properly evaluate the bottom-hole pressure conditions.[1,53] Such standard procedures[117] help to determine how much increase in weight of the drilling fluid is needed to subdue further inflow of the gas when circulating the gas out of the hole, and when drilling operations and drilling fluid circulation resume. In this study, simulation of the shut-in processes has been modeled as stage 3.

Figure 5.2 shows the predictions of the bottom-hole pressure rise during well shut-in on gas-mud mixture up to the initial pressure stabilization of the well. This

figure presents the comparisons of prediction results by both Nickens approach and the developed model. As earlier discussed, Nickens model is based solely on the upward velocity of the gas bubbles during shut-in, while the developed model considers this initial pressure stabilization period as the wellbore storage influenced period. Hence, there are considerable differences existing in the predictions from the two approaches.

Two realistic practical aspects are lacking in the predictions by Nickens. The first being that immediately at shut-in, the bottom-hole pressure is predicted to sharply decrease due to lower hydrostatic pressure in the annulus caused by the presence of the gas bubbles. This period is indicated in **Fig. 5.2** with dashed oval. This consideration is impractical because the reservoir pressure being greater than the bottom-hole pressure at shut-in would not allow the bottom-hole pressure to sharply decrease as presented by Nickens. Rather, a continuous pressure building would result as presented by the developed model. The second aspect is the practical impossibility of recording the surface casing pressure rise at a time interval of 15 minutes[53] if Nickens model is used. The resulting rapid rise in the predictions by Nickens would predict early time pressure stabilization, which could erroneously mislead the drilling crew in assuming a lower bottom-hole pressure as being the reservoir pressure. Hence, attempts to control the gas kick using Nickens model could cause multiple gas kick occurrences at the same depth, which are usually experienced when improper control procedures are followed.

To further support the discussion of gradual bottom-hole pressure rise during the initial stabilization period, a reproduction of the experimental results at the

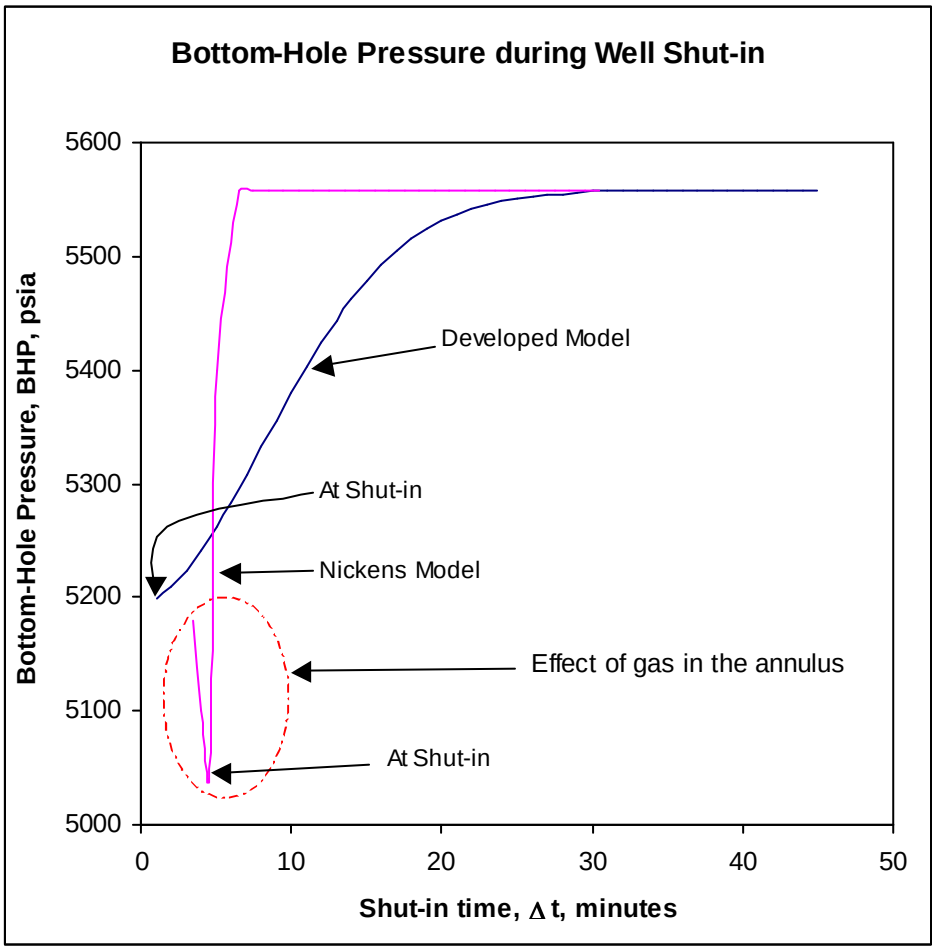

Fig. 5.2 – Comparison of the predictions for bottom-hole pressure rise by Nickens model and the developed model

Louisiana State University LSU-Goldking No. 1 Well[118] is presented in **Fig. 5.3**. The details of the experiment can be found in the cited reference. However, a summary of the test procedure is as follows. After initiating a gas kick with nitrogen gas injection at the bottom-hole through a tube passed from the surface to the bottom-hole, an initial mud pit gain was 11.8 bbl. At this time, the annulus was closed to prevent further outflow of the mud from the annulus, but gas injection continued, which, in reality, simulates the continuous pressurization of the annular fluid by the reservoir. The results show gradual pressure build-up or rise in the system without any initial bottom-hole drop. This is indicated in **Fig. 5.3** as the first shut-in period. Such period is considered as the wellbore storage period because more gas could be injected into the closed annulus to attain the initial wellbore pressure rise during shut-in. Practically, this initial pressure stabilization period is the critical period for estimating the reservoir pressure, which guides the amount of drilling mud weight-up needed.

After attaining a desired casing pressure, the gas injection was stopped, and the casing pressure was maintained by bleeding the mud from the well. This is the second experimental period shown as the mud-bled period in **Fig. 5.3**. Undoubtedly, after the initial pressure stabilization, any subsequent pressure rise at the surface and at the bottom-hole would be due to the continuous closeness of the leading gas bubble to the surface choke. In practice, mud is bled from the wellbore to maintain a desired casing pressure. Maintenance of slightly higher pressure above the initial stabilization of casing pressure helps to achieve a slightly greater bottom-hole pressure than the reservoir pressure. This is the safety pressure margin that allows mud to be periodically bled from the annulus without allowing the bottom-hole pressure to fall

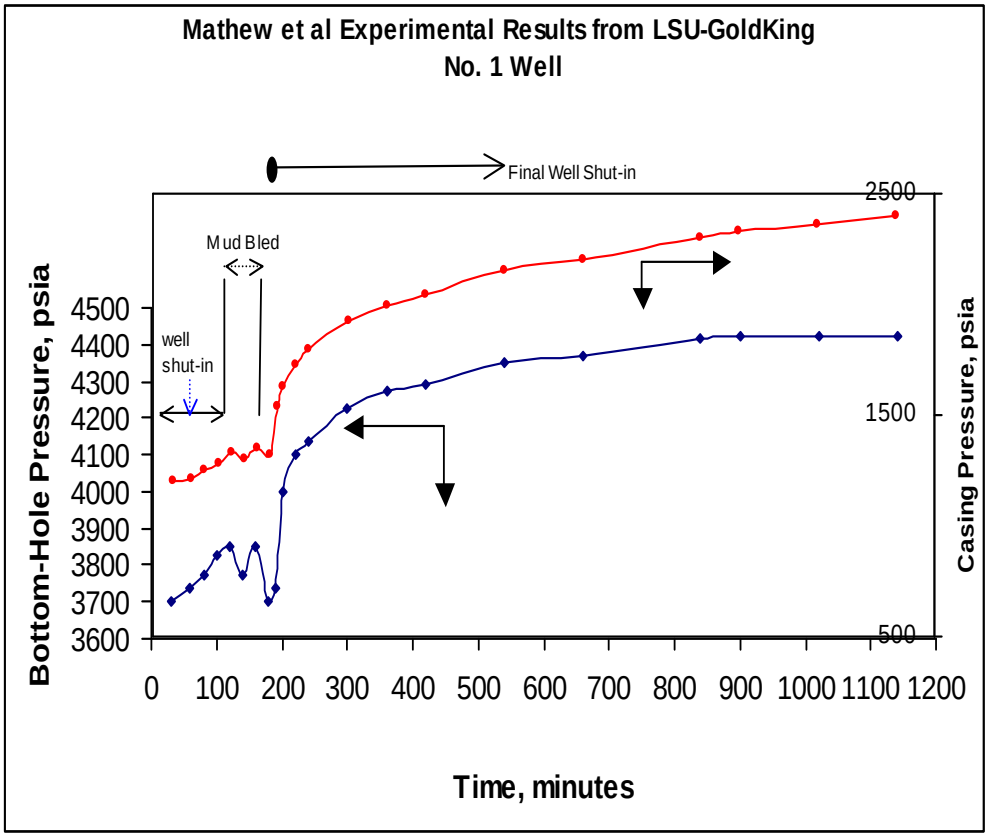

Fig. 5.3- Reproduced plots of the gas kick experimental results at the LSU-Goldking well no. 1[118]

below the reservoir pressure. During this period, any drop in the bottom-hole pressure is as a result of gas bubble expansion, which consequently lowers the equivalent hydrostatic pressure of the gas/mud mixture in the annulus with constant casing pressure.

The final shut-in period shown in **Fig. 5.3** was conducted when the leading gas bubble reaches the surface choke line. A sharp increase in the casing pressure, which also causes sharp increase in the bottom-hole pressure, is due to the high internal pressure of the gas bubbles that is exerted on the surface choke. Although, the experiment procedures did not present how the upward bubble migration affects the rate of wellbore pressure rise, however, some conclusions could be drawn from the experimental results. First, gradual wellbore pressure rise occurs starting from the time a well is shut-in up to the initial pressure stabilization period, that is dominated by wellbore storage. Secondly, rapid wellbore (surface casing and bottom-hole) pressure rise starts when the first gas bubble reaches the surface choke.

Presented in **Fig. 5.4** are the results of another study[86] that utilized bubble upward migration velocity as the determining factor for wellbore pressure rise after shut-in. However, gas pseudopressure was used to analyze the gas behavior. Clearly, one could conclude that the initial influence of the reservoir pressure, referred to as the wellbore storage period, is completely omitted. Rather, it is presented as a no pressure rise period followed by a sharp casing pressure rise, which should produce sharp bottom-hole pressure build-up.

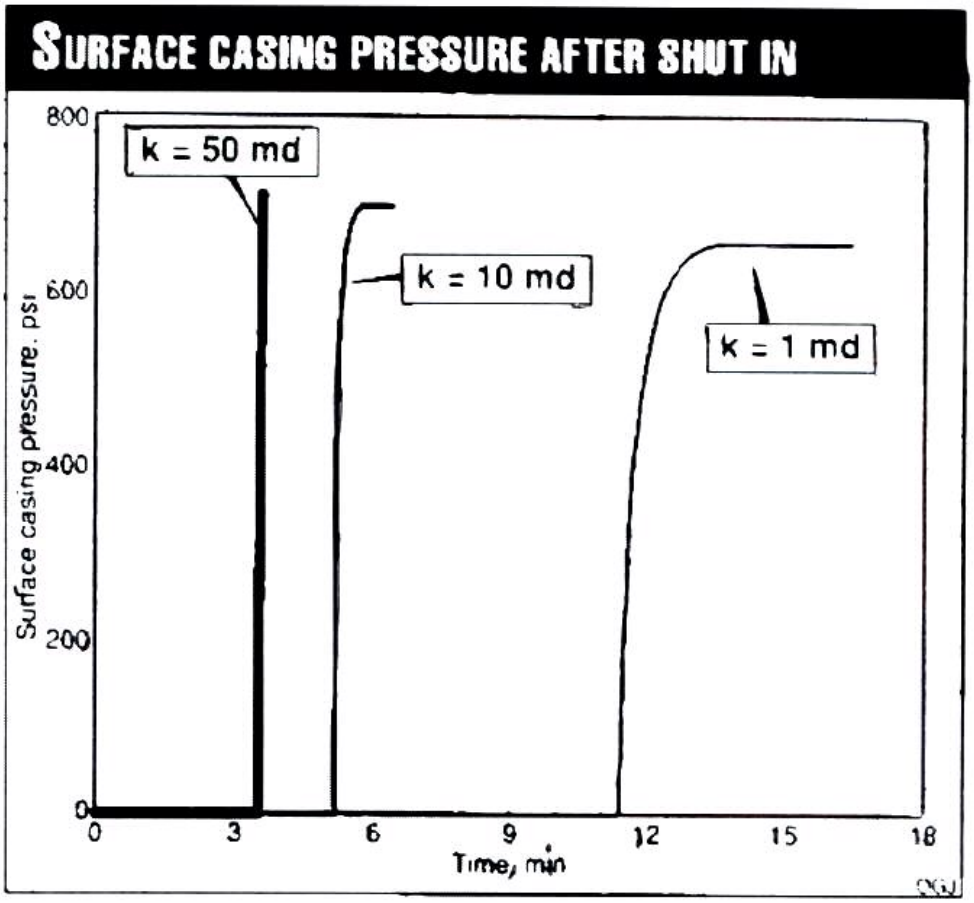

Fig. 5.4 – Surface casing pressure rise without wellbore storage effect considerations[86]

5.3 Quantitative Prediction of Gas Inflow During Under-balanced Drilling

One of the advantages of under-balanced drilling is the ability to evaluate the productivity of a reservoir during drilling operations.[119] Other benefits are the reduced formation damage, higher penetration rate especially in hard rocks, and lower cost of drilling operations if under-balanced could consistently be maintained.[120] However, from the real-time bottom-hole pressure measurements while drilling, it is obvious that continuous maintenance of under-balanced conditions at the bottom-hole is difficult. Pressure surges that occur during some subsidiary operations such as pipe connections and surveys tend to jeopardize the achievement of complete elimination of formation damage.[121]

From the recent literatures, reservoir evaluation has been approached through the estimation of the reservoir fluids flow rates into the wellbore. Assumption of the reservoir fluid inflow rate being the difference in the drilling fluid surface injection rate and the fluid outflow rate from the annulus.[122-128] So far, efforts in modeling reservoir fluid inflow have been concentrated on the oil inflow.[122-128] Considering the existence of other forces such as interfacial tension that is associated with gas inflow into a liquid system, different flow rates, and different physical characteristics that exist among the different phases of the reservoir fluids, it would be inappropriate to assume the same procedures for predominantly oil, and predominantly gas inflow into a liquid system.

Therefore, considering the fact that the induction of gas kick is due to the existence of under-balanced pressure conditions at the bottom-hole, the modeling

procedures presented in Chapter 3 could then be used for predicting the total volume of gas inflow while drilling. This is possible if under-balanced condition is maintained at the bottom-hole. An advantage of this prediction approach over those that depend on the difference between the fluid injection and fluid outflow rates is that the increasing fluid outflow rate from the annulus due to the gas expansion is eliminated. Likewise, the influence of the unloading wellbore storage on the total fluid outflow rate from the annulus is eliminated. The unloading effect causes the measured outflow rate to be higher than the reservoir fluid inflow rate at the bottom-hole if no fluid injection into the drillstring is permitted.

Unfortunately, all of these additional flow rates cannot be individually measured, and thus, the reservoir fluid inflow rate at the bottom-hole cannot be practically modified for their influences. Not recognizing the impact of such additional flow rates could cause misjudgment of the inflow capabilities of the gas into the wellbore. By predicting gas volume at the instant of inflow into the wellbore, better judgment on the production capability of the gas reservoir could be ascertained.

5.4 Estimation of the Gas Reservoir Permeability and Pore- Pressure

Prediction of reservoir characteristics during under-balanced drilling is undoubtedly a complex and cumbersome task. Recent studies[122-128] on the subject have shown efforts being made to judiciously utilize the available measurable information during the underbalanced drilling to gain insights on characterizing the reservoirs being drilled. Apart from the study by Kneissl[125], all other studies are based on alterations of both the reservoir pressure and suitable reservoir permeability values

in commercial reservoir and wellbore transient simulators to predict the measurable bottom-hole pressure during underbalanced drilling.

On the contrary, Kneissl[125] resolved the fluid inflow equation for two drilled incremented intervals to obtain two equations with two unknown variables (reservoir pressure and reservoir permeability). Solving the resulting equations simultaneously could yield the estimates for the reservoir pressure and permeability. However, the reservoir fluid inflow rate for each of these incremental intervals is assumed known through a downhole flow meter. If, however, a downhole flow meter is absent, such reservoir fluid inflow rate is assumed as the difference between the surface outflow rate and the injection rate.[125] In practice, Biswas et al[128] stated that direct inflow rate measurement from reservoir is presently impossible during underbalanced drilling.

5.4.1 Improving on the Existing Approaches

An obvious oversight from estimating reservoir inflow rate from surface flow measurements (injection and outflow rates) is the fact that the total fluid outflow rate from the annulus is not the sum of the injection, reservoir production and wellbore storage rates as always being assumed. It is a fact that there are considerable differences in the rate at which the drilling fluid is injected into the drill string at the surface and the rate of its ejection at the bit-reservoir contact. Therefore, the most appropriate approach should, rather, have been the following expression:

$$Q_{s,ann} = Q_{bit,ej}(t) + Q_{res}(t) + Q_{wbs}(t) \qquad \ldots 5.1$$

Where,

$$Q_{bit,ej} = f\left(Q_{s,inj},\ f_{dp},\ bit\ nozzle\ sizes,\ hole\ depth,.....\right) \qquad \ldots 5.2$$

$Q_{bit,ej}$ = rate of drilling fluid ejection at the bit-reservoir contact

$Q_{s,ann}$ = total fluid outflow rate from the annulus

Q_{res} = rate of reservoir fluid inflow

Q_{wbs} = contributions to the outflow rate due to wellbore storage effect

In **Eq. 5.1**, Q_{wbs} includes the outflow rate contribution from the rate of gas bubble expansion (unloading) and compressions (loading) as the case may be. Ability to individually measure the various flow rates at the RHS of **Eq. 5.1** would significantly improve on the analyses of the currently existing approaches. However, it is difficult, if not impossible, to estimate the expansion and/or contraction rates of all the gas bubbles existing at different depths inside the annulus. Hence, inaccurate estimation of wellbore storage effect could introduce significant error in the final prediction of reservoir pressure and permeability using this approach.[128]

5.4.2 Proposed Approach for Estimating the Reservoir Pressure and Permeability

From previous discussions, it is clear that the contribution of the wellbore storage effect to the fluid outflow rate from the annulus is practically impossible to be quantitatively evaluated. A better approach of adequately minimizing the uncertainties surrounding this event is to shut-in the well. By so doing, all of the gas bubbles would not expand any further, which eliminates the unloading aspect of the wellbore storage effect. This approach narrows down the uncertainties to only the

loading aspect of wellbore storage, which has been simulated in Chapter 4 of this study.

Also during well shut-in, measuring and/or determining the rates of fluid injection into the drill pipe, fluid ejection rate at the bit-reservoir contact, and the outflow rate are eliminated. This, consequentially, allows reservoir fluid inflow analysis to be solely dependent on the reservoir response to the wellbore conditions. However, any analysis to be conducted during well shut-in must be fast enough to avoid the bottom-hole status reaching overbalanced conditions.

Judging from the presently existing approaches, the procedures for estimating the reservoir pressure and permeability is by statistical alteration of these properties to history match the measurable bottom-hole pressure. That is, one of the reservoir properties is assumed known or kept constant while the other property is altered. However, there has always been difficulty in matching the flowing bottom-hole pressure when these reservoir properties are simultaneously and randomly varied.[126-127] Therefore, parametric sensitivity study is performed to determine which of the two reservoir parameters is most sensitive to the analysis. Using the well shut-in model presented in Chapter 4, the reservoir pressure and the reservoir permeability were separately varied. **Figure 5.5** shows the bottom-hole pressure rise during well shut-in on gas inflow. The effects of keeping the reservoir permeability constant and varying the reservoir pressures at intervals of 50-psi (5558, 5608, and 5658-psi) and 200-psi (5558 and 5358-psi) are displayed. On the other hand, **Fig. 5.6** shows the effects of keeping the reservoir pressure constant and varying the reservoir permeability at intervals of 100-md (300 and 400-md) and 350-md (400 and 50-md). From these

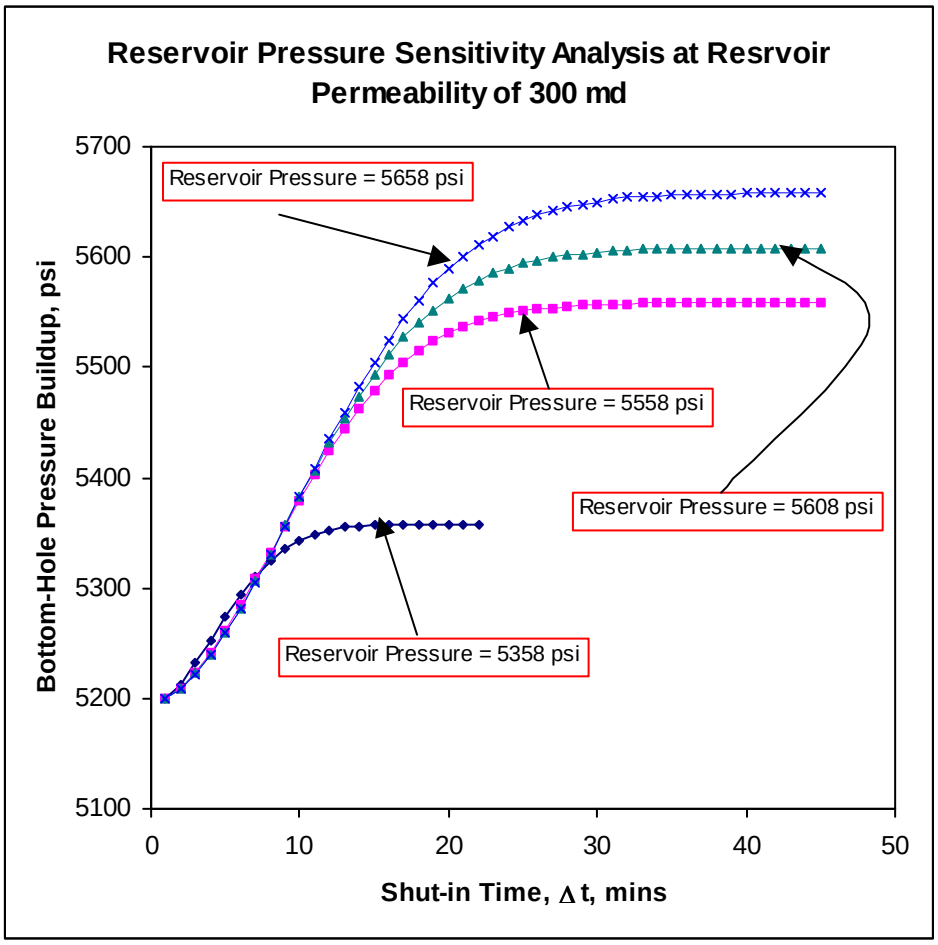

Fig. 5.5 – Reservoir pressure sensitivity study at constant reservoir permeability.

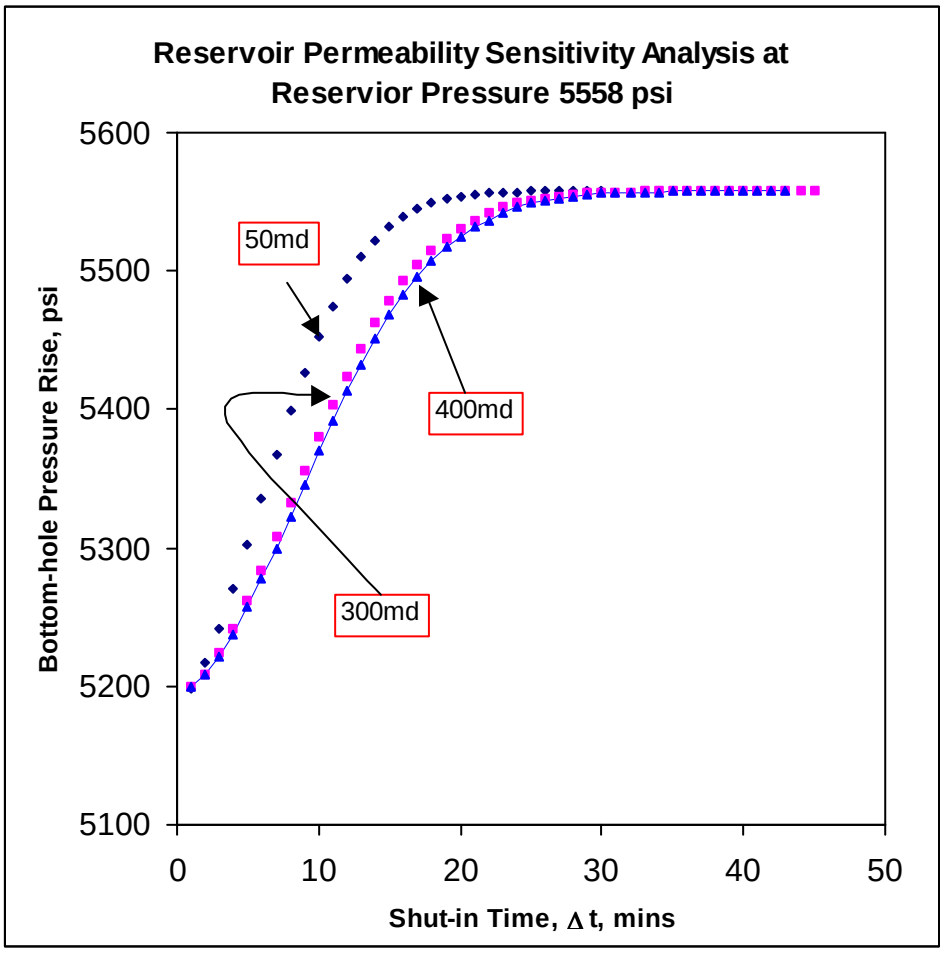

Fig. 5.6 – Reservoir permeability sensitivity study at constant reservoir pressure.

analyses, it is clear that the reservoir pressure is the most sensitive of the two reservoir properties because at smaller varying interval, than that of the permeability, it causes larger differences in the bottom-hole pressure at a particular shut-in time. These observations indicate that systematic variation of these parameters needs to be adopted to achieve speedy and meaningful results. Lack of such systematic variation could probably cause the poor prediction of the reservoir pressure and permeability as, also, presented by Vefring et al[127].

5.5 Summary

An existing published analytical model of Nickens[55], and a field experiment of a gas kick by Mathews and Bourgoyne[118] have been used to validate the two models developed and analyzed in Chapters 3 and 4. The field experiment confirms that bottom-hole pressure starts to build immediately the well is shut-in, as presented in this study, and the bottom-hole pressure does not rise sharply during this period. This shows that the similar approaches used by the various existing models are practically less adequate in predicting the initial pressure stabilization time from which the reservoir pressure is estimated, which also determines the success of a gas kick control.

In predicting the productivity capabilities of a gas reservoir, it has been shown that analyzing the gas inflow at the sand-wellbore face would better determine how well the reservoir actually produces without significant influences by the various wellbore conditions. A wellbore condition of pressure reduction on the gas as it flows to the surface would result in gas expansion, which then could indicate false

productivity capability of the gas reservoir if outflow production rate of the gas is used to evaluate the reservoir.

A more controllable approach for estimating the reservoir pressure and permeability during underbalanced drilling was introduced. Also, correction to the currently used surface flow rates approach was provided. It was indicated that the assumption of the difference in the fluid injection rate into the drill pipe and the fluid outflow rate from the annulus being taken as the inflow rate from the reservoir is incorrect. Also, the influence of wellbore loading and unloading (wellbore storage effect) cannot be quantitatively estimated in practice. In order to simplify or reduce the complexity of estimating reservoir properties (reservoir pressure and permeability) during under-balanced drilling, a well shut-in approach was presented. Sensitivity study showed that for gas reservoir, the reservoir pressure is more sensitive to the analysis than the reservoir permeability. Hence, in estimating any of these properties, better prediction or measured data matching could be obtained when the less sensitive property is held constant while the more sensitive property is varied.

CHAPTER SIX

CONCLUSIONS AND RECOMMENDATION

6.1 Conclusions

1. Two models were developed: gas bubbly model that is applicable to all of the three stages; and, a wellbore pressure build-up model that is based on the increasing annular fluid density during well shut-in was applied to stage 3 only. The gas bubbly model showed greater magnitude of reduction in the apparent gas bubble size, and the wellbore pressure build-up model showed greater reduction in the bottom-hole pressure change after certain shut-in period for the cases of gas formations with high permeability that are subjected to the same rate of increasing wellbore pressure.
2. Since the gas inflow into a denser fluid system is bubbly in nature while liquid inflow is streaky, it is paramount to incorporate the forces of the viscous, surface tension, inertia, and the buoyancy that are responsible for gas bubble formation or development in modeling gas inflow scenarios.
3. During the opened wellbore stages (stages 1 and 2), increase in permeability of the gas formations causes increase in the bubble sizes/volumes under the same conditions of drilling and other reservoir properties. Consequentially, there is increase in the rate at which the surface mud pit rises during these stages.

4. Assumption of radial flow of gas into partially penetrated wellbores of ≤ 1-ft for the modeling conditions stipulated in this study has proven to be inadequate for gas formations of considerable vertical permeability. Hence, for such short partial penetration into gas formations, a hemispherical inflow expression would be more appropriate.
5. Porosity effect on gas production is not apparent at smaller drilled gas formation interval. However, for long interval, based on cumulative gas produced, gas formation with lower porosity produces more gas volume than one with higher porosity due to the greater pore space compression. This was in agreement with the published data. Occurrence of this effect at the near wellbore could also contribute to additional near wellbore damage. This shows that a gas formation with significant porosity variation throughout the formation could have varying pore space compression, and hence varying internal porosity damages. This effect could trigger increasing permeability impairment, and hence, limit the ultimate recovery from such gas formation.
6. Permeability and the initial annular gaseous volume before shut-in play significant roles in determining the duration for pressure stabilization as well as quantitatively determining the rate of further gas inflow during shut-in. For formations with different permeability but with equal initial annular gaseous volume, the rate of gas inflow, during shut-in, decreases more rapidly for the highly permeable formations.

7. During bottom-hole pressure rise, gas formations with higher permeability allow higher rate of backpressure transmission from the wellbore into the gas formation to curtail further gas inflow.
8. In agreement with the experimental results from another author, the simulation results from this study showed that there is continuous bottom-hole pressure rise from shut-in to pressure stabilization. Existing approaches, otherwise, have indicated initial sharp drop in bottom-hole pressure immediately at shut-in. Such drop in the initial bottom-hole pressure has been simulated to be due to the reduced annular fluid density by the presence of the gas in the wellbore liquid system.
9. Small gas density variation during pressure build-up inside a shut-in wellbore, as always practically assumed, has been theoretically proven. However, such small gas density variation that is practically considered non-influential to wellbore pressure build-up has been shown to single-handedly generate considerable bottom-hole pressure build-up.

6.2 Recommendation

Numerical approach for adopting an approximate expression for the dimensionless pseudo-pressure transformation term for analytical procedures is required if analysis at partial penetration depth controlled by hemispherical flow is desired.

NOMENCLATURE

A = Arbitrary constant

A_t = Total crossectional area across the tri-cone bit nozzles, in^2

B = Arbitrary constant

BOP = Blow-Out-Preventer

B_g = Gas Formation Volume Factor, FVF, cu ft/SCF, bbls/SCF

c_g = Reservoir or formation gas compressibility, psi^{-1}

C_d = Nozzle discharge coefficient, constant = 0.95

d = Pipe or collar inside diameter, in

d_{bit} = Bit diameter, in

$d_{nz1,2,3}$ = Diameter of the bit nozzle 1, 2, and 3, in

d_H = Hydraulic diameter of the reservoir, ft

d_o = Orifice diameter, in

d_{Db} = Bubble diameter, ft

D = Gas supply opening, i.e Orifice diameter, cm

D_{bh} = Vertical depth of wellbore, ft

$\overline{D}_p$ = Average sand particle or grain diameter, ft

F_{ST} = Downward or opposing force on the bubble development due to the surface tension of the drilling fluid, lb_f

F_{vis} = Viscous force, lb_f

F_I = Inertia force, lb_f

F_{BF} = Buoyancy force, lb_f

g = Acceleration due to gravity, constant = 32.174 ft/sec^2

G = Discharge constant for the gas supply opening, i.e. Orifice

h = Formation interval or height drilled, ft

h_k = Length of the gas kick, ft

h_w = Vertical depth of the entire wellbore, ft

k = Formation permeability, md

L_{dp}, L = Vertical Length of drill pipes, ft

L_{dc}, L = Vertical Length of drill collars, ft

LHS = Left-Hand-Side of an expression

M = Virtual mass, lb

N_{RE} = Reynolds Number, dimensionless

ppg = pounds per gals

P_{res} = Formation or reservoir pressure, psi

P_{bh} = Total Bottom hole pressure opposing bubble formation, psi

P_{wb} = Bottom-hole circulating pressure from the nozzle jetting action, psia

P_D = Dimensionless Wellbore or Bottomhole pressure parameter

P_{hyd} = Hydrostatic pressure of drilling fluid, psi

P_{frac} = Formation fracture pressure, psi

P_{ob} = Overburden pressure, psi

q_g = Formation gas flow rate, scf/D, cuft

q_l = Drilling fluid flow rate, constant, gal/min (gpm)

r_b = Expanding radius of the forming bubble, ft

r_H = Hydraulic radius of the reservoir, ft

r_o = radius of the orifice opening, cm

r_w = Well bore bottom hole radius, ft

R = Dynamic combined modulus, psi

RHS = Right-Hand-Side of an expression

ROP = Rate of penetration, ft/hr

SIDPP = Shut-in Drill Pipe Pressure after pressure stabilization at the surface, psi

t = Time required to drill an interval of a formation, hr

t_b = Bubble expansion time, hr

t_D = Dimensionless time parameter

T_{bh} = Bottom hole temperature, ^{o}R

V_B = Bubble Volume at equalization of forces, cu ft

Z_g = Reservoir or formation gas compressibility factor,

Greek Symbols

v_s = Sonic or Seismic velocity, ft/s

$v_{s,\max}$ = Sonic velocity at the onset of unloading effect, ft/s

σ_v = Matrix effective vertical stress, psi

$\sigma_{v,\max}$ = Matrix effective stress at the onset of unloading effect, psi

μ_p, μ_l = Drilling fluid plastic or liquid viscosity, cp

ρ_{lC} = Bottom hole circulating mud density, ppg

$\bar{v}_{dc}$ = Average drilling fluid velocity through the drill collars, ft/sec

ρ_l = Drilling fluid or mud or liquid density, lb_m/ft^3, ppg

ρ_g = Gas density, constant, lb_m/ft^3, ppg

ρ_k = Density of the gas kick, ppg

$\Delta\rho$ = $\rho_l - \rho_g$, ppg

ρ_{lN} = Mud density equivalent of the normal pore pressure gradient at that depth,

σ = Surface tension of the drilling fluid, lb_f/ft

μ_g = gas viscosity, cp

λ_g = annular gas volumetric fraction

ϕ = Formation porosity, fraction

ΔP_{pump} = Discharge pressure differential from the surface mud pump, psi

Subscripts

B = Bubble status at the equalization of forces

Db = Bubble status at detachment, after forces equalization

wb = conditions at the exit of the bit nozzles downhole

spg = surface pit gain

res = reservoir conditions

fl = fluid

1 = A Numeric that signifies stage 1 of gas inflow

2 = A Numeric that signifies stage 2 of gas inflow

REFERENCES

1. Moore, P. L.: Drilling Practices Manual, 2nd Ed., PennWell Publishing Company, Tulsa, Oklahoma, 1986, Pg. 586

2. Fertl, W. H.: Abnormal Formation Pressures, Else Scientific Publishing Company, Amsterdam, Oxford – New York, 1976

3. Fertl, W. H., and Timko, D. J.: "Parameters for Identification of Overpressure Formations", SPE 3223

4. Gill, J. A.: "Shale Minerology and Overpressure: Some Case Histories of Pressure Detection Worldwide Utilizing Consistent Shale Minerology Parameters", SPE 3890.

5. Terzaghi, K., and Peck, R. B.: Soil Mechanics in Engineering Practice, John Wiley & Sons, Inc., N.Y., 1948.

6. Hubbert, M. K., and Rubey, W. W.: "Role of Fluid Pressure in Mechanics of Overthrust Faulting. Part I", Bull. GSA, Feb. 1959, 70

7. Keith, L. A., and Rimstidt, J. D.: "A Numerical Compaction Model of Overpressuring in Shales", Mathematical Geology, Vol. 17, No. 2, 198

8. Doyen, P. M., Psaila, D. E., den Boer, L. D., and Jans, D.: "Reconciling Data at Seismic and Well log Scales in 3-D Earth Modeling," SPE 38698.

9. Gurevich, A. E., and Chilingar, G. V.: "Abnormal Pressures in Azerbaijan: A Brief Critical Review and Recommendations", Journal of Petroleum Science and Engineering, 13, (1995) Pg 125 – 135.

10. Harper, D.: "New Findings from Over Pressure Detection Curves in Tectonically Stressed Beds", SPE 2781

11. Qiuguo, L., Heliot, D., Liangxiao, Z., and Yuxin, C.: "Abnormal Pressure Detection and Wellbore Stability Evaluation in Carbonate Formations of East Sichuan, China," IADC/SPE 59125

12. Jackson, T. S., Gorrara, A. J., and Chmela, W.: "Coiled Tubing Seismic While Drilling," SPE 68416

13. Jorden, J. R., and Shirley, O. J.: “Application of Drilling Performance Data to Overpressure Detection”, JPT, November 1966, Pg 1387-1394.

14. Sugimura, Y. et al.: “Development for Acoustic Sensing System Ahead of the Bit for Detection of Abnormally High-Pressured Formation”, SPE 56700.

15. Holbrook, P. W., and Hauck, M. L.: “A Petrophysical-Mechanical Math Model for Real-Time Wellsite Pore Pressure/Fracture Gradient Prediction,” SPE 16666.

16. Herbert, W. E., and Young, F. S.: “Estimation of Formation Pressure with Regression Models of Drilling Data”, JPT, January 1972, Pg 9-15

17. Bourgoyne, Jr. A. T., and Young, F. S.: “A Multiple Regression Approach to optimal Drilling and Abnormal Pressure Detection”, SPEJ, August 1974, Pg 371-384.

18. Ransom, R. C.: “A Method For Calculating Pore Pressures From Well Logs”, The Log Analyst, March-April, 1986, Pg 72 – 76.

19. Herring, E. A.: “Estimating Abnormal Pressures from Log Data in the North Sea”, SPE 4301.

20. Alixant, J, and Desbrandes, R.: “Explicit Pore-Pressure Evaluation: Concept and Application,” SPE Reprint Series, No. 49 – Pore Pressure and Fracture Gradients, 1991, Pg. 50 – 56.

21. Hottman, C. E., and Johnson, R. K.: “Estimation of Formation Pressures from Log-Derived Shale Properties”, JPT, June 1965, Pg 717 – 722

22. Foster, J. B., Whalen, H. E.: “Estimation of Formation Pressures from Electrical Surveys – Offshore Louisiana”, JPT, February, 1966, Pg 165 - 171

23. Matthews, W. R., and Kelly, J.: “How to Predict Formation Pressure and Fracture Gradient”, OGJ, Feb. 20, 1967, Pg 92-106.

24. Pennebaker, Jr., E. S.: “Seismic Data Indicate Depth, Magnitude of Abnormal Pressures”, World Oil, June 1968, Pg 73 – 77

25. Eaton, Ben A.: “The Effect of Overburden Stress on Geopressure Prediction from Well Logs”, JPT, August, 1972, Pg 929 – 934

26. Eaton, Ben., A.: “The Equation for Geopressure Prediction from Well Logs”, SPE 5544

27. Stein, N.: “Seismic Data used to Predict Formation Pressures”, OGJ, Nov. 30, 1992, Pg 55-58

28. Weakley, R. R.: “Use of Surface Seismic Data to Predict Formation Pore Pressures (Sand Shale Depositional Environments),” SPE/IADC 18713.

29. Weakley, R. R.: “Recalibration Techniques for Accurate Determinations of Formation Pore Pressures from Shale Resistivity”, SPE 19563

30. Weakley, R. R.: “Use of Surface Seismic Data to Predict Formation Pore Pressure Worldwide,” SPE 21752

31. Bilgeri, D., and Ademeno, E. B.: “Predicting Abnormally Pressured Sedimentary Rocks,” Geophysical Prospecting 30, 608-621, 1982

32. Bowers, G. L.: “Pore Pressure estimation from Velocity Data: Accounting for Overpressure Mechanisms besides Under-compaction,” SPE Drilling and Completion, June 1995, Pg 89 - 95

33. Guzman, C. E., Davenport, H. A., and Wilhelm, R.: “Calibration Method helps in Seismic Velocity Interpretation,” OGJ, Nov. 3, 1997, Pg 44-54.

34. Reynolds, E. B.: “Predicting Overpressure Zones with Seismic Data,” World Oil, 171, 78 – 82.

35. Badri, M. A., Sayers, C., Hussein, R. A., and Graziano, A.: “Pore Pressure Prediction using Seismic Velocities and Log Data in the offshore Nile Delta, Egypt”, SPE 68195, March, 2001

36. Martinez, R. D., Schroeder, J. D., and King, G. A.: “Formation Pressure Prediction with Seismic Data from the Gulf of Mexico,” SPE Formation Evaluation, March 1991, Pg 27-32.

37. Atencio, M., Sanchez, V., Breda, E., Fronza, S., Saavedra, B., Hansen, T., and Souza, J.: “Well Logs and 3D Seismic Data Integration using Geostatistical Methods, Lomas del Cuy Field – Golfo San Jorge Basin – Argentina,” SPE 64628

38. Dutta, N. C.: "Shale compaction and abnormal pore pressures: A model of geopressures in the Gulf Coast Basin," 53rd Annual International Meeting, Society of Exploration Geophysicists, Expanded Abstracts, 83, Session S20.2, 1983

39. Whilhelm, R., Franceware, L. B., and Guzman, C. E.: "Seismic Pressure-Prediction Method Solves Problem common in Deepwater Gulf of Mexico," OGJ, Sept. 14, 1998, Pg 67-75

40. Audet, D. M.: "Compaction and Overpressuring in Pleistocene Sediments on the Louisiana Shelf, Gulf of Mexico," Marine and Petroleum Geology, 1996, Vol. 13, No. 5, Pg 467-474.

41. Foster Jr., J.: "Pore-pressure plot accuracy increased by multiple trend lines", OGJ, May 7, 1990, Pg 100 – 108

42. Serebryakov, V. A., Chilingar, G. V., and Katz, S. A.: "Methods of Estimating and Predicting Formation Pressures", Journal of Petroleum Science and Engineering, 13, (1995) Pg 113 – 123.

43. Evers, J. F., and Ezeanyim R.: "Prediction of Abnormal Pressures in Wyoming Sedimentary basins Using Well Logs", SPE 11859

44. Owolabi, O. O., Okpobiri, G. A., and Obomanu, I. A.: "Prediction of Abnormal Pressures in the Niger Delta Basin Using Well Logs", SPE 21575 or CIM/SPE 90-75

45. Aremu, O. J., and Osisanya, S. O.: "Re-Examination of Offset Field-Data Calibration for the Purpose of Abnormal Pressure Prediction," a paper OTC 15251 presented at the 2003 Annual Offshore Technology Conference held in Houston, Texas, U.S.A., 5-8 May, 2003

46. Yoshida, C., Ikeda, S., and Eaton, B. A.: "An Investigative Study of Recent Technologies Used for Prediction, Detection, and Evaluation of Abnormal Formation Pressure and Fracture Pressure in North and South America", IADC/SPE 36381, Pg 131-151.

47. Yassir, N. A. and Bell, J. S.: "Abnormally High Fluid Pressures and Associated Porosities and Stress Regimes in Sedimentary Basins," SPE Formation Evaluation, March 1996, Pg 5-10.

48. Cheney, W., and Kincaid, D.: Numerical Mathematics and Computing, Fourth Edition, Brooks/Cole Publishing Company, 1999, Pg. 317.

49. Bassiouni, Z.: Theory, Measurement, and interpretation of Well Logs, SPE Textbook Series, Vol. 4.

50. Bourgoyne, A. T., Chenevert, M. E., Millheim, K. K., and Young Jr., F. S.: Applied Drilling Engineering, SPE Textbook Series, Vol. 2, 1991, Pg 261.

51. Investigation of blowout and fire, Eugene Island block 284, OCS-G 0991 Well A-13, Gulf of Mexico off the Louisiana coast, published by the U.S. Dept. of the Interior, Mineral Management Service, March 1, 2001

52. Investigation of October 1982 blowout and fire, Eugene Island Block 361, Gulf of Mexico, published by the U. S. Geological Survey

53. Grace, R. D.: Advanced Blowout and Well Control, Gulf Publishing Company, Houston, Texas, 1994, Pg. 395

54. Maus, L. D., Tannich, J. D., and llfrey, W. T.: "Instrumentation Requirements for Kick Detection in Deep Water," JPT, August 1979, Pg. 1029 –1034

55. Nickens, H. V.: "A Dynamic Computer Model of a Kicking Well," SPE Drilling Engineering, June 1987, Pg. 159 –173

56. Levy, S.: Two-Phase Flow in Complex Systems, John Wiley & Sons, 1999

57. Wallis, G. B.: One-Dimensional Two-Phase Flow, McGraw-Hill, Inc., 1969, Pg. 408

58. Davies, R. M., and Taylor, G.: "The mechanics of large bubbles rising through extended liquids and through liquids in tubes," Proceedings of the Royal Society, 1950, Vol. 200A, Pg. 375-390

59. Harmathy, T. Z.: "Velocity of Large Drops and Bubbles in Media of Infinite or Restricted Extent," AIChE Journal, June 1960, Vol. 6, No. 2, Pg. 281-288

60. White, E. T., and Beardmore, R. H.: "The Velocity of Rise of Single Cylindrical Air Bubbles through Liquids Contained in Vertical Tubes," Chemical Engineering Science, 1962, Vol. 17, Pg. 351-361

61. Nicklin, D. J., Wilkes, J. O., and Davidson, J. F.: "Two-Phase Flow in Vertical Tubes," Transactions of the Institution of Chemical Engineers, 1962, Vol. 40, Pg. 61-68

62. Taitel, Y., Bornea, D., and Dukler, A. E.: "Modeling Flow Pattern Transitions for Steady Upward Gas-Liquid Flow in Vertical Tubes," AIChE Journal, Vol. 26, No. 3, May 1980, Pg. 345-354

63. Davidson, J. F., and Schuler, B. O. G.: “Bubble Formation at an Orifice in a Viscous Liquid,” Transaction of the Institution of Chemical Engineers, Vol. 38, 1960, Pg. 144 –154

64. Ramakrishnan, S., Kumar, R., and Kuloor, N. R.: “Studies in Bubble Formation – I: Bubble Formation under constant Flow Conditions,” Chemical Engineering Science, 1969, Vol. 24, Pg. 731 – 747

65. Satyanarayan, A., Kumar, R., and Kuloor, N. R.: “Studies in Bubble Formation – II: Bubble Formation under constant Pressure Conditions,” Chemical Engineering Science, 1969, Vol. 24, Pg. 749 – 761

66. Sullivan, S. L., Jr., Hardy, B. W., and Holland, C. D.: “Formation of Air Bubbles at Orifices Submerged Beneath Liquids,” AIChE Journal, Vol. 10, No. 6, November 1964, Pg. 848 – 854

67. Kumar, R., and Kuloor, N. R.: “Blasenbildung in nichtviskosen Flussigkeiten unter konstanten Flieβbedingungen,” Chemie Technik, Vol. 19, No. 11, November 1967, Pg. 657 – 660

68. Davidson, J. F., and Schuler, B. O. G.: “Bubble Formation at an Orifice in an Inviscid Liquid,” Transaction of the Institution of Chemical Engineers, Vol. 38, 1960, Pg. 335 –342

69. Milne-Thompson, L. M.: Theoretical Hydrodynamics, The Macmillan Company,U.S.A., 1968, Pg. 743

70. Swope, R. D.: “Single Bubble Formation at Orifices Submerged in Viscous Liquids,” The Canadian Journal of Chemical Engineering, Vol. 49, April 1971, Pg. 169 – 174

71. Davies, R. M., and Taylor, G. I.: “The Mechanics of Large Bubbles Rising through Extended Liquids and through Liquid in Tubes,” Proceedings of the Royal Society of London, Series A, Vol. 200, 1950, Pg. 375 – 390

72. Rader, D. W., Bourgoyne, A. T., Jr., and Ward, R. H.: “Factors Affecting Bubble Rise Velocity of Gas Kicks,” Journal of Petroleum Technology, May 1975, Pg. 571 – 584

73. Hinze, J. O.: “Fundamentals of the Hydrodynamic Mechanism of Splitting in Dispersion Processes,” American Institute of Chemical Engineers Journal (AIChE), Vol. 1, No. 3, September 1955, Pg. 289 – 295

74. Hinze, J. O.: Turbulence – An Introduction to Its Mechanism And Theory, McGraw-Hill Book Company, Inc., 1959, Pg. 586.

75. Sleicher, C. A., Jr.: “Maximum Stable Drop Size in Turbulent Flow,” AIChE Journal, Vol. 8, No. 4, September 1962, Pg. 471 – 477

76. Sevik, M., and Park, S. H.: “The Splitting of Drops and Bubbles by Turbulent Fluid Flow,” Journal of Fluids Engineering, March 1973, Pg. 53 – 60

77. Zamora, M., Broussard, P. N., and Stephens, M. P.: “The Top 10 Mud-Related Concerns in Deepwater Drilling Operations,” paper SPE 59019 presented at the International Petroleum Conference and Exhibition in Villahermosa, Mexico, Feb. 1-3, 2000

78. LeBlanc, J. L. and Lewis, R. L.: “A Mathematical Model of a Gas Kick,” JPT August 1968, Pg. 888-898

79. Mathews, J. L.: Upward Migration of Gas Kick in a Shut-in Well, MS Thesis, Louisiana State University, Baton Rouge (1980)

80. Nickens, H. V.: “A Dynamic Computer Model of a Kicking Well: Part II – Model Predictions and Conclusions,” SPE 14184 paper presented at the 60th Annual Technical Conference and Exhibition in Las Vegas, NV, September 2-25, 1985

81. Zuber, N., and Findlay, J. A.: “Average Volumetric Concentration in Two-Phase Flow Systems,” Journal of Heat Transfer, Nov. 1965, Pg. 453 – 468

82. Johnson, A. B., and White, D. B.: “Gas-Rise Velocities During Kicks,” SPE Drilling Engineering, December 1991, Pg. 257-263

83. Hoberock, L. L., and Stanbery, S. R.: “Pressure Dynamics in Wells During Gas Kicks: Part 2 – Component Models and Results,” JPT, August 1981, Pg. 1367-1378

84. Thomas, D. C., Lea, J. F. Jr., and Turek, E. A.: “Gas Solubility in Oil-Based Drilling Fluids: Effects on Kick Detection,” SPE Reprint Series (Well Control) No. 42, 1996, Pg. 46 – 55.

85. White, D. B., and Walton, I. C.: “A Computer Model for Kicks in Water- and Oil-Based Muds,” a paper IADC/SPE 19975 presented at the 1990 IADC/SPE Drilling Conference in Houston, Texas, Feb. 27 – Mar. 2, 1990.

86. Choe, J., and Juvkam-Wold, H. C.: “Well Control Model Analyses Unsteady State, Two-Phase Flow,” Oil & Gas Journal, Dec. 2, 1996, Pg. 68-77

87. Bird, R. B., Stewert, W. E., and Lightfoot, E. N.: Transport Phenomena, John Wiley & Sons, New York, 1976, Pg. 780

88. Tiab, D., and Donaldson, E. C.: Petrophysics – Theory and Practice of Measuring Reservoir Rock and Fluid Transport Properties, Gulf Publishing Company, Student Ed., Houston, Texas, 1996, Pg. 706

89. Azbel, D.: Two-Phase Flows in Chemical Engineering, Cambridge University Press, New York, 1981, Pg. 311

90. Gatlin, C.: Petroleum Engineering –Drilling and Well Completions, Prentice-Hall Inc., Englewood Cliffs, N.J., 1960, Pg. 341

91. Craft, B. C., and Hawkins, M.: Applied Petroleum Reservoir Engineering, 2nd Ed., Revised by Terry, R. E., Prentice-Hall, Inc., 1991, Pg. 431

92. Ahmad, W. R., DeJesus, J. M., and Kawaji, M.: "Falling Film Hydrodynamics in Slug Flow," Chemical Engineering Journal, Vol. 53, No. 1, Pg. 123 – 130, 1998

93. Fair, W. B.: 'Pressure Buildup Analysis With Wellbore Phase Redistribution," SPEJ, April 1981, Pg. 259 – 270

94. Fair W. B.: "Generalization of Wellbore Effects in Pressure-Transient Analyses," SPE Formation Evaluation Journal, June 1996, Pg. 114 – 119

95. Earlougher, R. C., Jr.: Advances in Well Test Analysis, Monograph Series, Society of Petroleum Engineers, Dallas, TX, Vol. 5, Pg. 264

96. Mathews, C. S.: "Analysis of Pressure Build-Up and Flow Test Data," Journal of Petroleum Technology, September 1961, Pg. 862 – 870

97. Griffith, P., and Wallis, G. B.: "Two-Phase Slug Flow," Journal of Heat Transfer, August 1961, Pg. 307 – 320

98. Thomas, D. C., and Lea, J. F., Jr.: "Blowouts – A Computer Simulation Study," a paper SPE 11375 presented at the 1983 SPE/IADC Drilling Conference, New Orleans, Feb. 20 – 23, 1983

99. Lee, J.: Well Testing, SPE Textbook Series, Vol. 1, 1982, Pg. 159

100. Stegemeier, G. L., and Mathews, C. S.: "A Study of Anomalous Pressure Build-Up Behavior," Petroleum Transactions, AIME, Vol. 213, 1958, Pg. 44 – 50

101. Pitzer, S. C., Rice, J. D., and Thomas, C. E.: "A Comparison of Theoretical Pressure Build-Up Curves with Field Curves Obtained from Bottom-Hole Shut-in Tests," Petroleum Transactions, AIME, Vol. 216, 1959, Pg. 416 – 419.

102. Hegeman, P. S., Haliford, D. L., and Joseph, J. A.: "Well-Test Analysis with Changing Wellbore Storage," SPE Formation Evaluation, September 1993, Pg. 201 – 207

103. Hasan, A. R., and Kabir, C. S.: "Modeling Changing Storage During a Shut-in Test," paper SPE 24717 presented at the 67th Annual Technical Conference and Exhibition, Washington, DC, October 4 – 7,1992

104. Hasan, A. R., and Kabir, C. S.: "A Mechanistic Approach to Understanding Wellbore Phase Redistribution," paper SPE 26483 presented at the SPE 68th Annual Technical Conference and Exhibition, Texas, October 3 – 6, 1993

105. Beliveau, D., and Fair, P. S.: "Phase Behavior Impacts of Supercompressible Fluids on Pressure Transient Analyses," paper SPE 28423 presented at the SPE 69th Annual Technical Conference and Exhibition, New Orleans, September 25 – 28, 1994

106. Al-Haddad, S., LeFlore, M., and Lacy, T.: "Changing Wellbore Storage Effects in Gas Well Testing," paper SPE 38723 presented at the SPE Annual Technical Conference and Exhibition, Texas, October 5 – 8, 1997

107. Vasquez-Cruz, M. A., and Camacho-Velazquez, R. A.: "Analysis of Short Transient Tests Affected by Changing Wellbore Storage," SPE Reservoir Evaluation and Engineering, June 1998, Pg. 261 – 267

108. Spiegel, M. R.: Mathematical Handbook of Formulas and Tables – Schaum's Outline Series, published by the McGraw-Hill Companies, Inc., 1997, Pg. 271

109. Otake, T., Tone, S., Nakao, K., and Mitsuhashi, Y.: "Coalescence and Breakup of Bubbles in Liquids," Journal of Chemical Engineering Science, Vol. 32, 1977, Pg. 377 – 383

110. Cunha, J. C., and Rosa, F. S. N.: "Underbalance Drilling Technique Improves Drilling Performance – A Field Case History," a paper IADC/SPE 47802 presented at the IADC/SPE Asia Pacific Drilling Conference, Jakarta, Indonesia, September 7 – 9, 1998

111. Lage, A. C. V. M, and Time, R. W.: "Mechanistic Model for Upward Two-Phase Flow in Annuli," a paper SPE 63127 presented at the SPE Annual Technical Conference and Exhibition, Dallas, TX., October 1 – 4, 2000

112. Lage, A. C. V. M, and Time, R. W.: "An Experimental and Theoretical Investigation of Upward Two-Phase Flow in Annuli," a paper SPE 64525 presented at the SPE Asia Pacific Oil and Gas Conference and Exhibition, Brisbane, Australia, October 16 – 18, 2000

113. Osisanya, S. O.: PE 3313 – Drilling and Completion Manual, Mewbourne School of Petroleum and Geological Engineering, University of Oklahoma

114. Brodkey, R. S.: The Phenomena of Fluid Motions, Addison-Wesley Publishing Company, U.S.A., 1967, Pg. 737

115. Tarvin, J. A., Walton, I. C., Wand, P., and White, D. B.: "Analysis of a Gas Kick Taken in a Deep Well Drilled With Oil-Based Mud," a paper SPE 22560 presented at the 66th Annual Technical and Exhibition in Dallas, TX, Oct. 6 – 9, 1991

116. Cheremisinoff, N. P., and Gupta, R.: Handbook of Fluids in Motion, Ann Arbor Science Publishers, Michigan, U.S.A., 1983, Pg. 1202

117. "Ocean Margin Drilling Program: Final Report, Vol. III," National Science Foundation, 1980.

118. Mathews, J. L., and Bourgoyne, A. T.: Well Control - How to Handle a Gas Kick Moving up a Shut-in Well, SPE Reprint Series, No. 42, 1996, Pg. 22-28

119. Beiseman, T., and Emeh, V.: Underbalanced Operations – An Introduction to Underbalanced Drilling, SPE Reprint Series, No. 54, 2002, Pg. 27 – 52

120. Bennion, D. B., Thomas, F. B., Bietz R. F., and Bennion, D. W.: Underbalanced Operations – Underbalanced Drilling: Praises and Perils, SPE Reprint Series, No. 54, 2002, Pg. 17 – 25

121. Yurkiw, F. J., Churcher, P. L., Edmunds, A. C., Wasslen, R. D., and Schmigel, K. A.: Underbalanced Operations – Optimization of Underbalanced Drilling Operations to Improve Well Productivity, SPE Reprint Series, No. 54, 2002, Pg. 55 – 62

122. Kardolus, C. B., and van Kruijsdijk, C. P. J. W.: "Formation Testing While Underbalanced Drilling," a paper SPE 38754 presented at the Annual Technical Conference and Exhibition, San Antonio, Texas, Oct. 5-8, 1997

123. Larsen, L., and Nilsen, F.: "Inflow Predictions and Testing While Underbalanced Drilling," a paper SPE 56684 presented at the Annual Technical Conference and Exhibition, Houston, Texas, Oct. 3-6, 1999

124. Hunt, J. L., and Rester, S.: "Reservoir Characterization During Underbalanced Drilling: A New Model," a paper SPE 59743 presented at SPE/CERI Gas Technology Symposium, Calgary, Alberta, Canada, April 3-5, 2000

125. Kneissl, W.: "Reservoir Characterization Whilst Underbalanced Drilling," a paper SPE/IADC 67690 presented at the SPE/IADC Drilling Conference, Amsterdam, The Netherlands, Feb. 27 – March 1, 2001

126. Lorentzen, R. J., Fjelde, K. K., Frøyen, J., Lage, A. C. V. M., Nævdal, G., and Vefring, E. H.: "Underbalanced Drilling: Real Time Data Interpretation and Decision Support," a paper SPE/IADC 67693 presented at the SPE/IADC Drilling Conference, Amsterdam, The Netherlands, Feb. 27 – March 1, 2001

127. Vefring, E. H., Nygaard, G., Fjelde, K. K., Lorentzen, R. J., Nævdal, G., and Merlo, A.: "Reservoir Characterization during Underbalanced Drilling: Methodology, Accuracy, and Necessary Data," a paper SPE 77530 presented at the Annual Technical Conference and Exhibition, San Antonio, Texas, Sep. 29 – Oct. 2, 2002

128. Biswas, D., Suryanarayana, P. V., Frink, P. J., and Rahman, S.: "An Improved Model to Predict Reservoir Characteristics During Underbalanced Drilling," a paper SPE 84176 presented at the Annual Technical Conference and Exhibition, Denver, Colorado, U.S.A., Oct. 5-8, 2003

129. Newman, G. H.: "Pore-Volume Compressibility of Consolidated, Friable, and Unconsolidated Reservoir Rocks Under Hydrostatic Loading," Journal of Petroleum Technology (JPT), February 1973, Pg. 129 – 134.

130. Aremu, O. J., and Osisanya, S. O.: "Reduction of Wellbore Effects on Gas Inflow Evaluation Under Underbalanced Conditions," a paper SPE/IADC 91586 presented at the 2004 SPE/IADC Underbalanced Technology Conference and Exhibition, Houston, Texas, U.S.A., Oct. 11-12, 2004

131. Sahin, A., Menouar, H., Ali, A. Z., and Saner, S.: "Patterns of Variation of Permeability Anisotropy in a Carbonate Reservoir," a paper SPE 81472 presented at the 13th SPE Middle East Oil Show and Conference held in Bahrain, April 5 – 8, 2003.

132. Craft, B. C., and Hawkins, M.: Applied Petroleum Reservoir Engineering, 2nd Edition, Prentice Hall Inc., New Jersey, 1991, Pg 431

133. McCain, W. D., Jr.: The Practice of Reservoir Engineering, Elsevier Science B. V., 1994

134. Al-Hussainy, R., Ramey, H. J., and Crawford, P. B.: "The Flow of Real Gases Through Porous Media," Journal of Petroleum Technology, May 1966, 624-636

135. Slider, H. C.: Worldwide Practical Petroleum Reservoir Engineering Methods, PennWell Publishing Company, Oklahoma, 1983, Pg 826

136. Al-Hussainy, R., and Ramey, H. J., Jr.: "Application of Real Gas Flow Theory to Well Testing and Deliverability Forecasting," Journal of Petroleum Technology, May 1966, 637-642

137. Chatas, A. T.: "Unsteady Spherical Flow in Petroleum Reservoirs," SPEJ, June, 1966, Pg 102-114

138. Joseph, J. A., and Koederitz, L. F.: "Unsteady-State Spherical Flow With Storage and Skin," SPEJ, December 1985, Pg. 804-822

139. Chaudhry, V. K., Guerrero, E. T., and Carter, R. D.: "Effect of Spherical Flow in Gas Well Deliverability," SPE 2218, Sept. 29 – Oct. 2, 1968

140. Culham, W. E.: "Pressure Buildup Equations for Spherical Flow Regime Problems," SPEJ, December 1974, Pg. 545-555

141. Mott, R. L.: Applied Fluid Mechanics, 5th edition, published by Prentice-Hall, Inc., 2000, Pg. 597

APPENDIX A

A1. Radial-Cylindrical Differential Flow Equation

Assume a reservoir elemental volume between radius r and r+Δr from the center of the wellbore of formation height of h ft as shown in the figure below.[132]

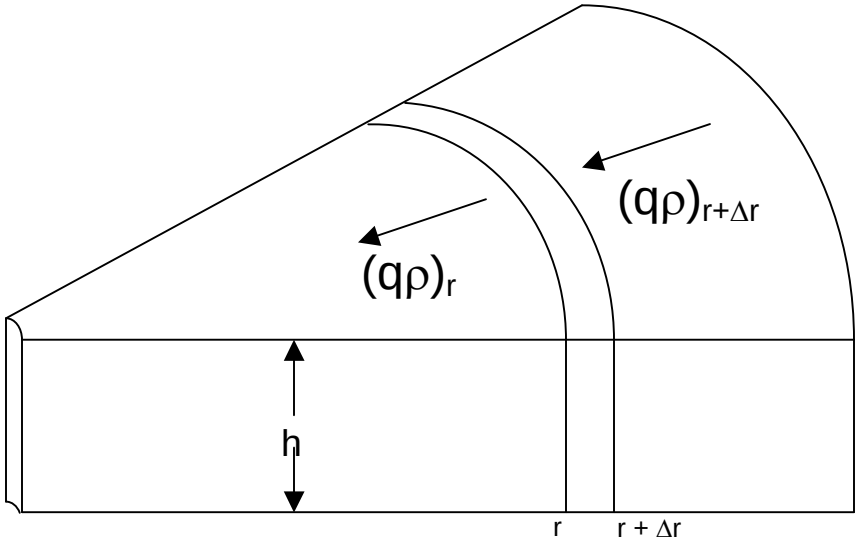

Fig. A1 – Schematic of radial flow of fluid

The mass balance of the gas entering and leaving the elemental volume is given as follows:

$$\begin{bmatrix}\text{Mass entering}\\ \text{the elemental}\\ \text{volume}\end{bmatrix} - \begin{bmatrix}\text{Mass leaving}\\ \text{the elemental}\\ \text{volume}\end{bmatrix}_{\Delta t} = \begin{bmatrix}\text{Rate at which mass}\\ \text{accumulates in the}\\ \text{elemental volume}\end{bmatrix}_{\Delta t} \quad \ldots \text{A1}$$

As indicated in the figure,

$(qB\rho)_{r+\Delta r}$ - $(qB\rho)_r$ = Rate of fluid accumulation during time interval Δt … A2

Where, the flow rate, q, is defined in SCF/day, B is the formation volume factor in bbl/SCF, and ρ is the density of the gas.

The rate of fluid accumulation is obtained by expressing the bulk volume of the element as:

$$V_{bel} = \pi\left(r + \Delta r\right)^2 h - \pi r^2 h \qquad \ldots \text{A3}$$

Expansion of Eq. A3 gives the following:

$$V_{bel} = \pi h\left(r^2 + 2r\Delta r + \left(\Delta r\right)^2\right) - \pi r^2 h$$

If Δr^2 is taken to be negligible compared to the remaining terms, the following expression is obtained for the bulk volume of the element.

$$V_{bel} = 2\pi r \Delta r h$$

The pore volume in which the fluid is retained is expressed as:

$$V_{pel} = 2\pi r \Delta r h \phi$$

And the mass of the fluid in the pore spaces is given as:

$$\text{Mass of fluid} = \rho V_{pel} = 2\pi r \Delta r h \rho \phi$$

Therefore, the rate of fluid accumulation in the element during the time interval Δt is given as follows:

$$\text{Rate of mass accumulation} = \frac{2\pi r \Delta r h\left[\left(\phi\rho\right)_{t+\Delta t} - \left(\phi\rho\right)_t\right]}{\Delta t} \qquad \ldots \text{A4}$$

The mass entering the elemental volume at velocity, υ, in bbl/(day-ft^2) through the cylindrical surface area of $2\pi\left(r + \Delta r\right)h$ within the time interval, Δt, hours, is given as:

$$\left(qB\rho\right)_{r+\Delta r} = \left(2\pi h\left(r + \Delta r\right)\left(\left(5.615/24\right)\rho\upsilon\right)\right)_{r+\Delta r} \qquad \ldots \text{A5}$$

And the mass leaving the elemental volume within the interval time, Δt, hours, is given as:

$$\left(qB\rho\right)_r = \left(2\pi hr\left(\left(5.615/24\right)\rho\upsilon\right)\right)_r \qquad \ldots \text{A6}$$

Substituting equations 4 through 6 into Eq. A2 results to the following:

$$2\pi h(0.234)\left[\left((r+\Delta r)\rho\upsilon\right)_{r+\Delta r} - r(\rho\upsilon)_r\right] = \frac{2\pi r\Delta rh\left[(\rho\phi)_{t+\Delta t} - (\rho\phi)_t\right]}{\Delta t} \quad \ldots \text{A7}$$

Dividing through both sides of the Eq. A7 by $2\pi r\Delta rh$ and taken the limit as each term Δr and Δt approaches zero, we have:

$$(0.234)\left[\left(\frac{(r\rho\upsilon)_{r+\Delta r} - (r\rho\upsilon)_r}{\Delta r}\right) + \frac{1}{r}(\rho\upsilon)\right] = \frac{\left[(\rho\phi)_{t+\Delta t} - (\rho\phi)_t\right]}{\Delta t} \quad \ldots \text{A8}$$

$$0.234\frac{\partial}{\partial r}(\rho\upsilon) + \frac{1}{r}(\rho\upsilon) = \frac{\partial}{\partial t}(\rho\phi) \quad \ldots \text{A9}$$

Equation A9 can be written as:

$$\frac{0.234}{r}\frac{\partial}{\partial r}(r\rho\upsilon) = \frac{\partial}{\partial t}(\rho\phi) \quad \ldots \text{A10}$$

Darcy's equation for laminar flow is defined as:

$$\upsilon = -0.001127\frac{k}{\mu}\frac{\partial p}{\partial r} \quad \ldots \text{A11}$$

Where,

υ - the apparent velocity, bbls/(day-ft^2)

k - permeability, md

μ - fluid viscosity, cp

p - pressure, psia

The negative sign signifies that the pressure drop is taken in the same direction of increasing radius. However, in the reservoir, and as indicated in the above figure, since the flow of fluid is towards the wellbore, the pressure drop is taken in the direction of decreasing radius from the center of the wellbore. Hence, the negative sign can be dropped. Therefore, combining equations A10 and A11, we have:

$$\frac{0.0002637}{r}\frac{\partial}{\partial r}\left(\rho r\frac{k}{\mu}\frac{\partial p}{\partial r}\right)=\frac{\partial}{\partial t}(\rho\phi) \qquad \ldots \text{A12}$$

The RHS term of equation A12 can be expanded as follows:

$$\frac{\partial}{\partial t}(\rho\phi)=\rho\frac{\partial\phi}{\partial t}+\phi\frac{\partial\rho}{\partial t} \qquad \ldots \text{A13}$$

By applying Chain rule of differentiation to the first differential term in equation A13, we have:

$$\frac{\partial\phi}{\partial t}=\frac{\partial\phi}{\partial p}\cdot\frac{\partial p}{\partial t} \qquad \ldots \text{A14}$$

The formation compressibility is expressed as follows[132]:

$$c_f=\frac{1}{\phi}\frac{\partial\phi}{\partial p} \qquad \ldots \text{A15}$$

Combining equations A14 and A15 result in the following expression:

$$\frac{\partial\phi}{\partial t}=c_f\phi\frac{\partial p}{\partial t} \qquad \ldots \text{A16}$$

Substituting equation A16 into A13 results to:

$$\frac{\partial}{\partial t}(\rho\phi)=\rho c_f\phi\frac{\partial p}{\partial t}+\phi\frac{\partial\rho}{\partial t} \qquad \ldots \text{A17}$$

Equation A17 is substituted into equation A12 to give:

$$\frac{0.0002637}{r}\frac{\partial}{\partial r}\left(\rho r\frac{k}{\mu}\frac{\partial p}{\partial r}\right)=\rho\phi c_f\frac{\partial p}{\partial t}+\phi\frac{\partial\rho}{\partial t} \qquad \ldots \text{A18}$$

Equation A18 is the general partial differential equation used to describe radial flow of any fluid in porous media under laminar flow. It is recognized that the pressure gradient of gas increases at the wellbore due to the expansion of the gas at the lower wellbore pressure, and thus higher velocity. This should create turbulence flow at the wellbore. Such near-wellbore turbulence gas flow can be attributed to excessive drop

in pressure at the wellbore, which can easily be achieved if the wellbore is full of gas and the well is produced at the surface under Absolute Open Flow (AOF).

However, during underbalanced drilling, flow of gas into the wellbore is minimized to reduce the rate of gas flaring at the surface. This implies that the gas flow into the wellbore is controlled by the surface annular choke and the bottom-hole circulating pressure during drilling. All these means of control reduce the pressure gradient at the wellbore, and thus minimize any turbulence flow of gas at the wellbore. Moreover, this study incorporates some other forces at the bottom-hole (viscous, surface tension and inertia forces) that further control the flow of gas into the wellbore. Hence, any turbulent flow that may occur during underbalanced drilling is assumed negligible in this study. That is why equation A18 is considered appropriate for this study.

Diffusivity equation of compressible fluid under transient flow regime

The real gas equation and the gas compressibility expression are respectively given as[133]:

$$pV = znRT \quad \ldots \text{A19}$$

$$c_g = \frac{1}{p} - \frac{1}{z}\frac{\partial z}{\partial p} \quad \ldots \text{A20}$$

Equation A19 can be written in terms of gas density as:

$$\rho = \frac{pM}{zRT} \quad \ldots \text{A21}$$

Where,

p - gas pressure, psia

z - gas deviation factor

R - universal gas constant,

n - number of moles of the gas

M - gas mass, lb

T - gas temperature, ^{o}R

Differentiating the gas density with respect to variable t gives:

$$\frac{\partial \rho}{\partial t} = \frac{\partial \rho}{\partial p} \cdot \frac{\partial p}{\partial t} \qquad \ldots \text{A22}$$

Differentiating equation A21 with respect to pressure, p, gives:

$$\frac{\partial \rho}{\partial p} = \frac{M}{zRT} + \frac{pM}{RT}\left(-\frac{1}{z^2}\frac{\partial z}{\partial p}\right) \qquad \ldots \text{A23}$$

Substituting equation A20 into equation A23 gives:

$$\frac{\partial \rho}{\partial p} = \frac{M}{RT}\left[\frac{1}{z} + \frac{p}{z}\left(c_g - \frac{1}{p}\right)\right] = \frac{Mc_g p}{zRT} \qquad \ldots \text{A24}$$

Equation A22 now becomes:

$$\frac{\partial \rho}{\partial t} = \frac{Mc_g p}{zRT} \cdot \frac{\partial p}{\partial t} \qquad \ldots \text{A25}$$

Substituting equations A21 and A25 into equation D18 gives:

$$\frac{0.0002637}{r}\frac{\partial}{\partial r}\left(\frac{pM}{zRT} r \frac{k}{\mu}\frac{\partial p}{\partial r}\right) = \frac{pM}{zRT}\phi c_f \frac{\partial p}{\partial t} + \frac{pMc_g}{zRT}\phi \frac{\partial p}{\partial t} \qquad \ldots \text{A26}$$

Re-arranging equation A26 leads to:

$$\frac{1}{r}\frac{\partial}{\partial r}\left(r \frac{p}{\mu z}\frac{\partial p}{\partial r}\right) = \frac{\phi c_t p}{0.0002637 zk}\frac{\partial p}{\partial t} \qquad \ldots \text{A27}$$

Where $c_t = c_f + c_g$ for single phase gas saturated reservoir.

c_t - the total compressibility of the system

Due to the large compressibility of the gas compared to the formation compressibility, $c_t \approx c_g$.

To solve equation A27 for the gas pressure, the following transformation was introduced by Al-Hussainy et al[134]

$$\psi_p = 2\int_{p_r}^{p} \frac{p}{\mu z} dp \qquad \ldots \text{A28}$$

Where ψ_p is the gas pseudopressure.

Differentiating equation A28 with respect to variable p gives:

$$\frac{\partial \psi_p}{\partial p} = \frac{2p}{\mu z} \qquad \ldots \text{A29}$$

Applying Chain rule of differentiation to equation A29 gives:

$$\frac{\partial \psi_p}{\partial r} = \frac{\partial \psi_p}{\partial p} \cdot \frac{\partial p}{\partial r} \qquad \ldots \text{A30}$$

Substitution of equation A29 into equation A30, re-arranging leads to:

$$\frac{\partial p}{\partial r} = \frac{\mu z}{2p} \frac{\partial \psi_p}{\partial r} \qquad \ldots \text{A31}$$

The gas pseudopressure is again differentiated with respect to variable t and the Chain rule of applied as follows:

$$\frac{\partial \psi_p}{\partial t} = \frac{\partial \psi_p}{\partial p} \cdot \frac{\partial p}{\partial t} \qquad \ldots \text{A32}$$

Substituting equation A29 into equation A32 leads to the following expression:

$$\frac{\partial p}{\partial t} = \frac{\mu z}{2p} \frac{\partial \psi_p}{\partial t} \qquad \ldots \text{A33}$$

Equations A31 and A33 are substituted into equation A27 to give:

$$\frac{1}{r}\frac{\partial}{\partial r}\left(r\frac{\partial \psi_p}{\partial r}\right) = \frac{\mu\phi c_t}{0.0002637k}\frac{\partial \psi_p}{\partial t} \quad \ldots \text{A34}$$

Expanding equation A34 leads to:

$$\frac{\partial^2 \psi_p}{\partial r^2} + \frac{1}{r}\frac{\partial \psi_p}{\partial r} = \frac{\phi\mu c_t}{0.0002637}\frac{\partial \psi_p}{\partial t} \quad \ldots \text{A35}$$

Equation A35 is the diffusivity equation for compressible flow inside porous media. Although it looks linear in appearance, it is actually non-linear because of the inherent gas viscosity and gas deviation factor that are still dependent on the pressure. The pressure transformation using the gas pseudopressure expression just simplified the diffusivity equation in order to by-pass the assumption of negligible pressure gradient at the wellbore. It is generally believed that assuming negligible pressure drop for gas flow into a predominant gas well is inappropriate because pressure will surely drop at the well as production continues.

Therefore, unsteady-state flow is inevitable for gas flow inside a gas reservoir. In order to achieve steady state gas flow, there should be a constraint to excessive pressure drop at the wellbore or a flow across the boundary at the same rate at which gas in produced at the wellbore.[134]

Steady state radial transient flow equation

In order to generalize the radial flow of gas into a wellbore at different wellbore pressure that leads to different pressure gradient and thus, different flow conditions, the gas flow rate into the wellbore is considered at the standard condition, which is similar for every gas production from any gas reservoir.[135]

Therefore, expressing the gas flow rate in standard cubic feet per day (MSCF/d), and considering the same n moles of gas under the prevailing reservoir conditions and at the surface conditions, the real gas equations at these two different conditions can be equated as follows:

$$\frac{p_{sc}q}{T_{sc}} = \frac{p_r q_r}{z_r T_r} \qquad \ldots \text{A36}$$

Where,

p_{sc} - standard pressure conditions, 14.67 psia

q - gas flow rate at standard conditions, MSCF/d

T_{sc} - standard temperature condition, $60^oF = 520^oR$

p_r - average reservoir gas pressure, psia

q_r - gas flow rate from the reservoir into the wellbore, SCF/d

T_r - bottom-hole temperature, ^oR

z_r - gas deviation factor under reservoir conditions

Re-arranging equation A36 and converting the gas flow rate into the wellbore into barrels per day to conform to the unit of gas velocity as expressed in equation A11, the following is obtained:

$$q_r B_g = \frac{0.02827 q T_r z_r}{5.615 p_r} \qquad \ldots \text{A37}$$

Equating equations A11 and A37 and removing the subscript r since we are dealing with only reservoir condition results to:

$$\frac{0.005034 qTz}{(2\pi rh)p} = 0.001127 \frac{k}{\mu}\frac{dp}{dr} \qquad \ldots \text{A38}$$

Using the pseudopressure transformation introduced by Al-Hussainy et al[134] expressed in equations A28 through A31, equation A38 can be re-written as follows:

$$\frac{0.005034qT}{(2\pi rh)(0.001127)k} = \frac{1}{2}\frac{d\psi_p}{dr} \quad \ldots \text{A39}$$

Definite integration of both sides of equation A39 is as follows:

$$\frac{0.005034qT}{(2\pi h)(0.001127)k}\int_{rw}^{re}\frac{dr}{r} = \frac{1}{2}\int_{\psi_{bhf}}^{\psi_{pi}} d\psi_p \quad \ldots \text{A40}$$

Evaluation of equation A40 gives:

$$\frac{0.711qT}{kh}\ln\left(re/rw\right) = \frac{\psi_{pi} - \psi_{bh}}{2} \quad \ldots \text{A41}$$

Equation A41 becomes:

$$q = \frac{kh(\psi_{pi} - \psi_{bh})}{1.424\,T\ln\left(re/rw\right)} \quad \ldots \text{A42}$$

In accordance with the approach by Al-Hussainy et al[134], a dimensionless real gas pseudopressure can be expressed as:

$$\psi_D(r_D, t_D) = \frac{kh(\psi_{pi} - \psi_p)}{1.424\,\mathrm{q}T} \quad \ldots \text{A43}$$

Where,

$$r_D = \frac{r}{r_w} \quad \ldots \text{A44}$$

$$t_D = \frac{kt}{\phi(\mu c_g)_i r_w^2} \quad \ldots \text{A45}$$

Equation A43 indicates that the dimensionless gas pseudopressure is directly proportional to the drop in the pseudopressures, which analogous to the flow of

slightly compressible fluid. However, in equation A45, the product of the gas viscosity and the gas compressibility must be evaluated at the initial conditions of the gas reservoir.

Therefore, replacing the pseudopressure differential terms in equation A35 with the dimensionless pseudopressure terms leads to:

$$\frac{\partial^2 \psi_D}{\partial r_D^2} + \frac{1}{r_D}\frac{\partial \psi_D}{\partial r_D} = \frac{\partial \psi_D}{\partial t_D} \qquad \ldots \text{A46}$$

Again, equation A46 is similar to the differential expression for flow of slightly compressible fluid inside porous media under unsteady state conditions. Equation A46 was solved by Al-Hussainy et al[134] using finite difference approach with one initial and two boundary conditions.

The initial condition at t = 0, the pressure everywhere in the system is the initial reservoir pressure.

That is,

$$\psi_D\left(t_D = 0\right) = 0 \qquad \ldots \text{A47}$$

The first boundary condition is that, at the wellbore constant gas mass flux is achieved at every time by imposing constant pressure drop at the bottom hole during underbalanced drilling operation.

That is,

$$\rho\upsilon = \frac{qB}{A}\rho = \frac{pM}{zRT}\cdot 0.001127\frac{k}{\mu}\left(\frac{\partial p}{\partial r}\right)_{r=rw} \qquad \ldots \text{A48}$$

Substituting equation A31 into equation A48 converts the pressure differential term to the pseudopressure differential term as follows:

$$\rho\upsilon = \frac{qB}{A}\rho = 0.001127\frac{kM}{2RT}\cdot\left(\frac{\partial\psi_D}{\partial r}\right)_{r=rw} \quad \ldots \text{A49}$$

The second boundary condition is obtained by considering the gas reservoir as infinite acting in size. That is,

$$\psi_D(r=\infty) = 0 \quad \ldots \text{A50}$$

Due to the non-linearity of the resulting diffusivity equation for the compressible fluid, Al-Hussainy et al[134] numerically solved this diffusivity equation and compared results with the dimensionless pressure solution obtained for the flow of slightly compressible fluid. These authors stated that the dimensionless real gas pseudopressure drop, $\psi_D(r_D,t_D)$ is similar to the dimensionless pressure drop $\psi_D(r_D,t_D)$, for a gas reservoir producing at constant flow rate at short time of production without the influence of the outer boundary of the reservoir. That is,

At $t_D < (t_D)_{pss}$, $\psi_D(t_D) = p_D(t_D)$

That is, equation D43 becomes:

$$\psi_D(r_D,t_D) = p_D(r_D,t_D) = \frac{kh(\psi_{pi}-\psi_{bh})}{1.424\,\mathrm{q}T} \quad \ldots \text{A51}$$

Al-Hussainy and Ramey[136] approximated the expression for the dimensionless pressure as follows:

$$p_D(t_D) = \frac{1}{2}[\ln t_D + 0.80907], \text{ for } 100 \le t_D \le \frac{1}{4}\left(\frac{r_e}{r_w}\right)^2 \quad \ldots \text{A52}$$

Since, the production from a gas reservoir during underbalanced drilling is for a short time, and noting in equation A52 the time limit for infinitely acting reservoir

considered in this study, these approximations were considered adequate for this study.

The pseudopressure terms in equation A51 was approximated to their respective squared-pressure terms because the difference between the wellbore and the reservoir pressure is generally less than 2000 psi during any underbalanced drilling. Therefore, the following were obtained by applying the pseudopressure transformation presented by Al-Hussainy et al[134].

Choosing an arbitrary base pressure[134], p_b, of difference less 2000 psi from the average or initial reservoir pressure and the wellbore pressure, the following is obtained by relating this base pressure to the reservoir pressure:

$$\psi_i = 2\int_{p_b}^{p_i} \frac{p}{z\mu} dp \qquad \ldots \text{A53}$$

Since the difference between the P_i and P_b is assumed to be less than 2000 psi, the product of the viscosity-deviation factor for these two pressures is assumed constant. By integrating equation A53, the following is obtained.

$$\psi_i = \frac{p_i^2 - p_b^2}{\bar{z}\bar{\mu}} \qquad \ldots \text{A54}$$

Similar procedures are conducted for the wellbore or bottom-hole pressure to arrive at:

$$\psi_{wf} = \frac{p_{bh}^2 - p_b^2}{\bar{z}\bar{\mu}} \qquad \ldots \text{A55}$$

Subtracting equation A55 from equation A54 leads to:

$$\psi_i - \psi_{wf} = \frac{p_i^2 - p_{bh}^2}{\bar{z}\bar{\mu}} \quad \ldots \text{A56}$$

If the flow rate is expressed in Mcuft/hr, and equation A56 is substituted into equation A51 we have:

$$q = \frac{kh\left(p_i^2 - p_{bh}^2\right)B_g}{34176\,\bar{z}\bar{T}\bar{\mu}p_D} \quad \ldots \text{A57}$$

Where,

B_g - the gas formation volume factor, cuft/scf

Modeling Considerations for the assumed Radial-Cylindrical Gas Inflow

As previously expressed, maintenance of constant pressure difference between the reservoir pressure and the bottomhole pressure created by the underbalanced drilling is crucial during the drilling operation. Included in equation A57 is the surface tension effect in the term for the total bottom-hole pressure imposed on the gas bubble. This inclusion seems to alter the difference in the squared-pressure terms from constancy because of the varying bubble size, but it is actually not since the surface tension is negligible. However, the term is included for completeness. Therefore, in accordance with the requirement of constant pressure difference (drop) during underbalanced drilling, the pressure difference in equation A57 is approximately constant.

Another consideration is the solution for the transient flow period in solving for the dimensionless pseudopressure. The corresponding dimensionless pressure term, P_D, in equation A57 is evaluated as a constant value because of the condition of a constant rate of penetration of the bit. This requires that the drill time for any

additionally drilled 1 inch of the interval be constant. For example, if the rate of penetration (ROP) is 30ft/hr, the corresponding drill time for 1 inch is 10 seconds (0.0027778 hr). This drill time in hours is substituted into the t_D expression that is used to evaluate the P_D expression. When additional 1 inch of interval is drilled during the next 10 seconds, a total formation interval of 2 inches would have been exposed. However, the total gas volume inflow into the wellbore at the end of drilling this additional 1 inch is for the period of 10 sec (0.002778 hr). This sequence continues for every additional 1 inch.

A2. Radial-Spherical Diffusivity Flow Equation

Spherical flow of fluids inside a reservoir has been considered to occur when a "spherical wellbore exists as a point sink within a massive reservoir. A special case of spherical flow is the "hemispherical" flow geometry.[134,135,137 140] These flow geometries are used to explain some pressure transient behaviors that are noticed on log-log plots of pressure derivatives.

Chatas[137] defined a spherical reservoir system existing at any instant of time as a system of two concentric hemispheres having their physical properties of interest varying along the radial distance only. A hemispherical flow of fluid is considered for analysis when a well partially penetrate a massive reservoir, whereas a spherical flow analysis is conducted when relatively small perforation interval is situated in the middle of a massive reservoirs. Since this study involves a partially penetrated well into gas reservoirs, a schematic diagram of hemispherical flow are presented in figure A2.

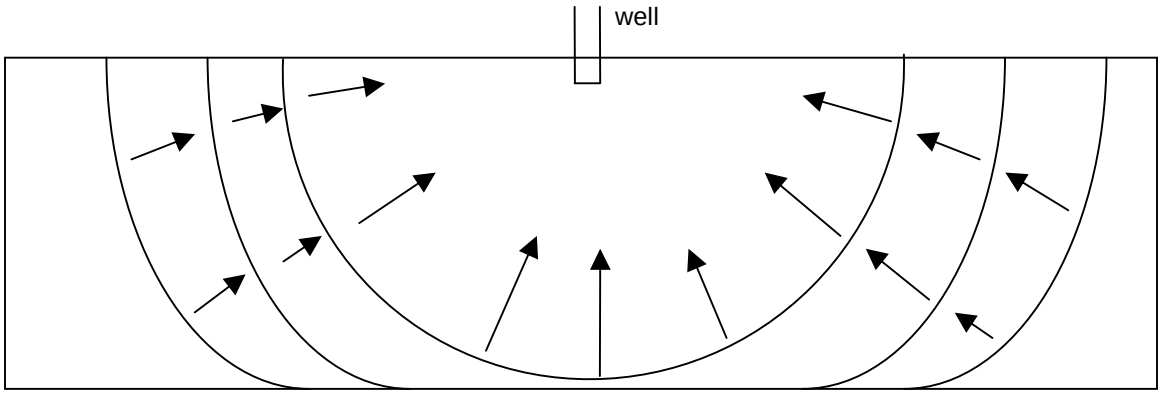

Fig. A2 – Reservoir cross section illustrating hemispherical fluid flow towards a partially penetrated well in a massive reservoir

Flow of fluids in a homogeneous and isotropic spherical geometry is generally represented as:

$$\frac{1}{r^2}\frac{\partial}{\partial r}\left(r^2\frac{\partial \Phi}{\partial r}\right)+\frac{1}{r\sin\theta}\frac{\partial}{\partial \theta}\left(\sin\theta\frac{\partial \Phi}{\partial \theta}\right)+\frac{1}{r^2}\frac{1}{\sin^2\theta}\frac{\partial^2 \Phi}{\partial \varphi^2}=\frac{\phi\mu c_t}{k}\frac{\partial \Phi}{\partial t} \qquad \ldots \text{A58}$$

The fluid potential Φ is represented as:

$$\Phi = p - \rho g z \qquad \ldots \text{A59}$$

Where,

r, θ, φ - spherical coordinates

p - fluid pressure, atm

ρ - fluid density, g/cc

g - gravitational force, cm/sec^2

z - vertical direction, cm

Considering the fact that geologic sands are laid down with sizable horizontal permeability and some vertical permeability, flow in the angular directions can be assumed negligible. Hence, the differential terms $\frac{\partial \Phi}{\partial \theta}$ and $\frac{\partial \Phi}{\partial \varphi}$ are neglected. Therefore, fluid flow in solely radial direction in a spherical geometry is represented as:

$$\frac{1}{r^2}\frac{\partial}{\partial r}\left(r^2\frac{\partial \Phi}{\partial r}\right)=\frac{\phi\mu c_t}{k}\frac{\partial \Phi}{\partial t} \qquad \ldots \text{A60}$$

Assuming that the hydraulic or gravitational force of the driving force is negligible compared to the pressure gradient. Then, equation D60 becomes:[138]

$$\frac{1}{r^2}\frac{\partial}{\partial r}\left(r^2\frac{\partial p}{\partial r}\right)=\frac{\phi\mu c_t}{k}\frac{\partial p}{\partial t} \qquad \ldots \text{A61}$$

Equation A61 is typically applied for analyzing liquid flow in spherical geometry.[138] For the flow of real gases, equation A61 can be transformed into a similar expression derived for the radial-cylindrical flow geometry. Therefore, equation A61 is written for real gas flow as:

$$\frac{1}{r^2}\frac{\partial}{\partial r}\left(r^2\frac{p}{\mu z}\frac{\partial p}{\partial r}\right)=\frac{\phi p c_t}{zk}\frac{\partial p}{\partial t} \qquad \ldots \text{A62}$$

For real gases, introduction of the pseudopressure transformation, ψ_p, as given by Al-Hussainy et al[134], into equation A62 leads to:

$$\frac{1}{r^2}\frac{\partial}{\partial r}\left(r^2\frac{\partial \psi_p}{\partial r}\right)=\frac{\phi\mu c_t}{k}\frac{\partial \psi_p}{\partial t} \qquad \ldots \text{A63}$$

Expanding equation A63, we have:

$$\frac{\partial^2\psi_p}{\partial r^2}+\frac{2}{r}\frac{\partial \psi_p}{\partial r}=\frac{\phi\mu c_t}{k}\frac{\partial \psi_p}{\partial t} \qquad \ldots \text{A64}$$

As presented for the radial-cylindrical geometry, equation A64 is not a linear differential equation as it seems. Therefore, a similar numerical evaluation is required to be able to relate the corresponding dimensionless pseudopressure to the readily available solution of dimensionless pressure expressions for the flow of slightly compressible liquid.

Steady State Equation for Hemispherical Flow for Compressible Fluids

The surface area of a hemisphere is given as:

$$A_{sp}=2\pi r^2 \qquad \ldots \text{A65}$$

Where r is the radial distance in the spherical or hemispherical geometry, which is different from the actual wellbore radius.[134,135,137-140] As expressed for the radial-cylindrical flow geometry under equation A37,

$$q_r B_g = \frac{0.02827 q T_r z_r}{5.615 p_r} \quad \ldots \text{A37}$$

Equating equation A37 to the Darcy's equation, dropping the subscript r, and substituting equation A65, we have:

$$\frac{0.005034 q T z}{\left(2\pi r^2\right) p} = 0.001127 \frac{k}{\mu} \frac{dp}{dr} \quad \ldots \text{A66}$$

Again, the negative sign in the Darcy's equation has been dropped for the same reason as stated while deriving the equation for the radial-cylindrical flow geometry. Replacing the pressure gradient term in equation A66 by the pseudopressure term, we have:

$$\frac{0.711 q T}{k r^2} = \frac{1}{2} \frac{\partial \psi_p}{\partial r} \quad \ldots \text{A67}$$

Integrating equation A67, we have

$$\frac{0.711 q T}{k} \int_{r_{sp}}^{re} \frac{dr}{r^2} = \frac{1}{2} \int_{\psi_p}^{\psi_{pi}} d\psi_p \quad \ldots \text{A68}$$

Equation A68 becomes:

$$\frac{1.424 q T}{k} \left(\frac{1}{r_{sp}} - \frac{1}{r_e} \right) = \left(\psi_{pi} - \psi_p \right) \quad \ldots \text{A69}$$

Re-arranging equation A69 leads to:

$$q = \frac{k\left(\psi_{pi} - \psi_{p}\right)}{1.424T\left(\frac{1}{r_{sp}} - \frac{1}{r_e}\right)} \quad \ldots \text{A70}$$

By taking an arbitrary base pressure[134] having a pressure difference less than 2000 psi with both the average or initial reservoir pressure and the wellbore pressure, we have:

$$q = \frac{k\left(p_i^2 - p_r^2\right)}{1.424T\left(\frac{1}{r_{sp}} - \frac{1}{r_e}\right)} \quad \ldots \text{A71}$$

Equation A71 is the same as presented by Slider[135], and by Chaudhry et al[139] through the application of Forchheimier equation with turbulent effects. As presented by Chaudhry et al[139], the effect of turbulence on pressure drop decreases with increase in the shot density. Since this study considers gas flow into an open-hole, the effect of turbulence on pressure drop can be assumed minimal.

In accordance with Joseph and Koederitz[138], the following dimensionless groups can be defined to numerically solve the radial-hemispherical diffusivity in equation A64.

$$\psi_D = \frac{kr_{sp}\left(\psi_{pi} - \psi_{p}\right)}{1.424qT} \quad \ldots \text{A72}$$

$$t_D = \frac{kr_{sp}^2 t}{\phi\mu c r^4}; \quad r \geq r_{sp} \quad \ldots \text{A73}$$

$$r_D = 1 - \frac{r_{sp}}{r}; \quad \text{r} \geq r_{sp} \quad \ldots \text{A74}$$

Since there is nothing as spherically drilled wellbore, the spherical radius r_{sp} is related to the radius of a cylindrically drilled wellbore as:[135]

$$\left(2\pi rh + \pi r^2\right) = 2\pi r_{sp}^2 \quad \ldots \text{A75}$$

The spherical radius can then be obtained in terms of the actual wellbore radius, r, as:

$$r_{sp} = \sqrt{\frac{2hr + r^2}{2}} \quad \ldots \text{A76}$$

Where,

r - radius of the cylindrically drilled wellbore, ft

h - drilled formation height, ft

Modeling Considerations

As stated by all authors[134,135,137-140], the application of hemispherical flow to partially penetrated is considered when the partially penetrated well is situated in massive reservoirs. The massiveness of the reservoirs could be a characteristic of oil reservoirs. However, most gas reservoirs, which are the focus for this study, are relatively thinner in productive interval. Therefore, application of transient radial flow has consistently be applied to the gas inflow into the wellbore for gas.[55,84]

Another consideration, as analyzed by the authors [134,135,137-140], is in relating the depth of the partially penetrated well to the entire formation interval during analysis. Unfortunately, the actual interval of the producing formation is not known until the formation is completely drilled. Since, this study considered partial well penetration and the entire height of the producing formation is not certain, the best approximation is to consider radial flow throughout the portions of the formation drilled. As discussed in the simulation results, the transition depth above which the

spherical (or hemispherical flow) should be applied becomes apparent. However, such transition depth is not known *a priori* unless it is first assumed that the gas inflow into the wellbore during underbalanced drilling is radial-transient flow.

A3. Derivation of Viscous Drag Forces

There are two basic types of viscous forces. These are the pressure or form drag and the friction drag forces. The form viscous force is referenced to the maximum cross-sectional area of a sphere perpendicular to the growth direction of the bubble, while the friction drag is referenced to the surface area of a sphere. The friction drag is more applicable when the sphere is moving.[141] The general expression for a drag force is given as:[141]

$$F_D = C_D\left(\frac{\rho\upsilon^2}{2}\right)A \qquad \ldots \text{A77}$$

Where C_D is the laminar drag coefficient given as:

$$C_D = \frac{24}{N_R} \qquad \ldots \text{A78}$$

N_R is the Reynold's number that is generally represented as:

$$N_R = \frac{\rho D\upsilon}{\mu} \qquad \ldots \text{D79}$$

Substituting equations A78 and A79 into equation A77 gives:

$$F_D = \frac{12\mu\upsilon A}{D} \qquad \ldots \text{A80}$$

The form viscous force is obtained by substituting parameter A in equation A80 with the maximum cross sectional area of a sphere, $A = \frac{\pi D^2}{4}$ to get:

$$F_D = 3\pi\mu\upsilon D = 6\pi\mu\upsilon r \qquad \ldots \text{A81}$$

The expression friction drag is obtained by substituting the parameter A in equation A80 with the surface area of a sphere, $A = \pi D^2$ to give:

$$F_D = 12\pi\mu\upsilon D = 24\pi\mu\upsilon \mathrm{r} \qquad \ldots \text{A82}$$

Equation A81 which is generally referred to as the Stoke's law had been considered for modeling in this study rather than the friction viscous force since there is an opposing pressure to the bubble growth which acts on the maximum cross sectional area of the growing bubble perpendicularly.

APPENDIX B

B1. COMPUTER PROGRAM INTERFACE FORMS FOR COMPUTATIONS

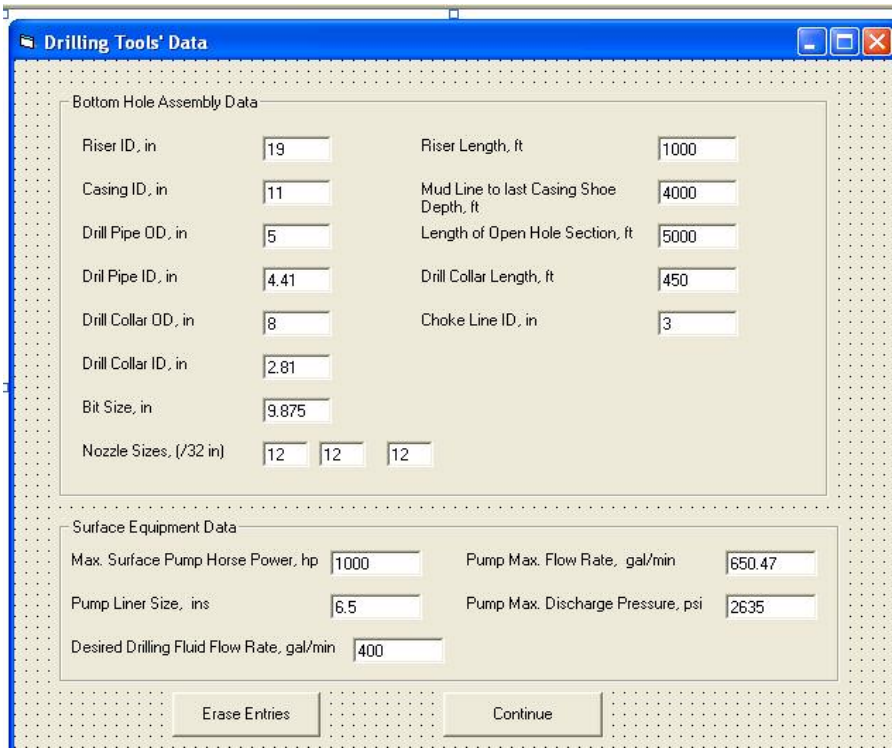

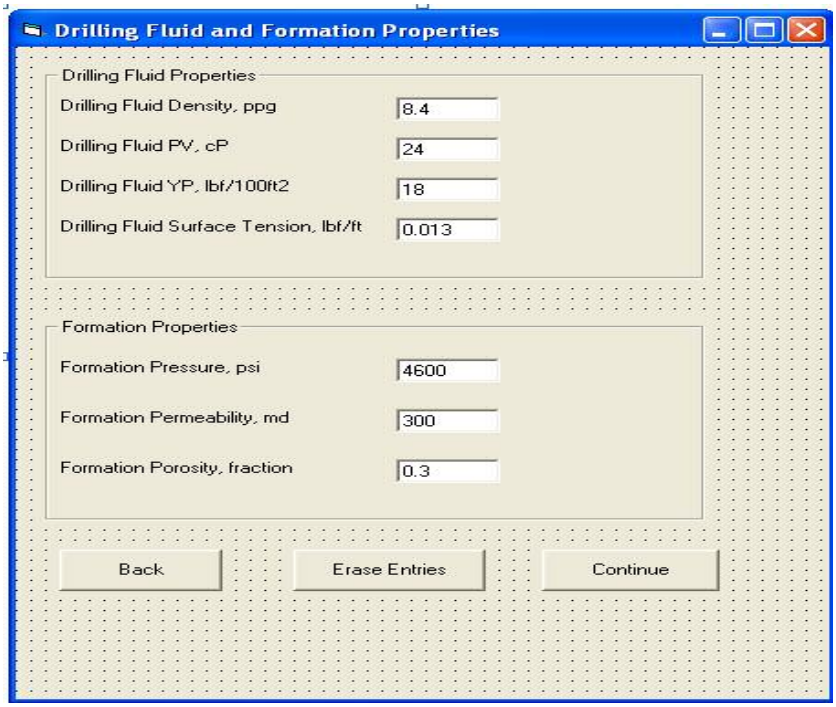

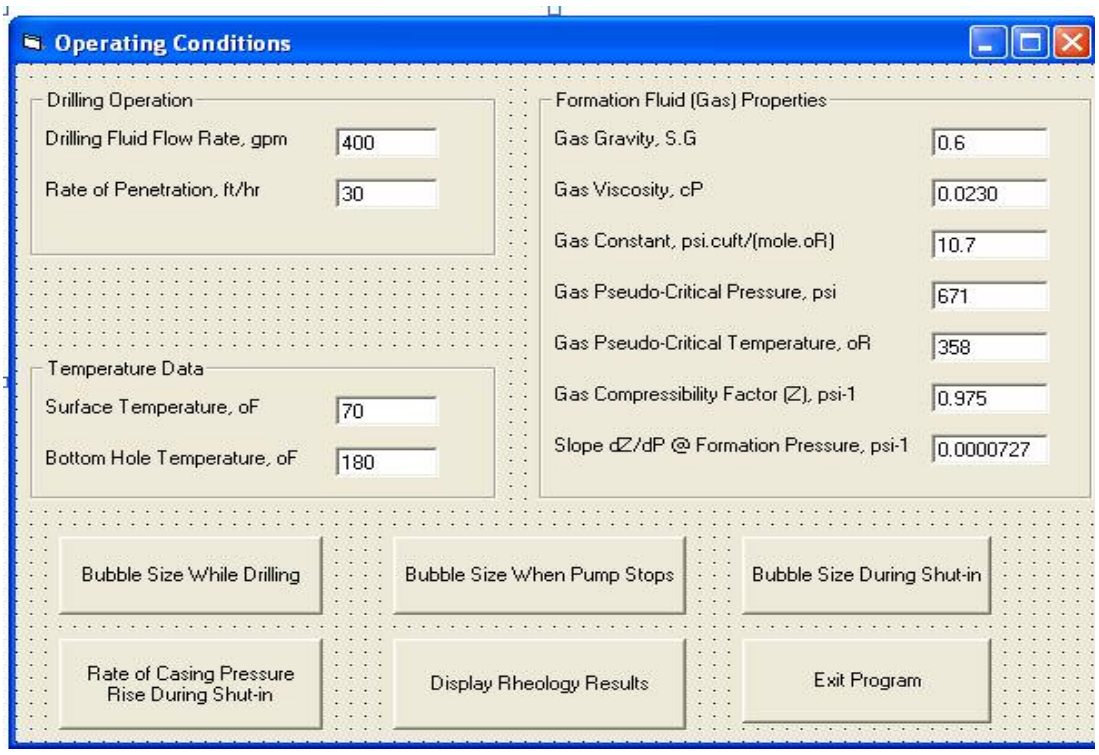
Operating Conditions
Drilling Operation
Drilling Fluid Flow Rate, gpm
400
Rate of Penetration, ft/hr
30
Temperature Data
Surface Temperature, oF
70
Bottom Hole Temperature, oF
180
Formation Fluid (Gas) Properties
Gas Gravity, S.G
0.6
Gas Viscosity, cP
0.0230
Gas Constant, psi.cuft/(mole.oR)
10.7
Gas Pseudo-Critical Pressure, psi
671
Gas Pseudo-Critical Temperature, oR
358
Gas Compressibility Factor (Z), psi-1
0.975
Slope dZ/dP @ Formation Pressure, psi-1
0.0000727
Bubble Size While Drilling
Bubble Size When Pump Stops
Bubble Size During Shut-in
Rate of Casing Pressure Rise During Shut-in
Display Rheology Results
Exit Program

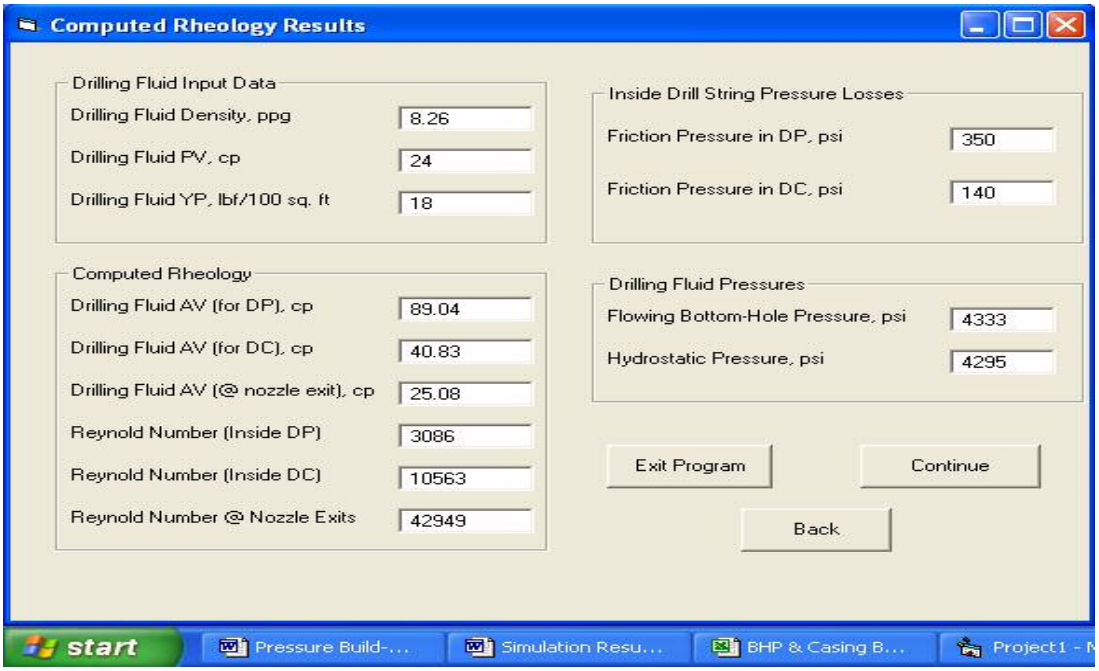
Computed Rheology Results
Drilling Fluid Input Data
Drilling Fluid Density, ppg
8.26
Drilling Fluid PV, cp
24
Drilling Fluid YP, lbf/100 sq. ft
18
Computed Rheology
Drilling Fluid AV (for DP), cp
89.04
Drilling Fluid AV (for DC), cp
40.83
Drilling Fluid AV (@ nozzle exit), cp
25.08
Reynold Number (Inside DP)
3086
Reynold Number (Inside DC)
10563
Reynold Number @ Nozzle Exits
42949
Inside Drill String Pressure Losses
Friction Pressure in DP, psi
350
Friction Pressure in DC, psi
140
Drilling Fluid Pressures
Flowing Bottom-Hole Pressure, psi
4333
Hydrostatic Pressure, psi
4295
Exit Program
Continue
Back
start
Pressure Build-...
Simulation Resu...
BHP & Casing B...
Project1 - M

B2. COMPUTER PROGRAMMING CODES

```
'Programmer    :  O. Jacob Aremu
'Description   :  This program models the size variations of gas bubbles at the
'                 wellbore-sand face contact for gas inflow during drilling
'                 operations, and wellbore pressure build-up computations
'Date          :  May, 2005
'Purpose       :  As a partial fulfillment of the degree of PhD at the Mewbourne
'                 School of Petroleum and Geological Engineering

Option Explicit

Dim tD As Double, PD1 As Double, PD As Double, Y As Double, gasFloRat As Double, A As Double, B As Double
Dim omega As Double, sip As Double, romanG As Double, diff As Double, romanh As Double, linerFact As Double
Dim pitVolIncres As Double, denConst As Double, counter As Integer, i As Integer, j As Integer
Dim error As Double, x As Double, sim_error(120) As Double, numIter(120) As Double, bubbIncre As Double

Dim TimCompClos As Double, piC As Double, deltSC As Double, Jc As Double, Yint As Double
Dim tDs As Double, PDs As Double, Ic As Double, shutInTime As Double, FormFt As Double
Dim totGasVol As Double, SeriesConstC As Double, JcArgC As Double, nc As Integer
Dim SeriesSumC As Double, SeriesTermC As Double, m As Integer, facto As Double
Dim tanz As Double, atanh As Double, SeriesConstT As Double, JcArgT As Double, nt As Integer
Dim SeriesSumT As Double, SeriesTermT As Double, deltST As Double, Arg As Double
Dim LstSeriTermC As Double, LstSeriTermT(1 To 2880) As Double, timCount As Integer
Dim Press(1 To 2880) As Double, tanh(1 To 2880) As Double, shInGasFlo(1 To 2880) As Double
Dim P_DConst As Double, shInGasDen(1 To 2880) As Double, CsgPress(1 To 2880) As Double
Dim gasFrac As Double, annVol As Double, CsgPressC As Double, shInGasDenC As Double

Dim riserID As Double, casingID As Double, DpOD As Double, DpID As Double, DcOD As Double
```

```
Dim DpOpHol As Double, annFlDen As Double, gasDenP As Double, gasMass As Double, ExpGasVol As Double
Dim DcID As Double, bitDia As Double, bitNoz(2) As Double, nozArea As Double, totDepth As Double
Dim pumpMaxFloRat As Double, pumpMaxPress As Double, check As Double, prod As Double
Dim nozDisCoef As Double, chokeID As Double, surfPumpMaxHp As Double, riserDep As Double
Dim casMudLnDep As Double, openHolInt As Double, DcLen As Double, drillTime As Double
Dim rw As Double, rop As Double, gasVis As Double, gasGrav As Double, gasConst As Double
Dim gasPcP As Double, gasPcT As Double, gasPrP As Double, gasPrT As Double, Z As Double
Dim gasDen As Double, gasComp As Double, gasFVF As Double, ZPslope As Double, totFricPress As Double
Dim mudFloRat As Double, surfPumpPres As Double, mudDen As Double, mudPV As Double
Dim mudYP As Double, mudAV As Double, mudSurfTen As Double, DpVel As Double, DpLen As Double
Dim DcVel As Double, nozVel As Double, DpRe As Double, DcRe As Double, nozRe As Double
Dim DpFricPress As Double, DcFricPress As Double, flowBHP As Double, mudHydPress As Double
Dim formPress As Double, formPerm As Double, formPoro As Double, bhTemp As Double
Dim h(120) As Double, surfTemp As Double, bubbleVol(120) As Double, bubbleSize(120) As Double


' This section computes the variations in the bubble size that while the drilling
' proceeds. That is, gas influx has not been noticed. It is assummed that about
' 5 feet of the formation has been drilled before suspecting influx.


Private Sub cmdDrillgasSize_Click()

Dim gasFloRatNum As Double, gasFloRatDen As Double

rop = Val(txtROP.Text)
   drillTime = (1 / 12) / rop  'Same Drill Time, hours

For counter = 0 To 60
   If counter = 0 Then
   h(counter) = 0
```

```
' Assigning value zero (0) to bubble size if the height, h, into the formation is zero

bubbleVol(counter) = 0
bubbleSize(counter) = 0
Else

h(counter) = h(counter - 1) + (1 / 12)

'Importing inputs from other Forms and assigning the inputs to
' variables

formPoro = Val(frmMudFormPpties.txtFormPoro.Text)
formPerm = Val(frmMudFormPpties.txtFormPerm.Text)
formPress = Val(frmMudFormPpties.txtFormPress.Text)
rw = Val(frmDrillToolsData.txtBitSize.Text) / 24
mudDen = Val(frmMudFormPpties.txtMudDen.Text)
riserDep = Val(frmDrillToolsData.txtRiserLength.Text)
casMudLnDep = Val(frmDrillToolsData.txtMudLnCasDep.Text)
openHolInt = Val(frmDrillToolsData.txtOpenHolLen.Text)
surfPumpMaxHp = Val(frmDrillToolsData.txtPumpMaxHp.Text)
pumpMaxPress = Val(frmDrillToolsData.txtPumpMaxDischargePress.Text)
DpID = Val(frmDrillToolsData.txtDpID.Text)
DpOD = Val(frmDrillToolsData.txtDpOD.Text)
DcID = Val(frmDrillToolsData.txtDcID.Text)
DcOD = Val(frmDrillToolsData.txtDcOD.Text)
mudPV = Val(frmMudFormPpties.txtMudPV.Text)
mudSurfTen = Val(frmMudFormPpties.txtMudSurfTen.Text)
DcLen = Val(frmDrillToolsData.txtDcLen.Text)

'Assigning inputs in the present form to variables for computation

Z = Val(txtgasCompFact.Text)
ZPslope = Val(txtSlopedZdP.Text)
gasVis = Val(txtgasVisc.Text)
mudFloRat = Val(txtMudFloRat.Text)  '(gpm)
bhTemp = Val(txtBHTemp.Text) + 460        'oR
gasGrav = Val(txtgasSG.Text)           'S.G
gasConst = Val(txtgasConst.Text)

'Calculating the Gas compressibility, Cg

gasComp = (1 / formPress) - ((1 / Z) * ZPslope)  '(psi-1)

' Calculating the Dimensionless time, tD, Pressure, PD
```

```
   tD = ((0.0002634) * formPerm * drillTime) / (formPoro * gasVis * gasComp * (rw
^ 2))
   'PD1 = Log(tD) / 2.30258509            'Note the LOG in VB is Natural Logarithm
(Ln)
   PD = (1 / 2) * (Log(tD) + (81 / 100))

   ' Computing the mud ejection pressure, Pbit, from the bit nozzles during drilling

      ' calculating the surface pump discharge pressure at the current operating mud
flow rate.

      pumpMaxFloRat = (1714 * surfPumpMaxHp) / pumpMaxPress

      frmDrillToolsData.txtPumpMaxFloRat.Text = Str(pumpMaxFloRat)

      'Since a specific pump is rated for its Max Hp, Max Flow rate and Max
discharge pressure
      'and as the flow rate through any pump increases the discahrge pressure should
increase
      'too. Therefore, to approximate the discharge pressure at any flow rate, as long
as
      'the flow rate and discharge pressure are not beyond the ratings of the pump,
      'a liner factor that expresses the proportionality between the parameters is
adopted.

      linerFact = pumpMaxFloRat / pumpMaxPress

      'Therefore, at a desired operating mud flow rate, the corresponding pump
discharge
      'for a pump of certain liner size is estimated as follows

      surfPumpPres = mudFloRat / linerFact    '(psi)

      ' Calculating the mud velocities inside the Drill pipe and the Drill collars
      DpVel = mudFloRat / (2.448 * (DpID ^ 2))     '(ft/sec)
      DcVel = mudFloRat / (2.448 * (DcID ^ 2))     '(ft/sec)

      'This initial simulation imposes turbulent flow inside the Drill String.

      DcFricPress = (((mudDen ^ 0.75) * (DcVel ^ 1.75) * (mudPV ^ 0.25)) / (1800 *
(DcID ^ 1.25))) * DcLen
      DpLen = (riserDep + casMudLnDep + openHolInt) - DcLen
      DpFricPress = (((mudDen ^ 0.75) * (DpVel ^ 1.75) * (mudPV ^ 0.25)) / (1800 *
(DpID ^ 1.25))) * DpLen

      ' Total frictional pressure inside the drill string follows:
```

```
totFricPress = DpFricPress + DcFricPress

' Calculating the total crossectional area of the bit nozzles

For i = 0 To 2
   If i = 0 Then
   bitNoz(i) = Val(frmDrillToolsData.txtNozzle1.Text)
   ElseIf i = 1 Then
   bitNoz(i) = Val(frmDrillToolsData.txtNozzle2.Text)
   ElseIf i = 2 Then
   bitNoz(i) = Val(frmDrillToolsData.txtNozzle3.Text)
   End If
Next i

nozArea = ((22 / 7) / (64 ^ 2)) * ((bitNoz(0)) ^ 2 + (bitNoz(1)) ^ 2 + (bitNoz(2)) ^ 2)

' Assigning a constant to the nozzle discharge coefficient

nozDisCoef = 0.95

' Estimating the mud ejection pressure from the bit nozzles, at the bottom hole during drilling

flowBHP = (0.052 * mudDen * (DpLen + DcLen)) + surfPumpPres - totFricPress - (0.0008074 * (DcVel ^ 2) * mudDen) - ((0.00008311 * mudDen * (mudFloRat ^ 2)) / ((nozDisCoef * nozArea) ^ 2))

'The beginning of iterative steps that are required to estimate bubble sizes

bubbleVol(counter) = 0

x = 0
diff = 1
error = 0
prod = 1

'A device for reducing the number of iterations as the exposed formation interval increases
'This help to speed up the time used to obtain results

If counter = 1 Then
bubbIncre = 0.00000001
ElseIf bubbleVol(counter - 1) < 1 Then
```

```
' Re-assigning the last bubble volume calculated to another variable for manipulation

check = bubbleVol(counter - 1)

'Reducing the decimal places of the increment for the next iteration process

Do While check < 1
check = check * 10
prod = prod * 10
Loop

bubbIncre = 1 / (prod * 100)

ElseIf bubbleVol(counter - 1) > 1 Then
bubbIncre = 0.001

End If

'Calculating the gas Formation Volume Factor, FVF

gasFVF = 0.02829 * ((Z * bhTemp) / formPress)        'Bg (Cuft/SCF)

' Evaluating the numerator expression of the gas flow rate equation

romanh = (formPerm * gasFVF) / (34176 * bhTemp * gasVis * Z)


' Iteration process begins

Do While Abs(error) < Abs(diff)
diff = Abs(error)

x = x + 1

bubbleVol(counter) = bubbleVol(counter) + bubbIncre

Y = flowBHP + (((88 / 21) ^ (1 / 3)) * (mudSurfTen / (72 * (bubbleVol(counter) ^ (1 / 3)))))

'gasFloRatNum = (formPerm * h(counter) * ((formPress ^ 2) - (Y ^ 2)) * gasFVF)

' The gas flow rate is then estimated as follows:

gasFloRat = (formPerm * h(counter) * ((formPress ^ 2) - (Y ^ 2)) * gasFVF) / (34176 * PD * bhTemp * gasVis * Z) 'cuft/hr
```

```
    ' Evaluating the denominator expression of the gas flow rate equation

    'gasFloRatDen = (24 * 1424 * PD * bhTemp * gasVis * Z)

    'gasFloRat = gasFloRatNum / gasFloRatDen              '(ft3/hr)

    'Evaluation of the model parameters follows:

    A = (formPress ^ 2) - (Y ^ 2)

    B = ((mudSurfTen / 72) * A * Y) - (((21 / 88) * bubbleVol(counter)) ^ (1 / 3) * (A
^ 2))

    'romanh = (formPerm * gasFVF) / (gasFloRatDen / PD)

    gasDen = (28.97 * gasGrav * formPress) / (Z * gasConst * bhTemp)

    denConst = (gasDen + (((11 * 7.48) / 16) * mudDen))

    omega = ((2 / 9) * ((romanh * h(counter)) / PD) ^ 2 * denConst * B) /
bubbleVol(counter)

    sip = ((((romanh * h(counter) * A) ^ 2) * denConst) / ((36 * (22 / 7)) ^ (1 / 3))) /
(bubbleVol(counter) ^ (2 / 3))

    romanG = (3 * A * ((22 / 7) ^ (1 / 3)) * mudPV * (romanh * h(counter) / PD)) /
(47980.8 * (6 ^ (1 / 3)) * (bubbleVol(counter) ^ (1 / 3)))

    'Subtracting all the RHS expressions from the LHS expression results in the error

    error = (bubbleVol(counter) * ((7.48 * mudDen) - gasDen)) - (omega + sip +
romanG + ((0.00082 * (22 / 7) * formPoro * mudSurfTen) / (3 * (1 - formPoro))))

    If x = 1 Then
    diff = Abs(error) + 1
    End If

    Loop

    End If
' Computing the bubble size or diameter

bubbleSize(counter) = (((6 / (22 / 7)) * bubbleVol(counter)) ^ (1 / 3)) * 12
sim_error(counter) = Abs(diff)
numIter(counter) = x
```

```
Next counter

frmResults.Show

' Setting the format for the result table

frmResults.msgResultTable.ColWidth(0) = 2000
frmResults.msgResultTable.ColWidth(1) = 2000
frmResults.msgResultTable.ColWidth(2) = 2000
frmResults.msgResultTable.ColWidth(3) = 2000
frmResults.msgResultTable.ColWidth(4) = 2000

' Setting the headings

frmResults.msgResultTable.Row = 0
frmResults.msgResultTable.Col = 0
frmResults.msgResultTable.Text = "Height (h) Drilled"
frmResults.msgResultTable.Col = 1
frmResults.msgResultTable.Text = "Bubble Volume"
frmResults.msgResultTable.Col = 2
frmResults.msgResultTable.Text = "Bubble size (diameter)"
frmResults.msgResultTable.Col = 3
frmResults.msgResultTable.Text = "Sim. Error"
frmResults.msgResultTable.Col = 4
frmResults.msgResultTable.Text = "No of Iterations"
frmResults.msgResultTable.Row = 1
frmResults.msgResultTable.Col = 0
frmResults.msgResultTable.Text = "  ft "
frmResults.msgResultTable.Col = 1
frmResults.msgResultTable.Text = " cuft "
frmResults.msgResultTable.Col = 2
frmResults.msgResultTable.Text = "inch(es)"
frmResults.msgResultTable.Col = 3
frmResults.msgResultTable.Text = ""
frmResults.msgResultTable.Col = 4
frmResults.msgResultTable.Text = "Absolute"

' Printing result table on a different form

For counter = 0 To 60
j = counter + 3

frmResults.msgResultTable.Row = j
frmResults.msgResultTable.Col = 0
frmResults.msgResultTable.Text = Str(Round(h(counter), 2))
```

```
frmResults.msgResultTable.Col = 1
frmResults.msgResultTable.Text = Str(Round(bubbleVol(counter), 4))
frmResults.msgResultTable.Col = 2
frmResults.msgResultTable.Text = Str(Round(bubbleSize(counter), 2))
frmResults.msgResultTable.Col = 3
frmResults.msgResultTable.Text = Str(Round(sim_error(counter), 8))
frmResults.msgResultTable.Col = 4
frmResults.msgResultTable.Text = Str(numIter(counter))


'frmResults.picResults.Print "drillTime  =  "; drillTime
'frmResults.picResults.Print "tD   = "; tD
'frmResults.picResults.Print "PD  =  "; PD
'frmResults.picResults.Print "Y  =  "; Y
'frmResults.picResults.Print "gasFloRat  =  "; gasFloRat
'frmResults.picResults.Print "A  = "; A
'frmResults.picResults.Print "B = "; B
'frmResults.picResults.Print "omega  = "; omega
'frmResults.picResults.Print "sip  = "; sip
'frmResults.picResults.Print "romanG  = "; romanG
'frmResults.picResults.Print "diff  = "; diff
'frmResults.picResults.Print "Bubble Size or Diameter  = "; bubbleSize(counter)
'frmResults.picResults.Print "gasComp  = "; gasComp
'frmResults.picResults.Print "FlowBhP  = "; flowBHP
'frmResults.picResults.Print "gasFVF  = "; gasFVF
'frmResults.picResults.Print "surface Pump press = "; surfPumpPres
'frmResults.picResults.Print "Dp Vel  = "; DpVel
'frmResults.picResults.Print "Dc Vel  = "; DcVel
'frmResults.picResults.Print "Dc fric  = "; DcFricPress
'frmResults.picResults.Print "Dp Length  = "; DpLen
'frmResults.picResults.Print "Dp fric  = "; DpFricPress
'frmResults.picResults.Print "tot fric  = "; totFricPress
'frmResults.picResults.Print "Nozzle area  = "; nozArea
'frmResults.picResults.Print "Gas density  = "; gasDen
'frmResults.picResults.Print "Log(tD)  = "; PD1

Next counter

' The following are the graph codes

'frmResults.picResults.Scale (0, 0.1)-(120, 0) 'Specify coordinate system
'frmResults.picResults.Line (-5, 0)-(100, 0)     'Draw x-axis
'frmResults.picResults.Line (0, -1)-(0, 10)      'Draw y-axis
'For counter = 0 To 120
'  frmResults.picResults.PSet (h(counter), bubbleVol(counter))
'Next counter
```

```
End Sub

Private Sub cmdExit_Click()
Unload frmOperatingCond

End Sub

Private Sub cmdShutInGasSize_Click()

Dim gasFloRatNum As Double, gasFloRatDen As Double

'Importing inputs from other Forms and assigning the inputs to
   ' variables

   formPoro = Val(frmMudFormPpties.txtFormPoro.Text)
   formPerm = Val(frmMudFormPpties.txtFormPerm.Text)
   formPress = Val(frmMudFormPpties.txtFormPress.Text)
   rw = Val(frmDrillToolsData.txtBitSize.Text) / 24
   mudDen = Val(frmMudFormPpties.txtMudDen.Text)
   riserDep = Val(frmDrillToolsData.txtRiserLength.Text)
   casMudLnDep = Val(frmDrillToolsData.txtMudLnCasDep.Text)
   openHolInt = Val(frmDrillToolsData.txtOpenHolLen.Text)
   surfPumpMaxHp = Val(frmDrillToolsData.txtPumpMaxHp.Text)
   pumpMaxPress = Val(frmDrillToolsData.txtPumpMaxDischargePress.Text)
   DpID = Val(frmDrillToolsData.txtDpID.Text)
   DpOD = Val(frmDrillToolsData.txtDpOD.Text)
   DcID = Val(frmDrillToolsData.txtDcID.Text)
   DcOD = Val(frmDrillToolsData.txtDcOD.Text)
   mudPV = Val(frmMudFormPpties.txtMudPV.Text)
   mudSurfTen = Val(frmMudFormPpties.txtMudSurfTen.Text)
   DcLen = Val(frmDrillToolsData.txtDcLen.Text)
   bitDia = Val(frmDrillToolsData.txtBitSize.Text)     'New for this section
   casingID = Val(frmDrillToolsData.txtCasingID.Text)  'New for this section

   'Assigning inputs in the present form to variables for computation

   Z = Val(txtgasCompFact.Text)
   ZPslope = Val(txtSlopedZdP.Text)
   gasVis = Val(txtgasVisc.Text)
   mudFloRat = Val(txtMudFloRat.Text)  '(gpm)
   bhTemp = Val(txtBHTemp.Text) + 460        'oR
   gasGrav = Val(txtgasSG.Text)          'S.G
   gasConst = Val(txtgasConst.Text)
   TimCompClos = Val(txtTimeToClose.Text)      'Seconds - New for this section
   FormFt = Val(txtFormInt.Text)              'feet - New for this section
```

```
    totGasVol = Val(txtTotGasVol.Text)          'cuft - total annular gas volume
                                                '       at reservoir pressure
    'Calculating the Gas compressibility, Cg

    gasComp = (1 / formPress) - ((1 / Z) * ZPslope)  '(psi-1)

    'Calculating the gas Formation Volume Factor, FVF

    gasFVF = 0.02829 * ((Z * bhTemp) / formPress)        'Bg (Cuft/SCF)- Repeated

    ' Computing the hydrostatic pressure of the mud in the drillpipe

    totDepth = riserDep + casMudLnDep + openHolInt

    mudHydPress = 0.052 * mudDen * totDepth

    'Convert the time to completely close the well into hours

    TimCompClos = TimCompClos / 3600        ' Now in "HOURS"

    Ic = ((0.0002634) * formPerm) / (formPoro * gasVis * gasComp * (rw ^ 2))
    Jc = (Log(Ic) + (81 / 100))

    gasDen = (28.97 * gasGrav * formPress) / (Z * gasConst * bhTemp) 'lbm/cuft -
repeated

    gasDenP = gasDen * (8.33 / 62.4) 'lbm/gal or ppg

    P_DConst = (formPress - ((1 / gasComp) * Log(gasDenP)))       'Pressure-Density
constant

    DpOpHol = openHolInt - DcLen

    annVol = (22 / (7 * 4 * 144)) * ((DcLen * (bitDia ^ 2 - DcOD ^ 2)) + (DpOpHol *
(bitDia ^ 2 - DpOD ^ 2)) + (casMudLnDep * (casingID ^ 2 - DpOD ^ 2)))

    'Estimating the total annular gas mass just at Shut-in

    gasMass = gasDen * totGasVol

    'Estimating the annular average gas density just at Shut-in

    shInGasDenC = Exp((mudHydPress - P_DConst) * gasComp) 'ppg

    'Estimating the Expanded volume of the gas just at Shut-in
```

```
   ExpGasVol = gasMass / (shInGasDenC * 7.491)

   gasFrac = ExpGasVol / annVol

   piC = (2 * (formPerm * FormFt * gasFVF)) / (34176 * Exp(Jc) * gasComp *
ExpGasVol * bhTemp * gasVis * Z)

   tD = (Ic * (1 / 60))        'Note duration of Bubble size formation is set
                               'at 1 minute tally with rate of pressure buildup

   PD = (1 / 2) * (Log(tD) + (81 / 100))     'Note the LOG in VB is Natural Logarithm
(Ln)
   '-------------------------------------------------------------------------------------------
   'Computing the series obtained through integration

   shutInTime = TimCompClos

   JcArgC = (Jc + Log(shutInTime))

   nc = 0          'Number of series terms to achieve the cut-off

   Do
      nc = nc + 1

      'computing the factorial
      m = 1
      facto = 1

      Do While m <= nc
      facto = facto * m
      m = m + 1
      Loop    ' End of Factorial computation

      SeriesTermC = (JcArgC ^ nc) / (nc * facto)
      SeriesSumC = SeriesSumC + SeriesTermC

   Loop Until SeriesTermC <= 0.001

   LstSeriTermC = SeriesTermC      'Storing the value of the last series term
                                   'for the constant of integration

   deltSC = Log(JcArgC) + SeriesSumC

   tanz = mudHydPress / formPress

   'Computing approximate derived function of ArcTangent
```

```
   atanh = Log((1 + tanz) / (1 - tanz)) / 2

   Yint = ((1 / formPress) * atanh) - (piC * deltSC)     'A Constant for the remaining computations

  '-------------------------------------------------------------------------------------------

   'Computing the Constant of integration for the Casing Pressure
   'Use the reservoir pressure and gas density at that condition

   annFlDen = ((shInGasDenC * gasFrac) + (mudDen * (1 - gasFrac)))

   CsgPressC = (mudHydPress - (0.052 * annFlDen * (casMudLnDep + openHolInt)))

   'Computing the pressure buildup

   nt = 0
   timCount = 0
Do
      timCount = timCount + 1
      If timCount = 1 Then
         shutInTime = ((1 / 60) - shutInTime)
      Else
         shutInTime = timCount / 60      'Shut-in time in hours
      End If

      JcArgT = (Jc + Log(shutInTime))

      nt = 0          'Number of series terms to achieve the cut-off

      Do
      nt = nt + 1

      'computing the factorial
      m = 1
      facto = 1

         Do While m <= nt
         facto = facto * m
         m = m + 1
         Loop    ' End of Factorial computation

      SeriesTermT = (JcArgT ^ nt) / (nt * facto)
      SeriesSumT = SeriesSumT + SeriesTermT
```

```
      Loop Until SeriesTermT <= 0.001       'Ending the each term computation and
total summation

   LstSeriTermT(timCount) = SeriesTermT       'Storing the value of the last series
term
                                  'for the constant of integration
   deltST = Log(JcArgT) + SeriesSumT

   Arg = (formPress * ((piC * deltST) + Yint)) 'Argument term for the pressure
computation

   tanh(timCount) = (Exp(Arg) - Exp(-1 * Arg)) / (Exp(Arg) + Exp(-1 * Arg))

   Press(timCount) = (formPress * tanh(timCount))

   ' Calculating the Dimensionless Shut-in time, tDs, and Pressure, PDs

   tDs = (Ic * shutInTime)

   PDs = (1 / 2) * (Log(tDs) + (81 / 100))       'Note the LOG in VB is Natural
Logarithm (Ln)

   'Calculating the diminishing gas influx rate during shut-in

   shInGasFlo(timCount) = (formPerm * FormFt * ((formPress ^ 2) -
(Press(timCount) ^ 2)) * gasFVF) / (34176 * PDs * bhTemp * gasVis * Z) 'cuft/hr

   'Computing the Casing Pressure

   shInGasDen(timCount) = Exp((Press(timCount) - P_DConst) * gasComp) 'ppg

   annFlDen = ((shInGasDen(timCount) * gasFrac) + (mudDen * (1 - gasFrac)))

   CsgPress(timCount) = (Press(timCount) - (0.052 * annFlDen * (casMudLnDep +
openHolInt)))

 Loop Until Press(timCount) >= formPress       'End of pressure built for each shut-in
time
'In the above expression USE "Round(Press(timCount)) = formPress" for Shut-in
Bubble sizes;,
                  'and "Press(timCount) >= formPress" for Build-up pressures


'-----------------------------------------------------------------------------------------------
-
```

```
'-------------------------------------------------------------------------------------------------------
---------

' Displaying Pressure Build-Up results

frmShutInResults.Show

' Setting the format for the result table

frmShutInResults.msgShutInResults.ColWidth(0) = 1000
frmShutInResults.msgShutInResults.ColWidth(1) = 1000
frmShutInResults.msgShutInResults.ColWidth(2) = 1500
frmShutInResults.msgShutInResults.ColWidth(3) = 1500
frmShutInResults.msgShutInResults.ColWidth(4) = 1000
frmShutInResults.msgShutInResults.ColWidth(5) = 1500
frmShutInResults.msgShutInResults.ColWidth(6) = 1000
frmShutInResults.msgShutInResults.ColWidth(7) = 1500

' Setting the headings

frmShutInResults.msgShutInResults.Row = 0
frmShutInResults.msgShutInResults.Col = 0
frmShutInResults.msgShutInResults.Text = "Shut-In Time"
frmShutInResults.msgShutInResults.Col = 1
frmShutInResults.msgShutInResults.Text = "Shut-In Time"
frmShutInResults.msgShutInResults.Col = 2
frmShutInResults.msgShutInResults.Text = "Series Last Term"
frmShutInResults.msgShutInResults.Col = 3
frmShutInResults.msgShutInResults.Text = "Hyperbolic Tangent"
frmShutInResults.msgShutInResults.Col = 4
frmShutInResults.msgShutInResults.Text = "BHP"
frmShutInResults.msgShutInResults.Col = 5
frmShutInResults.msgShutInResults.Text = "Gas Influx Rate"
frmShutInResults.msgShutInResults.Col = 6
frmShutInResults.msgShutInResults.Text = "Gas Density"
frmShutInResults.msgShutInResults.Col = 7
frmShutInResults.msgShutInResults.Text = "Casing Pressure"
frmShutInResults.msgShutInResults.Row = 1
frmShutInResults.msgShutInResults.Col = 0
frmShutInResults.msgShutInResults.Text = "  mins "
frmShutInResults.msgShutInResults.Col = 1
frmShutInResults.msgShutInResults.Text = " Hours "
frmShutInResults.msgShutInResults.Col = 2
frmShutInResults.msgShutInResults.Text = ""
frmShutInResults.msgShutInResults.Col = 3
frmShutInResults.msgShutInResults.Text = ""
```

```
frmShutInResults.msgShutInResults.Col = 4
frmShutInResults.msgShutInResults.Text = "  psi  "
frmShutInResults.msgShutInResults.Col = 5
frmShutInResults.msgShutInResults.Text = "  cuFt/hr  "
frmShutInResults.msgShutInResults.Col = 6
frmShutInResults.msgShutInResults.Text = " lbm/gal "
frmShutInResults.msgShutInResults.Col = 7
frmShutInResults.msgShutInResults.Text = "  psi  "

' Printing result table on a different form

For counter = 0 To timCount
j = counter + 3

If counter = 0 Then

frmShutInResults.msgShutInResults.Row = j
frmShutInResults.msgShutInResults.Col = 0
frmShutInResults.msgShutInResults.Text = Str(counter)
frmShutInResults.msgShutInResults.Col = 1
frmShutInResults.msgShutInResults.Text = Str(counter)
frmShutInResults.msgShutInResults.Col = 2
frmShutInResults.msgShutInResults.Text = Str(Round(LstSeriTermC, 4))
frmShutInResults.msgShutInResults.Col = 3
frmShutInResults.msgShutInResults.Text = Str(Round(atanh, 3))
frmShutInResults.msgShutInResults.Col = 4
frmShutInResults.msgShutInResults.Text = Str(Round(mudHydPress))
frmShutInResults.msgShutInResults.Col = 5
frmShutInResults.msgShutInResults.Text = Str(counter)
frmShutInResults.msgShutInResults.Col = 6
frmShutInResults.msgShutInResults.Text = Str(Round(shInGasDenC, 3))
frmShutInResults.msgShutInResults.Col = 7
frmShutInResults.msgShutInResults.Text = Str(Round(CsgPressC))

Else

frmShutInResults.msgShutInResults.Row = j
frmShutInResults.msgShutInResults.Col = 0
frmShutInResults.msgShutInResults.Text = Str(counter)
frmShutInResults.msgShutInResults.Col = 1
frmShutInResults.msgShutInResults.Text = Str(Round((counter / 60), 3))
frmShutInResults.msgShutInResults.Col = 2
frmShutInResults.msgShutInResults.Text = Str(Round(LstSeriTermT(counter), 4))
frmShutInResults.msgShutInResults.Col = 3
frmShutInResults.msgShutInResults.Text = Str(Round(tanh(counter), 3))
frmShutInResults.msgShutInResults.Col = 4
```

```
frmShutInResults.msgShutInResults.Text = Str(Round(Press(counter)))
frmShutInResults.msgShutInResults.Col = 5
frmShutInResults.msgShutInResults.Text = Str(Round(shInGasFlo(counter), 3))
frmShutInResults.msgShutInResults.Col = 6
frmShutInResults.msgShutInResults.Text = Str(Round(shInGasDen(counter), 3))
frmShutInResults.msgShutInResults.Col = 7
frmShutInResults.msgShutInResults.Text = Str(Round(CsgPress(counter)))

End If

Next counter


'-------------------------------------------------------------------------
'-------------------------------------------------------------------------------------------------------
---------


End Sub
```

APPENDIX C

C1. EXAMPLE OF SIMULATION RESULTS FOR COMPUTED APPARENT GAS BUBBLE SIZES

K = 300 md, q = 387 gpm, Porosity = 0.3, Mud PV = 24 cp
Mud YP = 18 lbf/100ft^2

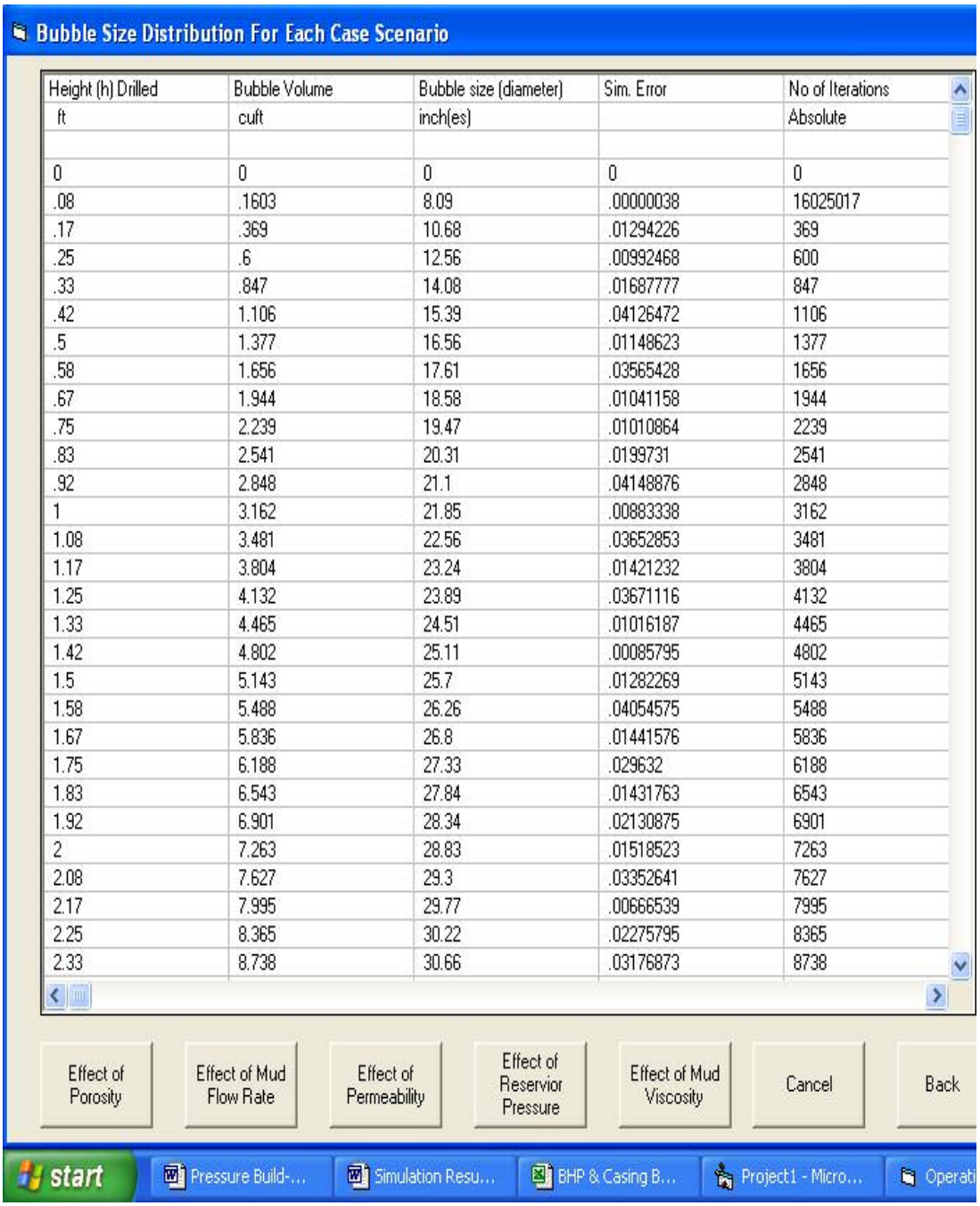

Height (h) Drilled	Bubble Volume	Bubble size (diameter)	Sim. Error	No of Iterations
ft	cuft	inch(es)		Absolute
0	0	0	0	0
.08	.1603	8.09	.00000038	16025017
.17	.369	10.68	.01294226	369
.25	.6	12.56	.00992468	600
.33	.847	14.08	.01687777	847
.42	1.106	15.39	.04126472	1106
.5	1.377	16.56	.01148623	1377
.58	1.656	17.61	.03565428	1656
.67	1.944	18.58	.01041158	1944
.75	2.239	19.47	.01010864	2239
.83	2.541	20.31	.0199731	2541
.92	2.848	21.1	.04148876	2848
1	3.162	21.85	.00883338	3162
1.08	3.481	22.56	.03652853	3481
1.17	3.804	23.24	.01421232	3804
1.25	4.132	23.89	.03671116	4132
1.33	4.465	24.51	.01016187	4465
1.42	4.802	25.11	.00085795	4802
1.5	5.143	25.7	.01282269	5143
1.58	5.488	26.26	.04054575	5488
1.67	5.836	26.8	.01441576	5836
1.75	6.188	27.33	.029632	6188
1.83	6.543	27.84	.01431763	6543
1.92	6.901	28.34	.02130875	6901
2	7.263	28.83	.01518523	7263
2.08	7.627	29.3	.03352641	7627
2.17	7.995	29.77	.00666539	7995
2.25	8.365	30.22	.02275795	8365
2.33	8.738	30.66	.03176873	8738

C1 (contd.)

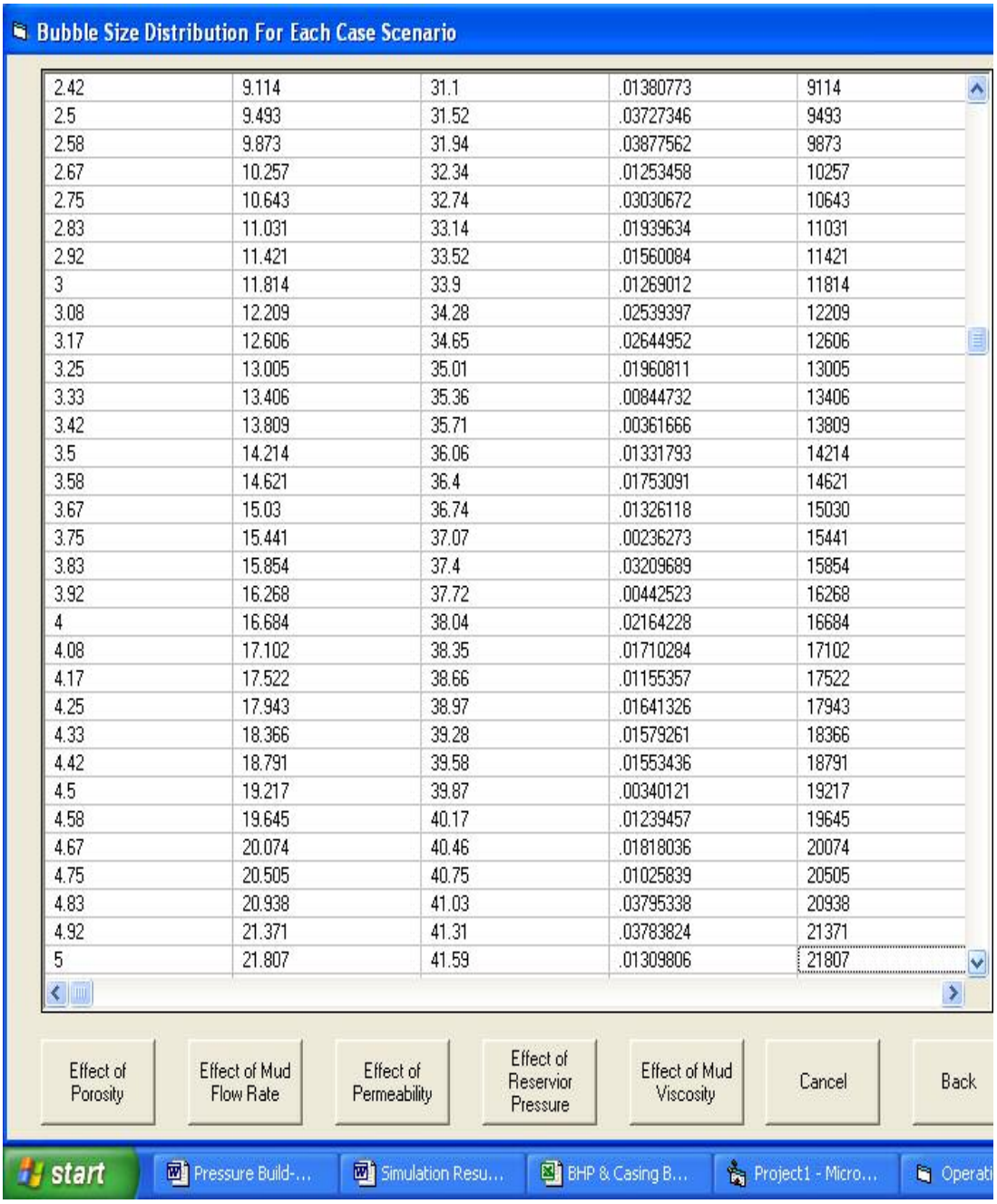
Bubble Size Distribution For Each Case Scenario
2.42 9.114 31.1 .01380773 9114
2.5 9.493 31.52 .03727346 9493
2.58 9.873 31.94 .03877562 9873
2.67 10.257 32.34 .01253458 10257
2.75 10.643 32.74 .03030672 10643
2.83 11.031 33.14 .01939634 11031
2.92 11.421 33.52 .01560084 11421
3 11.814 33.9 .01269012 11814
3.08 12.209 34.28 .02539397 12209
3.17 12.606 34.65 .02644952 12606
3.25 13.005 35.01 .01960811 13005
3.33 13.406 35.36 .00844732 13406
3.42 13.809 35.71 .00361666 13809
3.5 14.214 36.06 .01331793 14214
3.58 14.621 36.4 .01753091 14621
3.67 15.03 36.74 .01326118 15030
3.75 15.441 37.07 .00236273 15441
3.83 15.854 37.4 .03209689 15854
3.92 16.268 37.72 .00442523 16268
4 16.684 38.04 .02164228 16684
4.08 17.102 38.35 .01710284 17102
4.17 17.522 38.66 .01155357 17522
4.25 17.943 38.97 .01641326 17943
4.33 18.366 39.28 .01579261 18366
4.42 18.791 39.58 .01553436 18791
4.5 19.217 39.87 .00340121 19217
4.58 19.645 40.17 .01239457 19645
4.67 20.074 40.46 .01818036 20074
4.75 20.505 40.75 .01025839 20505
4.83 20.938 41.03 .03795338 20938
4.92 21.371 41.31 .03783824 21371
5 21.807 41.59 .01309806 21807
Effect of Porosity
Effect of Mud Flow Rate
Effect of Permeability
Effect of Reservior Pressure
Effect of Mud Viscosity
Cancel
Back
start
Pressure Build-...
Simulation Resu...
BHP & Casing B...
Project1 - Micro...
Operati

C2. EXAMPLE OF CASING AND BOTTOM-HOLE PRESSURE BUILD-UP SIMULATION RESULTS

K = 50 md (Initial Gas Volume = 81.74 ft^3)

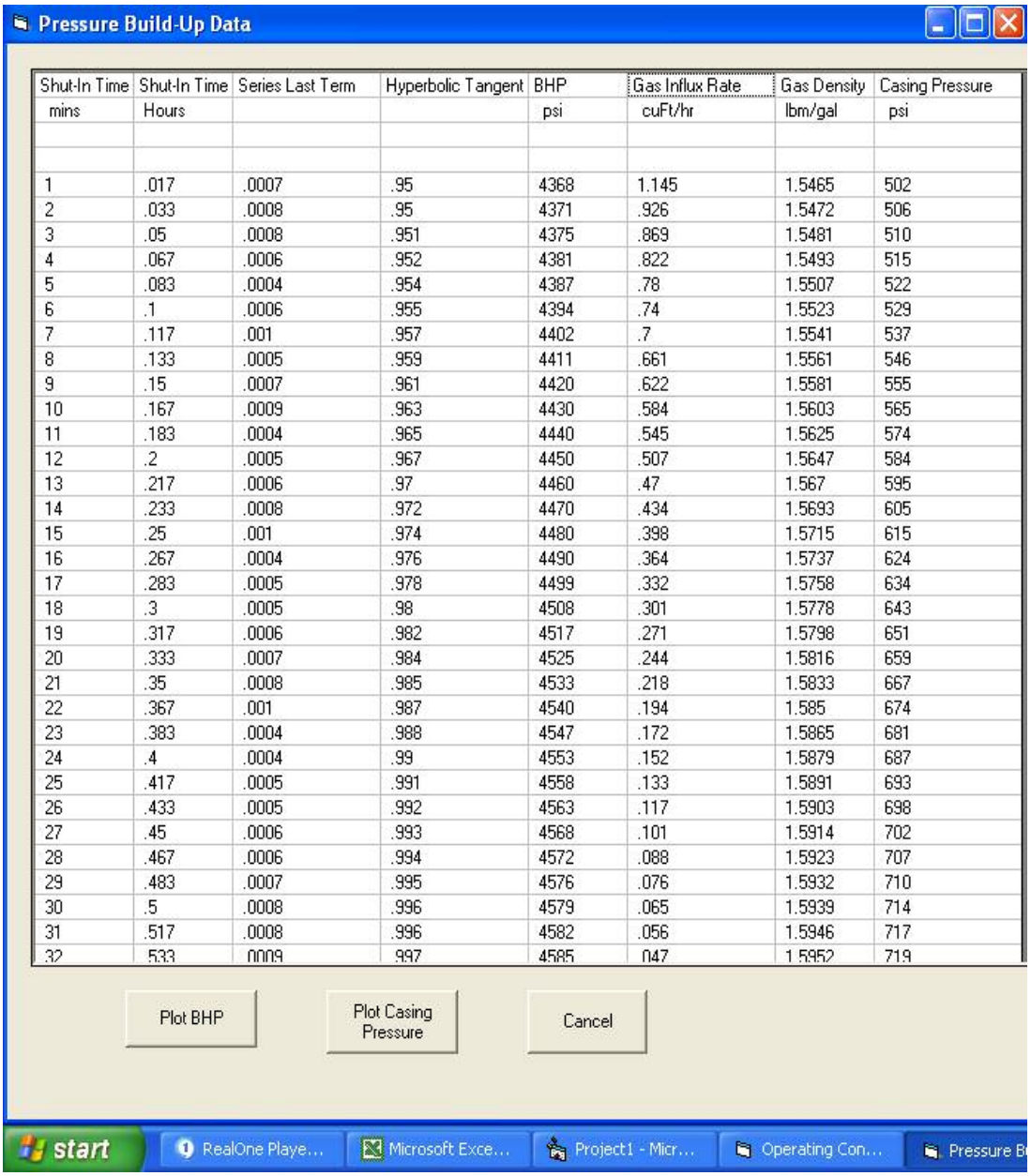

Shut-In Time	Shut-In Time	Series Last Term	Hyperbolic Tangent	BHP	Gas Influx Rate	Gas Density	Casing Pressure
mins	Hours			psi	cuFt/hr	lbm/gal	psi
1	.017	.0007	.95	4368	1.145	1.5465	502
2	.033	.0008	.95	4371	.926	1.5472	506
3	.05	.0008	.951	4375	.869	1.5481	510
4	.067	.0006	.952	4381	.822	1.5493	515
5	.083	.0004	.954	4387	.78	1.5507	522
6	.1	.0006	.955	4394	.74	1.5523	529
7	.117	.001	.957	4402	.7	1.5541	537
8	.133	.0005	.959	4411	.661	1.5561	546
9	.15	.0007	.961	4420	.622	1.5581	555
10	.167	.0009	.963	4430	.584	1.5603	565
11	.183	.0004	.965	4440	.545	1.5625	574
12	.2	.0005	.967	4450	.507	1.5647	584
13	.217	.0006	.97	4460	.47	1.567	595
14	.233	.0008	.972	4470	.434	1.5693	605
15	.25	.001	.974	4480	.398	1.5715	615
16	.267	.0004	.976	4490	.364	1.5737	624
17	.283	.0005	.978	4499	.332	1.5758	634
18	.3	.0005	.98	4508	.301	1.5778	643
19	.317	.0006	.982	4517	.271	1.5798	651
20	.333	.0007	.984	4525	.244	1.5816	659
21	.35	.0008	.985	4533	.218	1.5833	667
22	.367	.001	.987	4540	.194	1.585	674
23	.383	.0004	.988	4547	.172	1.5865	681
24	.4	.0004	.99	4553	.152	1.5879	687
25	.417	.0005	.991	4558	.133	1.5891	693
26	.433	.0005	.992	4563	.117	1.5903	698
27	.45	.0006	.993	4568	.101	1.5914	702
28	.467	.0006	.994	4572	.088	1.5923	707
29	.483	.0007	.995	4576	.076	1.5932	710
30	.5	.0008	.996	4579	.065	1.5939	714
31	.517	.0008	.996	4582	.056	1.5946	717
32	.533	.0009	.997	4585	.047	1.5952	719

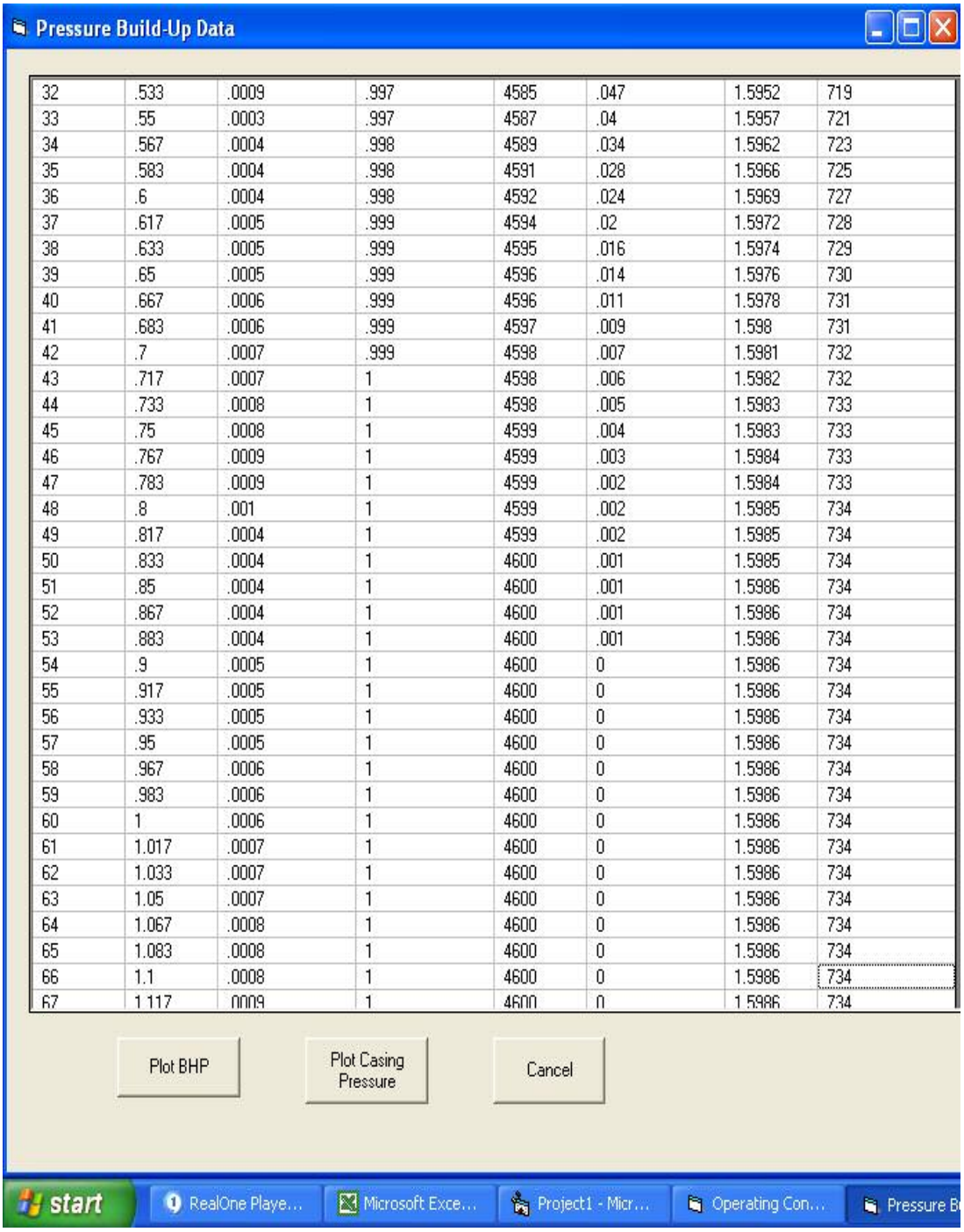

32	.533	.0009	.997	4585	.047	1.5952	719
33	.55	.0003	.997	4587	.04	1.5957	721
34	.567	.0004	.998	4589	.034	1.5962	723
35	.583	.0004	.998	4591	.028	1.5966	725
36	.6	.0004	.998	4592	.024	1.5969	727
37	.617	.0005	.999	4594	.02	1.5972	728
38	.633	.0005	.999	4595	.016	1.5974	729
39	.65	.0005	.999	4596	.014	1.5976	730
40	.667	.0006	.999	4596	.011	1.5978	731
41	.683	.0006	.999	4597	.009	1.598	731
42	.7	.0007	.999	4598	.007	1.5981	732
43	.717	.0007	1	4598	.006	1.5982	732
44	.733	.0008	1	4598	.005	1.5983	733
45	.75	.0008	1	4599	.004	1.5983	733
46	.767	.0009	1	4599	.003	1.5984	733
47	.783	.0009	1	4599	.002	1.5984	733
48	.8	.001	1	4599	.002	1.5985	734
49	.817	.0004	1	4599	.002	1.5985	734
50	.833	.0004	1	4600	.001	1.5985	734
51	.85	.0004	1	4600	.001	1.5986	734
52	.867	.0004	1	4600	.001	1.5986	734
53	.883	.0004	1	4600	.001	1.5986	734
54	.9	.0005	1	4600	0	1.5986	734
55	.917	.0005	1	4600	0	1.5986	734
56	.933	.0005	1	4600	0	1.5986	734
57	.95	.0005	1	4600	0	1.5986	734
58	.967	.0006	1	4600	0	1.5986	734
59	.983	.0006	1	4600	0	1.5986	734
60	1	.0006	1	4600	0	1.5986	734
61	1.017	.0007	1	4600	0	1.5986	734
62	1.033	.0007	1	4600	0	1.5986	734
63	1.05	.0007	1	4600	0	1.5986	734
64	1.067	.0008	1	4600	0	1.5986	734
65	1.083	.0008	1	4600	0	1.5986	734
66	1.1	.0008	1	4600	0	1.5986	734
67	1.117	.0009	1	4600	0	1.5986	734

APPENDIX D

D. PLOT OF ANNULAR GAS DENSITY AGAINST THE SHUT-IN TIME

